NON-REDUCTIVE BIOMINERALIZATION OF U(VI)-PHOSPHATE MINERALS THROUGH THE ACTIVITIES OF MICROBIAL PHYTASES

A Dissertation
Presented to
The Academic Faculty

by

Kathleen R. Salome

In Partial Fulfillment
of the Requirements for the Degree
Doctor of Philosophy in the
School of Earth and Atmospheric Sciences

Georgia Institute of Technology
August 2013

NONREDUCTION BIOMINERAZLIATION OF U(VI)-PHOSPHATE MINERALS THROUGH THE ACTIVITIES OF MICROBIAL PHYTASES

Approved by:

Dr. Martial Taillefert, Advisor
School of Earth and Atmospheric Sciences
Georgia Institute of Technology

Dr. Patricia A. Sobecky
School of Biological Sciences
University of Alabama

Dr. Thomas J. DiChristina
School of Biology
Georgia Institute of Technology

Dr. Ellery Ingall
School of Earth and Atmospheric Sciences
Georgia Institute of Technology

Dr. Samuel M. Webb
Stanford Synchrotron Radiation Lightsource

Date Approved: 05/17/2013

For Sittie

Whose love, smiles, and conversation

I will forever miss

ACKNOWLEDGEMENTS

I would like to thank my advisor, Dr. Martial Taillefert, for his support and guidance over the last six years. Without his dedication to undergraduate research and enthusiasm for scientific discovery, I would not be the scientist I am today. I especially thank him for fostering my independence and encouraging me to pursue new ideas. I wish to thank my committee members, Dr. Patricia Sobecky, Dr. Thomas DiChristina, Dr. Samuel Webb, and Dr. Ellery Ingall, whose recommendations have improved this dissertation. A special thanks to Dr. Samuel Webb for help in EXAFS fitting and to Dr. Thomas DiChristina for indulging all of my biology-related questions.

Thank you to all my past and present lab mates who made sometimes tedious lab work much more interesting: Melanie Stephanie, Morris, Jordon, Deidre, Lin, Anna, Keaton, Eryn, and Nicole. A very special thank you to Nadia Szeinbaum for all of her microbiological help. I would especially like to thank Dr. Melanie Beazley for the countless hours she spent helping me with research problems both in the lab and from afar. I feel honored to consider you a mentor and friend.

I would also like to thank the School of Earth and Atmospheric Sciences for providing me with this opportunity, and the National Science Foundation for providing me with funding to pursue my graduate research.

I am blessed with an amazing family, without whom I would not be the person I am today. Thank you for always supporting me in every decision I make. Finally, I would especially like to thank my loving husband, David, whose love, support, and encouragement carried me through the toughest times of this experience. I love you, and I can't wait to see what challenges life brings us next.

TABLE OF CONTENTS

LIST OF TABLES

LIST OF FIGURES

LIST OF SYMBOLS AND ABBREVIATIONS

ΣPO_4^{3-}	Sum of all orthophosphate species
IP_6	Inositol hexaphosphate, phytate, phytic acid
DOE	Department of Energy
EXAFS	Extended X-ray Absorption Fine Structure
IC	Ion Chromatography
ICP-MS	Inductively-coupled Plasma Mass Spectrometry
ORFRC	Oak Ridge Field Research Center
DIC	Dissolved Inorganic Carbon
SIXPACK	Sam's Interface for XAS Package
SSRL	Stanford Synchrotron Radiation Lightsource
XANES	X-ray Absorption Near-Edge Spectroscopy
XAS	X-ray Absorption Spectroscopy
NSAP	Non-specific Acid Phosphatase
MUP	4-methylumbelliferyl phosphate

SUMMARY

Remediation of the large quantity of uranium contaminated soils and groundwater at Department of Energy facilities across the United States remains a daunting task. Bioremediation, which involves either direct or indirect enzymatic transformation of uranium to immobile forms, is preferable to traditional remediation techniques which generally require physical removal of contaminants, rendering them cost-prohibitive and impractical. As subsurface geochemical conditions vary tremendously between contaminated sites, a one-size fits all approach when developing bioremediation strategies is not ideal.

In environments characterized by low pH and/or high nitrate, the biomineralization of U(VI)-phosphate minerals represents a uniquely suited bioremediation method involving microbially-mediated hydrolysis of organophosphates coupled to a chemical precipitation of sparingly soluble U(VI)-phosphate minerals. Unlike the widely studied bioreduction, this technique is not inhibited by low pH, fluctuating redox conditions, or elevated concentrations of common co-contaminants. Thus, the overall objective of this research is to further demonstrate the utility of U(VI)-phosphate biomineralization strategies and to investigate the use of phytate, a naturally-occurring and abundant organophosphate, to promote this process.

In this study, biomineralization of U(VI)-phosphate minerals promoted by addition of glycerol-2-phosphate (G2P) was shown to outcompete bioreduction in anaerobically-maintained sediment microcosms containing contaminated soils from the Oak Ridge Field Research Center (ORFRC), even at pH 7.0 when bioreduction should be

favorable. Sufficient orthophosphate was liberated by indigenous microorganisms to precipitate U(VI)-phosphate minerals both at low and circumneutral pH as determined by wet chemical extractions and X-ray absorption spectroscopy. In addition, the activities of nitrate-reducing bacteria were shown to be G2P-dependent, while iron reduction occurred independently of organophosphate addition.

Addition of phytate to aerobic soils slurries containing ORFRC soils also resulted in significant production of inorganic phosphate. The natural microbial community hydrolyzed phytate and liberated inorganic phosphate which was coupled to U(VI)-phosphate mineral formation and formation of ternary sorption complexes. Two-phytase positive microorganisms, *Bradyrhizobium* sp. and *Variovorax* sp., were isolated from these soil slurries, and experiments with increasing concentrations of uranium revealed that phytate hydrolysis by *Variovorax* sp. is induced as a uranium detoxification mechanism which was confirmed with development of a kinetic model to describe this process.

Finally, U(VI)-phosphate minerals were shown to be stable in low pH and/or low DIC environments, indicating the biomineralization of U(VI)-phosphate minerals may be uniquely suited for remediation of acidic contaminated subsurfaces. Phytate sorption to ORFRC soils was shown to be significant, but not complete, suggesting phytate should remain bioavailable to subsurface microorganisms. In addition, significant phytate was extracted from cereal bran using acidic solvents, demonstrating bran may represent an inexpensive and abundant phytate source for use in U(VI)-phosphate biomineralization strategies.

Overall, the results of this study demonstrate the utility of U(VI)-phosphate biomineralization in a wide range of geochemical conditions, including at low pH when bioreduction is unfavorable. Significantly, phytate hydrolysis by subsurface microorganisms coupled to precipitation of U(VI)-phosphate minerals was demonstrated for the first time, suggesting that phytate may represent an ideal organophosphate to promote this process, and cereal bran was identified as a possible commercially available and inexpensive source of this compound.

CHAPTER 1

INTRODUCTION

1.1 Overview and Motivations

Since the end of the cold war era in 1991, the United States Department of Energy (DOE) has shifted its focus from nuclear proliferation to remediation of over 120 legacy nuclear weapons facilities and test sites spread over 36 states which are currently contaminated with toxic heavy metals and radionuclides (DOE, 1997; NABIR, 2003). The current DOE waste inventory includes 6.4 trillion liters of contaminated groundwater, 40 million cubic meters contaminated solids and solid wastes, and 3 million cubic meters of waste buried in landfills (DOE, 1997; NABIR, 2003). Due to the scale of contamination at DOE facilities, traditional remediation techniques such as pump and treat have proven to be cost-prohibitive and inefficient approaches for treating contaminated soil and groundwater (Dawson and Gilman, 2001; Jardine, 2006; Mackay and Cherry, 1989). Therefore, the DOE has shifted focus to the investigation of *in situ* remediation strategies as relatively inexpensive and noninvasive alternatives to more traditional remediation methods (NABIR, 2003).

To encourage field-scale research of *in situ* remediation techniques in natural conditions, the Department of Energy developed a multi-year Integrated Field Research Challenge (IFRC) Project funded by the DOE's Subsurface Biogeochemical Research (SBR) program. This project established three field research sites: the uranium mill tailings site in Rifle, CO, the Hanford 300 former plutonium production facility in Hanford, WA, and the former Y-12 weapons development plant in Oak Ridge, TN. The

research presented in this dissertation revolves around the Oak Ridge Field Research Center (ORFRC) in Oak Ridge, TN, which is contaminated with uranium and other heavy metals originating from the former Y-12 nuclear weapons plant (Brooks, 2001). Four unlined nuclear waste disposal ponds, known as the S-3 ponds, were constructed in 1951 and received approximately 10 million liters of acidic uranium nitrate waste per year until 1983 (Figure 1.1) (Brooks, 2001; Jardine, 2006). The infiltration of waste into groundwater resulted in multiple contaminant plumes extending from the S-3 ponds and large secondary sources of contamination (Brooks, 2001). In 1988, the sludge was allowed to settle, and the liquid waste was treated for organic and metal contaminants and discharged into East Fork Poplar Creek (Brooks, 2001). The ponds and the remaining sludge were capped to prevent rainwater infiltration, and the area is currently used as a parking lot (Figure 1.1) (Brooks, 2001). Due to the nature of waste stored at Oak Ridge, groundwater at the ORFRC is characterized by low pH, high nitrate, and high uranium.

Figure 1.1 The S-3 waste disposal ponds (left), located near the former Oak Ridge Y-12 weapons plant, were constructed in 1951 and received waste until 1983 (Brooks, 2001). In 1988, the ponds were capped with asphalt to prevent infiltration (right), and the area is now used as a parking lot (Brooks, 2001). Picture from http://public.ornl.gov/orifc.

In fact, the pH of groundwater near the S-3 storage ponds has been recorded as low as 2.8, while nitrate and uranium concentrations have been observed as high as 654 mM and 252 μM, respectively (Jardine, 2006).

Currently, the primary *in situ* remediation strategies being pursued to mitigate the wide-spread uranium contaminations present at DOE managed sites are bioremediation techniques, which involve microbially-mediated transformations of hazardous chemicals to more benign chemical forms. Bioremediation, while well-established for organic contaminants (NABIR, 2003), has only recently been considered a viable technology for remediation of heavy-metals and radionuclides (Lovley and Phillips, 1992a; Lovley et al., 1991; Macaskie et al., 2000; Macaskie et al., 1992; Senko et al., 2002). For metals and radionuclides, which are often toxic to subsurface microorganisms (Suzuki and Banfield, 1999), bioremediation usually involves a decrease in solubility through detoxification mechanisms such as metal reduction (Lovley et al., 1991), precipitation (Macaskie et al., 1992), and biosorption (Macaskie and Basnakova, 1998). In addition, geochemical processes such as adsorption, precipitation, and chemical reduction, which effect the bioavailability of toxic metals (Suzuki and Banfield, 1999), should also be considered in any remediation strategy.

1.2 Uranium Occurrence in Nature

There are 17 known isotopes of uranium, all of which are radioactive with half-lives ranging from 10^5 to 10^9 years (NABIR, 2003). However, in nature uranium primarily exists as the isotopes ^{234}U (0.0057%), ^{235}U (0.719%), and ^{238}U (99.275%) which decay with half-lives of 2.47×10^5, 7.10×10^8, and 4.51×10^9 years, respectively

(Langmuir, 1997). Uranium, the most abundant naturally occurring actinide, has an average crustal abundance of 2.7 µg/g and tends to concentrate in silica-rich igneous rock such as granite (up to 15 µg/g) and phosphate rocks (20 – 120 µg/g) (Langmuir, 1997). The largest known uranium ore deposits are located in Canada, South Africa, Australia, Namibia, and the United States (Cotton et al., 1999). Uranium in seawater remains constant at 0.03 µM (Langmuir, 1997). However, uranium concentrations in natural freshwaters can vary between 0.42 nM in reducing groundwater to 0.5 µM in oxidizing groundwater and may be as high as 84 µM in mine tailing leachates (Langmuir, 1997), and the factors affecting these concentrations range from source rock uranium content and leachability to seasonal climate variability (Langmuir, 1978).

1.3 Controls on Aqueous Uranium Speciation in Natural Waters

The aqueous chemistry of uranium is highly complex largely due to its redox and complexation properties. Uranium exists in +3,+4, +5, and +6 oxidation states and has an atomic number of 92 and an atomic mass of 238.03 g mol^{-1} (Langmuir, 1997). U(III) is seldom found in nature as it is only favored in highly reducing and acidic conditions (Lehto and Hou, 2011). Pentavalent uranium may exist as the UO_2^+ ion over a narrow redox range and is more common than U(III) (Lehto and Hou, 2011). However, U(V) readily disproportionates into U(IV) and U(VI) (Langmuir, 1997) (Equation 1-1).

$$2UO_2^+ \rightarrow UO_2^{2+} + UO_{2\,(s)} \quad (1\text{-}1)$$

As such, the most common oxidation states of uranium in natural environments are U(IV) and U(VI). In reducing environments, U(IV) dominates and readily precipitates as the mineral uraninite $UO_{2\,(s)}$ (Langmuir, 1997). Upon transition to oxidizing conditions,

however, uraninite is reoxidized to U(VI) in the form of the uranyl ion UO_2^{2+} . The uranyl ion is highly stable and soluble over a wide range of geochemical conditions (Murphy and Shock, 1999), including most environmentally relevant pH. The stability of the uranyl ion may be attributed to its linear structure (Figure 1.2a) and strong covalent bonds between the uranium and oxygen atoms which remain intact during complexation (Figure 1.2b) and precipitation (Chernyaev, 1966; Cotton et al., 1999). Upon complexation, the uranyl ion is coordinated by 4, 5, or 6 ligands that are arranged in the equatorial plane of uranyl in a square bipyramidal, pentagonal bipyramidal, or hexagonal bipyramidal pattern depending on the ligand included (Figure 1.2b) (Burns, 1999).

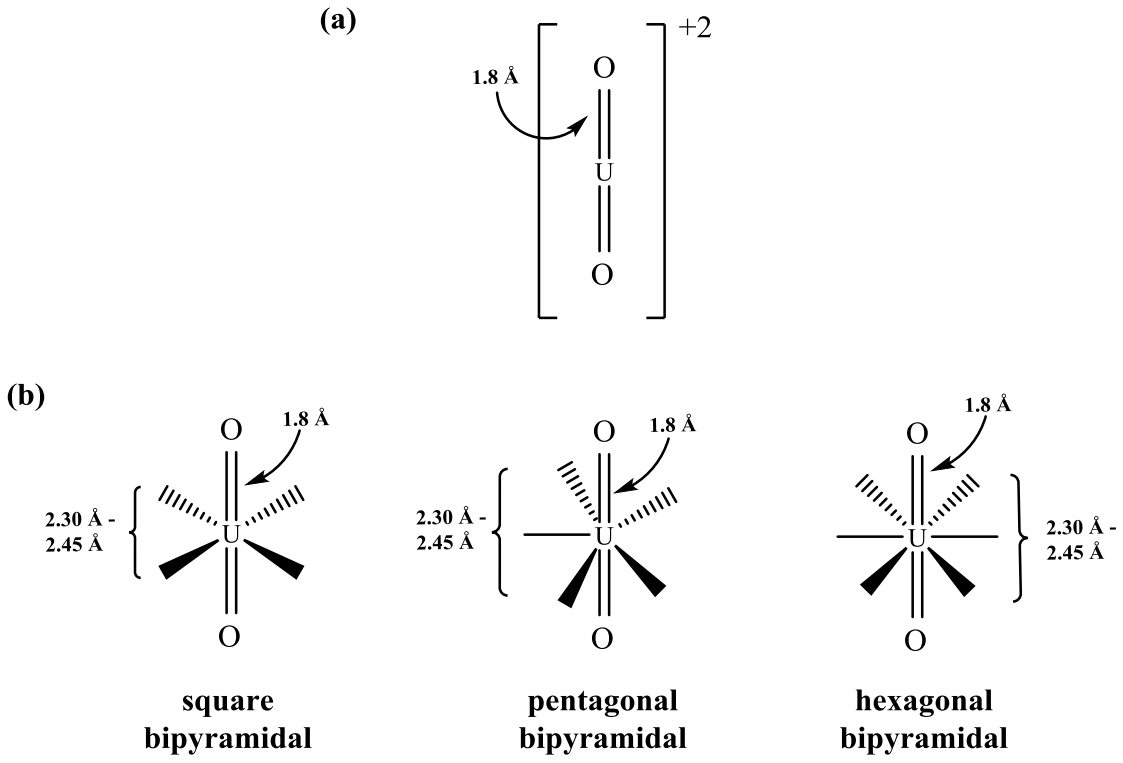

Figure 1.2 (a) The linear uranyl ion (UO_2^{2+}) displays axial oxygen bond length of 1.8 Å and (b) may be coordinated by 4, 5, or 6 equatorial ligands with bond lengths between 2.30Å and 2.45 Å.

While the axial uranium-oxygen bond of the uranyl ion displays a bond length of 1.80 Å (Burns, 1999) corresponding to strong covalent bonds, the equatorial oxygen bonds between uranium and coordinating ligands are longer and weaker (Burns, 1999) with typical lengths ranging between 2.30 Å and 2.45 Å depending on the bonding environment (Figure 1.2b) (Beazley et al., 2011; Burns, 1999; Webb et al., 2006). In addition, a*b inito* molecular orbital calculations demonstrate p-orbital electron donation from equatorial oxygen atoms into the empty d- and f- orbitals of the central U(VI) atom as the primary bonding mechanism for equatorial ligand complexation (Burns, 1999).

When considering uranium mobility in contaminated systems, U(VI) complexation chemistry is vastly important as the uranyl ion is highly soluble (i.e. mobile) and either hydrolyzes or forms strong coordination complexes at most environmentally relevant pH (Langmuir, 1997). Below pH 4.0, the dominant form of aqueous U(VI) is the free uranyl ion (Figure 1.3a, 1.3b). However, above pH 4 in the absence of competing ligands, the uranyl ion hydrolyzes to form moderately weak monomeric (low uranium concentrations) (Figure 1.3a) or polymeric (elevated uranium concentrations) (Figure 1.3b) aqueous hydroxide complexes according to the general hydrolysis reactions below (Eq. 1-2, 1-3) (Finch and Murakami, 1999a).

$$UO_2^{2+} + yH_2O \rightarrow UO_2(OH)_y^{(2-y)} + yH^+ \quad (1\text{-}2)$$

$$xUO_2^{2+} + yH_2O \rightarrow (UO_2)_x(OH)_y^{(2x-y)} + yH^+ \quad (1\text{-}3)$$

In typical groundwater (U_T = 10^{-8} M) at circumneutral pH with no competing ligands present, the dominant uranyl hydroxide complexes are UO_2OH^+, $UO_2(OH)_{2\ (aq)}$, and $UO_2(OH)_3^-$ (Figure 1.3a). However, upon introduction of competing ligands, uranyl

hydroxide species become less important as the uranyl ion is a hard acid and binds strongly to oxygen containing ligands such as carbonate and phosphate (Suzuki and Banfield, 1999). In addition, sulfate complexes may become important in low pH sulfidic waters when sulfide oxidation occurs (Finch and Murakami, 1999a).

Perhaps the most important driver of uranyl mobility in natural environments is carbonate. Carbonate forms strong bidentate complexes with U(VI) at or above pH 7.0 when carbonate is deprotonated (Figure 1.3c, 1.3d, 1.3e, 1.3f) (Langmuir, 1997), and these complexes may be particularly important in groundwater where P_{CO2} is sometimes as high as 10^{-2} bar (Figure 1.3e, 1.3f) (Langmuir, 1997). Uranyl carbonate complexes only minimally adsorb to iron oxides due to their negative charge (Figure 1.4a, 1.4b, 1.4c) (Katsoyiannis, 2007), and the presence of elevated carbonate concentrations may promote both U(IV) and U(VI) mineral dissolution (De Pablo et al., 1999; Liu et al., 2004; Sowder et al., 2001; Ulrich et al., 2009), which is greatly enhanced by the presence of bacterial cells (Katsenovich et al., 2012). In addition, elevated calcium concentrations present in high pH environments may promote the formation of ternary calcium-uranyl-carbonate complexes (Table 1.1), which further inhibit U(VI) sorption (Fox et al., 2006; Meleshyn et al., 2009; Stewart et al., 2010) and biological reduction by lowering the reduction potential of uranyl to less energetically favorable values (Brooks et al., 2003; Luo et al., 2007b). Thus, the presence of carbonates in natural systems where ambient pH is often in the circumneutral range frequently drives uranium mobility through complexation reactions.

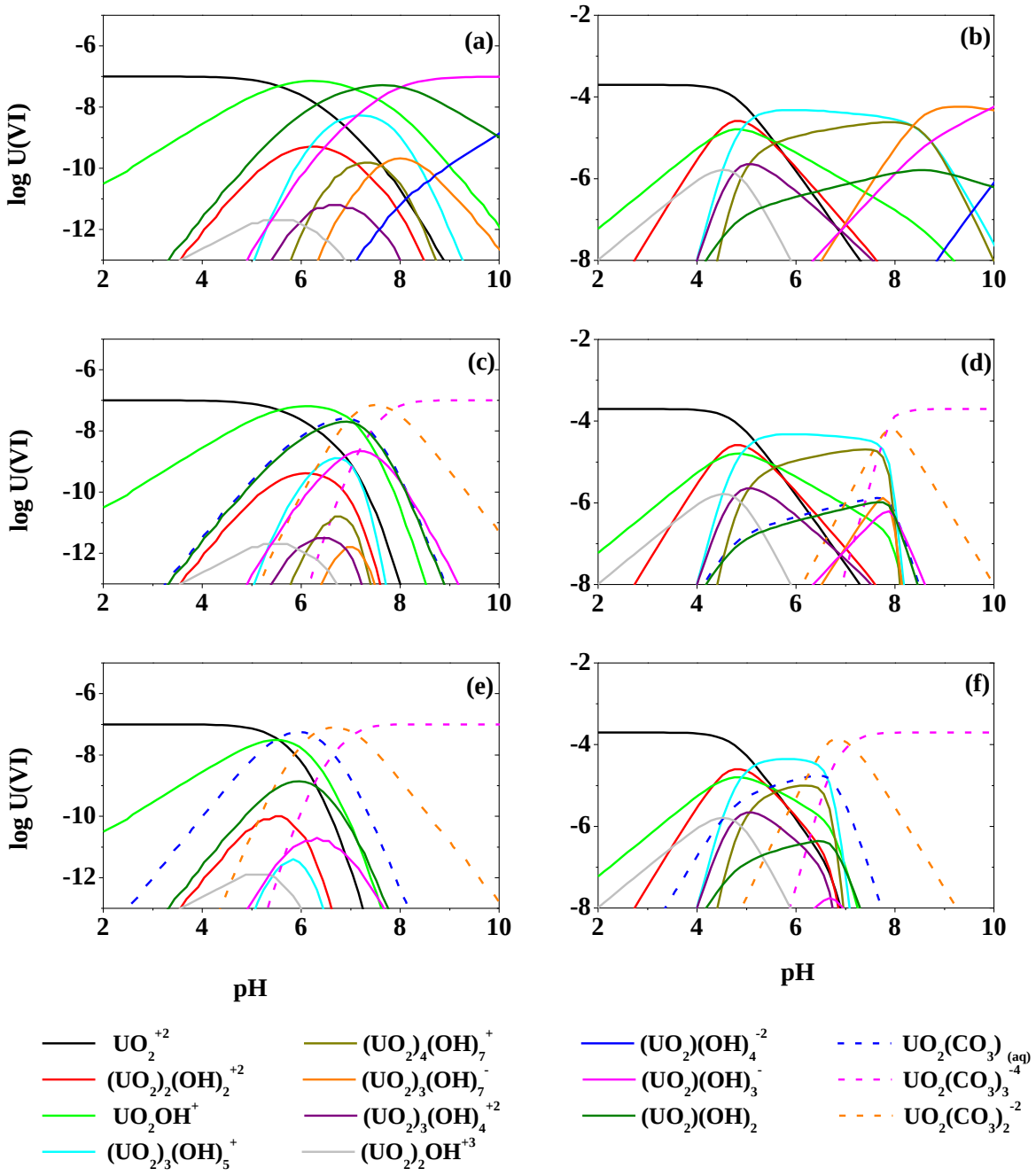

Figure 1.3 Speciation of 10^{-8} M U(VI) [(a), (c), (e)] and 200 µM U(VI) [(b), (d), (f)] at 25°C and I = 0.1 M without carbonate [(a) and (b)], at equilibrium with atmospheric CO_2 (P_{CO2} = $10^{-3.5}$ bar) [(c) and (d)], and in the presence of elevated carbonate found in groundwaters (P_{CO2} = $10^{-2.0}$ bar) [(e) and (f)] as predicted by MINEQL (Schecher and McAvoy, 2001) updated with the thermodynamic constants listed in Table 1.1.

1.4 Solid-phase Controls on Uranium Mobility in Natural Systems

Adsorption to iron oxides represents the dominant process controlling uranium mobility in natural systems (Figure 1.4a), although sorption to clay minerals may become important in low pH environments (pH < 4.0) when sorption to metal oxides is no longer favorable or at circumneutral pH in iron deficient sediments (Zheng et al., 2003). Generally, iron is prevalent in most terrestrial systems and represents a highly reactive mineral surface for the sorption of metal cations (Tessier et al., 1996). The reactivity of surface hydroxyl groups on iron oxide minerals is dependent on system pH and the pH_{ZPC} of each mineral (Stumm and Morgan, 1996). The pH_{ZPC} for goethite and hematite, common soil iron oxides, ranges between 5.9 and 6.7 for goethite and between 4.2 and 6.9 for hematite (Langmuir, 1997), and adsorption of uranyl is highest at or above ~ pH 6.5 when surface hydroxyl groups on iron oxides are deprotonated. At lower pH (pH < 5.0), aqueous U(VI) adsorbs strongly to manganese oxides given their low pH_{zpc} (Han et al., 2007) and even to ferric oxides despite the net positive charge of both uranyl hydroxide complexes and metal oxides (Han et al., 2007; Hsi and Langmuir, 1985; Waite et al., 1994). In addition, the presence of inorganic phosphate may enhance U(VI) sorption to ferric oxides at low pH through the formation of ternary surface complexes (Cheng et al., 2004; Payne et al., 1996).

Precipitation reactions may also significantly affect uranium mobility depending on the prevailing environmental conditions. If groundwaters become reducing, U(VI) may be chemically or biologically reduced to the sparingly soluble (~ 10^{-8} M) uranous ion $UO_{2\ (aq)}$ and reductively precipitate as uraninite (Figure 1.5) (Finch and Murakami, 1999a; Langmuir, 1997) or non-uraninite U(IV) minerals if competing ligands such as

orthophosphate are present (Bernier-Latmani et al., 2010; Fletcher et al., 2010; Sharp et al., 2011). At pH > 6, the surface-catalyzed chemical U(VI) reduction by Fe(II) adsorbed onto crystalline iron oxides (Behrends and Van Cappellen, 2005; Jeon et al., 2005; Liger et al., 1999; Regenspurg et al., 2009) and other minerals (Chakraborty et al., 2010; Regenspurg et al., 2009) is efficient. Dissolved sulfide (Ho and Miller, 1986; Kosztolanyi et al., 1996; Mohagheghi et al., 1985) and sulfide minerals (i.e. H_2S, FeS) (Beyenal et al., 2004; Marsili et al., 2007; Wersin et al., 1994) have also been shown to reduce U(VI) chemically.

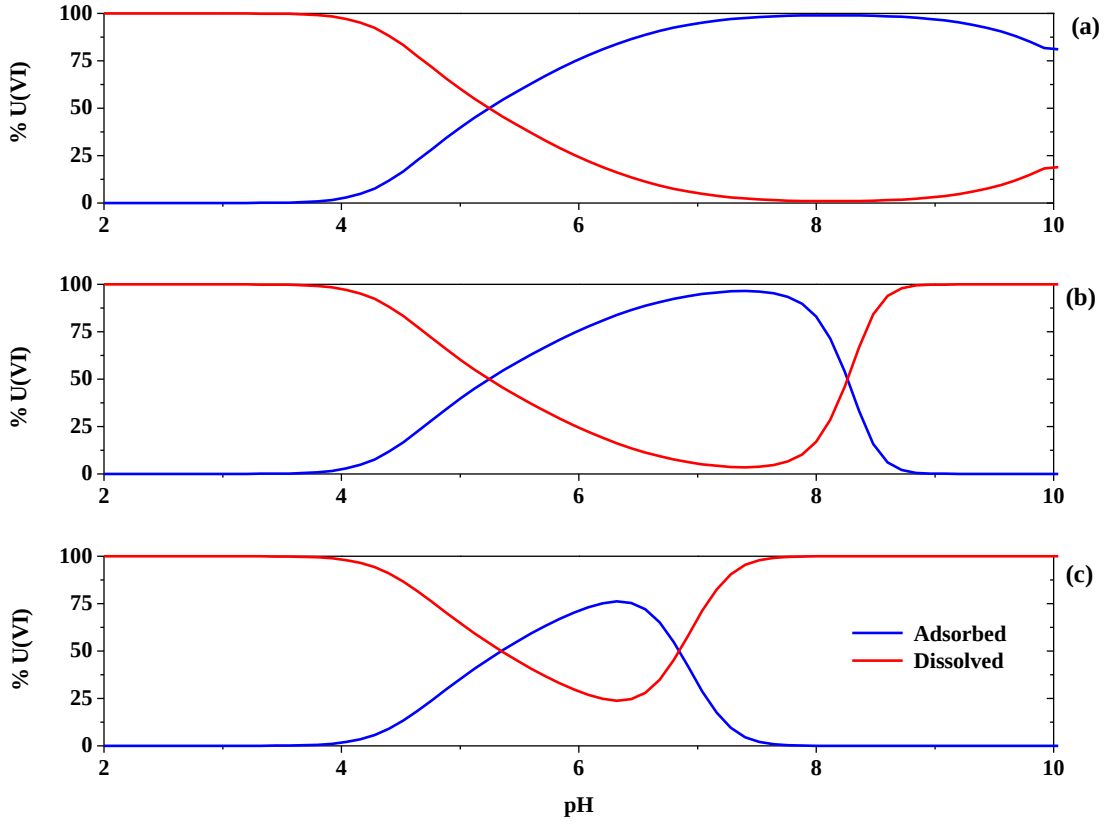

Figure 1.4 Adsorption of 200 µM (UO_2^{+2}) onto amorphous Fe-oxides (0.53 g/L) as a function of pH at (a) P_{CO2} = 0 bar, (b) P_{CO2} = $10^{-3.5}$ bar, and (c) P_{CO2} = $10^{-2.0}$ bar, representative of elevated carbonate in groundwaters, as predicted by MINEQL (Schecher and McAvoy, 2001) and updated with the thermodynamic constants listed in Table 1.1. A double-layer sorption model (600 m^2/g) was included in the calculations.

Interestingly, the dominant minerals in uranium ore are uraninite [$UO_{2\ (s)}$] and coffinite [$USiO_{4\ (s)}$] (Langmuir, 1997), both reduced minerals, indicating reductive precipitation may represent an important control on uranium mobility in natural systems.

In oxidizing environments, U(VI) may precipitate with oxyanions to form a highly diverse group of uranyl minerals (Burns, 1999). In high pH (pH ≥ 7) environments, schoepite [$\beta UO_3 \bullet 2H_2O$] precipitation may be significant (Figure 1.6a, 1.6b) but only in the absence of carbonate (Figure 1.6c, 1.6d) (Langmuir, 1997). In addition, uranyl precipitates to form silicate (uranophane) arsenate, molybdate, and vanadate (i.e. carnotite and tyuyamunite) minerals, which may be important when reduced uranium and vanadium minerals are oxidized simultaneously (Finch and Murakami, 1999a).

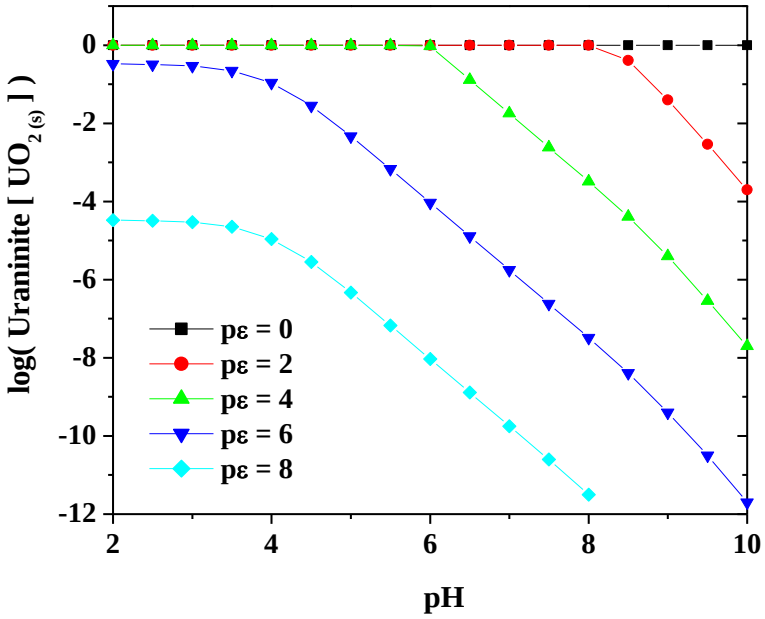

Figure 1.5 Speciation of 200 µM uranium as a function of pH and pε. The reductive precipitation of uraninite is favored at low pε and high pH.

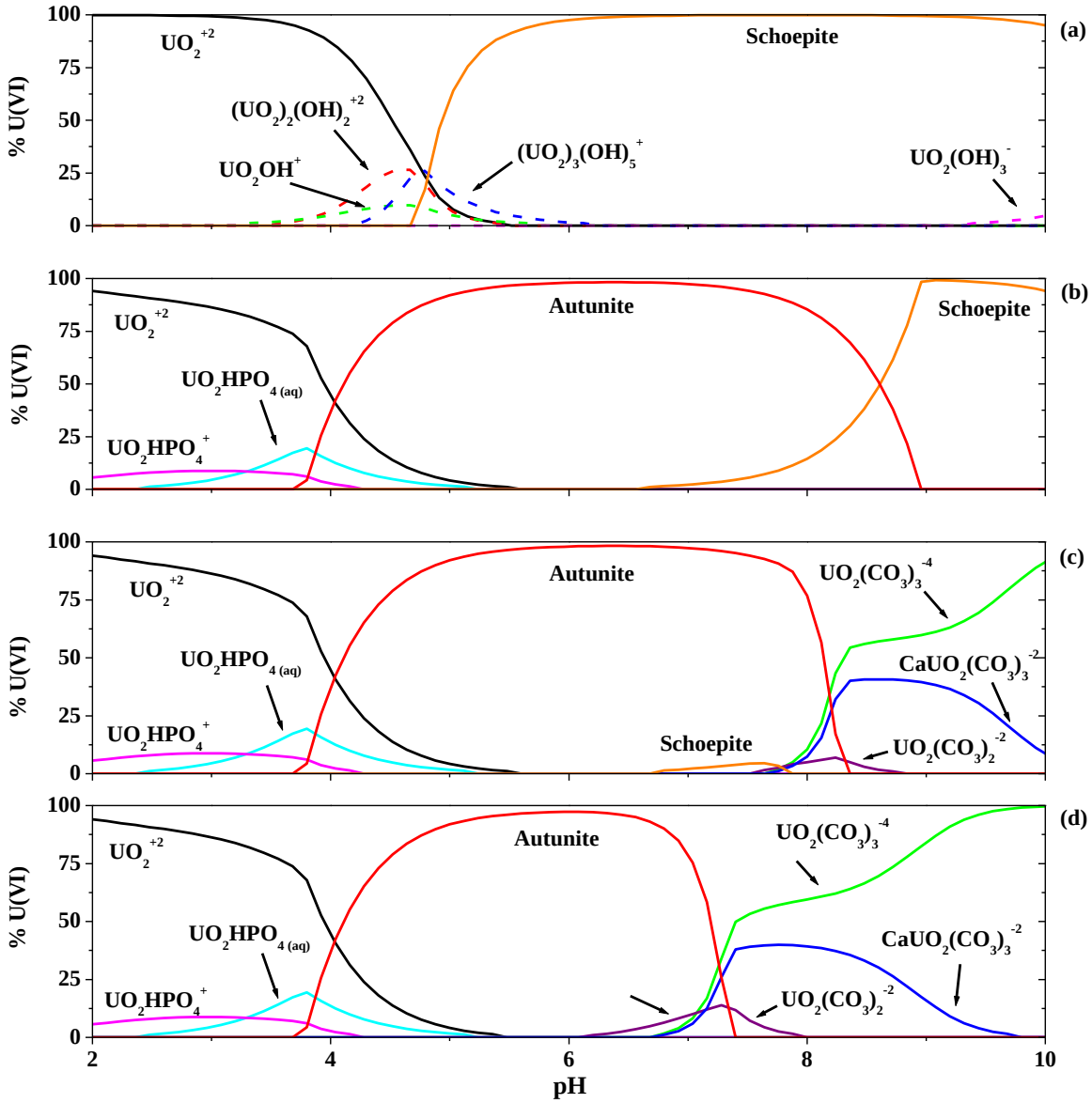

Figure 1.6 Precipitation of autunite [$Ca(UO_2)_2(PO_4)_2$] and schoepite [$UO_3 \bullet 2H_2O$] with 200 µM UO_2^{+2} and 200 µM Ca^{2+} as a function of pH at (a) P_{CO2} = 0 bar and 0 µM ΣPO_4^{3-}, (b) P_{CO2} = 0 bar and 200 µM ΣPO_4^{3-} (c) P_{CO2} = $10^{-3.5}$ bar and 200 µM ΣPO_4^{3-}, and (c) P_{CO2} = $10^{-2.0}$ bar and 200 µM ΣPO_4^{3-}, representative of elevated carbonate in groundwaters (Langmuir, 1997), as predicted by MINEQL (Schecher and McAvoy, 2001) updated with the thermodynamic constants listed in Table 1.1.

Between pH 4.0 and 8.0, uranyl also forms sparingly soluble complexes with phosphate (Figure 1.6b, 1.6c, 1.6d). In groundwaters where $\log([PO_4^{3-}]_T/[CO_3^{2-}]_T) > -0.3$, phosphate should outcompete carbonate for uranyl complexation (Finch and Murakami, 1999a). Additionally, carbonate-induced autunite dissolution rates are minimum between pH 5.0 and 6.0 (Wellman et al., 2007) when autunite formation is most favorable, and chernikovite [$(UO_2)H(PO_4)•4H_2O$] and metaautunite [$Ca(UO_2)_2(PO_4)_2•xH_2O$] are stable in the presence of 1 mM carbonate over yearly timescales (Sowder et al., 2001). Thus, in groundwater containing 200 μM U(VI), 200 μM Ca^{2+}, 200 μM ΣPO_4^{3-}, and atmospheric pCO_2 ($10^{-3.5}$ bar), uranyl phosphate mineral formation is seemingly unaffected by the presence of carbonate below pH 8.0 (Figure 1.6c). Contrastingly, the presence of carbonate significantly inhibits schoepite precipitation in these conditions (Figure 1.6c), demonstrating the presence of carbonate may significantly enhance uranium mobility above circumneutral pH. Uranyl phosphate minerals are ubiquitous in nature with over 70 identified minerals and U:P stoichiometric ratios varying between 1:1 (autunite and meta-autunite groups) and 1:2 (walpurgite group) (Finch and Murakami, 1999a). In fact, U(VI)-phosphate minerals have been identified in sediments from several contaminated sites, including the ORFRC (Kelly et al., 2005; Roh et al., 2000; Stubbs et al., 2006) and the Hanford 300 Area facility (Arai et al., 2007; Catalano et al., 2006), among others, suggesting uranyl phosphate precipitation may represent a natural attenuation mechanism for uranium immobilization at contaminated sites.

Phosphate may also influence uranium mobility indirectly through its strong interactions with soil iron oxides and other minerals. Sorption of phosphate to iron oxides may also indirectly inhibit reductive precipitation of U(IV) minerals by blocking

iron surfaces and limiting microbial iron reduction (Borch et al., 2007). At low pH, phosphate may enhance U(VI) sorption to alumina (Guo et al., 2006). In addition, phosphate readily adsorbs to soils below pH 7.0 when iron oxides are positively charged (Dideriksen and Stipp, 2003), resulting in a change in the average surface charge of the iron oxide (Payne et al., 1996) and a shift in the U(VI) sorption edge to a lower pH through the formation of ternary $\equiv Fe{-}OPO_3{-}UO_2$ surface complexes (Cheng et al., 2004). In fact, ternary U(VI)-phosphate surface complex formation may be a precursor to the precipitation of uranyl phosphate minerals (Sato et al., 1997). In reduced systems where uranium reduction occurs, aqueous phosphate also drives U(IV) solid-phase speciation through precipitation of monomeric U(IV)-phosphate precipitates in place of uraninite (Bernier-Latmani et al., 2010; Boyanov et al., 2011).

Table 1.1. Most updated (2012) uranium complexation reactions and thermodynamic stability constants (T = 25°C, I = 0, P = 1bar)

Reaction	Log K
Hydrolysis Reactions	
$UO_2^{2+} + H_2O \rightarrow UO_2OH^+ + H^+$	-5.2[a,b,c]
$UO_2^{2+} + 2H_2O \rightarrow UO_2(OH)_2 + 2H^+$	-12.15[c]
$UO_2^{2+} + 3H_2O \rightarrow UO_2(OH)_3^- + 3H^+$	-20.25[c]
$UO_2^{2+} + 4H_2O \rightarrow UO_2(OH)_4^{2-} + 4H^+$	-32.4[c]
$2UO_2^{2+} + H_2O \rightarrow (UO_2)_2OH^{3+} + H^+$	-2.7[b,c]
$2UO_2^{2+} + 2H_2O \rightarrow (UO_2)_2(OH)_2^{2+} + 2H^+$	-5.62[a,b,c]
$3UO_2^{2+} + 4H_2O \rightarrow (UO_2)_3(OH)_4^{2+} + 4H^+$	-11.9[b,c]
$3UO_2^{2+} + 5H_2O \rightarrow (UO_2)_3(OH)_5^+ + 5H^+$	-15.6[a,b,c]
$3UO_2^{2+} + 7H_2O \rightarrow (UO_2)_3(OH)_7^- + 7H^+$	-32.2[c]
$4UO_2^{2+} + 7H_2O \rightarrow (UO_2)_4(OH)_7^+ + 7H^+$	-21.9[a,b,c]
Uranyl Carbonate Complexes	
$UO_2^{2+} + CO_3^{2-} \rightarrow UO_2CO_{3\ (aq)}$	9.94[c]
$UO_2^{2+} + 2CO_3^{2-} \rightarrow UO_2(CO_3)_2^{2-}$	16.61[c]
$UO_2^{2+} + 3CO_3^{2-} \rightarrow UO_2(CO_3)_3^{4-}$	21.84[c]
$Ca^{2+} + UO_2^{2+} + 3CO_3^{2-} \rightarrow CaUO_2(CO_3)_3^{2-}$	27.18[d]
$2Ca^{2+} + UO_2^{2+} + 3CO_3^{2-} \rightarrow CaUO_2(CO_3)_{3\ (aq)}$	30.7[d]
Uranyl Phosphate Complexes	
$UO_2^{2+} + PO_4^{3-} \rightarrow UO_2PO_4^-$	13.23[b,c]
$UO_2^{2+} + HPO_4^{2-} \rightarrow UO_2HPO_{4\ (aq)}$	7.24[b,c]
$UO_2^{2+} + H_3PO_4^0 \rightarrow UO_2H_2PO_4^+ + H^+$	1.12[a,b,c]
Sorbed Uranyl Complexes	
$2 \equiv Fe(st)OH + UO_2^{2+} \rightarrow (\equiv Fe(st)O)_2UO_2 + 2H^+$	-2.57[e]
$2 \equiv Fe(wk)OH + UO_2^{2+} \rightarrow (\equiv Fe(wk)O)_2UO_2 + 2H^+$	-6.28[e]
$\equiv Fe(st)OH + UO_2^{2+} + H_2PO_4^- \rightarrow \equiv Fe(st)PO_4UO_2 + H_2O + H^+$	9.51[f]
$\equiv Fe(wk)OH + UO_2^{2+} + H_2PO_4^- \rightarrow \equiv Fe(wk)PO_4UO_2 + H_2O + H^+$	7.84[f]
$2 \equiv Fe(st)OH + UO_2^{2+} + H_2CO_3^* \rightarrow (\equiv Fe(st)O)_2UO_2CO_3^{2-} + 4H^+$	-12.3[b]
$2 \equiv Fe(wk)OH + UO_2^{2+} + H_2CO_3^* \rightarrow (\equiv Fe(wk)O)_2UO_2CO_3^{2-} + 4H^+$	-16.4[b]
U(VI) Solids	
$UO_2^{2+} + 3H_2O \rightarrow UO_3 \bullet 2H_2O_{(s)}$ (schoepite) $+ 2H^+$	-5.2[a]
$Ca^{2+} + 2UO_2^{2+} + 2PO_4^{3-} \rightarrow Ca(UO_2)_2(PO_4)_{2\ (s)}$ (autunite)	44.7[a]

[a] (Langmuir, 1997), [b] (Grenthe et al., 1992), [c] (Guillaumont et al., 2003), [d] (Dong and Brooks, 2006), [e] (Waite et al., 1994), [f] (Romero-Gonzalez et al., 2007)

1.5 Remediation of Uranium in Contaminated Subsurfaces

1.5.1 Traditional Remediation Techniques

A variety of physical, chemical, and biological techniques exist for remediation of uranium at contaminated sites. Natural attenuation, or the exploitation of naturally occurring processes to achieve long-term ecosystem restoration, represents the least invasive and least expensive method for uranium remediation (Gavrilescu et al., 2009), though, the feasibility of this approach varies greatly with the chemical, biological, and physical properties of the contaminated site (Gavrilescu et al., 2009). For small-scale contaminations, physical remediation techniques such as soil capping or excavation (Gavrilescu et al., 2009) may be effective. However, these techniques become prohibitively expensive and inefficient for the geographically expansive contaminations often present at DOE managed facilities (Dawson and Gilman, 2001; Jardine, 2006; Mackay and Cherry, 1989). Chemical remediation approaches include chemical degradation/transformation, volatilization, chemical oxidation/reduction, precipitation, adsorption/desorption processes, and permeable reactive barriers (Gavrilescu et al., 2009) and may be coupled to the physical removal of contaminated media in remediation processes such as pump and treat (Mackay and Cherry, 1989).

1.5.2 Bioremediation Techniques

Bioremediation describes the process of harnessing microbial metabolism to transform and/or degrade contaminants (Gavrilescu et al., 2009). Biologically-mediated reduction of U(VI), or bioreduction, is currently the primary bioremediation technique studied for the immobilization of uranium in contaminated subsurface environments

(Fredrickson et al., 2000; Ganesh et al., 1999; Lovley and Phillips, 1992b; Lovley et al., 1991; North et al., 2004; Sanford et al., 2007; Wade and DiChristina, 2000). Currently, several strains of metal-reducing and sulfate-reducing bacteria are known to reduce U(VI), including members of the genus *Shewanella* (Blakeney et al., 2000; Lovley et al., 1991), *Desulfovibrio* sp. (Lovley, 1993; Lovley and Phillips, 1992b), *Geobacter* sp. (Jeon et al., 2004; Lovley et al., 1991), and *Anaeromyxobacter dehalogens* (Sanford et al., 2007), and *in situ* bioreduction of U(VI) has been demonstrated at the ORFRC (Wu et al., 2006b) and other contaminated sites (Senko et al., 2002). Unfortunately, bioreduction is inhibited at pH < 7 and in elevated nitrate concentrations (Finneran et al., 2002b; Wu et al., 2006a; Wu et al., 2006b). In addition, the uraninite mineral product may not remain stable in fluctuating chemical conditions as uraninite is readily oxidized to the mobile U(VI) upon reintroduction of oxygen in groundwater recharge areas (Langmuir, 1997; Murphy and Shock, 1999) and by NO_2^- (Beller, 2005; Moon et al., 2007; Wu et al., 2010), $Fe(OH)_3$ (Senko et al., 2002; Senko et al., 2005b; Wan et al., 2005; Zeng and Giammar, 2011), and MnO_2 (Fredrickson et al., 2002; Wang et al., 2013b) under reducing conditions. Thus, the long term instability of uraninite coupled with the inhibitory effects of co-contaminants on U(VI) reduction favors investigation of alternative remediation techniques applicable in both reducing and oxidizing conditions.

The biomineralization of insoluble U(VI)-phosphate minerals through the activities of microbial phosphatases represents a possible complementary bioremediation technique to the widely studied bioreduction. As mentioned previously, U(VI) forms sparingly soluble and stable (Jerden and Sinha, 2003) phosphate minerals over a broad range of environmental conditions (pH 4 - 8) (Ohnuki et al., 2004; Wellman et al., 2007;

Zheng et al., 2006). However, direct addition of inorganic phosphate to subsurface environments drastically decreases soil hydraulic conductivity (Wellman et al., 2006) and may limit orthophosphate transport throughout contaminant plumes. Consequently, research has concentrated primarily on the addition of an exogenous organophosphate source to stimulate microbially-mediated orthophosphate production coupled to a chemical precipitation of sparingly soluble U(VI)-phosphate minerals (Beazley et al., 2007, 2009; Macaskie et al., 1995; Martinez et al., 2007; Montgomery et al., 1995; Shelobolina et al., 2009). To fulfill their phosphate requirements, most microorganisms secrete non-specific acid phosphohydrolases (NSAP, phosphatases), a group of periplasmic or membrane-bound enzymes that catalyze the hydrolysis of organic phosphoester bonds at acidic to circumneutral pH (Rossolini et al., 1998). Uranium removal coupled to microbial phosphatase activity has been demonstrated in both aerobic and anaerobic conditions and at both acidic and circumneutral pH by the facultative anaerobe *Rahnella* sp. Y9602 (Beazley et al., 2007, 2009; Martinez et al., 2007), in anaerobic circumneutral pH conditions by *Cellumonas* sp. (Sivaswamy et al., 2011), and in low-pH aerobic conditions by *Citrobacter* sp. (Macaskie et al., 1995; Montgomery et al., 1995), *Bacillus* sp. (Merroun et al., 2011), and *Sphingomonas* sp. (Merroun et al., 2011). In addition, uranium removal in aerobically-maintained contaminated sediments has been achieved through stimulation of the phosphatase activities of indigenous bacteria (Beazley et al., 2011; Shelobolina et al., 2009).

Thus far, biomineralization studies have predominantly investigated the addition of synthetic organophosphates, such as glycerol-2-phosphate (G2P) (Figure 1.7a) and glycerol-3-phosphate (G3P) (Figure 1.7b), to subsurface environments to promote uranyl-

phosphate mineral formation (Beazley et al., 2007, 2009; Beazley et al., 2011; Martinez et al., 2007; Shelobolina et al., 2009). Inositol hexaphosphate (IP_6) (Figure 1.7c), also known as phytate (salt) or phytic acid (metal-free), is synthesized by plants for phosphorus storage and, consequently, represents the dominant organophosphate in most terrestrial environments (Turner et al., 2002) making it an attractive alternative to synthetically derived substrates. The chemical precipitation of U(VI) by phytate has been investigated (Knox et al., 2008; Nash et al., 1998; Seaman et al., 2003). However, phytate-promoted biomineralization of U(VI)-phosphate minerals has been only limitedly explored.

1.5.3 Inositol Phosphate Biochemistry

Inositol hexaphosphate is a phosphorylated inositol with six attached phosphate groups (Figure 1.7c) (Turner et al., 2002). The *myo*- inositol form of IP_6 is the by far the most abundant of the nine stereoisomers found in the environment, perhaps because it is the sole isomer with only one axial phosphate group (Figure 1.7c) (Parthasarathy and Eisenberg, 1991). The six phosphate groups on phytic acid carry twelve ionizable protons (Figure 1.7c) (Turner et al., 2002) with pK_as ranging from 1.1 to 12.0 as determined by ^{31}P nuclear magnetic resonance chemical shifts (Table 1.2) (Costello et al., 1976). With six pK_as below 3.0 (Table 1.2), phytic acid carries a highly negative charge (-6 to -9) at environmentally relevant pH. As such, phytic acid efficiently chelates multivalent cations, including Ca^{2+}, Zn^{2+}, Mg^{2+}, Mn^{2+}, and Cu^{2+} (Turner et al., 2002; Wodzinski and Ullah, 1996), especially above circumneutral pH (Shvets et al., 1991).

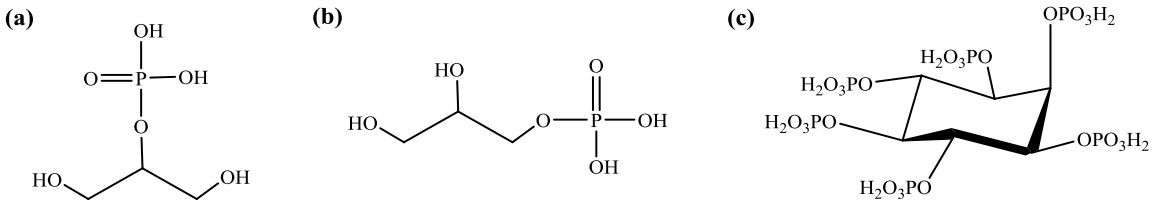

Figure 1.7 Chemical structure of (a) glycerol-2-phosphate (G2P), (b) glycerol-3-phosphate (G3P), and (c) myo-inositol hexakisphosphate (IP_6).

In addition to chelating metals, phytate interacts strongly with soil sorbents, including metal oxides and natural organic matter (Degroot and Golterman, 1993; Johnson et al., 2012). In fact, phytate inhibits orthophosphate sorption and actually displaces sorbed inorganic phosphate from iron oxides (Degroot and Golterman, 1993).

Although IP_6 remains chemically stable at all environmentally relevant pH and is not hydrolyzed by conventional phosphohydrolases (Turner et al., 2002), enantioselective phytase enzymes may catalyze its hydrolysis to lower inositol derivatives (IP_X, x: 1-5) and inorganic phosphate (Irving and Cosgrove, 1971; Parthasarathy and Eisenberg, 1991). Importantly, once hydrolysis of the initial phosphate group from IP_6 is achieved, hydrolysis of lower inositol derivatives (IP_X, x: 1-5) may be catalyzed either by phytase or any non-specific acid or alkaline phosphatase (Marko-Varga and Gorton, 1990; Meek and Nicoletti, 1986; Shan et al., 1994). Phytase enzymes are a substrate-specific subclass of phosphomonoesterases produced by plants, animals, and microorganisms (Oh et al., 2004) with variable pH optimum, molecular weight, structure, and metal cofactor required for enzyme activation (Shin et al., 2001). Plant phytases have been studied in a variety of species including barley, bean, corn, cottonseed, grass seeds, lettuce seed, white mustard seed, pea, potato, radish, rice, rye, sorghum, soybean, and wheat, while animal phytases have been mostly isolated from digastric mammals (Cosgrove, 1980).

Table 1.2 Acid dissociation (pK_a) constants of phytic acid as determined by ^{31}P nuclear magnetic resonance chemical shifts (Costello et al., 1976)

pK_{a1}	pK_{a2}	pK_{a3}	pK_{a4}	pK_{a5}	pK_{a6}	pK_{a7}	pK_{a8}	pK_{a9}	pK_{a10}	pK_{a11}	pK_{a12}
1.1	1.5	1.5	1.7	2.1	2.1	5.7	6.9	7.6	10.0	10.0	12.0

Additionally, a broad range of phytase-producing microorganisms have been identified in a wide variety of environments. Usually, fungi produce extracellular phytase (Oh et al., 2004; Rao et al., 2009; Shimizu, 1993), while bacteria produce intracellular phytase. Phytases from *Bacillus* and *Enterobacter* sp., however, are extracellular enzymes (Mukhametzyanova et al., 2012) and phytase from *E. coli* is a periplasmic enzyme (Greiner and Sajidan, 2008). Generally, bacterial phytase biosynthesis is triggered in phosphate-limited conditions and, thus, is thought to be controlled by the *Pho* regulon which regulates expression of genes involved in the uptake and assimilation of phosphate (Kertesz et al., 1994; Vershinina and Znamenskaya, 2002; Wanner, 1993). However, *E. coli* phytase, the most robustly characterized bacterial phytase, is not under control of the *Pho* regulon (Greiner, 2007), suggesting the function and regulation of bacterial phytases may be highly variable.

Based on their optimum pH, phytases may be classified broadly as either acid or alkaline phytases. Acid phytases include the subclasses purple acid phosphatases (PAPs) and histidine acid phosphatases (HAPs) which both display optimum catalytic activity at acidic pH and exhibit a range of specific phytase activity. In addition, acid phytases are inhibited by elevated concentrations of monovalent and divalent cations (Oh et al., 2004), and the final product of phytase-catalyzed IP_6 hydrolysis is IP_1 as the final phosphate group on IP_1 cannot be liberated by phytase (Turner et al., 2002). Purple acid phosphatases, also known as tartrate-resistant acid phosphatases due to their insensitivity

to tartrate inhibition, are highly abundant in plants and are thought to mediate phosphorus acquisition and redistribution (Kuang et al., 2009). They occur as homodimeric glycoproteins with a Fe(III)-Zn(II) metal pair in their active site (Rao et al., 2009), and the current proposed mechanism for PAP-catalyzed phytate hydrolysis involves formation of a Zn(II)-substrate complex which undergoes nucleophilic attack by an Fe(III) bound hydroxide group (Klabunde et al., 1996; Strater et al., 1995). Histidine acid phosphatases are the most common class of acid phytase and are widespread among microorganisms (Mukhametzyanova et al., 2012). Additionally, all HAPs share the conservative N- and C- terminal active site motifs RHGXRXP and HD, respectively, which become proximate during folding and impart catalytic activity to the enzyme (Mukhametzyanova et al., 2012). Phytate hydrolysis by HAPs occurs in a two-step process involving a nucleophilic attack by the active site histidine to form a phospho-histidine intermediate followed by hydrolysis of the intermediate compound and liberation of inorganic phosphate (Shin et al., 2001; Vincent et al., 1992), and the aspartic acid residue of the C-terminal conserved HD motif is thought to act as a proton donor to the oxygen atom in the phosphomonoester bond (Oh et al., 2004).

Unlike acid phytases, alkaline phytases consist of a class of enzymes known as β-propeller phytases (BPPs) which share a sequence identity of 90-98% with each other but display no homology with any other known group of phosphatases and lack the RHGXRXP and HD active site conservative motifs found in HAPs (Mullaney and Ullah, 2007; Yao et al., 2012). Although β-propeller phytases have almost exclusively been characterized in *Bacillus* sp. (Fu et al., 2008; Kerovuo et al., 1998; Kim et al., 1998), BPPs from *Shewanella oneidensis* MR-1 (Cheng and Lim, 2006) and *Pedobacter*

nyackenesis MJ11 CGMCC 2503 (Huang et al., 2009) have also been investigated, and bioinformatic studies indicate BPPs may be widespread in prokaryotes (Cheng and Lim, 2006; Lim et al., 2007). Interestingly, while acid phytases are inhibited by calcium (Kim et al., 1998), BPPs require calcium for enzyme function (Ha et al., 2000). The binding of six calcium ions by highly ion-specific sites in the protein globule imparts thermostability to the enzyme, and the binding of three additional calcium ions by non-specific sites at the surface of the phytate molecule transitions phytate to a preferable conformer for biding with phytase enzymes (Ha et al., 2000). In addition to the BPP calcium binding sites, there is also one high-affinity phosphate binding site which attracts and orients the phytate molecule and a second phosphate binding site where cleavage occurs (Oh et al., 2001). Because of the affinity phosphate binding site, BPPs preferentially hydrolyze inositol phosphates with adjacent bound phosphate groups resulting in a final BPP phytate hydrolysis product of IP_3 with alternating phosphorylated and unphosphorylated positions on the inositol ring (Shin et al., 2001).

1.6 Research Scope and Objectives

Due to the highly varied nature of uranium contaminated environments, a one-size fits all remediation approach is unlikely to succeed. Due to their unique ambient geochemistry, contaminated sites such as the ORFRC, where low pH and elevated nitrate concentrations drive subsurface biogeochemistry, present a particularly difficult challenge. Interestingly, a flourishing microbial community exists that has adapted to these harsh conditions (Green et al., 2010; Spain and Krumholz, 2011) and thus, may potentially be exploited in the development of novel bioremediation strategies. The overall objective of this research is to explore the possible avenues for promoting

microbially-catalyzed *in situ* uranium bioremediation at contaminated sites characterized by acidic pH and high levels of co-contaminants.

Previous work has identified bacterial isolates from the ORFRC that express phosphatase activity in the presence of synthetic organophosphates in both aerobic and anaerobic conditions (Beazley et al., 2007, 2009; Martinez et al., 2007). Additionally, uranium removal coupled to the phosphatase activity of the natural microbial community at Oak Ridge has been demonstrated in aerobic flow-through reactors amended with G3P (Beazley et al., 2011). The primary goal of this study is to assess the phytase activity of the ORFRC natural microbial community and to determine whether phytase expression by this community liberates sufficient inorganic phosphate to precipitate sparingly soluble U(VI)-phosphate minerals. Specifically, this dissertation details experiments investigating the following hypotheses: 1) U(VI)-phosphate biomineralization promoted by ORFRC microorganisms outcompetes bioreduction in reducing sediments; 2) OFRFC microorganisms promote U(VI)-phosphate mineral formation via enzymatic hydrolysis of phytate; and 3) the U(VI)-phosphate mineral product of biomineralization remains stable in a variety of geochemical conditions.

In order to accurately understand the evolving geochemical and microbial dynamics involved in U(VI)-phosphate biomineralization, a large number of analytical tools were used to elucidate overall aqueous composition and solid-phase uranium speciation, and Chapter II of this dissertation outlines the various analytical techniques employed in this study. Dissolved constituents were quantified by inductively-coupled plasma mass spectrometry (dissolved uranium), ion chromatography (anions, organophosphates, low molecular weight organic acids), and spectrophotometric

techniques (phosphate, Fe(II), nitrite). A combination of solid-phase sequential extractions and synchrotron-based X-ray absorption spectroscopy were used to determine the speciation and molecular structure of solid-phase associated uranium.

Although U(VI)-phosphate biomineralization has been demonstrated in anaerobic conditions, the competition dynamic between uranium biomineralization and bioreduction has not been thoroughly examined. Chapter III investigates this competition in anaerobically maintained static microcosms containing contaminated ORFRC sediments buffered at either pH 5.5 or 7.0. The objectives of this work were (1) to determine whether nitrate-, iron-, or sulfate-reducing conditions are most conducive to U(VI)-phosphate biomineralization through the activity of endogenous ORFRC microbial phosphatases and (2) to determine whether the biomineralization of U(VI)-phosphate minerals outcompetes uranium bioreduction in conditions favorable to bioreduction (i.e. pH 7.0, low nitrate).

Previously, U(VI)-phosphate biomineralization was demonstrated with synthetic organophosphate sources. In Chapter IV, the ability of endogenous ORFRC microorganisms to hydrolyze phytate, a naturally-occurring and abundant organophosphate, and liberate inorganic phosphate was investigated in aerobic soils slurries containing contaminated ORFRC soils. The objectives of this work were (1) to explore the phytase activity of the ORFRC natural microbial community at pH 5.5 and 7.0, (2) to determine the dependence of this phytase activity on the addition of an electron donor, and (3) to examine the biomineralization of U(VI)-phosphate minerals coupled to microbial phytase activity.

The work in Chapter V builds on the establishment of substantial phytase activity exhibited by the ORFRC natural microbial community by elucidating the mechanisms of phytate hydrolysis by phytase-positive ORFRC microorganisms. *Variovorax paradoxus* sp., an acid-tolerant denitrifier isolated from the soils slurries discussed in Chapter IV, was assayed for its ability to mineralize phytate and liberate inorganic phosphate in aerobic conditions with varying concentrations of uranium. The objectives of this work were (1) to demonstrate phytase activity by an ORFRC bacterial isolate, (2) to determine what geochemical conditions induce phytase expression by this bacterial strain, and (3) to investigate the effect of increasing uranium concentrations on the production of phytase enzymes.

Prior to implementing a bioremediation strategy in contaminated environments, predictive models must be developed to determine the long-term stability and distribution of mitigated contaminants. Thus, a diagnostic model for phytate hydrolysis by *Variovorax* sp. was developed in Chapter VI of this dissertation. The objectives of this work were (1) to develop a kinetic model to accurately describe phytate hydrolysis promoted by *Variovorax* and (2) to apply this model to incubations amended with increasing uranium concentrations to determine the effect of uranium on phytate hydrolysis by *Variovorax* species.

To determine the viability of U(VI)-phosphate biomineralization promoted by microbially-mediated phytate hydrolysis as a remediation strategy, Chapter VII of this dissertation investigates the stability of the resulting uranium precipitates and the bioavailability of the phytate substrate. The objectives of this work were (1) to demonstrate the stability of U(VI)-phosphate minerals in a wide range of geochemical

conditions, (2) to validate a sequential extraction technique for differentiating between U(VI)-phosphate and U(VI)-phytate precipitates, (3) to characterize phytate sorption to ORFRC soils, and (4) to investigate the potential of utilizing an inexpensive phytate source in U(VI)-phosphate biomineralization strategie.

Finally, Chapter VIII synthesizes the results of this dissertation, discusses the efficacy of utilizing phytate as an organophosphate to promote U(VI)-phosphate biomineralization, identifies new questions posed by the results of this research, and presents recommendations for future investigations.

Appendices are found at the end of this dissertation. Appendix A contains supporting information for Chapter III of this dissertation. Appendix B contains supporting information for Chapter IV of this dissertation. Appendix C contains supporting information for Chapter V of this dissertation. Appendix D contains supporting information for Chapter VI of this dissertation.

CHAPTER 2

ANALYTICAL TECHNIQUES

2.1 Inductively-Coupled Plasma Mass Spectrometry

Total dissolved uranium concentrations were measured using an Agilent 7500a Series system inductively-coupled plasma mass spectrometer (ICP-MS). Samples were filtered through a 0.2 µm polyethersulfane membrane filter (PES, Millipore) and diluted in 2% trace metal grade nitric acid (Fisher) prepared with Nanopure water (Barnstead). Standards ranging from 0 to 10 nM were prepared using uranyl acetate (Spectrum) acidified in 2% trace metal grade nitric acid. Standard curves were measured every 20 samples and at the beginning and end of each run, and holmium and bismuth (500 ng/L) were used as internal standards (SPEX certiPrep) in both standards and samples to correct for instrument drift (Figure 2.1). River Water Certified Reference Material for Trace Metals (SLRS-5, 100 ng/L U, National Research Council Canada, Ottowa, Canada), 2% trace metal grade nitric acid blanks, and calibration check standards (500 ng/L) were measured every 10 samples as quality controls (Figure 2.1). Using this procedure, the U detection limit was 0.03 nM and quality control samples were typically within 10% of their reported values. The analytical error on duplicate samples was usually less than 3% relative standard deviation (RSD).

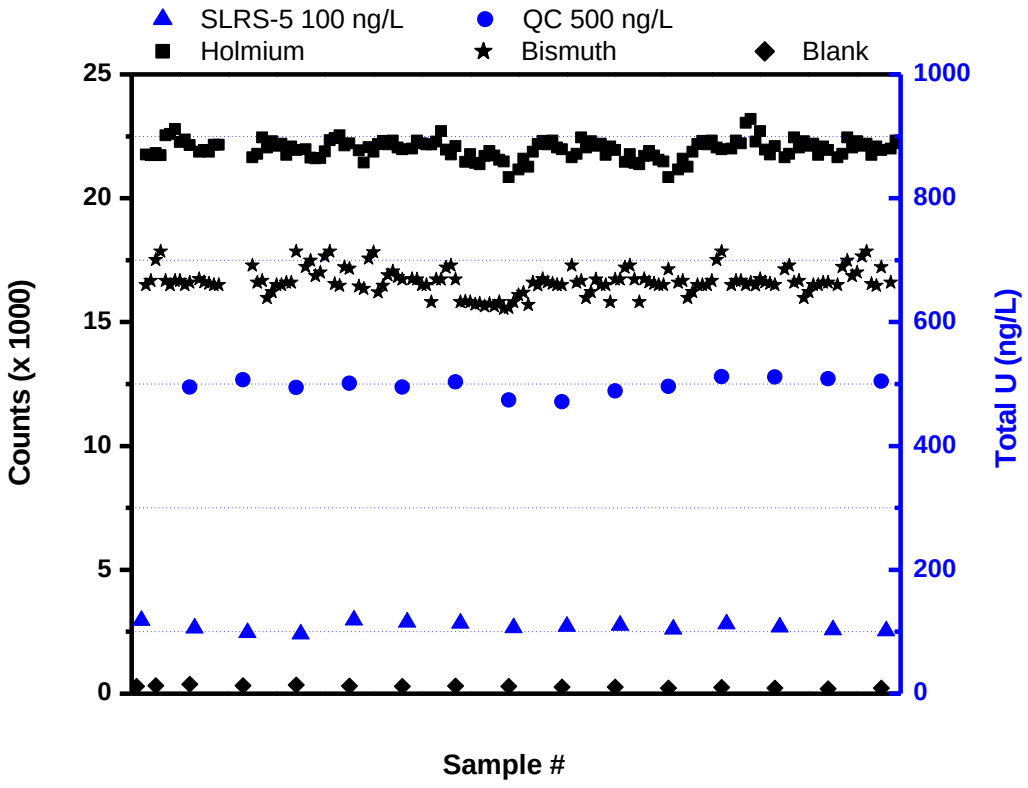

Figure 2.1 Inductively-coupled plasma mass spectrometry (ICP-MS) detector counts for internal standards and quality control samples. Internal standards (holmium and bismuth and calibration blanks are shown on the left axis (black symbols) and quality control samples SLRS-5 and 500 ng/L U check standard are shown on the right axis (blue symbols).

2.2 Colorimetry

2.2.1 Inorganic Phosphate

Inorganic phosphate was quantified using the colorimetric method of Murphy and Riley (1962) for the portion of this dissertation presented in Chapter 3. All samples reserved for phosphate determination were filtered through a 0.2 µm PES membrane filter (Millipore) and frozen until analysis, and all chemicals used for standard and reagent preparation were reagent grade (Fisher). Standards ranging from 0 to 25 µM were prepared using NaH_2PO_4 dissolved in Nanopure water (Barnstead). A 50 µL aliquot

of a freshly made molybdate reagent containing 1.6 mL Ascorbic Acid (0.31 M), 0.8 mL potassium antimonyl tartrate (4.2 mM), 4 mL sulfuric acid (2.8 M), and 1.6 mL ammonium molybdate (0.023 M) was added to 0.5 mL of filtered samples and standards. Blue color was allowed to develop for 20 minutes and absorbance at 885 nm was measured using a Milton Roy Spectronic 501 spectrophotometer with a detection limit of 2.5 µM. Analytical error on duplicate samples was less than 5% RSD.

As phytate interferes with the original spectrophotometric method for orthophosphate detection described above, inorganic phosphate in the presence of phytate was quantified using a modified spectrophotometric technique developed by Heinonen and Lahti (1981) for the portion of this dissertation presented in Chapter 5. Standards ranging from 0 to 1 mM were prepared using NaH_2PO_4 dissolved in Nanopure water (Barnstead). First, a 0.4 mL aliquot of freshly made molybdate reagent containing 2.5 mL ammonium molybdate (10 mM), 2.5 mL sulfuric acid (2.5 M), and 5.0 mL acetone was combined with 0.2 mL of filtered sample/standard and mixed thoroughly. Then, a 20 µL aliquot of 1.0 M citric acid was added to each sample/standard, and the yellow color was allowed to develop for 10 minutes prior to spectrophotometric detection at 410 nm using a Milton Roy Spectronic 501 spectrophotometer. The detection limit for phosphate detection with this method was 100 µM and the analytical error on duplicate samples was less than 5% RSD.

2.2.2 Nitrite

Nitrite was immediately analyzed using the colorimetric method of Grasshoff (1983). Standards ranging from 0 to 20 µM were prepared using dried $NaNO_2$ dissolved in Nanopure water (Barnstead). Reagents and standards were prepared using reagent

grade chemicals (Fisher) and stored in the dark at 4°C until use. A 20 µL aliquot of sulphanilamide reagent (5.8 mM sulphanilamide, 1.21 M HCl) was added to 1 mL of sample and allowed to react for one minute. Then, a 20 µL aliquot of N-1-napthylethylenediamine dihydrochloride (0.97 mM, NED) was added to each sample, and the pink color was allowed to develop for 15 minutes prior to spectrophotometric detection at 530 nm using a Milton Roy Spectronic 501 spectrophotometer. The detection limit for nitrite detection was 1.0 µM and the analytical error on duplicate samples was less than 4% RSD.

2.2.3 Iron

Fe(II) was quantified using the ferrozine method developed by Stookey (1970). Adsorbed Fe(II) was quantified by difference of total Fe(II), measured in unfiltered acidified samples, and dissolved Fe(II) determined in filtered samples. Acidified standards ranging from 0 to 15 uM were prepared using ferrous ammonium sulfate. Reagents and standards were prepared using reagent grade chemicals (Fisher) and stored in the dark at 4°C until use. A 1 mL aliquot of ferrozine reagent (5 mM ferrozine salt, 0.5 M ammonium acetate, 0.05 M HCl) was combined with 100 µL sample and 900 µL Nanopure water (Barnstead), and purple color was allowed to develop for 10 minutes prior to spectrophotometric detection at 562 nm using a Milton Roy Spectronic 501 spectrophotometer. The detection limit for Fe(II) detection was 2 µM and the analytical error on duplicate samples was less than 3% RSD.

2.3 Ion Chromatography

2.3.1 Inorganic Anions

Concentrations of NO_3^-, G2P (Chapter 3 of this dissertation), ΣPO_4^{3-} (Chapter 4 and Chapter 6 of this dissertation), and SO_4^{2-} were quantified by ion chromatography (IC) using a Dionex GP-50 high-performance liquid chromatography (HPLC) pump and conductivity detector (Dionex, CD-20) coupled to an Analytical Instrument Systems, Inc. integrator (LCC 100). An anion exchange analytical column (Dionex AS14, 4 x 250mm) and guard column (Dionex AG14, 4 x 50mm) were used in line with an AMMS-300 (4-mm, Dionex) suppressor. Operating conditions included a carbonate buffer eluent (1 mM $NaHCO_3$/ 3 mM Na_2CO_3) containing 10% acetonitrile to facilitate G2P elution with a 1 mL min^{-1} flow rate and a 25 mN H_2SO_4 regenerant. All reagents and standards were prepared using reagent grade chemicals (Fisher) unless otherwise specified. Mixed standards ranging from 0 to 300 µM were prepared using $NaNO_3$, G2P (Sigma Aldrich), NaH_2PO_4, and Na_2SO_4 dissolved in Nanopure water (Barnstead). Typical elution times ranged between 5 and 10 minutes (Figure 2.2a) and calibration curves (Figure 2.2b) were analyzed at the beginning and end of each run to account for instrument drift.

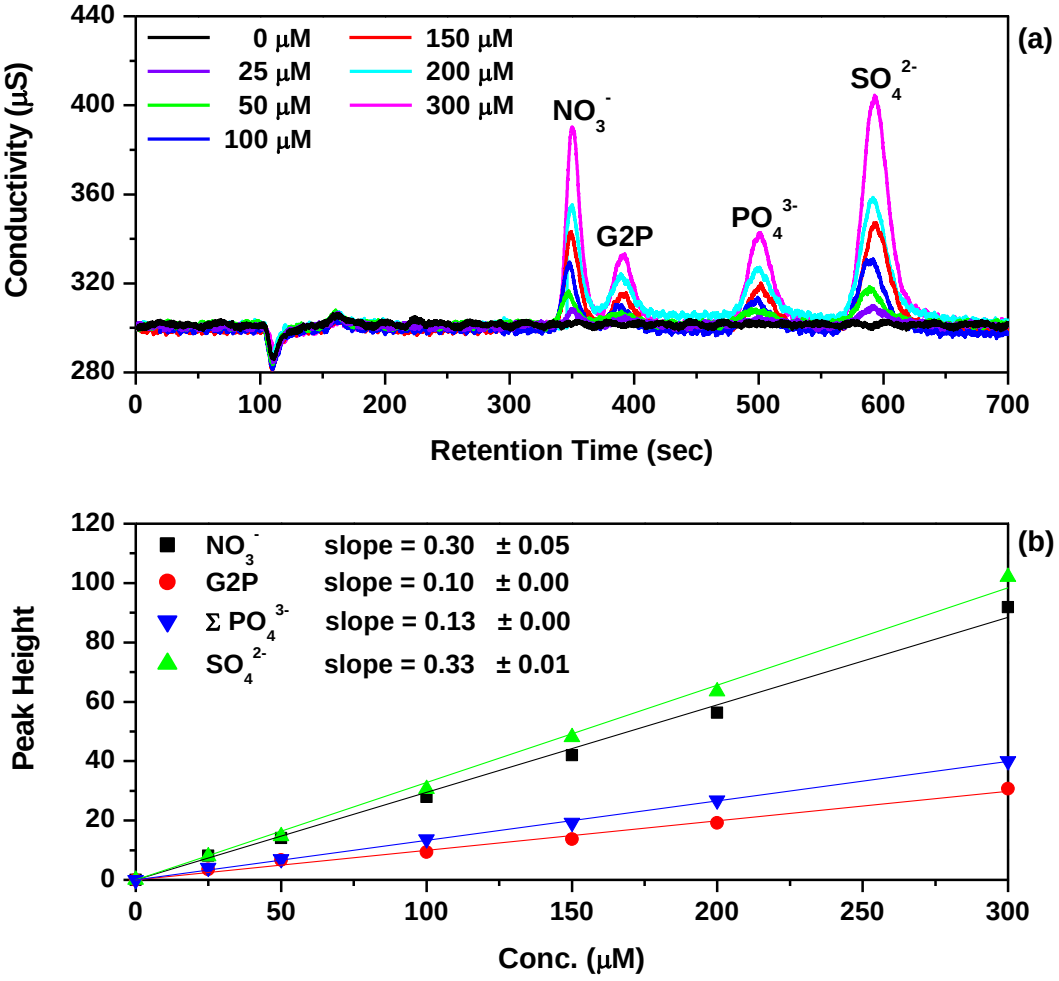

Figure 2.2 Typical (a) Chromatograms and (b) calibration curves for NO_3^-, G2P, ΣPO_4^{3-}, and SO_4^{2-} as determined by ion chromatography with conductivity detection.

2.3.2 Low Molecular Weight Organic Acids

For Chapter 5 of this dissertation, the consumption of lactate and possible production of other low molecular weight organic acids during respiration by *Variovorax paradoxus* sp. was quantified by IC using a Dionex GP-50 HPLC pump and conductivity detector (Dionex, CD-20) coupled to an Analytical Instrument Systems, Inc. integrator (LCC 100). An ion-exclusion column (Dionex IonPac ICE-AS6) was used in line with an AMMS-300 (4-mm, Dionex) suppressor. Operating conditions included a 0.4 mM heptafluorobutyric acid (HFBA) eluent with a 1 mL min-1 flow rate and a 5 mN Tetrabutylammonium hydroxide (TBA-OH) regenerant. All reagents and standards were prepared using reagent grade chemicals (Acros) unless otherwise specified. Mixed standards ranging from 0 to 3 mM were prepared using sodium lactate (Fisher) and sodium acetate (Fisher) dissolved in Nanopure water (Barnstead). Typical elution times ranged between 10 and 15 minutes and calibration curves were analyzed at the beginning and end of each run to account for instrument drift.

2.3.3 Inositol Phosphates

Inositol phosphates (IP_2 – IP_6) were quantified using a modified chromatographic separation coupled to spectrophotometric detection (Rounds and Nielsen, 1993) with a Dionex ICS-3000 dual pump chromatography system. IP_x (x = 2:6) standards ranging from 0 to 125 µM were prepared using inositol hexaphosphate, inositol pentaphosphate, inositol tetraphosphate, inositol triphosphate, and inositol bisphosphate purchased from Sigma Aldrich and diluted in Nanopure water (Barnstead). Separation was achieved with an OmniPac PAX-100 guard column (4 x 40 mm), and eluent flow conditions included a 23 minute linear gradient (0.5 mL/min) from 0.01 M 1-methylpiperazine (pH 4.0) to

0.375 M $NaNO_3$ in 0.01 M 1-methylpiperazine (pH 4.0). Following separation, 0.015% (w/v) $FeCl_3 \cdot 6H_2O$ in 0.15% (w/v) sulfosalicylic acid (pH 1.8) was introduced (0.5 mL/min) as a post-column reagent. Absorbance at 500 nm was monitored after thorough mixing, and IP_X species were recorded as negative absorbance peaks in suppression mode (Figure 2.3a). Due to the doublet peak observed for IP_2 (Figure 2.3a) possibly caused by partial separation of different IP_2 isomers, calibration curves were determined using peak area rather than peak height (Figure 2.3b). As IP_2, IP_3, IP_4, and IP_5 salts are prohibitively expensive, the pilot ion method was used to quantify each species. One set of standards was prepared and analyzed (5 replicates) to establish an accurate ratio of the calibration slope of IP_6 to the calibration slopes of IP_2, IP_3, IP_4, and IP_5, respectively. In all subsequent measurements, IP6 calibration curves were used with these ratios to determine the sensitivity with respect to each intermediate species (IP_2, IP_3, IP_4, IP_5). Those ratios and their associated errors are as follows: IP_6/IP_5 1.56 ± 0.06, IP_6/IP_4 3.26 ± 0.04, IP_6/IP_3 4.76 ± 0.16, and IP_6/IP_2 1.60 ± 0.02.

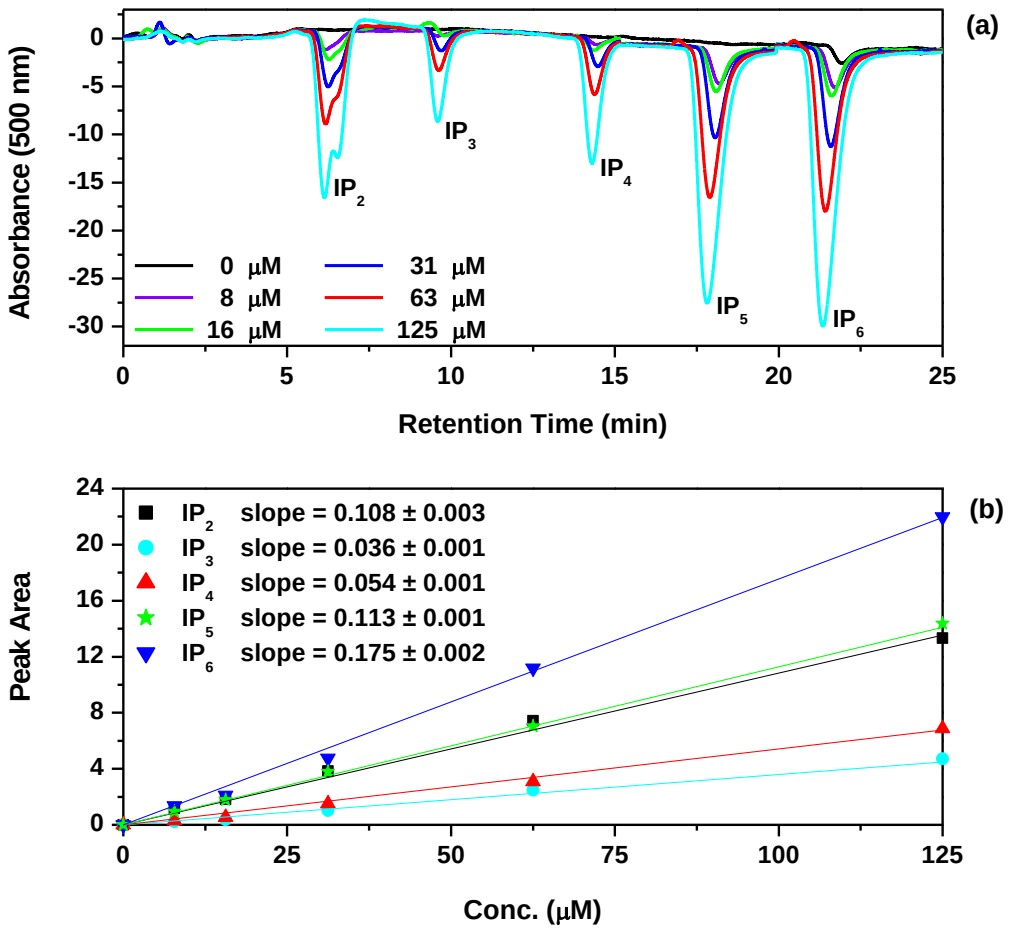

Figure 2.3 (a) Chromatogram and (b) calibration curves for IP_2, IP_3, IP_4, IP_5, and IP_6 as determined by chromatographic separation with gradient elution coupled to spectrophotometric detection. Peaks are recorded as a decrease in absorbance at 500 nm.

2.4 Synchrotron X-ray Absorption Spectroscopy

X-ray absorption spectroscopy (XAS) was performed at the Stanford Synchrotron Radiation Lightsource (SSRL) on beam lines 10-2 (winter 2009) and 4-1 (Summer 2012) with spot sizes of 0.2 x 0.43 mm and 4 x 18 mm, respectively. For the XAS analysis discussed in Chapter 3 of this dissertation, soil samples were loaded into windowed Lexan sample holders sealed with Kapton tape in an anaerobic chamber (Coy Laboratory

Instruments, Inc.), and maintained anoxic in a sealed jar for transport to SSRL and under N_2 atmosphere during analysis at beam line 10-2. For the XAS analysis discussed in Chapter 4 of this dissertation, soil samples were loaded into windowed Lexan sample holders sealed with Kapton tape for analysis at beam line 4-1. All uranium L_{III}-edge XAS spectra were collected using a focused X-ray beam with a 23 keV harmonic rejection cutoff and a 13 element Ge detector. The incident energy was selected with a Si(220) monochromator crystal, and the energy for each beam line was calibrated to the yttrium K-edge (17038 eV). Transmission and fluorescence data were collected simultaneously between 16142 and 18014 eV. Energy resolution in the pre-edge, edge, and post-edge regions were 10 eV, 0.3 eV, and 1 eV, respectively. All EXAFS data were reduced using SIXPACK (Webb, 2005). Phase and amplitude files for EXAFS fittings were created with FEFF7 (Ankudinov et al., 1998; Zabinsky et al., 1995). Theoretical models were based on scattering paths expected for autunite-type group minerals (Catalano and Brown, 2004) and U(VI) adsorbed to iron oxihydroxides (Waite et al., 1994). The models were first tested on known chernikovite and U-$Fe_{(ads)}$ samples to ensure good agreement with previous fittings (Beazley et al., 2009, 2011). The U═Oax═U═Oax transoxido multiple scattering path (Allen et al., 1996; Bargar et al., 2000; Hudson et al., 1996) was included in all fits. The axial oxygen coordination number (N) for all reactors was set at two (Beazley et al., 2007, 2009; Beazley et al., 2011; Webb et al., 2006). To aid comparison between samples, the Debye-Waller factors (σ) were fixed for shells other than axial oxygen, a common practice for uranium EXAFS (Bargar et al., 2000; Beazley et al., 2009; Beazley et al., 2011; Webb et al., 2006). As Mn and Fe display similar backscattering intensities and phases in EXAFS, it is unlikely

to distinguish between them. Thus, a "sum" of Fe/Mn like neighbors were reported rather than distinct Fe and Mn shells. The addition of shells was considered to improve the quality of the EXAFS fit if a reduction in the reduced chi-square was observed (Webb et al., 2006; Webb et al., 2005).

2.4.1 Fitting EXAFS Spectra with SIXPACK

To model EXAFS spectra with SIXPACK (Webb, 2005), individual data spectra were loaded into the SAMVIEW module of SIXPACK to check for quality of data and to average multiple scans for a given sample. Once loaded into SAMVIEW, muF plots for each scan were checked for abnormalities. Then, individual fluorescence channels for each scan were observed using a column plot (ICRind), and channels with abnormal data were zeroed out. After all scans were quality corrected, the muF of all scans for an individual sample were averaged. This procedure was repeated for all samples, resulting in one average (.avg) file for each sample from a given set of experiments. Next, average files were background corrected using the background subtraction module of SIXPACK. Average files for all samples to be compared from a given set of experiments were loaded into the background subtraction module. The parameters Rbkg and dk were set to 1. Each average file was selected by double clicking (denoted by x next to file name). With one sample highlighted, E0 was set to 17170, k_{max} under plot options was changed to 12, and the k range for the spline region was set at 1 to 12. Parameters for other average files were duplicated accordingly (parameters→set all to current), and the mu and chi files for each sample average were saved. The resulting chi files were fit individually using the FEFF EXAFS fitting module of SIXPACK. The parameter dk was set to 3, and the option to plot the model fit along with the actual data was chosen for k and R (Plot

options). FEFF files were generated using FEFF7 (Ankudinov et al., 1998; Zabinsky et al., 1995), and paths were fit in order of increasing distance from uranium. Except for the axial oxygen coordination number which was set at two, coordination number, radial distance, and sigma were allowed to float for each path added. Sigma affects the broadness of the guassian curve for a given scattering path, and the range of acceptable values is 0.002 (peak is tall and thin) to 0.01 (peak is broad and short). After an acceptable fit was achieved, k and r were saved and the statistics chi squared, reduced chi squared, and Rfactor were recorded.

In heterogeneous systems where more than one mineral phase is expected, linear combination fitting using EXAFS spectra of defined end members may also be also useful. Linear combination fittings of EXAFS spectra can be performed in SIXPACK (Webb, 2005) using the linear least-squares fitting module. This module allows the user to load reference spectra as components along with the averaged mu file for a given sample. Constraints on the model fit are defined in the fit parameters toolbox. Before loading reference and data spectra, the energy boundaries (i.e. x-min, x-max) and x-weight of the fit must be specified. In addition, the user has the option of limiting component weights to non-negative values and requiring that the component weights sum to one. If energy calibrations are poor, energy scales of the reference and data spectra may be allowed (E) to float.

CHAPTER 3

THE ROLE OF ANAEROBIC RESPIRATION IN THE IMMOBILIZATION OF URANIUM THROUGH BIOMINERALIZATION OF PHOSPHATE MINERALS

Reproduced with permission from Salome, K. R.; Green, S. J.; Beazley, M. J.; Webb, S. M.; Kostka, J. E.; Taillefert, M. The role of anaerobic respiration in the immobilization of uranium through biomineralization of phosphate minerals.

Geochimica et cosmochimica acta. **106**, 344-363. Copyright 2012, Elsevier Ltd.

3.1 Abstract

Although bioreduction of uranyl ions (U(VI)) and biomineralization of U(VI)-phosphate minerals are both able to immobilize uranium in contaminated sediments, the competition between these processes and the role of anaerobic respiration in the biomineralization of U(VI)-phosphate minerals has yet to be investigated. In this study, contaminated sediments incubated anaerobically in static microcosms at pH 5.5 and 7.0 were amended with the organophosphate glycerol-2-phosphate (G2P) as sole phosphorus and external carbon source and iron oxides, sulfate, or nitrate as terminal electron acceptors to determine the most favorable geochemical conditions to these two processes. While sulfate reduction was not observed even in the presence of G2P at both pHs, iron reduction was more significant at circumneutral pH irrespective of the addition of G2P. In turn, nitrate reduction was stimulated by G2P at both pH 5.5 and 7.0, suggesting nitrate-reducing bacteria provided the main source of inorganic phosphate in these sediments. U(VI) was rapidly removed from solution in all treatments but was not

reduced as determined by X-ray absorption near edge structure (XANES) spectroscopy. Simultaneously, wet chemical extractions and extended X-ray absorption fine structure (EXAFS) spectroscopy of these sediments indicated the presence of U-P species in reactors amended with G2P at both pHs. The rapid removal of dissolved U(VI), the simultaneous production of inorganic phosphate, and the existence of U-P species in the solid phase indicate that uranium was precipitated as U(VI)-phosphate minerals in sediments amended with G2P. Thus, under reducing conditions and in the presence of G2P, bioreduction of U(VI) was outcompeted by the biomineralization of U(VI)-phosphate minerals and U(VI) sorption at both pHs.

3.2 Introduction

The United States Department of Energy (DOE) currently manages 120 nuclear legacy waste sites spread over 36 states contaminated with heavy metals and radionuclides, such as uranium (U) (DOE, 1997; NABIR, 2003). As the sheer volume of contaminated geomedia at these sites makes traditional remediation techniques (i.e. pump-and-treat, excavation) cost-prohibitive (Dawson and Gilman, 2001; Jardine, 2006; Mackay and Cherry, 1989), remedial efforts have focused on the development of alternative *in situ* technologies designed to immobilize contaminants in the subsurface.

As with other contaminants, the design of uranium *in situ* remediation techniques aims to capitalize on the geochemical properties of uranium in natural waters to immobilize it in the subsurface. Uranium mobility in groundwater is largely driven by ligand complexation (i.e. carbonate), adsorption to metal oxides, and precipitation reactions (i.e. formation of phosphate minerals, reduced metal oxides). In oxic

groundwater where U(VI) is the dominant oxidation state, uranium usually occurs as the highly mobile uranyl ion UO_2^{2+} (Langmuir, 1997). The dominant aqueous forms of uranyl in the environment include the free uranyl ion at low pH and positively charged hydroxyl complexes at circumneutral pH ($5 \leq pH \leq 6.5$) (Langmuir, 1997). At pH 5.0, aqueous U(VI) adsorbs strongly to manganese oxides given their low pH_{zpc} (Han et al., 2007) and even to ferric oxides despite the net positive charge of both uranyl hydroxide complexes and metal oxides (Han et al., 2007; Hsi and Langmuir, 1985; Waite et al., 1994). Ferric oxides represent one of the most important U(VI) sorbents in soils of the Oak Ridge Field Research Center (ORFRC), a well-studied nuclear legacy waste site in Oak Ridge, TN, and at pH 5.5 and 7.0 approximately 80% and 98% of U(VI) adsorbs to these soils (Barnett et al., 2002). In addition, the presence of inorganic phosphate may enhance U(VI) sorption to ferric oxides at low pH through the formation of ternary surface complexes (Cheng et al., 2004; Payne et al., 1996). In higher pH environments ($pH \geq 7.0$) and in the presence of elevated concentrations of carbonates, uranyl carbonate complexes represent the dominant form of U(VI) in solution (Langmuir, 1997). These complexes only minimally adsorb to iron oxides (Katsoyiannis, 2007), and the presence of elevated carbonate promotes both U(IV) and U(VI) mineral dissolution (De Pablo et al., 1999; Liu et al., 2004; Sowder et al., 2001; Ulrich et al., 2009). In addition, elevated calcium concentrations present in high pH environments may promote the formation of ternary calcium-uranyl-carbonate complexes, which further inhibit U(VI) sorption (Fox et al., 2006; Meleshyn et al., 2009; Stewart et al., 2010) and U(VI) reduction by lowering the reduction potential of uranium to less energetically favorable values (Brooks et al., 2003; Luo et al., 2007a). Therefore, uranium mobility in circumneutral pH environments

may be largely driven by carbonate dissolution and complexation reactions.

In reducing environments, uranium is either chemically or biologically reduced to insoluble U(IV) minerals, including uraninite (Finch and Murakami, 1999b; Langmuir, 1997) or non-uraninite minerals (Bernier-Latmani et al., 2010; Fletcher et al., 2010; Sharp et al., 2011). At pH > 6, the surface-catalyzed chemical U(VI) reduction by Fe(II) adsorbed onto crystalline iron oxides (Behrends and Van Cappellen, 2005; Jeon et al., 2005; Liger et al., 1999; Regenspurg et al., 2009) and other minerals (Chakraborty et al., 2010; Regenspurg et al., 2009) may also occur. Dissolved sulfide (Ho and Miller, 1986; Kosztolanyi et al., 1996; Mohagheghi et al., 1985) and sulfide minerals (Beyenal et al., 2004; Marsili et al., 2007; Wersin et al., 1994) have also been shown to reduce U(VI) chemically. In addition, several strains of metal-reducing and sulfate-reducing bacteria are capable of reducing U(VI) (reviewed in(Kostka and Green, 2011)), including members of the genus *Shewanella* (Blakeney et al., 2000; Lovley et al., 1991), *Desulfovibrio* sp. (Lovley, 1993; Lovley and Phillips, 1992b), *Geobacter* sp. (Jeon et al., 2004; Lovley et al., 1991), and *Anaeromyxobacter dehalogens* (Sanford et al., 2007). Biologically-mediated reduction of U(VI), or bioreduction, is currently the primary *in situ* remediation technique studied for the immobilization of uranium in subsurface environments (Fredrickson et al., 2000; Ganesh et al., 1999; Lovley and Phillips, 1992b; Lovley et al., 1991; North et al., 2004; Sanford et al., 2007; Wade and DiChristina, 2000), and *in situ* bioreduction of U(VI) has been demonstrated at the ORFRC (Wu et al., 2006b) and other contaminated sites (Senko et al., 2002). Unfortunately, bioreduction is inhibited at pH < 7 and in elevated nitrate concentrations (Finneran et al., 2002b; Wu et al., 2006a; Wu et al., 2006b). In addition, the uraninite mineral product may not remain

stable in fluctuating chemical conditions as uraninite is readily oxidized to the mobile U(VI) upon reintroduction of oxygen in groundwater recharge areas (Langmuir, 1997; Murphy and Shock, 1999) and by NO_2^- (Beller, 2005; Moon et al., 2007; Wu et al., 2010), $Fe(OH)_3$ (Senko et al., 2002; Senko et al., 2005b; Wan et al., 2005), and MnO_2 (Fredrickson et al., 2002) under reducing conditions. Thus, the long term instability of uraninite coupled with the inhibitory effects of co-contaminants on U(VI) reduction favors investigation of alternative remediation techniques applicable in both reducing and oxidizing conditions.

Biomineralization of insoluble U(VI)-phosphate minerals through the activities of microbial phosphatases represents a possible complementary bioremediation technique to bioreduction. U(VI) forms sparingly soluble and stable (Jerden and Sinha, 2003) phosphate minerals over a broad range of environmental conditions (pH 4 - 8) (Ohnuki et al., 2004; Wellman et al., 2007; Zheng et al., 2006), and uranium phosphate minerals have been identified in sediments from the ORFRC (Kelly et al., 2005; Roh et al., 2000; Stubbs et al., 2006) and the Hanford 300 Area facility, WA (Arai et al., 2007; Catalano et al., 2006), among others. As inorganic phosphate readily adsorbs to soils (pH $\leq$ ~7.0) or precipitates as minerals (pH $\geq$ ~ 4.0) ultimately decreasing the hydraulic conductivity of soils (Wellman et al., 2006), direct addition of inorganic phosphate to subsurface environments is not a viable field-scale remediation strategy. Thus, research has focused primarily on stimulating microbially-mediated phosphate production coupled to a chemical precipitation of sparingly soluble U(VI)-phosphate minerals (Beazley et al., 2007, 2009; Macaskie et al., 1995; Martinez et al., 2007; Montgomery et al., 1995; Shelobolina et al., 2009). To fulfill their phosphate requirements, most microorganisms

produce phosphatase enzymes, a class of non-specific enzymes that catalyze the hydrolysis of organic phosphoester bonds in a broad range of chemical conditions (Rossolini et al., 1998). Uranium removal coupled to phosphatase activity has been demonstrated in both aerobic and anaerobic conditions and at both acidic and circumneutral pH by the facultative anaerobe *Rahnella* sp. Y9602 (Beazley et al., 2007, 2009; Martinez et al., 2007) and in low-pH aerobic conditions by *Citrobacter* sp. (Macaskie et al., 1995; Montgomery et al., 1995). In addition, uranium removal in aerobically-maintained contaminated sediments has been achieved through stimulation of the phosphatase activities of indigenous bacteria (Beazley et al., 2011; Shelobolina et al., 2009). As phosphatases may also be activated in anaerobic conditions (Rossolini et al., 1998), U(VI)-phosphate biomineralization may compete with bioreduction in the presence of G2P. Interestingly, the competitive interaction between these two processes has yet to be investigated.

In this study, a combination of X-ray absorption spectroscopy, solid-phase extractions, and bulk chemical analyses was used to determine whether nitrate-, iron-, or sulfate-reducing conditions are most conducive to uranium removal through the activity of endogenous microbial phosphatases in contaminated sediments from the ORFRC. In addition, the competition between uranium reduction and the biomineralization of U(VI)-phosphate minerals under varying electron accepting conditions in both low and circumneutral pH environments was examined.

3.3 Experimental

3.3.1 Materials and Site Description

Contaminated sediments were collected during installation of a monitoring well in Area 3 of the ORFRC (well number: FWB120-08-40, core depth: 21-23'; courtesy of D. Watson, ORNL). Soil mineralogy of neighboring wells indicates a bulk soil particle size distribution (~1.5 m depth) as 31% sand, 50% silt, and 19% clay (Barnett et al., 2000). In addition, bulk soil Mn and Fe content in Oak Ridge have been quantified as 0.36 g/kg and 25.8 g/kg, respectively (Barnett et al., 2000), and uranium-bearing Fe and Mn minerals in Area 3 Oak ridge soils have been identified as polycrystalline ferrihydrite and goethite and poorly crystalline mixed Mn-Fe oxides (Stubbs et al., 2006). As Area 3 sediments are located closest to the former waste disposal ponds, they are generally characterized by low pH and high nitrate levels (Brooks, 2001). Chemical information for well FWB120 remains unavailable; however, the nearest neighboring well (~1 m) displays an average pH of 3.4, nitrate concentration of 30.4 mM, and sulfate concentration of 19.7 mM. Sediment cores were stored in the dark at 4°C and remained sealed until incubation.

3.3.2 Experimental Design

To simulate a variety of environmental conditions, static microcosms containing 125 g of contaminated ORFRC sediments homogenized under controlled atmosphere (1% H_2, 5% CO_2, 94% N_2) were incubated in duplicate in 1-L borosilicate glass reactors containing sterile artificial groundwater for a period of 70 days. In each treatment, 500 mL of artificial groundwater containing 17.1 mM NaCl, 2.0 mM $MgCl_2 \cdot 6H_2O$, 680 µM $CaCl_2 \cdot 2H_2O$, and 6.7 mM KCl was first degassed using UHP N_2, sealed, and autoclaved.

After cooling, filter-sterilized aliquots of selenite-tungstate solution (0.1%), trace elements solution (0.1%, Table A.1, Appendix A, (Bak, 1992)), $NaHCO_3$ (5 mM), and either 2-(N-Morpholino)ethanesulfonic acid (MES, 50 mM, pH 5.5) or 4-(2-hydroxyethyl)-1-piperazineethanesulfonic acid (HEPES, 50 mM, pH 7.0) were added to autoclaved groundwater in the presence or absence of filter-sterilized solutions of glycerol-2-phosphate (G2P) (Sigma Aldrich) and uranyl acetate (Spectrum) (Table 3.1). Reactors were buffered at pH 5.5 or 7.0 to establish conditions favorable to both U(VI)-phosphate biomineralization (pH 5.5) and bioreduction (pH 7.0). Excluding G2P, no external electron donor was added to the system. Reactors were sealed from the controlled atmosphere within an hour after addition of the reactants, such that the incubations were not significantly affected by H_2 and CO_2 gases. Sealed duplicate reactors were homogenized to ensure uniform groundwater composition prior to static incubation at room temperature in the dark.

At each time point, the following sampling protocol was followed to ensure that all samples were maintained anaerobic at all times. Microcosm sediment and groundwater were homogenized, and a subsample of the microcosm mixture was extracted under anaerobic atmosphere (1% H_2, 5% CO_2, and 94% N_2) through a septum using a polypropylene syringe with Teflon plunger (HSW) and a 18 gauge stainless steel needle (B & H). An aliquot of the homogenized mixture was added to a 0.5 M HCl solution to extract total Fe(II). The remaining mixture was centrifuged at 3300 rpm for 5 minutes. The supernatant was filtered through a 0.2 µm pore size polyethersulfane membrane filter (Puradisc, Whatman) and reserved for pH measurement (data not shown) and analysis of phosphate and nitrite. Other filtered aliquots were diluted in 2% trace

metal grade nitric acid for uranium analysis or preserved in 0.1 M HCl and stored at 4°C until dissolved Fe(II) quantification. The remaining filtered supernatant was frozen until analysis of sulfate, nitrate, and G2P. Finally, following completion of the incubations, sediments were collected for solid-phase chemical extraction, X-ray absorption near-edge spectroscopy (XANES), and extended X-ray absorption fine structure (EXAFS) analysis. Sediments were preserved at -80°C and under UHP N_2 atmosphere in Mason jars until analysis.

Table 3.1 pH, U(VI), G2P, and external terminal electron acceptor (TEA) conditions in each incubation conducted in duplicate in artificial groundwater.

Treatment	*pH*	*[U(VI)]*	*[G2P]*	*[TEA]*
U - amended control	5.5/7.0	300 µM	0 mM	0 mM
G2P - amended reactor	5.5/7.0	300 µM	5.0 mM	0 mM
NO_3^- - amended reactor	5.5	300 µM	5.0 mM	7.0 mM NO_3^-
NO_3^- - amended reactor	7.0	300 µM	0 mM	7.0 mM NO_3^-
SO_4^{2-} - amended reactor	5.5/7.0	300 µM	5.0 mM	9.4 mM SO_4^{2-}

3.3.3 Analytical Methods

3.3.3.1 Aqueous Phase Speciation

Dissolved uranium was measured in duplicate using an Agilent 7500a Series inductively coupled plasma mass spectrometer (ICP-MS). Standards were prepared using uranyl acetate (Spectrum) acidified in 2% trace metal grade nitric acid (Fisher). Holmium and bismuth were used as internal references in both standards and samples (SPEX certiPrep), and 2% trace metal grade nitric acid blanks and calibration check standards were used as quality controls. Phosphate, nitrite, and total/dissolved Fe(II) were quantified colorimetrically with a Milton Roy Spectronic 501 spectrophotometer. Phosphate was measured using the molybdenum blue method (Murphy and Riley, 1962),

nitrite was measured using a sulphanilamide/NED reagent mixture immediately after sampling (Grasshoff, 1983), and Fe(II) was measured using the ferrozine method (Stookey, 1970). Adsorbed Fe(II) was quantified by difference of total Fe(II), measured in unfiltered acidified samples, and dissolved Fe(II) determined in filtered samples. Sulfate, nitrate, and G2P were measured by ion chromatography using a Dionex GP-50 HPLC pump and conductivity detector (Dionex, CD-20) coupled to an Analytical Instrument Systems, Inc. integrator (LCC 100). An anion exchange analytical column (Dionex AS14, 4 x 250mm) and guard column (Dionex AG14, 4 x 50mm) were used in line with an AMMS-300 (4-mm, Dionex) suppressor. Operating conditions included a 10% acetonitrile, 1 mM $NaHCO_3$, and 3 mM Na_2CO_3 buffer eluent with a 1 mL min^{-1} flow rate and a 25 mN H_2SO_4 regenerant. All standard deviations reported for dissolved species represent the range of average concentrations found in duplicate reactors.

3.3.3.2 Rate Constant Calculations and Thermodynamic Modeling

Rate constants, k_{obs}, for NO_3^- consumption, G2P consumption, and U removal were calculated assuming pseudo-first-order reactions using the linear regression of the natural log of concentrations as a function of time (see details in supplementary information). The error reported for rate constants was propagated to include variations between duplicate incubations and standard error of the unweighted slope of linear regressions. Due to the apparent two-phased uranium removal, two separate uranium rate constants were calculated for pH 5.5 reactors; U_0 represents the rate constant calculated for days 0 – 4 and U_7 represents the rate constant calculated for days 7 – 31. Thermodynamic equilibrium calculations were performed in MINEQL+ (Schecher and McAvoy, 2001) for each reactor treatment. The theoretical composition of artificial

groundwater, modified to reflect the different treatments (Table 3.1), was included as the background solution in the thermodynamic calculations. For these calculations, total ΣPO_4^{3-} concentrations in all G2P-containing reactors were estimated assuming complete hydrolysis of the organophosphate compound, and total Fe(II) detected at 7 days was used to estimate the maximum Fe(II) production. Adsorption onto amorphous iron oxides was included using a double-layer sorption model with both low affinity and strong affinity sites and solid concentrations that reflected the composition of ORFRC soils (Barnett et al., 2002). Ionic strength was calculated, and the system was assumed to be closed to the atmosphere with a pH of 5.5 or 7.0 and total dissolved inorganic carbon concentrations fixed at 5 mM.

3.3.3.3 Solid phase uranium characterization

Solid phase uranium and phosphate eventually associated with the solid phase were quantified in duplicates in sediments collected following 70 days of incubation using a modified sequential extraction technique of Tessier et al. (1979). The following procedure was performed sequentially: (1) 4 mL of 1.0 M $MgCl_2$ (pH 7.0) was added to ~ 0.5 g sediment and agitated at 20°C for 1 hour to extract loosely adsorbed uranium; (2) 4 mL of 1.0 M sodium acetate (adjusted to pH 5.0 with 1.0 M HCl) was added and agitated at 20°C for 5 hours to dissolve uranium-phosphate minerals (Beazley et al., 2011); (3) 10 mL of 0.04 M $NH_2OH \bullet HCl$ in 25% (v/v) acetic acid was added and agitated at 96°C for 6 hours to remove Fe- and Mn-associated uranium; (4) 1.5 mL of 0.02 M HNO_3 and 2.5 mL of 30% H_2O_2 (pH 2.0) were added and agitated at 96°C for 2 hours, a second 1.5 mL aliquot of 30% H_2O_2 (pH 2.0) was added and agitated at 96°C for 3 hours, and a third 5 mL aliquot of 2.5 M NH_4OAc in 20% (v/v) HNO_3 was added and

agitated at 20°C for 1 hour to extract uranium bound to organics; and (5) 5 mL of 15.8 M HNO_3 was added and maintained at 85°C for 3 hours to extract the residual fractions (Gleyzes et al., 2002). After each extraction step, samples were centrifuged (1380 xG for 10 minutes), and supernatants were filtered (0.2 µm, PES Puradisc Whatman) and reserved for uranium analysis by ICP-MS and for phosphate quantification using the spectrophotometric technique of Murphy and Riley (1962). The pH of the samples for phosphate quantification in each extract was adjusted to ~ 4.0 with NaOH (10.0 M) or HCl (12.0 M) to allow for color development. Standards were prepared in extraction media and treated as described above.

X-ray absorption spectroscopy (XAS) was performed at the Stanford Synchrotron Radiation Lightsource (SSRL). Final samples (T = 70 days) from the U-amended controls, the G2P-amended reactors, nitrate-amended reactors, and the sulfate-amended reactors at both pH 5.5 and 7.0 were characterized by XAS, and an initial sample (T = 0 days) from pH 5.5 G2P-amended reactors was also examined. Sediment samples were loaded into windowed Lexan sample holders, sealed with Kapton tape in an anaerobic chamber (Coy Laboratory Instruments, Inc.), and maintained anoxic in a sealed jar for transport to SSRL and under N_2 atmosphere at the beam line. Uranium L_{III}-edge XAS spectra were collected at SSRL beam line 10-2 using a focused X-ray beam with a 23 keV harmonic rejection cutoff and a 13 element Ge detector. The incident energy was selected with a Si(220) monochromator crystal. Transmission and fluorescence data were collected simultaneously. Detection limits of around 5% weight are achieved in these conditions at beam line 10-2. All EXAFS data were reduced using SIXPACK (Webb, 2005). Phase and amplitude files for EXAFS fittings were created with FEFF7

(Ankudinov et al., 1998; Zabinsky et al., 1995). Theoretical models were based on scattering paths expected for autunite-type group minerals (Catalano and Brown, 2004) and U(VI) adsorbed to iron oxihydroxides (Waite et al., 1994). The models were first tested on known chernikovite and U-$Fe_{(ads)}$ samples to ensure good agreement with previous fittings (Beazley et al., 2009, 2011). The U═Oax═U═Oax transoxido multiple scattering path (Allen et al., 1996; Bargar et al., 2000; Hudson et al., 1996) was included in all fits. The axial oxygen coordination number (N) for all reactors was set at two (Beazley et al., 2007, 2009; Beazley et al., 2011; Webb et al., 2006). To aid comparison between samples, the Debye-Waller factors (σ) were fixed for shells other than axial oxygen, a common practice for uranium EXAFS (Bargar et al., 2000; Beazley et al., 2009; Beazley et al., 2011; Webb et al., 2006). The addition of shells was considered to improve the quality of the EXAFS fit if a reduction in the reduced chi-square was observed (Webb et al., 2006; Webb et al., 2005). As Mn and Fe display similar backscattering intensities and phases in EXAFS, it is unlikely to distinguish these two elements during the fitting procedure. Thus, rather than distinct Fe and Mn shells, a "sum" of Fe/Mn like neighbors was reported for all the treatments.

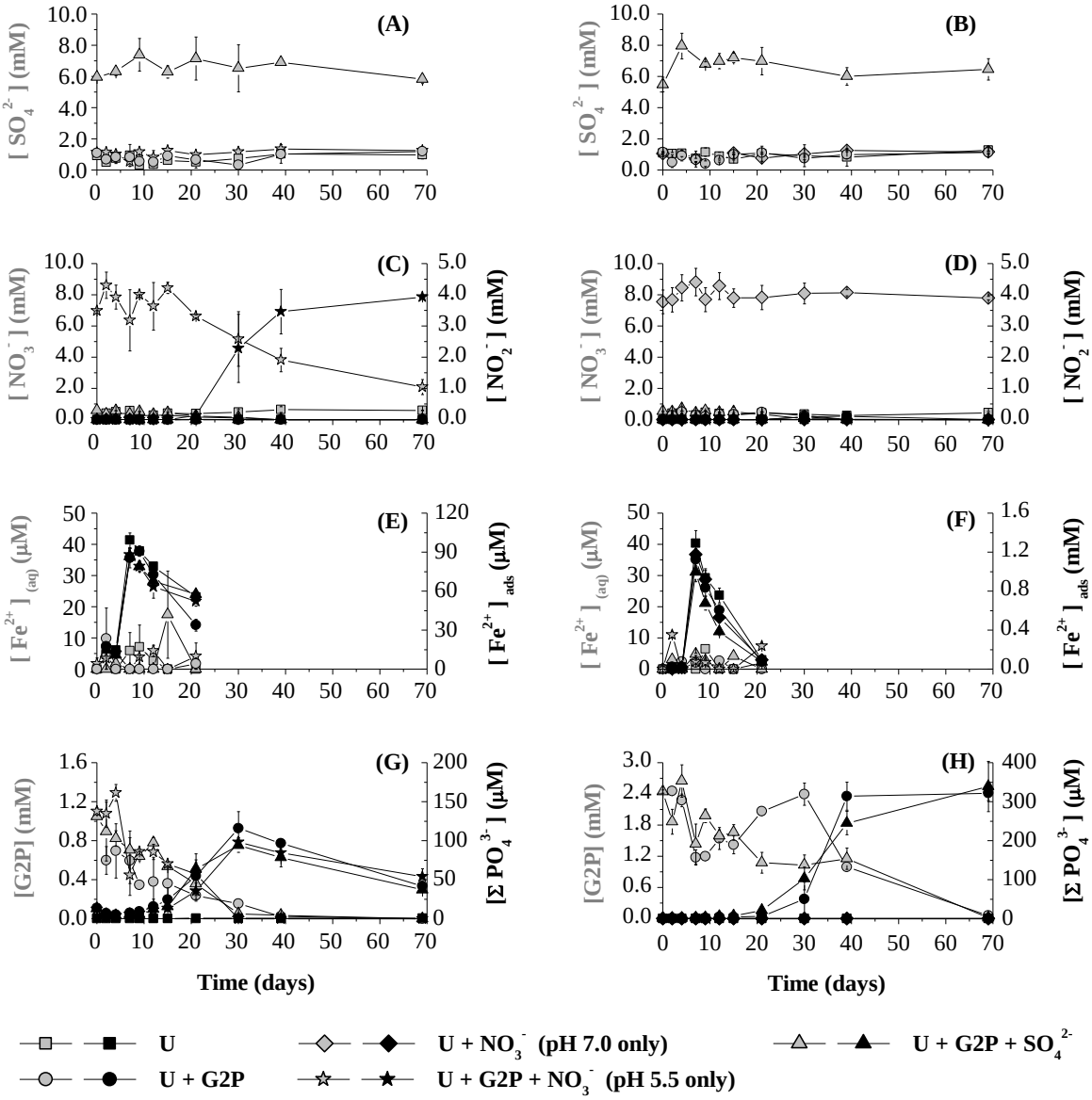

Figure 3.1 Evolution of SO_4^{2-} [(A) and (B)], NO_3^- and NO_2^- [(C) and (D)], $Fe^{2+}_{(aq)}$ and adsorbed Fe^{2+} [(E) and (F)], and Glycerol-2-phosphate (G2P) and $\sum PO_4^{3-}$ [(G) and (H)] as a function of time in pH 5.5 [(A), (C), (E), and (G)] and pH 7.0 [(B), (D), (F), and (H)] static microcosms amended with 300 µM UO_2^{2+} only; 300 µM UO_2^{2+} and 7 mM NO_3^- (pH 7.0 only); 300 µM UO_2^{2+} and 5 mM G2P; 300 µM UO_2^{2+}, 5 mM G2P, and 7 mM NO_3^- (pH 5.5 only); or 300 µM UO_2^{2+}, 5 mM G2P, and 9.4 mM SO_4^{2-}. Grey symbols represent chemical species on the left axes, while black symbols represent chemical species on the right axes. Error bars represent the range of average reported concentrations between duplicate reactors.

3.4 Results

3.4.1 Aqueous species

The pH remained constant for the duration of the experiments in both pH 5.5 and 7.0 reactors (data not shown). In all treatments without addition of external terminal electron acceptors (TEAs), background nitrate and sulfate concentrations exchanged from the original sediment after 3 hours of equilibration averaged 450 µM and 800 µM, irrespective of the pH of the incubations (Figure 3.1A-D). Although sulfate and nitrate were present in the U-amended controls, both nitrate and sulfate reduction were negligible without G2P addition (Figure 3.1A-D), even in pH 7.0 incubations in the presence of 7 mM NO_3^- (Figure 3.1D). After a phase lag of 15 days, the presence of G2P stimulated nitrate reduction at both pH 5.5 and 7.0 (Figure 3.1E-H) but not sulfate reduction, even in treatments containing elevated sulfate concentrations (Figure 3.1A-B), and complete depletion of nitrate was observed in G2P-containing reactors without NO_3^- addition after 39 days of incubation (Figure 3.1C-D). Pseudo-first-order rate constants for nitrate reduction in G2P-containing reactors unamended with nitrate were calculated to be 0.04 ± 0.01 d^{-1} and 0.07 ± 0.03 d^{-1} at pH 5.5 and 7.0 (Table 3.2). Although nitrate was removed in the sulfate-amended reactors, only ephemeral accumulation of nitrite was observed, while traces of nitrite were observed in the G2P-amended reactors with no external TEA (Figure 3.1C-D). In the nitrate-amended reactors at pH 5.5, nitrate concentrations were reduced from 7 to 2 mM over 70 days (Figure 3.1C) with a pseudo-first-order rate constant of 0.02 ± 0.004 d^{-1} (Table 3.2), and the accumulation of 4 mM nitrite was observed after a small phase lag (Figure 3.1C).

Table 3.2 Pseudo-first-order rate constants, k_{obs}, for consumption of NO_3^-, Fe(III), glycerol-2-phosphate (G2P), and dissolved U. For pH 7.0 reactors, only one uranium rate constant was calculated between days 0 and 30. Rate constants reported as N/A represent species that were not present in the given reactor treatment, and rate constants reported as 0 represent species that were not transformed between the initial and final sampling points. Values are reported in units of d^{-1}. Errors represent the standard error of the unweighted slope of linear regressions used to determine rate constants (details in supplementary material).

Treatment	*pH*	*NO_3^-*	*Fe(III)*	*G2P*	*U*
U - amended control	5.5	0	0.66 ± 0.01	N/A	0
	7.0	0	1.36 ± 0.03	N/A	0
G2P - amended reactor	5.5	0.04 ± 0.01	0.62 ± 0.02	0.05 ± 0.01	0.39 ± 0.01[a] 0.10 ± 0.01[b]
	7.0	0.07 ± 0.03	1.28 ± 0.01	0.10 ± 0.002	0.06 ± 0.01
SO_4^{2-} - amended reactor	5.5	0.04 ± 0.01	0.64 ± 0.01	0.05 ± 0.01	0.39 ± 0.09[a] 0.11 ± 0.02[b]
	7.0	0.06 ± 0.01	1.38 ± 0.04	0.09 ± 0.02	0.06 ± 0.01
NO_3^- - amended reactor	5.5	0.02 ± 0.004	0.54 ± 0.01	0.05 ± 0.02	0.46 ± 0.08[a] 0.10 ± 0.01[b]
	7.0	0	1.36 ± 0.02	N/A	0

[a] Calculated rate constant between day 0 and day 4 representing the initial uranium removal phase
[b] Calculated rate constant between day 7 and day 31 representing the secondary removal phase

Aqueous Fe(II) remained constant at ~ 10 µM in both pH 5.5 and pH 7.0 reactors throughout the 21 day sampling period (Figure 3.1E-F). In all pH 5.5 reactors, adsorbed Fe(II) remained constant at 15 µM until day 7 when a steep increase to 100 µM was observed (Figure 3.1E). A much more pronounced increase in adsorbed Fe(II) was detected in all pH 7.0 reactors, irrespective of the TEA present, with concentrations as high as 1.1 mM (Figure 3.1F). A pseudo-first-order rate constant for Fe(III) reduction of 0.61 ± 0.05 d^{-1} was calculated from total Fe(II) produced at pH 5.5, while an average

pseudo-first-order rate constant of 1.34 ± 0.04 d^{-1} was estimated for all treatments at pH 7.0 (Table 3.2). The increase in adsorbed Fe(II) was followed by a steady decrease to ~ 65 µM after 21 days of incubation in all reactors at both pH (Figure 3.1E-F). The same trends were observed in all reactors, regardless of the presence or absence of G2P.

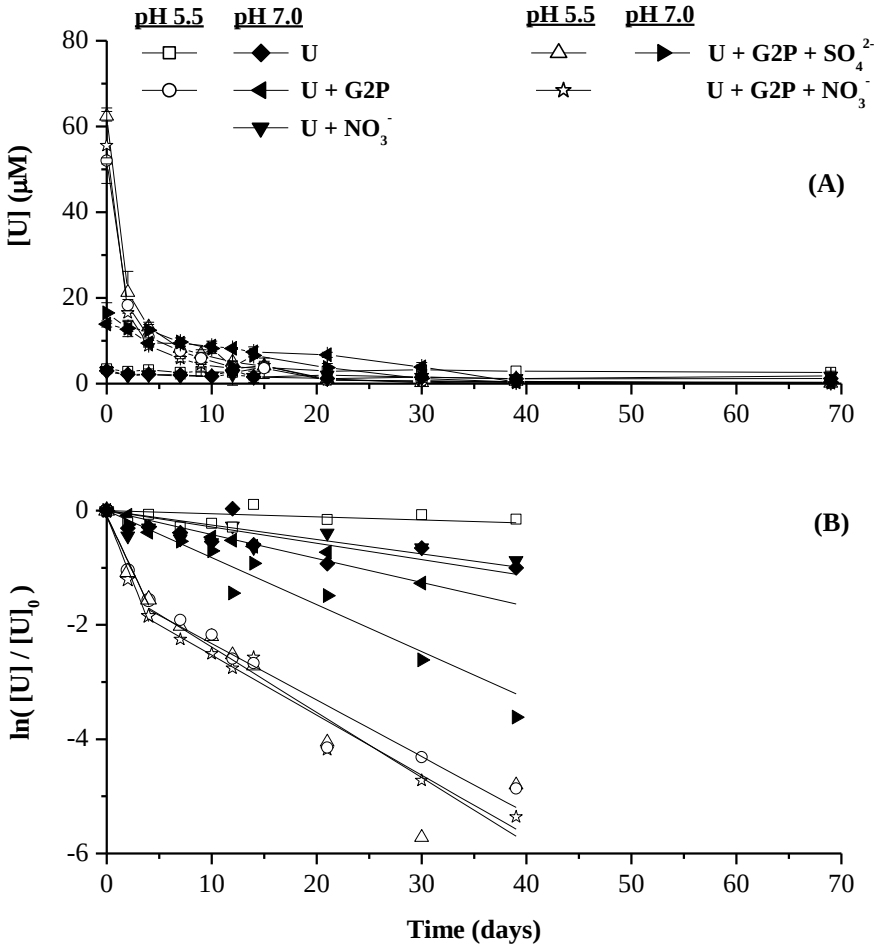

Figure 3.2 Evolution of A) Total dissolved uranium as a function of time in pH 5.5 (open symbols) and pH 7.0 (closed symbols) static microcosms amended with 300 µM UO_2^{2+} only; 300 µM UO_2^{2+} and 7 mM NO_3^- (pH 7.0 only); 300 µM UO_2^{2+} and 5 mM G2P; 300 µM UO_2^{2+}, 5 mM G2P, and 7 mM NO_3^- (pH 5.5 only); or 300 µM UO_2^{2+}, 5 mM G2P, and 9.4 mM SO_4^{2-}. Error bars represent the range of average reported values between duplicate reactors, and uranium standard deviations also include error associated with duplicate measurements. B) Linearization of total dissolved uranium in all reactors assuming pseudo-first-order with respect to uranium concentration. For pH 5.5 reactors, data points between 0 and 4 days have a distinct linear fit from data points between 7 and 39 days.

Although G2P-containing reactors were amended with 5 mM G2P, initial aqueous G2P concentrations averaged only 1 mM at pH 5.5 and 2.3 mM at pH 7.0 (Figure 3.1G-H), indicating adsorption of G2P onto ORFRC sediments is more significant at low pH. Complete removal of dissolved G2P was observed after 39 days of incubation (Figure 3.1G-H), and the pseudo-first-order rate constant for G2P consumption at pH 5.5 and 7.0 averaged 0.05 ± 0.02 d^{-1} and 0.10 ± 0.02 d^{-1}, respectively (Table 3.2). Dissolved phosphate was not detected in the U-amended controls or the pH 7.0 nitrate-amended reactors without G2P (Figure 3.1H). However, in all G2P-containing reactors at pH 5.5, up to 120 µM inorganic phosphate accumulated after 30 days of incubation followed by a slow linear decrease to 50 µM by day 70 (Figure 3.1G). Alternatively, in all pH 7.0 G2P-containing reactors, inorganic phosphate accumulated up to 350 µM after 39 days of incubation and remained around the same concentration for the remainder of the experiments (Figure 3.1H). This observed accumulation of phosphate is ~ 90% lower than expected if mass balance with G2P consumption was conserved, indicating that at both pH a significant fraction of phosphate was removed by adsorption onto the solid phase, uptake by microbial populations, and/or precipitation of phosphate minerals.

All reactors amended with 300 µM U but not G2P at both pH initially contained only 2 µM uranium in solution, and uranium concentrations remained at 2 µM for the duration of the incubations (Figure 3.2A). As U(VI) was instantaneously removed by precipitation or adsorption onto the solid phase and no temporal change in uranium concentration was observed in these treatments, the pseudo-first-order rate constants for this removal process were reported as zero (Table 3.2). In the presence of G2P, however, pH 5.5 reactors amended with 300 µM uranium displayed approximately 55 µM uranium

in solution at time zero, while the same reactors at pH 7.0 displayed only15 µM (Figure 3.2A). Rapid uranium removal to < 0.2 µM was observed in G2P-containing reactors at pH 5.5, and U remained immobilized for the duration of the experiment regardless of the type and presence of terminal electron acceptor (TEA) (Figure 3.2A). Interestingly, uranium removal at pH 5.5 was divided into two distinct phases, an initial phase between 0 and 4 days during which U(VI) removal occurred with an average pseudo-first-order rate constant of 0.41 ± 0.12 d^{-1} for all treatments, and a second phase between 7 and 30 days during which removal occurred with an average pseudo-first-order rate constant 0.10 ± 0.02 d^{-1} for all treatments (Table 3.2, Figure 3.2B). In contrast, the initial 15 µM uranium present in pH 7.0 reactors was steadily titrated out of solution over the 70 day sampling period to < 0.2 µM (Figure 3.2A) with a pseudo-first-order rate constant of 0.06 ± 0.01 d^{-1} (Table 3.2) regardless of the presence or absence of elevated sulfate concentrations.

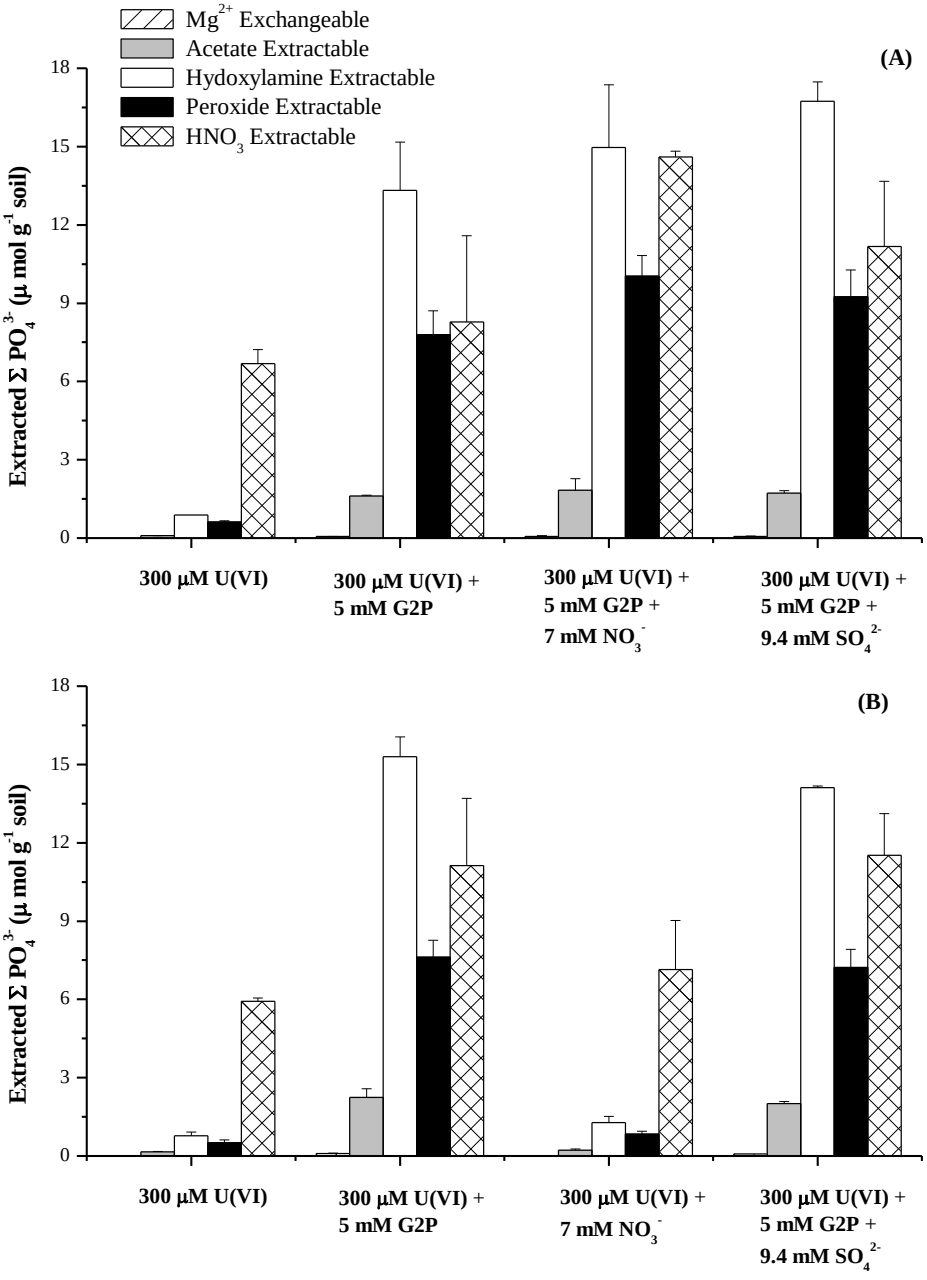

Figure 3.3 Solid phase-associated $\sum PO_4^{3-}$ extracted with uranium by the sequential extraction technique of Tessier (1979) from A) pH 5.5 and B) pH 7.0 sediments after 70 days of incubation. Bars represent the species extracted during each individual extraction step. A total of 4.4 (± 0.7) µmol g^{-1} soil ΣPO_4^{3-} was extracted from the untreated soils. All error bars represent the standard error of the mean calculated from duplicate reactors and duplicate extractions.

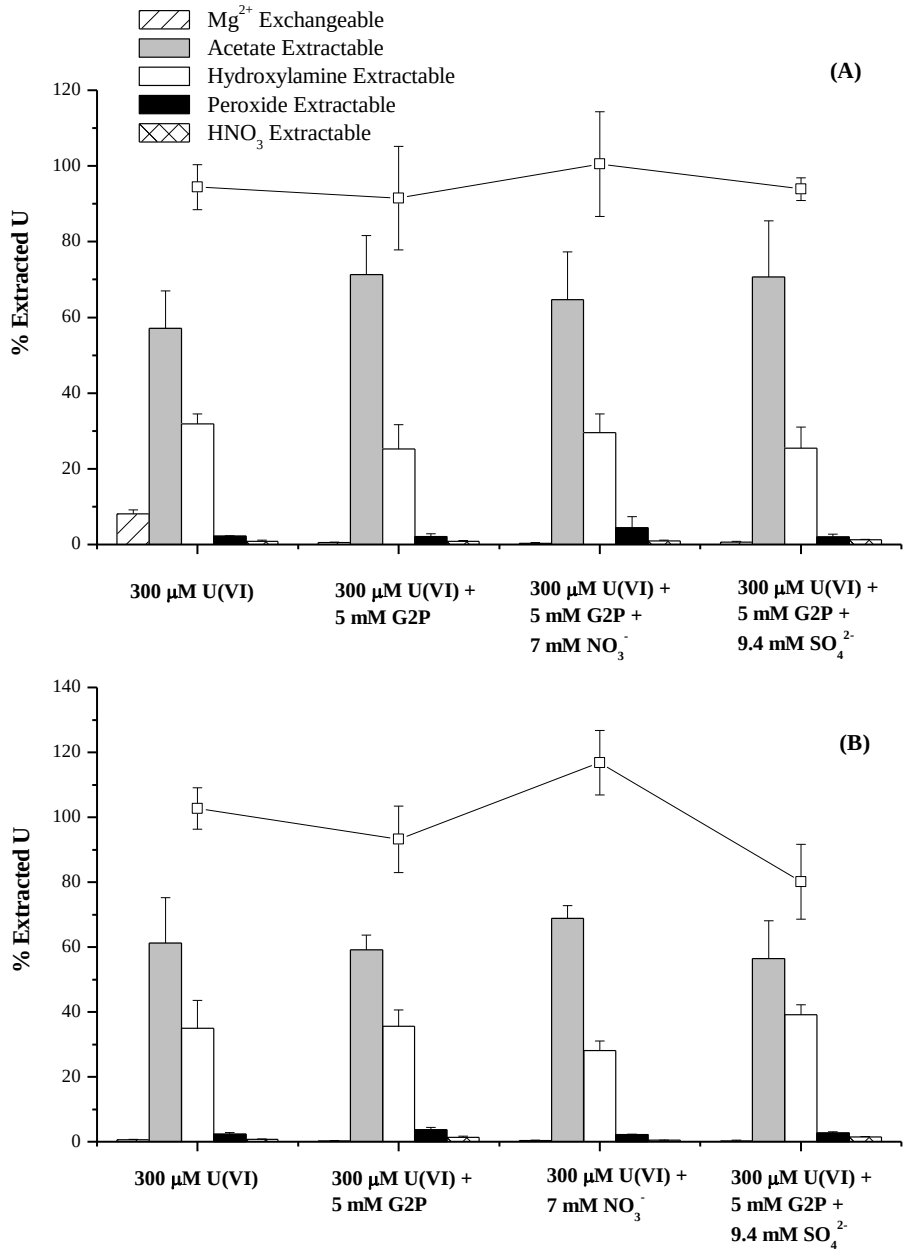

Figure 3.4 Solid phase-associated U extracted by the sequential extraction technique of Tessier (1979) from A) pH5.5 and B) pH 7.0 sediments after 70 days of incubation. A total of 0.7 (± 0) µmol g^{-1} soil U was extracted from the untreated soils. Bars represent percent uranium extracted in each individual extraction step with respect to the total extracted uranium in each treatment. Symbols represent the percent uranium recovered in each reactor with respect to the total mass of extractable uranium. All error bars represent the standard error of the mean calculated from duplicate reactors and duplicate extractions.

3.4.2 Solid-phase speciation of uranium and phosphate

A total phosphate concentration of 4.4 ± 0.7 µmol P g^{-1} was extracted in the original sediment prior to phosphate amendment. Not surprisingly, solid phase extractions of sediments revealed higher total extracted phosphate in all G2P-containing reactors than in reactors without G2P (Figure 3.3A-B). As expected, phosphate was not detected in the exchangeable fraction (Figure 3.3A-B), as phosphate should not exchange with Mg^{2+}. Without G2P, extracted phosphate was primarily concentrated in the residual fraction (Figure 3.3A-3B). In the presence of G2P, however, the distribution of extracted phosphate shifted towards hydroxylamine- and peroxide-extracted fractions and was not significantly affected by the pH and the presence or type of amended TEA (Figure 3.3A-B). As the organophosphate compound was in great excess of uranium in these incubations, the acetate-extractable phosphate fraction, which is representative of uranium-phosphate minerals, was relatively small in all reactors compared to the other treatments (Figure 3.3A-B).

The original unamended sediment contained a total concentration of 0.7 ± 0.02 µmol U g^{-1} soil or about 25% of the total extracted uranium after amendments of 300 µM U(VI). The acetate extractable uranium fraction constituted the largest fraction (~ 60%) of total extracted uranium in all reactor treatments, regardless of the pH (Figure 3.4A-B), followed by the hydroxylamine extractable fraction (~ 30%) as the second most abundant. Except for the exchangeable fraction in the pH 5.5 U-amended controls, other fractions did not contribute significantly to total extracted uranium (Figure 3.4A-B). Mass-balance on uranium from sequential extractions was respected (within error) in each treatment except for pH 7.0 reactors amended with G2P but no TEA (80.1 ± 11.5 %)

and pH 7.0 reactors amended with 5 mM NO_3^- but no G2P (116.8 ± 9.9 %) (Figure 3.4A-B). Further bulk characterization of solid-associated uranium by XAS provided information on the oxidation state and speciation of uranium in each reactor. The normalized and background-subtracted solid phase XANES spectra of samples from each treatment exhibited a uranium L_{III}-edge at ~ 17163 eV and a characteristic U(VI) shoulder between 17188 and 17200 eV, regardless of pH, indicating U(VI) as the main oxidation state of uranium in these systems (Figures 3.5A and 3.6A). In all pH 5.5 reactors, the k^3-weighted EXAFS fittings confirmed the presence of an axial oxygen shell at 1.80 Å (Figure 3.5B-C, Table 3.3). In addition, two distinct equatorial oxygen shells were evidenced which may be grouped into two subsets based on radial distance (R) from the central uranium atom. The first equatorial oxygen group clustered at approximately 2.30 Å with coordination numbers between 2.3 and 3.5. The second equatorial oxygen group clustered at approximately 2.45 Å with coordination numbers between 1.9 and 3.4. As expected at pH 5.5, carbon from carbonates was not found in the neighborhood of uranium in any reactor. In contrast, Mn and/or Fe shells between 3 and 3.5 Å were necessary in all pH 5.5 reactors to improve the fit. The interatomic distances for sorption complexes between Mn/Fe and U display a wide variety of distances, and these Mn/Fe values fall within the typical range reported elsewhere (Bargar et al., 2000; Webb et al., 2006). Finally, phosphorus shells at ~ 3.65 Å improved the fit in the G2P-amended reactors without external TEA (day 70) and in the presence of excess sulfate (day 70) and nitrate (T = 70).

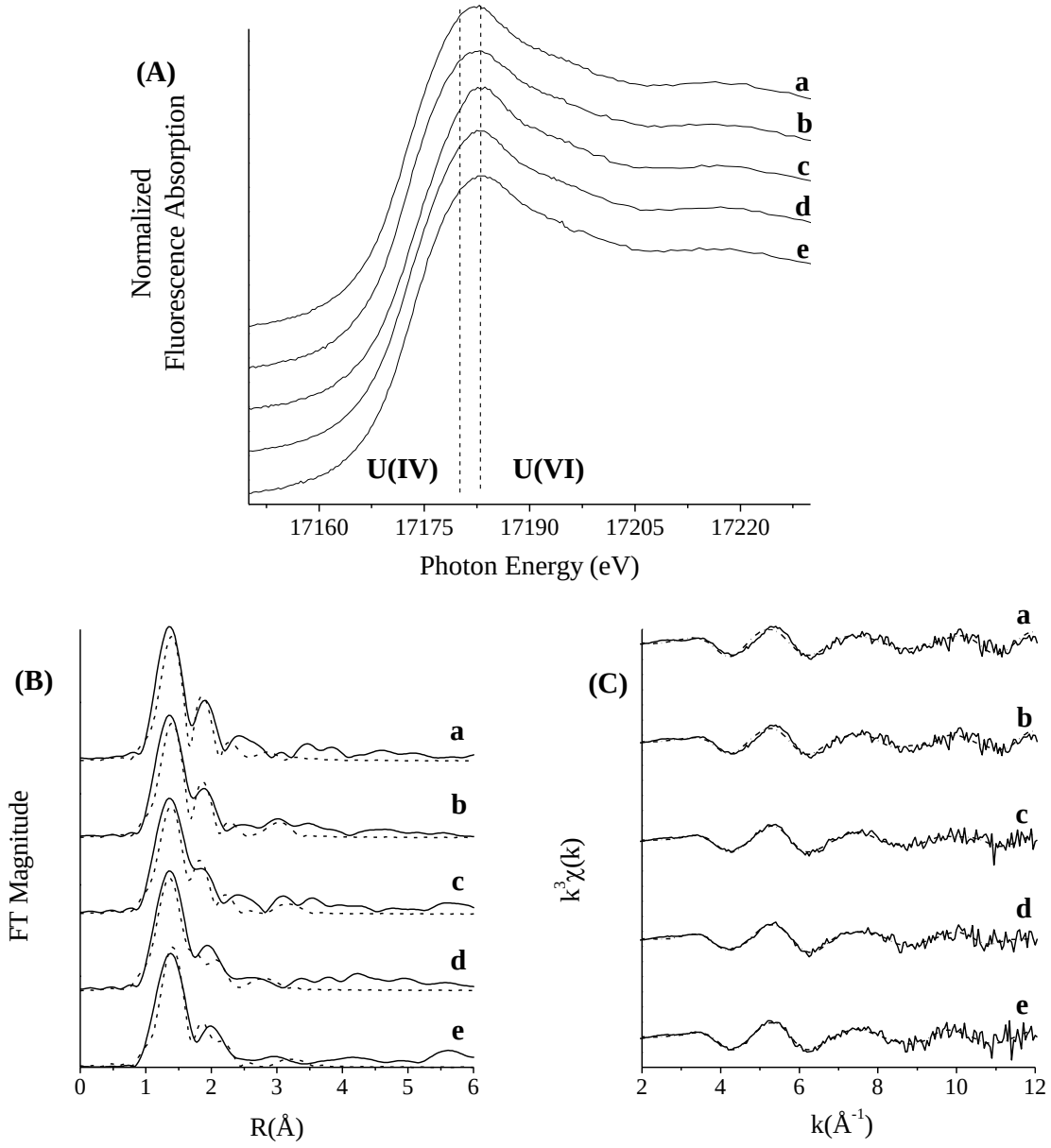

Figure 3.5 Uranium (A) XANES, (B) R-space, and (C) *k*-space diagrams of the L_{III}-edge EXAFS obtained from Area 3 sediments of the Oak Ridge Field Research Center incubated anaerobically in static microcosms for 70 days at pH 5.5. Treatments included a (300 µM U + 5 mM G2P, day 0), b (300 µM U + 5 mM G2P, day 70), c (300 µM U + 5 mM G2P + 7 mM NO_3^- , day 70), d (300 µM U + 5 mM G2P + 9.4 mM SO_4^{3-}, day 70), and e (300 µM U, day 70).

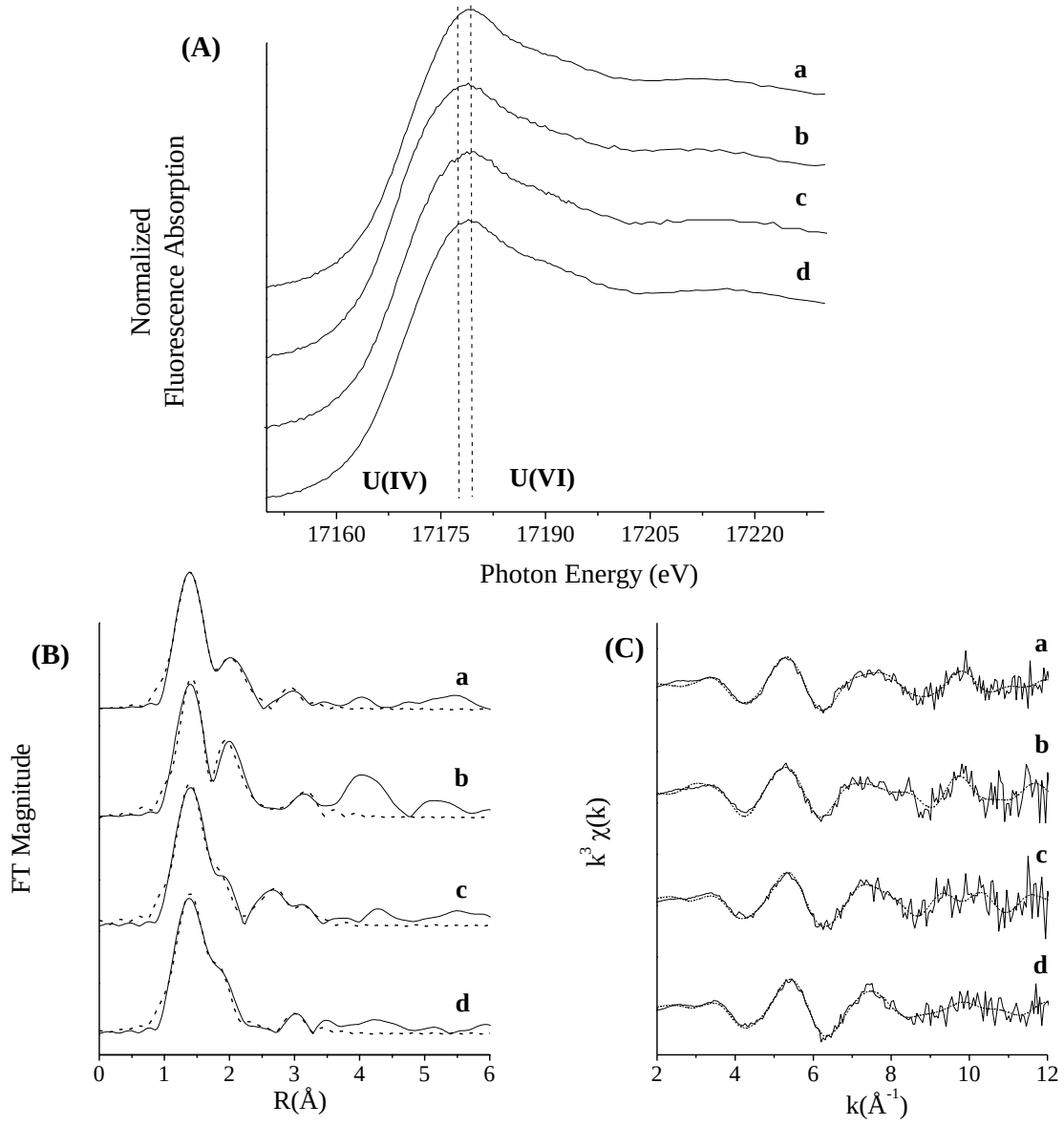

Figure 3.6 Uranium (A) XANES, (B) R-space, and (C) *k*-space diagrams of the L_{III}-edge EXAFS obtained from Area 3 sediments of the Oak Ridge Field Research Center incubated anaerobically in static microcosms for 70 days at pH 7.0. Treatments included a (300 µM U, T = 70 d), b (300 µM U + 7 mM NO_3^- , T = 70 d), c (300 µM U + 5 mM G2P, T = 70 d), and d (300 µM U + 5 mM G2P + 9.4 mM SO_4^{3-}, T = 70 d).

As observed at pH 5.5, the k^3-weighted EXAFS fittings of pH 7.0 sediments confirmed the presence of an axial oxygen shell at 1.83 Å (Figure 3.6B-C, Table 3.4). Similarly, two distinct equatorial oxygen shells were also observed in all pH 7.0 reactors. The first equatorial oxygen group clustered at approximately 2.25 Å with coordination numbers between 1.4 and 2.0, and the second equatorial oxygen group clustered at approximately 2.42 Å with coordination numbers between 1.6 and 3.7. As expected at pH 7.0, carbon was needed to improve the fit in the nitrate-amended reactors and the sulfate-amended reactors. Similarly, Mn and/or Fe shells between 3.2 and 3.5 Å were necessary in the pH 7.0 reactors to improve the fit. Finally, phosphorus shells at ~ 3.65 Å improved the fit in the G2P-amended reactors only.

3.5 Discussion

Both U(VI) bioreduction and the biomineralization of U(VI)-phosphate minerals are potentially viable approaches to immobilize uranium in contaminated subsurfaces. Bioreduction in low pH soils is typically promoted by buffering the pH to circumneutral values and introducing an electron donor, and U(VI) reduction usually occurs after complete reduction of nitrate (Madden et al., 2009; Nyman et al., 2006; Wu et al., 2006b) and may be concurrent with sulfate or iron reduction (Akob et al., 2008; Cardenas et al., 2010; Madden et al., 2009; Nyman et al., 2006). Biomineralization of U(VI)-phosphate minerals preferentially occurs in low to circumneutral pH conditions in both anaerobic and aerobic environments, provided that organophosphates are available (Beazley et al., 2007, 2009; Beazley et al., 2011; Macaskie et al., 1995; Martinez et al., 2007; Montgomery et al., 1995; Shelobolina et al., 2009). Although these processes potentially overlap in reducing conditions, the competition dynamic between adsorption,

U(VI)-phosphate biomineralization, and bioreduction has yet to be examined. To determine which anaerobic respiration process is most conducive to uranium removal through U(VI)-phosphate biomineralization and whether bioreduction can compete with biomineralization in G2P-amended sediments, this study investigated the relationship between these competing processes at pH 5.5 and 7.0 in the presence of iron oxides and elevated concentrations of sulfate or nitrate as terminal electron acceptors and G2P as the organophosphate source for U(VI)-phosphate biomineralization.

3.5.1 Terminal electron acceptor transformations

Although a variety of sulfate-reducing bacteria have been detected in ORFRC wells (Cardenas et al., 2010; Gihring et al., 2011), no evidence of sulfate reduction was observed in any treatment regardless of the presence or absence of G2P and pH conditions (Figure 3.1A-B): sulfate concentrations remained steady in all reactors, even after complete removal of nitrate and in the presence of elevated sulfate concentrations; the sediments remained brown, characteristic of the high iron content of ORFRC sediments, throughout the course of the experiment; and sulfide odors were not noticed. These findings are not consistent with past studies conducted with Oak Ridge sediments that observed substantial sulfate reduction after the system pH was raised to between 6.0 and 7.5 (Akob et al., 2008; Gu et al., 2005; Kelly et al., 2009; Kim et al., 2010; Madden et al., 2009; Wu et al., 2006b; Zhang et al., 2010). Electron donor limitations may have prevented sulfate reduction from occurring, as G2P represented the only carbon source added to these incubations. Ambiguous information is available on the ability of sulfate reducers to metabolize or assimilate glycerol, the by-product of G2P hydrolysis. Even though sulfate reduction coupled to glycerol oxidation was observed in acidic sediments

conditioned by acid mine drainage (Becerra et al., 2009), sulfate reduction is known to be highly electron donor dependent (Madden et al., 2009; Petrie et al., 2003), suggesting that glycerol may have limited the activity of sulfate-reducing bacteria.

Table 3.3 Fitting Parameters for U L_{III}-edge EXAFS derived using SIXPACK (Webb, 2005) in pH 5.5 reactors. Treatments include a (300 µM U, day 70), b (300 µM U + 5 mM G2P, day 0), c (300 µM U + 5 mM G2P, day 70), d (300 µM U + 5 mM G2P + 7 mM NO_3^- , day 70), and e (300 µM U + 5 mM G2P + 9.4 mM SO_4^{3-} , day 70). *N* represents U-ligand coordination number, R(Å) represents U-ligand distance.

Path	*Treatment*	*N*	*R(Å)*	σ^2	*Rfactor*	ΔE_0
$U\text{-}O_{ax}$	a	2.00	1.80 ± 0.01	0.002 ± 0.001	0.0556	11.4 ± 2.92
	b	2.00	1.79 ± 0.01	0.001 ± 0.000	0.0399	9.63 ± 2.01
	c	2.00	1.80 ± 0.01	0.002 ± 0.001	0.0367	9.99 ± 2.29
	d	2.00	1.79 ± 0.01	0.002 ± 0.001	0.0522	8.22 ± 2.87
	e	2.00	1.76 ± 0.01	0.002 ± 0.001	0.0345	2.82 ± 3.07
$U\text{-}O_{eq\ 2.30}$	a	2.34 ± 0.65	2.30 ± 0.03	0.003		
	b	3.49 ± 0.55	2.35 ± 0.01	0.003		
	c	3.01 ± 0.55	2.34 ± 0.02	0.003		
	d	3.14 ± 0.63	2.30 ± 0.02	0.003		
	e	2.94 ± 0.58	2.22 ± 0.02	0.003		
$U\text{-}O_{eq\ 2.45}$	a	2.60 ± 0.75	2.46 ± 0.03	0.003		
	b	2.14 ± 0.71	2.53 ± 0.02	0.003		
	c	1.86 ± 0.70	2.52 ± 0.03	0.003		
	d	2.33 ± 0.76	2.47 ± 0.03	0.003		
	e	3.44 ± 0.62	2.39 ± 0.02	0.003		
U-Mn/Fe	a	0.20 ± 0.39	3.54 ± 0.01	0.003		
	b	0.32 ± 0.29	3.29 ± 0.05	0.003		
	c	0.36 ± 0.54	3.41 ± 0.06	0.003		
	d	0.31 ± 1.99	3.52 ± 0.27	0.003		
	e	0.40 ± 0.28	3.28 ± 0.04	0.003		
U-P	a					
	b					
	c	0.17 ± 1.11	3.62 ± 0.33	0.003		
	d	0.57 ± 2.32	3.60 ± 0.40	0.003		
	e	0.75 ± 0.71	3.72 ± 0.06	0.003		

Errors are given for values which were allowed to float
No error means value was fixed or calculated from other parameters

Table 3.4 Fitting Parameters for U L_{III}-edge EXAFS derived using SIXPACK (Webb, 2005) in pH 7.0 reactors. Treatments include a (300 µM U, day 70), b (300 µM U + 7 mM NO_3^-, day 70), c (300 µM U + 5 mM G2P, day 70), and d (300 µM U + 5 mM G2P + 9.4 mM SO_4^{3-}, day 70). *N* represents U-ligand coordination number, R(Å) represents U-ligand distance.

Path	*Treatment*	*N*	*R(Å)*	σ^2	*Rfactor*	ΔE_0
$U\text{-}O_{ax}$	a	2.00	1.87 ± 0.01	0.008 ± 0.002	0.0252	13.9 ± 3.1
	b	2.00	1.86 ± 0.04	0.006 ± 0.003	0.0436	10.4 ± 3.6
	c	2.00	1.85 ± 0.03	0.005 ± 0.003	0.0555	7.45 ± 3.9
	d	2.00	1.78 ± 0.01	0.007 ± 0.001	0.0128	2.34 ± 1.4
$U\text{-}O_{eq\ 2.30}$	a	1.37 ± 0.49	2.30 ± 0.03	0.003		
	b	1.35 ± 1.6	2.28 ± 0.10	0.003		
	c	2.05 ± 2.5	2.25 ± 0.06	0.003		
	d	1.72 ± 0.31	2.20 ± 0.02	0.003		
$U\text{-}O_{eq\ 2.45}$	a	1.64 ± 0.58	2.46 ± 0.02	0.003		
	b	2.65 ± 2.19	2.44 ± 0.07	0.003		
	c	3.73 ± 3.22	2.42 ± 0.04	0.003		
	d	1.96 ± 0.37	2.35 ± 0.02	0.003		
U-C	a					
	b	1.19 ± 1.39	2.87 ± 0.06	0.003		
	c					
	d	1.67 ± 0.62	2.95 ± 0.03	0.003		
U-Mn/Fe	a	0.27 ± 0.14	3.43 ± 0.03	0.003		
	b	0.49 ± 0.42	3.47 ± 0.06	0.003		
	c	0.30 ± 0.43	3.18 ± 0.07	0.003		
	d	0.43 ± 0.16	3.24 ± 0.02	0.003		
U-P	a					
	b					
	c	1.02 ± 1.14	3.61 ± 0.06	0.003		
	d	0.62 ± 0.35	3.69 ± 0.03	0.003		

Errors are given for values which were allowed to float
No error means value was fixed or calculated from other parameters

Alternately, the background nitrate concentrations in the present study, reflective of the high nitrate levels at the ORFRC, may have prevented stimulation of sulfate-reducing bacteria. Nitrate-reducing bacteria are diverse and active in ORFRC soils (Spain and Krumholz, 2011), and a subset of the nitrate reducers that are metabolically active include members of the genera *Burkholderia*, *Ralstonia*, *Castellaniella*,

Herbaspirillum, *Dechloromonas*, *Zooglea*, *Rhodanobacter*, *Rhizobiaceae*, *Sphingomonas*, *Magnetospirillum*, and *Paenibacillus* (Akob et al., 2007; Green et al., 2010; Green et al., 2012; Mohanty et al., 2008). In addition, *Rahnella* sp. Y9602, a phosphatase-positive metal-resistant bacterium isolated from ORFRC soils (Martinez et al., 2006), is able to reduce nitrate anaerobically while promoting biomineralization of U(VI)-phosphate minerals (Beazley et al., 2009). The results of the present study confirm that G2P addition is sufficient to stimulate nitrate reduction by indigenous nitrate reducing bacteria of ORFRC sediments in varied pH conditions and variable nitrate concentrations (Figure 3.1C-D). The higher pseudo first-order rate constant at pH 7.0 compared to pH 5.5 (Table 3.2) indicates that nitrate reduction was more efficient at circumneutral pH, which is consistent with previous findings at the ORFRC (Edwards et al., 2007; Istok et al., 2004; Shelobolina et al., 2003). Simultaneously, only ephemeral nitrite accumulation was observed in incubations amended with G2P only and both G2P and sulfate regardless of pH (Figure 3.1C-D), likely due to further reduction of nitrite to other denitrification products or ammonia during dissimilatory nitrate reduction to ammonia (DNRA) (Herbert, 1999). In turn, 4 mM NO_2^- accumulated in pH 5.5 nitrate-amended reactors (Figure 3.1C), and comparison of nitrate reduction rates (-180.9 ± 11.6 μM d^{-1}) and net nitrite production rates at pH 5.5 (157.3 ± 4.7 μM d^{-1}) suggests denitrification or DNRA removed nitrite from this reactor at a rate of -23.6 ± 12.5 μM d^{-1}.

The accumulation of high NO_2^- concentrations in the pH 5.5 nitrate-amended reactors may also have had a toxic effect on denitrifying bacteria that is reflected in a decrease in the pseudo-first-order rate constant for nitrate reduction in nitrate-amended

reactors compared to G2P-amended and sulfate-amended reactors (Table 3.2). The nitrite toxicity effect is well documented and is evidenced in a wide variety of microorganisms. Proposed mechanisms include an increase in the permeability of the cytoplasmic membrane (Sijbesma et al., 1996) and the disruption of proton translocation stoichiometry (Rake and Eagon, 1980). In addition, elevated levels of nitrite have been shown to interfere with denitrification pathways, a phenomenon that is known to be exaggerated in anaerobic conditions (Bollag and Henninger, 1978; Meijer et al., 1979). These findings suggest that the accumulation of NO_2^- in the pH 5.5 nitrate-amended reactors may have resulted from the toxicity of NO_2^- on nitrite-reducing bacteria, while the relatively minimal NO_2^- concentrations detected in other incubations were likely not significant to affect nitrite-reducing bacteria.

Iron reduction was not significantly inhibited by elevated nitrate concentrations (Figure 3.1C-F) in contrast to what is known about the inhibitory effect of nitrate on iron reduction (Dichristina, 1992; Finneran et al., 2002a; Finneran et al., 2002b; Senko et al., 2002). In addition, iron reduction was unaffected by the presence of G2P (Figure 3.1E-F). However, a significant inhibition on iron reduction was apparent at pH 5.5 (Figure 3.1E), consistent with previous findings demonstrating that microbial growth is impacted in low pH conditions (Edwards et al., 2007). As Fe^{2+} production preceded nitrate removal and production of nitrite, chemical reduction of Fe^{3+} coupled to reoxidation of nitrite was likely not significant, and the observed production of Fe^{2+} was likely due to microbially-mediated G2P-independent iron reduction in the presence of nitrate (Figure 3.1C-F). These observations suggest that iron-reducing bacteria present at the ORFRC

may be active in nutrient- and electron donor-limited environments when nitrate-reducing bacteria remain dormant.

The rapid rise and decrease of adsorbed Fe^{2+} not balanced by accumulation of dissolved Fe^{2+} in all reactors regardless of pH (Figure 3.1E-F) suggests that Fe^{2+} was not desorbed via an ion exchange process and instead precipitated as a distinct mineral. XANES spectra confirmed the bulk oxidation state of uranium as U(VI) in all reactors (Figures 3.5A and 3.6A), suggesting the chemical oxidation of sorbed Fe^{2+} by U(VI) (Liger et al., 1999) was likely not significant at pH 7.0 or inhibited at pH 5.5. As thermodynamic calculations predicted little adsorption of Fe^{2+} at pH 5.5 (Table 3.5), the observed adsorption of Fe^{2+} in all reactor treatments may have been driven by formation of ternary $=Fe—OPO_3—Fe^{+}$ complexes with iron oxides. These complexes are well known to occur under both pH conditions and are thought to be precursors to the surface precipitation of iron phosphate minerals even in undersaturated conditions (Ler and Stanforth, 2003; Li and Stanforth, 2000), but they were not included in the thermodynamic model. Thus, despite the fact that equilibrium calculations predict undersaturation of vivianite [$Fe_3(PO_4)_2$] at both pHs in the conditions of the incubations (Table 3.5), the decrease in total Fe^{2+} coinciding with the accumulation of inorganic phosphate in solution (Figure 3.1E-H) could be explained by the formation of ternary iron phosphate complexes and subsequent surface-catalyzed precipitation of vivianite. This process should be investigated in future studies.

Table 3.5 Predicted solution equilibrium and solid phase saturation indices using MINEQL+ (Schecher and McAvoy, 2001) in pH 5.5 and 7.0 incubations assuming 5 mM ΣPO_4^{3-} was produced by G2P hydrolysis. Solution concentrations are reported in percent of total species. Each treatment (Table 3.1) was modeled using the maximum measured total Fe^{2+} concentration and initial conditions as input for all other species. A double layer sorption model onto amorphous Fe-oxide (3.2 g/L, 600 m^2/g surface area) was included in the calculations. Unless otherwise noted, log K values are as reported in Schecher and McAvoy (2001).

Species	*Log K*	*Treatment*			
		U - amended control	*G2P - amended reactor*	*SO_4^{2-} - amended reactor*	*NO_3^- - amended reactor*
pH 5.5					
UO_2^{2+}					
$UO_2CO_{3\,(aq)}$	9.94[a]	25.9%	0.1%	0.0%	0.1%
Fe(wk)OH-$UO_2(OH)_2$	-6.28[b]		0.0%	0.0%	0.0%
Fe(st)OH-$UO_2(OH)_2$	-2.57[b]		0.7%	0.3%	0.4%
Others	--	6.8%	--	--	--
PO_4^{3-}					
Fe(wk)H_2PO_4	31.29	--	44.7%	48.4%	48.4%
Fe(wk)HPO_4^-	25.39	--	45.5%	41.6%	41.6%
Others (Autunite)	--	--	9.9%	10.0%	10.0%
Fe^{2+}				9.8%	
Fe^{2+}		91.3%	93.4%	57.5%	94.7%
Fe(st)OH-$Fe(OH)^+$	-0.95[c]	0.0%	3.60%	2.70%	2.80%
Fe(wk)-$Fe(OH)^+$	-2.98[c]	6.8%	1.50%	1.10%	1.10%
Others	--	1.9%	1.5%	1.5%	1.4%
Solid Phase					
Schoepite	-5.2[d]	-0.981	-3.48	-3.84	-3.70
Na-Autunite	47.4	-28.4	0 (99.2% U)	0 (99.7% U)	0 (99.5% U)
Ca-Autunite	44.7[d]	-32.05	-3.51	-4.16	-3.88
K-Autunite	22.73[e]	-28.64	-0.19	-0.72	-0.44
Vivianite	36.0[f]	-40.62	-7.10	-6.99	-6.98
Siderite	10.24[g]	-3.24	-3.20	-3.25	-3.24
pH 7.0					
UO_2^{2+}					
$UO_2(CO_3)_2^{-2}$	16.61[a]	11.3%	0.1%	0.1%	12.3%
$CaUO_2(CO_3)_3^{-2}$	27.18[h]	28.4%	0.5%	0.2%	27.8%
$Ca_2UO_2(CO_3)_3^{0}$	30.7[h]	6.4%	0.2%	0.1%	6.0%
Fe(st)OH-$UO_2(OH)_2$	-2.57[b]	47.3%	0.0%	0.0%	47.3%
Others	--	6.6%	--	--	6.6%
PO_4^{3-}					
Fe(wk)H_2PO_4	31.29	--	23.7%	22.8%	--
Fe(wk)HPO_4^-	25.39	--	61.9%	62.6%	--
Others	--	--	14.4%	14.6%	--
Fe^{2+}					
Fe^{2+}		4.4%	38.2%	34.8%	4.5%
Fe(wk)-$Fe(OH)^+$	-2.98[c]	71.3%	47.8%	40.5%	71.1%
Fe(st)OH-$Fe(OH)^+$	-0.95[c]	22.3%	7.00%	8.60%	22.4%
Fe(wk)-$Fe(OH)_2$	-11.55[c]	1.9%	1.30%	1.10%	1.9%
Others	--	0.1%	5.7%	15.0%	0.1%
Solid Phase					
Schoepite	-5.2[d]	-2.32	-4.30	-4.50	-2.32
Na-Autunite	47.4	-32.21	0 (99.2% U)	0 (99.6% U)	-32.00
Ca-Autunite	44.7[d]	-35.95	-3.65	-4.29	-35.98
K-Autunite	22.73[e]	-32.42	-0.19	-0.72	-32.45
Vivianite	36.0[f]	-39.70	-0.63	-0.97	-39.72
Siderite	10.24[g]	-2.35	-1.34	-1.44	-2.36

[a] (Guillaumont et al., 2003), [b] (Waite et al., 1994),[c] (Appelo et al., 2002), [d] (Langmuir, 1997), [e] (Van Haverbeke et al., 1996), [f] (Nriagu, 1972), [g] (Singer and Stumm, 1970), [h] (Dong and Brooks, 2006)

3.5.2 Organophosphate Hydrolysis

Incubations in the presence of G2P clearly illustrate that organophosphate hydrolysis is significant in reducing conditions (Figure 3.1G-H) and stimulates anaerobic respiration (Figure 3.1C-D) compared to otherwise identical control incubations without G2P. The distribution of phosphate extracted simultaneously with uranium from the solid phase at the end of the incubations demonstrates that phosphate exists primarily in highly recalcitrant phases in the absence of organophosphate (Figure 3.3A-B), suggesting that anaerobic respiration is limited by the availability of phosphorus in these conditions. In contrast, the distribution of solid-phase associated phosphate shifts towards more reactive phases in the presence of G2P (Figure 3.3A-B). These findings imply the supply of labile organic carbon (i.e. glycerol) or phosphate to support the metabolism and growth of the indigenous microbial community represents the driving force for G2P hydrolysis. Previous studies have demonstrated glycerol oxidation coupled to iron (Petrie et al., 2003), sulfate (Qatibi et al., 1991), and uranium (Madden et al., 2007) reduction, while organophosphate hydrolysis by bacterially-derived phosphatase enzymes is thought to provide inorganic phosphorus either for nutrient assimilation or as a heavy-metal detoxification mechanism (Macaskie et al., 1992). As uranium reduction was not favored in these incubations and as G2P consumption in reactors amended with G2P was so intense (1.2-2.4 mM, Figure 3.1G-H) compared to the availability of uranium (300 μM) in these sediments, G2P was likely hydrolyzed by bacterially-derived phosphatases produced due to phosphorus or carbon limitations. In addition, G2P hydrolysis may have been enhanced at pH 7.0 (Table 3.2) in response to the decrease in adsorption of G2P onto iron oxides due to the repulsion between partially deprotonated iron oxides and

totally deprotonated G2P at that pH. As nitrate reduction is clearly promoted by the presence of G2P in solution compared to the unamended control (Figure 3.1D), the decrease in G2P adsorption and associated increase in G2P hydrolysis at pH 7.0 may have also promoted the increase in the pseudo-first order rate constants for nitrate reduction observed at circumneutral pH in the incubations amended with G2P compared to at pH 5.5 (Table 3.2). Indeed, factoring out initial concentration of G2P from the pseudo-first order rate constants reveals similar rate constants for nitrate reduction at both pH 5.5 and 7.0 (not shown). Finally, the disparity between G2P consumption and phosphate production in solution in all G2P-containing reactors (Figure 3.1G-H) indicates the existence of a significant phosphate removal mechanism other than U(VI)-phosphate biomineralization. Thermodynamic modeling suggests ~ 80% phosphate removal through adsorption in these incubations at both pH 5.5 and 7.0 (Table 3.5), and solid-phase extractions (Figure 3.3A-B) confirm large quantities of phosphate associated with iron and manganese oxides in these sediments. Thus, sorption was likely primarily responsible for phosphate removal with less significant contributions from precipitation of U(VI)-phosphate minerals and assimilation by the natural microbial community.

3.5.3 Fate of Uranium

Although each treatment received a 300 µM U(VI) amendment, approximately 20% of uranium at pH 5.5 and less than 5% at pH 7.0 remained in solution initially in each reactor (Figure 3.2A). As ~ 95% of uranium removal between pH 5.5 and 7.0 is achieved through sorption in ORFRC soils (Barnett et al., 2000) and inorganic phosphate was initially unavailable to support U(VI) removal through the biomineralization of U(VI)-phosphate minerals, the initial uranium removal observed in all reactors can be

attributed to adsorption. Important sorbents in ORFRC sediments include predominantly ferric and aluminum oxides (Brooks, 2001), which display a pH_{zpc} around 7.0 (Hsi and Langmuir, 1985; Langmuir, 1997; Stumm and Morgan, 1996), and in less extent manganese oxides (Barnett et al., 2000), which display a pH_{zpc} ranging between 1.3 and 7.3 (Langmuir, 1997). Aluminum oxides, however, are less likely to be involved in the removal of uranium at pH greater than 4.0 in the presence of iron oxides (Zheng et al., 2003). Indeed, bulk uranium EXAFS of both pH 5.5 and pH 7.0 reactors demonstrate uranium associated with Mn and/or Fe phases (Table 3.3, 3.4). At pH 5.5, U(VI) carries a positive (UO_2^{2+}) or neutral ($UO_2CO_{3\,(aq)}$) charge (Table 3.5), making it less likely to adsorb to positively charged soils than negatively charged G2P or orthophosphates which strongly competes for soil sorption sites, especially given their high concentration. In fact, thermodynamic modeling predicts ~ 70% adsorption of U(VI) at pH 5.5 in the absence of phosphate (U-control) as compared to ~ 1% adsorption in the presence of 5 mM phosphate from organophosphate hydrolysis (G2P-treatments) (Table 3.5). At pH 7.0, U(VI) is primarily present as neutral [$Ca_2UO_2(CO_3)_3$] and negatively charged species ($CaUO_2CO_3^{2-}$) (Table 3.5), and G2P is totally deprotonated. As evidenced by the initial two-fold increase in dissolved G2P at pH 7.0 compared to pH 5.5 (Figure 3.1D), G2P adsorbs less efficiently at pH 7.0 when surface sites shift towards more negative values. Thus, the decreased sorption of G2P allows for more complete sorption of U(VI) species and is reflected in the four-fold decrease in aqueous uranium at pH 7.0 versus pH 5.5 initially (Figure 3.2A). In a similar fashion, the initial adsorption of U(VI) at pH 7.0 is much higher in the absence (U-control) than in the presence of organophosphate.

Examination of the removal of uranium as a function of time reveals interesting

features. At pH 5.5, two kinetically-controlled uranium removal phases are observed in all G2P-containing reactors (Figure 3.2) in agreement with previous studies that demonstrated rapid adsorption of U(VI) to ferrihydrite within the first few hours of equilibration at pH 5.0 is followed by a secondary removal phase that lasts several days (Waite et al., 1994). The first removal phase that occurs between 0 and 4 days could be attributed to the diffusion-limited sorption of uranium in the crystal lattice of minerals or pores of the soil matrix (Davis and Kent, 1990; Waite et al., 1994), as during that time period hydrolysis of G2P was not significant as indicated by the relatively constant concentration of G2P in solution and the lack of production of inorganic phosphates (Figure 3.1G). The second phase that occurs between 4 and 40 days is attributed to the precipitation of uranium phosphate controlled by the hydrolysis of G2P, as previously demonstrated in pure cultures incubations with an organism isolated from the same site (Beazley et al., 2007 and 2009) and supported by the decrease in G2P, the simultaneous production of dissolved phosphate after a small phase lag (Figure 3.1G), and the thermodynamic calculations that predict precipitation of almost all uranium as autunite mineral (Table 3.5). In pH 7.0 reactors containing G2P, only one uranium removal phase was observed (Figure 3.2), suggesting that uranium carbonate complexes, the dominant form of dissolved uranium in the absence of inorganic phosphate at that pH (Table 3.5), do not promote the diffusion-limited removal process observed in the pH 5.5 incubations. The slightly lower pseudo-first-order rate constants calculated for the removal of uranium at pH 7.0 compared the second uranium removal phase at pH 5.5 (Table 3.2) may be attributed to the stabilization of uranium in solution by carbonates. Overall, these data suggest that similar U(VI) removal mechanisms were ongoing in the pH 7.0 incubations.

Indeed, thermodynamic calculations predict the majority of uranium is precipitated under the form of autunite minerals (Table 3.5).

Bioreduction is a commonly observed removal pathway for U(VI) in anaerobic conditions. In this study, however, XANES data did not show evidence of U(VI) reduction regardless of pH, even after complete nitrate removal (Figures 3.5A and 3.6A). These findings suggest that U(VI) reduction was inhibited in these incubations. Similar results were observed in both pure culture systems and sediment microcosms. Both manganese (Liu et al., 2002) and ferrihydrite (Wielinga et al., 2000) were shown to inhibit uranium reduction by acting as competitive terminal electron acceptors in pure cultures, while calcium was shown to inhibit reduction of U(VI) in pure cultures through the formation of ternary $Ca\text{-}UO_2\text{-}CO_3$ complexes which are less energetically favorable terminal electron acceptors than free uranyl ions (Brooks et al., 2003). In addition, uranium reduction in ORFRC sediments commonly occurs concurrently with sulfate reduction (Akob et al., 2008; Cardenas et al., 2010; Kostka and Green, 2011; Luo et al., 2007a; Madden et al., 2009; Nyman et al., 2006; Wu et al., 2006b). Although the exact mechanism of this coupling is unknown, it has recently been suggested that the observed U(VI) reduction is driven by the formation of iron sulfides and subsequent sulfide-catalyzed chemical reduction of U(VI) to U(IV) (Hyun et al., 2012). As no sulfate reduction was observed in the present incubations and $Ca\text{-}UO_2\text{-}CO_3$ aqueous species are predicted to dominate the speciation of U(VI) in solution (Table 3.5), it is unlikely that uranium reduction occurred over the experimental time scale of 70 days. Finally, the chemical oxidants NO_2^-, Fe(III), and/or possibly MnO_2, which can re-oxidize uraninite in reducing conditions (Fredrickson et al., 2002; Moon et al., 2007; Senko et al., 2002;

Senko et al., 2005a; Senko et al., 2005b; Wan et al., 2005), were present in great excess in these incubations suggesting any reduced uranium would have been destabilized.

The biomineralization of U(VI)-phosphate minerals represents an alternative U(VI) removal mechanism and has been demonstrated in both pure culture (Beazley et al., 2007; Macaskie et al., 1995; Martinez et al., 2007; Montgomery et al., 1995) and soil studies (Beazley et al., 2011; Shelobolina et al., 2009). The observed G2P consumption and subsequent production of inorganic phosphate support the hypothesis that U(VI)-phosphate biomineralization is an important contributor to U(VI) removal in these experiments, and the lack of observed uranium reduction is indicative of the formation of more stable U(VI)-phosphate minerals (Beazley et al., 2007; Beazley et al., 2011; Shelobolina et al., 2009). In all incubations, solid-phase extractions revealed uranium primarily associated with phosphate minerals (acetate extractable fraction) and bound to iron/manganese oxides (hydroxylamine extracted) (Figure 3.4A-B). While this was expected for G2P-containing reactors, uranium in the U-amended controls was also found in the acetate extractable fraction. This discrepancy is likely due to precipitation of schoepite during the pH 7.0 $MgCl_2$ extraction step designed to desorb loosely bound uranium (not shown) and does not reflect actual precipitation of U(VI)-phosphate minerals in reactors unamended with G2P. Thermodynamic calculations and EXAFS data support the formation of U-P minerals at both pH 5.5 and 7.0 (Table 3.3, 3.4, and 3.5). Equilibrium calculations predict 99% of uranium precipitates under the form of autunite minerals at both pHs (Table 3.5), even when uranium phosphate ternary complexes are included in the model. Following incubation for 70 days at pH 5.5 and 7.0, the fit for all G2P-containing reactors was improved by the inclusion of a U-P scattering path to the

EXAFS fitting (Table 3.4, Figure 3.5B). In contrast, the fit was not improved by the addition of a U-P EXAFS scattering path for the sample taken from G2P-amended reactors prior to incubation, supporting the hypothesis that the initial uranium removal by adsorption was followed by the biomineralization of U(VI)-phosphate minerals.

These findings have important implications for the design and implementation of uranium remediation strategies in contaminated subsurface environments. First, U(VI) biomineralization promoted by G2P hydrolysis appears to outcompete U(VI) bioreduction in nitrate- and iron-rich environments. Almost complete uranium removal may be achieved in high nitrate conditions found at some radionuclide-contaminated sites without the preconditioning steps (i.e. nitrate removal and pH adjustments) required to promote U(VI) bioreduction (Wu et al., 2006a). Eliminating these conditioning steps may help minimize the cost of remediation. In contrast, if sulfate-reducing microorganisms are not stimulated by organophosphate addition, nor involved in organophosphate hydrolysis as suggested by the findings of this study, sulfate-reducing conditions promoted by endogenous electron donors should lead to formation of uraninite and other U(IV) mineral products. Finally, the low phosphate levels in most subsurface environments are likely to favor phosphatase activity by native subsurface microbial populations. The fact that such activity occurs under both aerobic (Beazley et al., 2011; Shelobolina et al., 2009) and anaerobic conditions (this study), coupled to the fact that uranium phosphate minerals are highly stable in a wide range of redox conditions compared to U(IV) minerals, indicate that biomineralization of U(VI)- phosphate minerals may be particularly useful at contaminated sites subject to fluctuating redox conditions.

3.6 Conclusions

The instability of uraninite, even under reducing conditions, generates the need for an alternative bioremediation strategy to decrease the solubility of uranium in contaminated environments. Biomineralization of U(VI)-phosphate minerals, a possible complementary technique to bioreduction, has been shown to be applicable in both reducing and oxidizing environments, and the ability of ORFRC microbial isolates to metabolize G2P in aerobic conditions has been demonstrated. In this study, the competition dynamic between U(VI) bioreduction, U(VI)-phosphate biomineralization, and adsorption in the presence of G2P and alternate terminal electron acceptors was studied in anaerobically-maintained ORFRC contaminated sediments at two different pHs to determine which respiratory process is promoted by G2P in these sediments and its influence on the fate of uranium.

The addition of G2P to ORFRC Area 3 sediments was sufficient to stimulate reduction of nitrate at both pH 5.5 and 7.0 but not sulfate, even after complete removal of nitrate, suggesting the lack of a suitable electron donor for sulfate-reducing bacteria in these incubations. Although more efficient at pH 7.0, anaerobic respiration of iron oxides occurred at both pHs, even in the presence of high nitrate concentrations, and appeared to be unaffected by the addition of G2P. In turn, nitrate reduction depended on G2P hydrolysis and was enhanced at circumneutral pH, suggesting that G2P availability in the dissolved phase may control the intensity of anaerobic nitrate respiration in these sediments. High nitrate reduction rates simultaneously impacted nitrite-reducing microorganisms significantly, likely via accumulation of the toxic nitrite in solution. Hydrolysis of G2P was much more significant than the availability of uranium at both

pHs, suggesting that the hydrolysis of organophosphate in these sediments was activated by phosphate or carbon limitations rather than a uranium detoxification mechanism. Finally, almost complete removal of uranium through a combination of adsorption and precipitation of uranium phosphate minerals was observed at both pHs. Overall, the results of this study not only suggest that biomineralization of U(VI)-phosphate minerals may be complementary to bioreduction, but also that U(VI)-phosphate biomineralization may be preferable to bioreduction in certain environments due to its utility in a wide range of chemical and redox conditions.

3.7 Acknowledgements

This research was supported by the Office of Science (BER), US Department of Energy Grant No. DE-FG02-04ER63906. Portions of this research were carried out at the Stanford Synchrotron Radiation Lightsource, a national user facility operated by Stanford University on behalf of the US Department of Energy, Office of Basic Energy Sciences. The SSRL Structural Molecular Biology Program is supported by the Department of Energy, Office of Biological and Environmental Research, and by the National Institutes of Health, National Center for Research Resources, Biomedical Technology Program. We thank Dave Watson of Oak Ridge National Laboratory for providing ORFRC sediment cores and Eric Roden for providing thermodynamic stability constants of glycerol phosphate adsorption onto iron oxides.

CHAPTER 4

URANIUM BIOMINERALIZATION PROMOTED BY MICROBIALLY-MEDIATED PHYTATE HYDROLYSIS IN SUBSURFACE SOILS

Reproduced with permission from Kathleen R. Salome, Melanie J. Beazley, Samuel M. Webb, Patricia A. Sobecky, and Martial Taillefert
Submitted to *Environmental Science and Technology*, March 2013.

4.1 Abstract

The low solubility of uranium phosphate minerals makes them good candidates for the immobilization of U(VI) in contaminated environments. As inorganic phosphate is generally scarce in soils, the biomineralization of U(VI)-phosphate minerals via microbially-mediated organophosphate hydrolysis represents an attractive bioremediation strategy. In this study, contaminated soils were incubated aerobically in two pH conditions to examine the potential of utilizing phytate, a naturally-occurring and abundant organophosphate in soils, as a phosphorous source to promote U(VI)-phosphate biomineralization by natural microbial communities. While phytate hydrolysis was not evidenced at pH 7.0, complete hydrolysis was observed both with and without electron donor at pH 5.5, suggesting indigenous microorganisms express acidic phytases in these soils. The presence of uranium accelerated phytate hydrolysis and decreased the rate of hydrolysis of inositol intermediates as a result of a possible toxicity effect on the indigenous population. The abundant production of inorganic phosphate drastically decreased uranium solubility via formation of ternary sorption complexes and

precipitation of U(VI)-phosphate minerals. Overall, the results of this study demonstrate the ability of natural microbial communities to liberate phosphate from phytate in acidic soils and the potential utility of phytate-promoted biomineralization of U(VI)-phosphate minerals as a uranium immobilization strategy.

4.2 Introduction

Since the end of the cold war era, the Department of Energy (DOE) has shifted its focus from nuclear weapons proliferation to remediation of radionuclide and heavy metal contaminations found at its facilities across the United States (DOE, 1997), including the Oak Ridge Field Research Center (ORFRC) in Oak Ridge, TN. For over 30 years, four unlined storage ponds at the ORFRC received over 10 million liters of waste per year from uranium enrichment processes, resulting in a large volume of groundwater and soil contaminated with depleted uranium, nitric acid, heavy metals, and radionuclides (Brooks, 2001; Jardine, 2006). The numerous toxic contaminants at the ORFRC along with the sheer volume of contaminated geomedia command the development of creative *in situ* remediation solutions for environmental uranium contaminations (Istok et al., 2004; Kelly et al., 2008; North et al., 2004; Sitte et al., 2010; Van Nostrand et al., 2011; Wu et al., 2006a; Wu et al., 2006b).

The mobility of uranium in the subsurface is controlled by a combination of surface complexation reactions, precipitation reactions, and redox processes (Finch and Murakami, 1999b; Hsi and Langmuir, 1985; Langmuir, 1997). Uranium exists primarily as U(IV) or U(VI) depending on the prevailing environmental redox conditions. In reducing conditions, U(VI) may either be chemically or biologically reduced to U(IV) and precipitate as uraninite ($UO_{2(s)}$) (Finch and Murakami, 1999b; Langmuir, 1997) or

other non-uraninite U(IV) minerals (Boyanov et al., 2011; Fletcher et al., 2010). Despite recent studies demonstrating biogenic uraninite may be more stable than abiotically formed uraninite (Sharp et al., 2011; Ulrich et al., 2009), the presence of NO_2^- (Beller, 2005; Moon et al., 2007; Wu et al., 2010), Fe(III) (Senko et al., 2002; Senko et al., 2005b; Wan et al., 2005), or MnO_2 (Fredrickson et al., 2002) in reducing conditions or the reintroduction of oxygen (Langmuir, 1997; Murphy and Shock, 1999) may remobilize uraninite to soluble U(VI) species. In oxidizing conditions, U(VI) exists as the aqueous uranyl ion UO_2^{2+} and its hydroxyl complexes. Above pH 7.0, carbonates may enhance uranyl mobility by forming soluble uranyl-carbonate complexes and promoting the dissolution of U(IV) and U(VI) minerals (Langmuir, 1978, 1997). Contrastingly, below circumneutral pH, strong sorption to metal oxides and clays and the formation of highly stable and sparingly soluble precipitates with phosphate may limit uranyl mobility in the environment (Finch and Murakami, 1999b; Langmuir, 1997).

Thus far, *in situ* bioremediation of uranium contaminations has primarily focused on uraninite mineral formation via microbially-catalyzed reduction of U(VI), known as bioreduction (Istok et al., 2004; Lovley et al., 1991; North et al., 2004; Wade and DiChristina, 2000; Wu et al., 2006b). Unfortunately, the low pH, elevated nitrate, and oxidizing conditions present in the ORFRC subsurface may inhibit this process (Finneran et al., 2002b; Wu et al., 2006a; Wu et al., 2006b), making the precipitation of U(VI)-phosphate minerals a potentially appealing alternative to bioreduction at this site. As orthophosphate directly amended to the subsurface rapidly precipitates thus limiting substrate transport (Wellman et al., 2006), research has focused on the addition of organophosphates to subsurface sediments to promote microbially-mediated

organophosphate hydrolysis coupled to the chemical precipitation of sparingly soluble U(VI)-phosphate minerals in a process termed biomineralization (Beazley et al., 2007, 2009; Beazley et al., 2011; Macaskie et al., 1994; Shelobolina et al., 2009). To fulfill their phosphorus requirement when faced with nutrient limitations, microorganisms encode genes for various phosphohydrolase (phosphatase) enzymes to catalyze the hydrolysis of organophosphates and acquire orthophosphate (Macaskie et al., 1994). In addition, uranium stress may induce microbial phosphatase expression as a metal detoxification mechanism (Barnett et al., 2002; Knox et al., 2008; Macaskie et al., 1994). Although previous research has demonstrated U(VI)-phosphate precipitation coupled to microbial hydrolysis of predominantly synthetic organophosphates (Beazley et al., 2007, 2009; Beazley et al., 2011; Martinez et al., 2007; Shelobolina et al., 2009), the efficacy of utilizing naturally-occurring organophosphates to promote U(VI)-phosphate biomineralization has not been demonstrated.

Inositol hexaphosphate (IP_6), also known as phytate, is a phosphorylated inositol with six attached phosphate groups that is widely synthesized by plants for phosphorus storage and, therefore, represents the dominant organophosphate in most terrestrial environments (Turner et al., 2002). Although IP_6 remains chemically stable at all environmentally relevant pH and is not hydrolyzed by conventional phosphohydrolases (Turner et al., 2002), phytase enzymes may catalyze its hydrolysis to lower inositol derivatives (IP_X, x : 1 - 5) and inorganic phosphate (Irving and Cosgrove, 1974). Phytase enzymes are substrate-specific phosphatases of bacterial, fungal, or plant origin and are designated as either acidic or alkaline depending on their optimal pH for catalytic activity (Oh et al., 2004). Because of its highly negative charge above pH 2 (Figure

4.1a), phytate interacts strongly with soils (Degroot and Golterman, 1993; Johnson et al., 2012) and efficiently chelates metals to form sparingly soluble complexes (Martin and Evans, 1987; Turner et al., 2002). While the use of phytate to chemically precipitate U(VI) has been investigated (Knox et al., 2008; Nash et al., 1998; Seaman et al., 2003), the microbially-facilitated precipitation of U(VI)-phosphate minerals by phytate-mineralizing bacteria has yet to be examined. The objectives of this study were to investigate the phytase activity of the natural microbial community in pH conditions representative of ORFRC soils, examine the dependence of phytase activity on the addition of an electron donor, and determine the geochemical conditions required to induce U(VI)-phosphate biomineralization coupled to microbial phytase activity.

4.3 Materials and Methods

All experiments were conducted in artificial groundwater (Table B.1, Appendix B) buffered at either pH 5.5 or pH 7.0 with 50 mM 2-(N-Morpholino)ethanesulfonic acid (pH 5.5) or 50 mM 4-(2-hydroxyethyl)-1-piperazineethanesulfonic acid (pH 7.0).

4.3.1 Abiotic Precipitation of U(VI)-Phytate

To ensure phytate does not abiotically precipitate with uranium in the conditions of these incubations, triplicate solutions of 200 µM uranyl acetate (Spectrum) was equilibrated for 48 hours with 0, 0.05, 0.1, 0.2, 0.6, 1.0, 3.0, 5.0, and 10 mM Na-IP_6 (Sigma Aldrich) in artificial groundwater buffered at either pH 5.5 or pH 7.0. After equilibration, a small aliquot was filtered through a 0.2 µm pore size polyethersulfone (PES) membrane filter (Puradisc, Whatman) and preserved in 2% trace metal grade nitric acid for uranium analysis.

4.3.2 Soil Slurry Incubations

To assess the phytase activity of the natural microbial community, ORFRC contaminated soils (well number: FWB134-08-03, core depth: 6.5-7.5 m) collected during installation of a monitoring well in Area 3 were incubated in triplicate with artificial groundwater. Area 3 soils are located closest to the waste disposal ponds and are generally characterized by low pH and high nitrate levels (Brooks, 2001) as well as significant concentrations of Mn (0.36 g/kg) and Fe (25.8 g/kg) (Barnett et al., 2000). Soils were stored in the dark at 4°C and remained sealed until incubation at pH 5.5 and 7.0. In each treatment, homogenized soil was combined with filter-sterilized artificial groundwater (16 g/L) buffered at either pH 5.5 or 7.0. Incubation treatments included inositol hexaphosphate (Sigma Aldrich), glycerol (OmniPur) as electron donor, and uranyl acetate (Spectrum) as follows: 10 mM phytate only; 10 mM phytate and 10 mM glycerol; 10 mM phytate and 200 µM U(VI); or 10 mM phytate, 10 mM glycerol, and 200 µM U(VI). In addition, pH 7.0 incubations contained 10 mM $NaHCO_3$ to inhibit schoepite precipitation. Triplicate reactors were maintained aerobically (Martinez et al., 2007) in the dark and were agitated at 200 rpm and 30 °C using a Lab-Line 3525 shaker incubator. At each time point, part of a filtered aliquot (0.2 µm, PES Puradisc, Whatman) was preserved in 2% trace metal grade nitric acid for uranium analysis, and the remainder was frozen until analysis of inorganic phosphate (ΣPO_4^{3-}) and inositol phosphates. Following incubation, soils were collected and divided for characterization by solid-phase sequential extraction and X-ray absorption spectroscopy (XAS). Samples for XAS were preserved at -80°C in 50 mL centrifuge tubes until transport to the Stanford Synchrotron Radiation Lightsource (SSRL). Just before analysis, soils were

thawed, loaded into windowed Lexan sample holders, and sealed with Kapton tape.

4.3.3 Analytical Techniques

Dissolved uranium was measured with an Agilent 7500a Series inductively-coupled plasma mass spectrometer (ICP-MS) and ΣPO_4^{3-} was quantified by ion chromatography using previously described analytical procedures to ensure data accuracy and precision (Salome et al., 2013). Errors reported for uranium and phosphate measurements represent the standard deviation between triplicate incubations and the analytical error on duplicate measurements. Inositol hexaphosphate, inositol pentaphosphate (IP_5), inositol tetraphosphate (IP_4), inositol triphosphate (IP_3), and inositol bisphosphate (IP_2) (standards from Sigma Aldrich) were quantified using a modified chromatographic separation coupled to suppressed spectrophotometric detection at 500 nm (Rounds and Nielsen, 1993) with a Dionex ICS-3000 dual pump chromatography system. Separation was achieved with an OmniPac PAX-100 guard column (4 x 40 mm), and eluent flow conditions included a 23 minute linear gradient (0.5 mL/min) from 0.01 M 1-methylpiperazine (pH 4.0) to 0.38 M $NaNO_3$ in 0.01 M 1-methylpiperazine (pH 4.0). Following separation, 0.015% (w/v) $FeCl_3 \bullet 6H_2O$ in 0.15% (w/v) sulfosalicylic acid (pH 1.8) was introduced (0.5 mL/min) as post-column reagent through a reaction coil to ensure thorough mixing. Reported errors for IP_x (x = 1:6) species include analytical error and standard variation between triplicate incubations.

Solid phase uranium in soils collected following 16 days of incubation were quantified using a modified sequential extraction technique (1979). The following procedure was performed sequentially: (1) 1.0 M $MgCl_2$ in 10 mM nitrilotriacetic acid (NTA) (pH 4.5) was added and agitated at 20°C for 1 hour to extract the loosely adsorbed

fraction; (2) 1.0 M acetic acid (pH 5.0) was added and agitated at 20°C for 5 hours to dissolve uranium minerals; (3) 0.04 M NH_2OH • HCl in 25% (v/v) Acetic Acid was agitated at 96°C for 6 hours to remove Fe- and Mn-associated uranium; (4) 1.5 mL of 0.02 M HNO_3 and 2.5 mL of 30% H_2O_2 (pH 2.0) were agitated at 96°C for 2 hours, a second 1.5 mL aliquot of 30% H_2O_2 (pH 2.0) was added and agitated at 96°C for 3 hours, and a third 5 mL aliquot of 2.5 M NH_4OAc in 20% (v/v) HNO_3 was agitated at 20°C for 1 hour to extract the uranium fraction bound to organics; and (5) 15.8 M HNO_3 at 85°C was reacted for 3 hours to extract the residual fraction. After each extraction step, samples were centrifuged, and supernatants were filtered (0.2 µm, PES Puradisc Whatman) and reserved for uranium analysis by ICP-MS.

Soil samples after 16 days of incubation were characterized by XAS at the Stanford Synchrotron Radiation Lightsource (SSRL). Uranium L_{III}-edge XAS spectra were collected at SSRL beam line 4-1 using a focused X-ray beam with a 23 keV harmonic rejection cutoff and a 13 element Ge detector. The incident energy was selected with a Si(220) monochromator crystal and data was collected using fluorescence detection. Extended X-ray absorption fine structure (EXAFS) data for each incubation treatment was fitted using SIXPACK (Webb, 2005). Phase and amplitude files for EXAFS fittings were created with FEFF7 (Ankudinov et al., 1998; Zabinsky et al., 1995). The axial oxygen coordination number (N) for all modeled treatments was set at two. Since the Debye-Waller factors (σ) correlated highly with coordination numbers (N), σ's for some shells were each fixed at their average values, and the U═Oax═U═Oax transoxido multiple scattering path (Hudson et al., 1996) was included in all fits. Due to the similar backscattering intensities and phases of Mn and Fe in

EXAFS, a "sum" of Fe/Mn like neighbors was reported for all treatments rather than distinct Fe and Mn shells (Salome et al., 2013).

4.4 Results and Discussion

4.4.1 Abiotic Precipitation of Uranium and IP_6

In natural waters (pH 2-10), phytate carries a highly negative charge of between -6 and -9 (Figure 4.1a) and, thus, is expected to interact strongly with positively charged uranyl hydroxide complexes at or below circumneutral pH (Turner et al., 2002). Equilibration of increasing concentrations of phytate with 200 µM uranium revealed concentration-dependent uranyl solubilities at both pH 5.5 and 7.0 (Figure 4.1b), likely due to the highly negative charge of IP_6 at both pHs (Figure 4.1a). At $[IP_6]$:[U] ratios below 15:1, uranium formed precipitates with IP_6 at both pH 5.5 and 7.0 (Figure 4.1b). At or above $[IP_6]$:[U] ratios of 15:1, however, uranium predominantly remained in solution at both pHs (Figure 4.1b). Previous studies have demonstrated similar concentration-dependent uranyl solubility in the presence of other organophosphates (Beazley et al., 2007), and the increase in uranium solubility with elevated organophosphate concentration is thought to be caused by enhanced steric hindrance as organophosphate concentration increases. These findings have important implications for promotion of U(VI)-phosphate biomineralization by phytate, as the $[IP_6]$:[U] ratio likely determines whether chemical (low concentrations of phytate) or biological (high concentrations of phytate) sequestration processes will dominate.

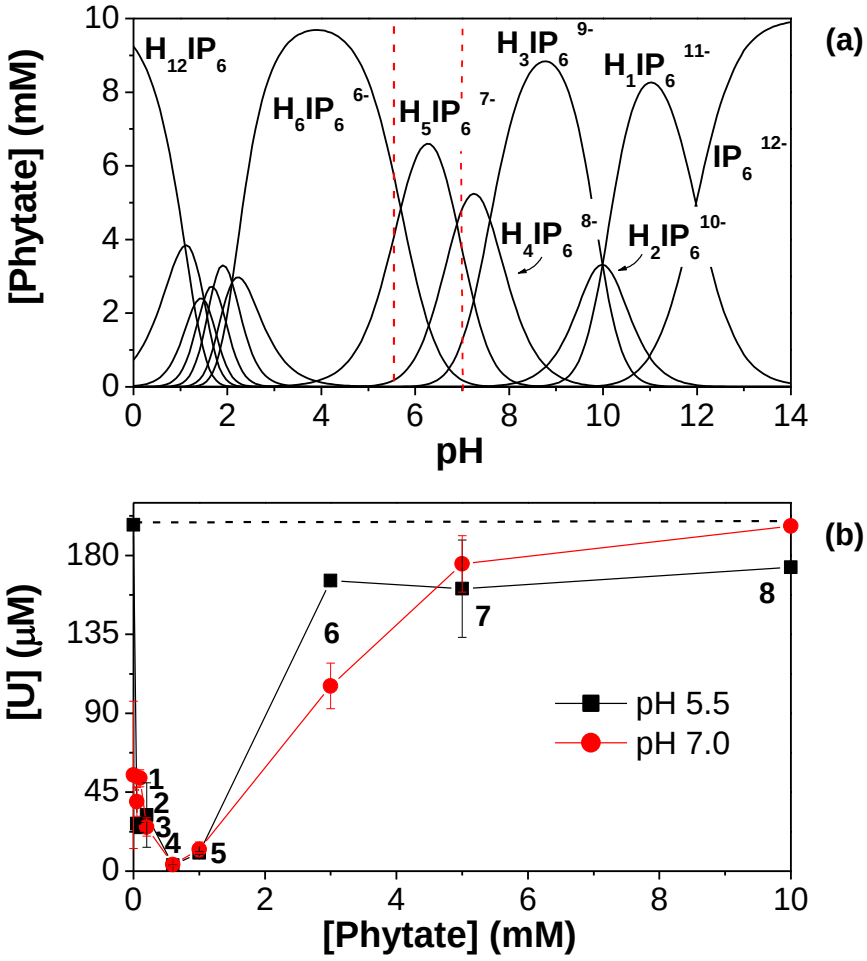

Figure 4.1 (a) Phytate (IP_6) speciation as a function of pH as calculated by MINEQL+ (Schecher and McAvoy, 2001) using pK_a values reported in Costello et al. (1976). Total phytate concentrations set at 10 mM. Vertical dashed lines represent the experimental conditions of the present study. (b) Uranium solubility in the presence of increasing concentrations of phytate at both pH 5.5 (black squares) and 7.0 (red circles) in artificial groundwater equilibrated for 1 week. Initial uranium concentration was 200 µM in all experiments (horizontal dashed line), and error bars represent variation between triplicate experiments and analytical error on duplicate measurements. Labels 1, 2, 3, 4, 5, 6, 7, and 8 represent [IP_6]:[U] molar ratios of 1:4, 1:2, 1:1, 3:1, 5:1, 15:1, 25:1 and 50:1.

4.4.2 Activities of Natural Phytases

All pH 5.5 soil slurry incubations amended with phytate liberated inorganic phosphate, although at different rates and to different extents depending on the treatment (Figure 4.2), suggesting phytate hydrolysis likely induced by phosphate starvation conditions (Mukhametzyanova et al., 2012) in these experiments. Interestingly, no inorganic phosphate was detected in any pH 7.0 reactor treatment (Figure 4.2), and IP_6 concentrations remained constant at ~ 9 mM in all pH 7.0 phytate-amended reactors over the duration of the incubations (Figure 4.3a-4.3d). These results indicate either that phytate hydrolysis is inhibited at pH 7.0 and phytate (~1 mM) is simply removed by adsorption onto ORFRS soils, or that phytate hydrolysis is limited (< 1 mM) and the inorganic phosphate released is consumed by incorporation into biomass or sorption onto the solid phase. As phytate adsorbs strongly to iron oxides at this pH (Degroot and Golterman, 1993; Johnson et al., 2012), it should outcompete inorganic phosphate for soil sorption sites (Degroot and Golterman, 1993). Thus, the more likely explanation for the observed phytate consumption in pH 7.0 incubations is an apparent lack of phytate hydrolysis at this pH. These findings, therefore, suggest that phytate hydrolysis by the ORFRC natural microbial community may be pH dependent, which is not surprising as phytase enzymes active at acidic and circumneutral and/or alkaline pH are expressed by different genes and display different catalytic mechanisms (Oh et al., 2004). In addition, alkaline phytase enzyme function could have been limited by the low concentration of calcium (200 µM) in the artificial groundwater (Ha et al., 2000).

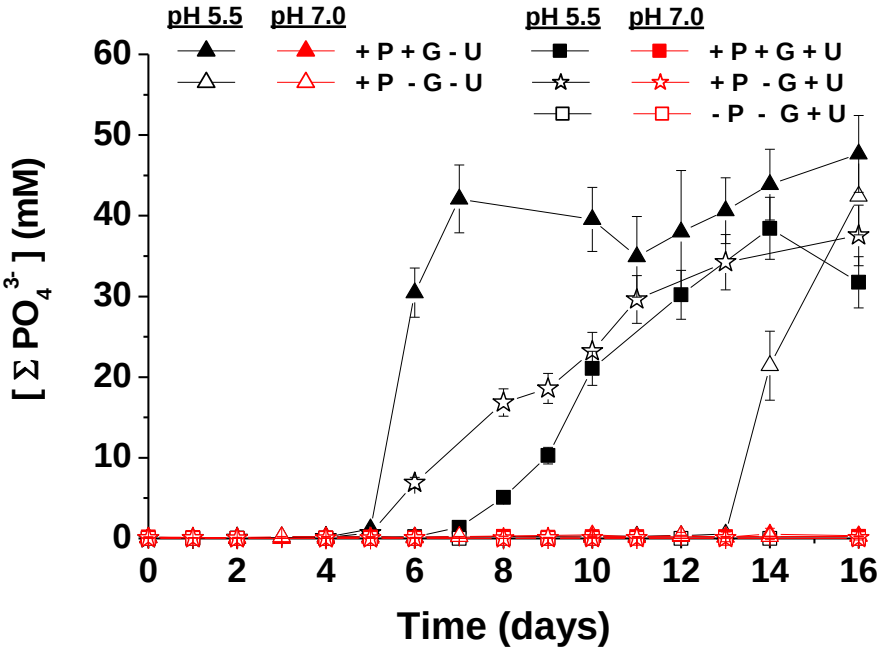

Figure 4.2 Evolution of inorganic phosphate (ΣPO_4^{3-}) as a function of time in pH 5.5 (black) and pH 7.0 (red) soil slurries containing 16 g/L Area 3 Oak Ridge Field Research Center soils and artificial groundwater amended with 10 mM phytate and 10 mM glycerol (+ P + G – U); 10 mM phytate only (+ P - G – U); 10 mM phytate, 10 mM glycerol, and 200 µM UO_2^{2+} (+ P + G + U); 10 mM phytate and 200 µM UO_2^{2+} (+ P - G + U) and 200 µM UO_2^{2+} only (- P - G + U). Closed symbols represent slurries amended with glycerol and triangles represent slurries without uranium. Error bars include variation between triplicate reactors and the analytical error on duplicate measurements.

An 8 day difference in lag phase for the initial release of extracellular phosphate was observed in pH 5.5 reactors amended with phytate and glycerol but no uranium compared to identical reactors amended with phytate only (Figure 4.2). As only endogenous electron donors were available in incubations without glycerol, the activity of the natural microbial community was likely stimulated by glycerol addition resulting in earlier phytate mineralization. Once this initial limitation was overcome, however, inorganic phosphate was liberated at a comparable net rate in reactors amended with phytate and glycerol (20.5 ± 5.1 mM d^{-1}) and reactors amended with phytate but no

external electron donor (13.5 ± 2.6 mM d^{-1}) (Figure 4.2), suggesting a similar organophosphate hydrolysis pathway in each of these conditions. As expected, the accumulation of aqueous orthophosphate coincided with consumption of IP_6 in both treatments (Figure 4.3a-4.3b), confirming the existence of phytase-producing subsurface microorganisms at the ORFRC. Mass balance considerations indicate that the sole inositol phosphate species not analyzed (IP_1) did not constitute a significant fraction of inositol phosphate intermediates in these incubations (1-12% of total P). Interestingly, despite displaying similar net orthophosphate production rates, the IP_6 consumption rate in pH 5.5 reactors with phytate and glycerol (2.5 ± 0.58 mM d^{-1}) was much higher than in identical reactors without exogenous electron donor (0.92 ± 0.22 mM d^{-1}). In addition, intermediate inositol phosphates did not accumulate significantly in these conditions (Figure 4.3a-4.3b). The similar orthophosphate production rates together with the different IP_6 consumption rates and the lack of accumulation of intermediate inositol phosphate in pH 5.5 phytate-amended incubations without uranium suggests that phosphate production was controlled by the hydrolysis of intermediate inositol phosphates independently from electron donor availability. While IP_6 hydrolysis requires catalysis by phytase enzymes (Irving and Cosgrove, 1974), hydrolysis of lower inositol phosphates may be catalyzed by phytase enzymes and/or non-specific phosphomonoesterase (phosphatase) enzymes (Turner et al., 2002). If phytase enzymes were primarily responsible for dephosphorylation of all inositol phosphates, each dephosphorylation step should likely be equally affected by electron donor concentrations. Thus, the almost complete lack of intermediate inositol phosphates (i.e. IP_2 – IP_5) in phytate-amended incubations without uranium (Figure 4.3a-4.3b) may

reflect the adaptability of the microbial community in these conditions and possibly suggests that phytase enzyme production drives the conversion of IP_6 to IP_5 and initiates glycerol-independent phosphatase enzyme production that facilitates dephosphorylation of intermediate inositol phosphate species.

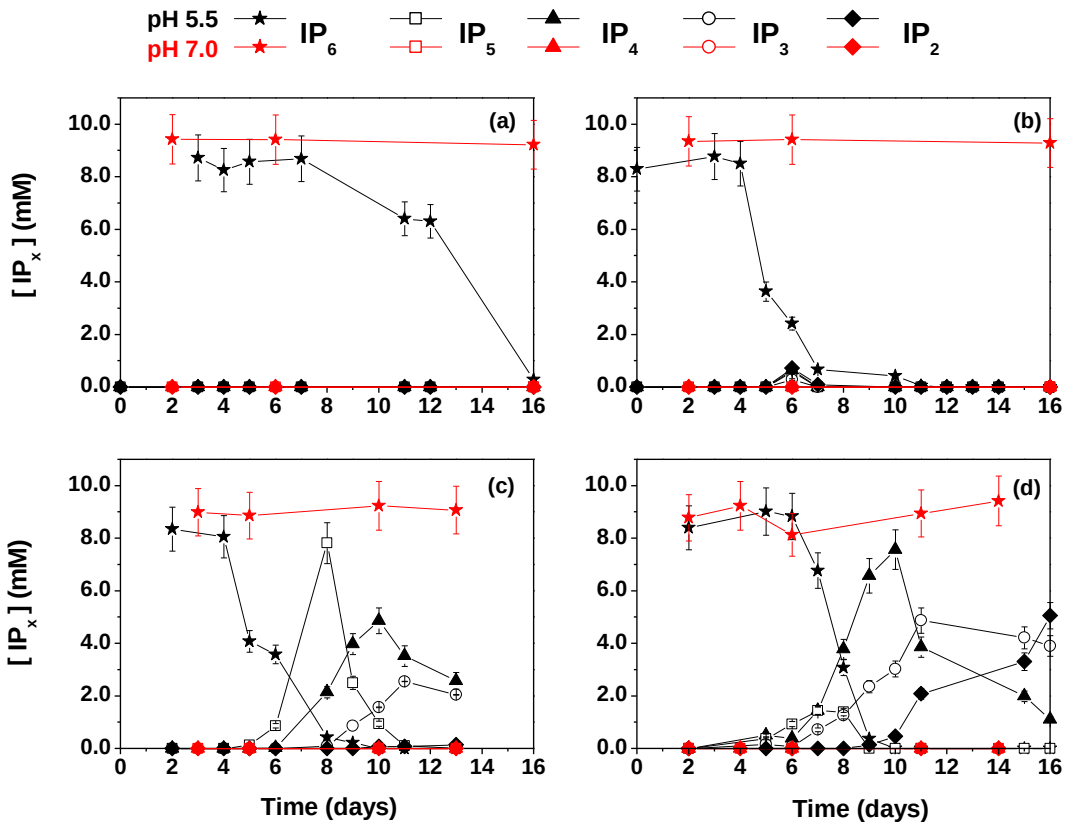

Figure 4.3 Evolution of inositol hexaphosphate (IP_6) and its lower derivatives (IP_x, x = 2:5) as a function of time in pH 5.5 (black) and pH 7.0 (red) slurries containing 16 g/L Area 3 Oak Ridge Field Research Center soils in artificial groundwater amended with a) 10 mM phytate; b) 10 mM phytate and 10 mM glycerol; c) 10 mM phytate, and 200 µM UO_2^{2+}; and d) 10 mM phytate, 10 mM glycerol, and 200 µM UO_2^{2+}. Reactors buffered at pH 7.0 were also amended with 10 mM dissolved inorganic carbon. Error bars include variation between triplicate reactors and analytical error from calibrations.

Surprisingly, the difference in lag phase for the onset of inorganic phosphate production between phytate-amended reactors with and without glycerol at pH 5.5 was eliminated upon introduction of 200 μM U(VI) (Figure 4.2). In fact, orthophosphate production in uranium-amended reactors containing phytate but no exogenous electron donor began 2 days before uranium-amended reactors containing both phytate and glycerol (Figure 4.2). Additionally, IP_6 consumption rates in uranium-amended reactors with phytate but no glycerol doubled (1.7 ± 0.38 mM d^{-1}) compared to identical reactors without uranium (0.92 ± 0.22 mM d^{-1}) at pH 5.5 (Figure 4.3a, 4.3c), while IP_6 consumption rates in phytate-amended reactors with glycerol and uranium (2.9 ± 0.21 mM d^{-1}) were comparable to identical reactors without uranium (2.5 ± 0.58 mM d^{-1}). Previous studies have proposed microbial phosphatase overexpression as a heavy metal detoxification mechanism in contaminated environments (Macaskie et al., 1994; Montgomery et al., 1995; Powers et al., 2002; Sobecky et al., 1996; Yong and Macaskie, 1995), and the increase in IP_6 consumption rate combined with the disappearance of the lag phase for the onset of orthophosphate production upon uranium addition suggest that microbial communities might have responded to this combined stress by expressing phytase. The increased production of phytase by ORFRC microorganisms in the presence of glycerol but no uranium, however, indicates that electron donor limitation may also affect bacterial metabolism.

Net orthophosphate production rates in pH 5.5 reactors containing both phytate and uranium decreased by more than threefold compared to identical reactors without uranium, regardless of the presence of external electron donor (Figure 4.2). This effect was probably due to an alteration of the hydrolysis kinetics of IP_5 through IP_2 in the

presence of uranium as evidenced by the significant accumulation of intermediate inositol phosphates in these conditions (Figure 4.3c-4.3d) compared to identical incubations without uranium (Figure 4.3a-4.3b). The decreased transformation rates of the intermediate inositol phosphates in the presence of uranium at pH 5.5 suggest an apparent uranium toxicity effect on the ORFRC microbial community possibly expressed either through the inhibition of phosphatase production and/or activity or through a shift in the dominant enzyme catalyzing IP_x (x = 1:5) hydrolysis from phosphatase to phytase. Given the complexity of the production and consumption kinetics of intermediate inositol phosphates, it is unlikely to distinguish between these two possible explanations for the observed decrease in IP_x (x = 2:5) transformation rates.

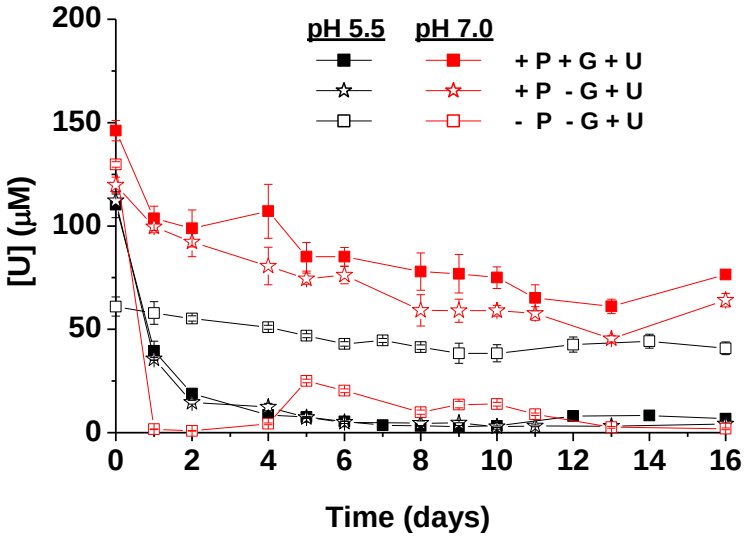

Figure 4.4 Evolution of dissolved uranium as a function of time in pH 5.5 (black) and pH 7.0 (red) soil slurries containing 16 g/L Area 3 Oak Ridge Field Research Center soils and artificial groundwater amended with 10 mM phytate, 10 mM glycerol, and 200 µM UO_2^{2+} (+ P + G + U); 10 mM phytate and 200 µM UO_2^{2+} (+ P - G + U); and 200 µM UO_2^{2+} only (- P - G + U). All pH 7.0 reactors also received 10 mM dissolved inorganic carbon (DIC). Closed symbols represent slurries amended with glycerol. Error bars represent variation between triplicate reactors and include the analytical error on duplicate measurements.

4.4.3 Fate of Uranium

Although 200 µM U(VI) was introduced into each uranium-amended reactor, significantly less dissolved uranium was measured within minutes after inoculation (Figure 4.4). Only 60 µM aqueous uranium was detected after 30 minutes in the pH 5.5 incubations without phytate, indicating that ~ 70% of uranium was immediately removed from solution by soil sorption. In comparison, the presence of 10 mM phytate at pH 5.5 resulted in a higher initial dissolved uranium concentration (110 µM), partly because uranium solubility is enhanced by formation of uranium-phytate complexes in these conditions (Figure 4.1b). As phytate is highly negatively charged at pH 5.5 (Figure 4.1a) and adsorbs strongly and irreversibly to iron oxides (Degroot and Golterman, 1993; Johnson et al., 2012), the apparent sorption of ~1 mM phytate initially (Figure 4.3a-4.3d) may have provided an additional mechanism to prevent adsorption of uranium onto the solid phase. Uranium concentrations in control incubations at pH 5.5 decreased only slightly from their initial values over the first 8 days (Figure 4.4), suggesting that uranium sorption was initially fast but incomplete. Contrastingly, 97% of the initial aqueous uranium was seemingly titrated from solution during early production of inorganic phosphate (Figure B.1) by day 8 in pH 5.5 incubations containing uranium, regardless of the presence of electron donor (Figure 4.4). This enhanced uranium removal could be attributed to the formation of stable U(VI)-phosphate minerals (Beazley et al., 2007; Beazley et al., 2011; Shelobolina et al., 2009), as ~ 40 mM inorganic phosphate was produced from IP_x (x = 1:6) hydrolysis (Figure 4.2) and/or the precipitation of U(VI)-IP_x minerals (Knox et al., 2008; Nash et al., 1998; Seaman et al., 2003) which may be further transformed to U(VI)-phosphate minerals (Nash et al., 1998). Indeed, thermodynamic equilibrium calculations detailed in the supplementary material (Table B.2, Appendix B)

predict that 100% of uranium should be precipitated as autunite at pH 5.5 given the degree of orthophosphate production in this system.

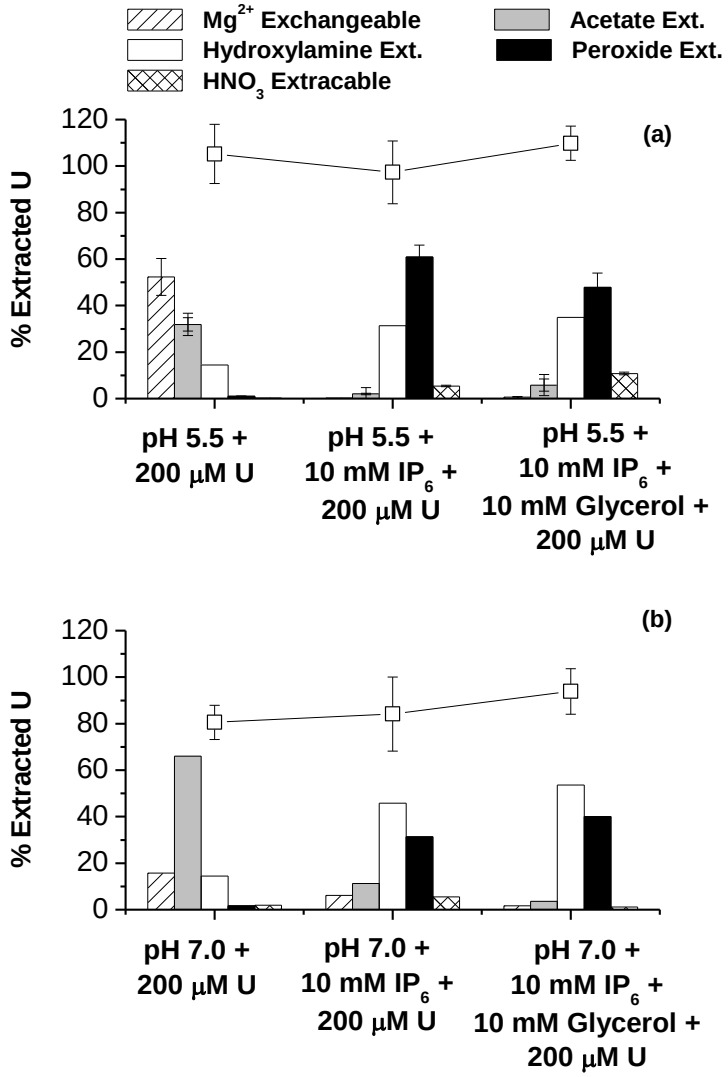

Figure 4.5 Solid phase-associated U in pH 5.5 (a) and pH 7.0 (b) soils after 16 days of incubation extracted using a modified sequential extraction technique of Tessier (1979). Bars represent the fraction of U extracted during each individual extraction step relative to total extracted uranium in each treatment. Symbols represent the percent uranium recovered in each treatment. All error bars include the variation between triplicate reactors and duplicate extractions.

In pH 7.0 reactors amended with 200 µM U(VI), aqueous uranium concentrations averaged ~130 µM initially and were not significantly affected by the presence or absence of phytate (Figure 4.4), likely due to the formation of uranium-carbonate complexes which inhibit sorption (Katsoyiannis, 2007). After the initial sampling point, however, aqueous uranium in pH 7.0 reactors without phytate decreased to 2 µM, probably due to the precipitation of thermodynamically favored schoepite in these conditions despite the addition of 10 mM carbonate (Table B.2, Appendix B). This drastic drop in aqueous uranium concentration was followed at day 5 by a brief remobilization and gradual removal down to 2 µM by the end of the incubations (Figure 4.4). Contrastingly, in all pH 7.0 reactors containing both uranium and phytate, dissolved uranium gradually decreased from 130 µM to 70 µM over the duration of the incubations (Figure 4.4). Combined with the lack of phytate hydrolysis (Figure 4.2 and 4.3a-4.d), these findings indicate the formation of aqueous U(VI)-phytate complexes increases uranium solubility by inhibiting uranium adsorption to ORFRC soils or sequestration via schoepite precipitation. Overall, the enhanced removal of dissolved uranium in phytate-amended reactors at pH 5.5, which displayed significant inorganic phosphate production from IP_6 hydrolysis compared to identical reactors at pH 7.0, demonstrates the efficiency of U(VI)-phosphate biomineralization promoted by phytase enzyme expression in low pH ORFRC soils.

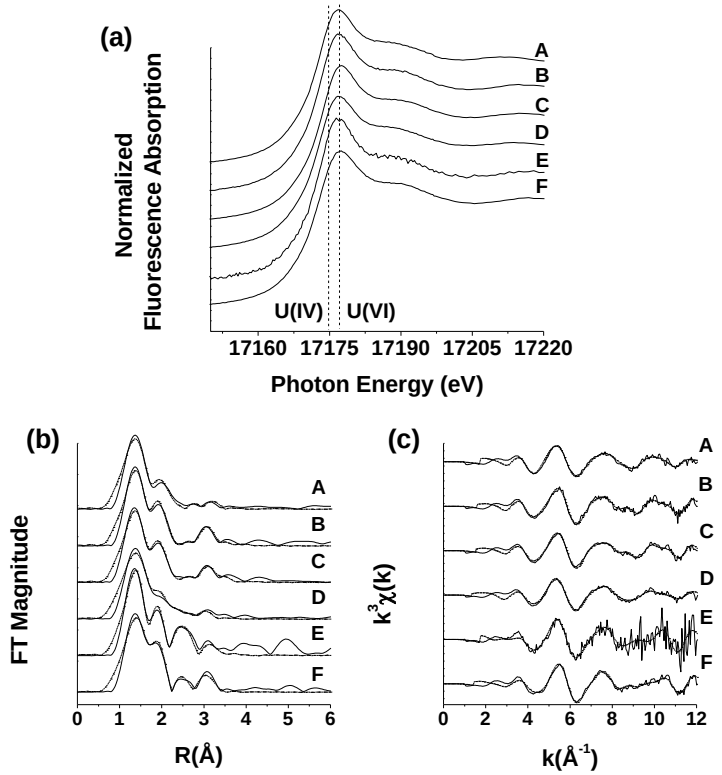

Figure 4.6 Uranium (a) XANES, (b) R-space, and (c) k-space diagrams of the L_{III}-edge EXAFS obtained from Area 3 soils of the Oak Ridge Field Research Center following aerobic incubation in soil slurries for 16 days at pH 5.5 and 7.0. Treatments included A: pH 5.5, 200 µM U; B: pH 5.5, 200 µM U + 10 mM IP_6; C: pH 5.5, 200 µM U + 10 mM IP_6 + 10 mM glycerol; D: pH 7.0, 200 µM U; E: pH 7.0, 200 µM U +10 mM IP_6; and F: pH 7.0, 200 µM U + 10 mM IP_6 + 10 mM glycerol.

4.4.4 Solid-phase Uranium Characterization

Sequential extractions of ORFRC sediments incubated at pH 5.5 and 7.0 in the presence of elevated uranium concentrations reveal a significant shift in solid-phase uranium speciation between slurries with and without phytate (Figure 4.5a, 4.5b). Without phytate, uranium was primarily associated with Mg^{2+} exchangeable, acetate extractable, and hydroxylamine extractable fractions at both pH 5.5 and 7.0 (Figure 4.5a, 4.5b), indicating the presence of loosely sorbed uranium species and uranium precipitates (i.e. schoepite) that is supported by thermodynamic predictions (Table B.2, Appendix B).

Interestingly, solid-phase uranium speciation shifts towards the more recalcitrant hydroxylamine extractable and peroxide extractable fractions upon introduction of phytate at both pHs (Figure 4.5a, 4.5b), indicating phytate addition triggers a change in the dominant uranium removal mechanism even when inorganic phosphate is not produced. Previous studies investigating U(VI)-phosphate biomineralization also demonstrated significant hydroxylamine-extractable uranium in Oak Ridge soils containing U(VI)-phosphate precipitates attributable either to the presence of strongly sorbed U(VI) or U(VI)-phosphate precipitates incorporated into iron oxides (Beazley et al., 2011; Salome et al., 2013). In the present incubations, the initial adsorption of both phytate (Figure 4.3a-4.3d) and uranium (Figure 4.4) indicates ternary $=Fe—IP_6—UO_2^{2+}$ surface complexes, in addition to iron-incorporated uranium-phosphate precipitates, may have contributed significantly to the hydroxylamine-extractable uranium fraction. Finally, chemical control experiments (data not shown) indicate that U(VI)-IP_x (x = 2:6) precipitates constitute the majority of the observed peroxide-extractable uranium fraction in these experiments.

Comparison of pH 7.0 and pH 5.5 dissolved uranium data in phytate-amended incubations (Figure 4.4) reveals that 40% more uranium was removed in pH 5.5 incubations which released 40 mM inorganic phosphate than in pH 7.0 incubations which did not produce orthophosphate, indicating that the additional uranium removed at pH 5.5 is attributable to a mechanism other than adsorption and/or diffusion of uranium into the crystal lattice of soil minerals. Solid-phase extractions also reveal that 50% of uranium was strongly adsorbed (hydroxylamine extractable) at pH 7.0 in the presence of phytate (Figure 4.5b) compared to only 30% at pH 5.5 (Figure 4.5a). Simultaneously, 35% of

uranium was found in the peroxide extractable fraction of the pH 7.0 incubations with little or no phytate hydrolysis (Figure 4.5b), while 60% of uranium was extracted by peroxide in pH 5.5 incubations. If the removal of uranium was mainly due to the formation of U-IP_6 precipitates, the peroxide extractable fraction of uranium should be similar at pH 5.5 and 7.0 given the highly negative charge on IP_6 at both pHs. These observations, therefore, suggest that approximately 35% of uranium is chemically precipitated with IP_6 at pH 7.0 (Figure 4.5b), while 70% of uranium is precipitated as a mixture of U-IP_x (x = 2:6) and U(VI)-PO_4^{3-} minerals at pH 5.5 (Figure 4.5a).

Examination of solid-phase uranium by XANES reveals a uranium L_{III}-edge at ~17163 eV and a characteristic U(VI) shoulder between 17187 and 17200 eV in all treatments (Figure 4.6a), confirming that uranium existed as U(VI) in these aerobic incubations. Additionally, the k^3-weighted EXAFS fittings confirmed the presence of an axial oxygen shell at 1.80 Å in all incubations (Figure 4.6b, 4.6c, Table B.3, Appendix B). The split equatorial oxygen shells at 2.25 Å and 2.41 Å required to improve EXAFS fittings in uranium-amended reactors without phytate at both pH (Table B.3, Appendix B) may indicate the presence of schoepite (Allen et al., 1996) or U(VI) ternary surface complexes on iron or manganese oxides with carbonates or other complexing ligands (Waite et al., 1994; Webb et al., 2006) and, thus, confirm thermodynamic predictions (Table B.2, Appendix B). Interestingly, only a single equatorial oxygen shell was required to improve the fit of uranium-amended reactors in the presence of phytate at pH 7.0 rather than the split equatorial shells observed in reactors without phytate (Table B.3, Appendix B). These findings indicate the presence of phytate may drive a shift in the dominant uranium removal mechanism between these treatments from surface-mediated

ternary complex formation to solution-mediated precipitation reactions, even when no phytate hydrolysis occurs. This shift in removal mechanism is also reflected by the shift in solid-phase speciation between pH 7.0 reactors with and without phytate determined by sequential extractions (Figure 4.5a, 4.5b). Past studies have demonstrated iron oxides as the primary U sorbent in Oak Ridge soils above pH 4.0 (Barnett et al., 2002; Zheng et al., 2003). Thus, the required inclusion of Mn/Fe EXAFS shells in all treatments demonstrates that sorption to metal oxides represents a prevalent uranium sink in this system (Figure 4.5, Table B.2, Appendix B), even in phytate-amended reactors where precipitation of U-phosphate phases is important. Phosphorus shells improved EXAFS fittings of pH 5.5 uranium-amended reactors with phytate only and with both phytate and glycerol (Figure 4.6b, 4.6c, Table B.3, Appendix B) in which significant inorganic phosphate was produced (Figure 4.2), suggesting that inorganic phosphate production in pH 5.5 reactors was sufficient to promote the precipitation of uranium-phosphate minerals. Assuming uranium adsorbed to metal oxides represented the primary phosphate-independent uranium sink for pH 5.5 incubations and that all U-P precipitates and ternary sorption complexes display U-P coordination numbers of one, the U-P coordination numbers exhibited by pH 5.5 uranium-containing reactors amended with phytate only (N = 0.39) or with phytate and glycerol (N = 0.55) (Table B.3, Appendix B) suggest that roughly 61% and 45% of uranium removal, respectively, may be attributed to uranium sorption directly to metal oxides. In contrast, a P-shell was not required to improve EXAFS fittings of solids from the pH 7.0 phytate-amended incubations, in which phytate hydrolysis did not occur, despite the apparent presence of U(VI)-phytate precipitates in phytate-amended reactors (Figure 4.5b). These results indicate that U(VI)-

phytate precipitates may not represent the dominant form of solid U at this pH. Likely, uranium sorption to ORFRC soils and precipitation of both schoepite and U(VI)-IP_6 solid phases contributed to uranium removal in pH 7.0 incubations.

4.4.5 Implications for *in situ* Bioremediation

Previous studies demonstrated the biomineralization of U(VI)-phosphate minerals by microbial phosphatase activity may be promoted by synthetic organophosphates in both aerobic (Beazley et al., 2007; Macaskie et al., 1995; Martinez et al., 2007; Montgomery et al., 1995; Shelobolina et al., 2009) and anaerobic conditions (Beazley et al., 2009), including in ORFRC soils (Beazley et al., 2011; Salome et al., 2013) . In this study, the hydrolysis of phytate with the concomitant release of inorganic phosphate by indigenous subsurface microorganisms in ORFRC sediments was demonstrated. Further, the inorganic phosphate from phytate hydrolysis at pH 5.5 enhanced uranium immobilization via biomineralization of U(VI)-phosphate minerals, even though uranium stress enhanced IP_6 hydrolysis and eventually decreased hydrolysis of intermediate inositol phosphate species. Interestingly, phytate hydrolysis was not observed in pH 7.0 incubations with the native ORFRC microbial community, suggesting that alkaline phytase is not produced by the natural microbial community at the ORFRC.

The biomineralization of U(VI)-phosphate minerals is an appealing remediation strategy for *in situ* uranium immobilization due to its utility in a wide range of geochemical conditions, including at contaminated sites like the ORFRC where fluctuating redox-conditions, elevated uranium and nitrate concentrations, and low pH create an environment unfavorable to bioreduction. To our knowledge, this is the first study demonstrating U(VI)-phosphate biomineralization promoted by microbially-

catalyzed phytate hydrolysis. As phytate is naturally abundant, relatively inexpensive, and potentially yields six moles of orthophosphate per mole of phytate, it represents an ideal organophosphate compound to promote this process. In addition, the lower net rates of transformation of inositol phosphate intermediates and the slower kinetics of production of inorganic phosphate in the presence of elevated uranium compared to non-contaminated sites would allow time for phytate and its inositol phosphate intermediates to migrate within the contaminant plume before hydrolysis occurs and, thus increase the surface area treated for uranium contamination. While phytate sorption may limit its transport, sorbed IP_6 may also represent a long term source of inorganic phosphate to contaminated environments. Previous concerns over increased uranium mobility in contaminated sediments upon phytate amendment (Seaman et al., 2003) seem to be unfounded, as phytate hydrolysis results in precipitation of any mobilized uranium in conditions which promote phytase expression. Additionally, phytate may chemically precipitate with uranium depending on its concentration, further decreasing aqueous uranium concentrations. At circumneutral pH in the presence of elevated phytate, however, uranium solubility may be enhanced if phytate hydrolysis does not occur. Thus, preliminary studies must be conducted prior to phytate amendment to ensure the indigenous microbial community of a particular contaminated site is able to express phytases.

4.5 Acknowledgements

This research was supported by the Office of Science (BER), US Department of Energy Grant No. DE-FG02-04ER63906. Portions of this research were carried out at the Stanford Synchrotron Radiation Lightsource, a national user facility operated by

Stanford University on behalf of the US Department of Energy, Office of Basic Energy Sciences. The SSRL Structural Molecular Biology Program is supported by the Department of Energy, Office of Biological and Environmental Research, and by the National Institutes of Health, National Center for Research Resources, Biomedical Technology Program. We thank Dave Watson of Oak Ridge National Laboratory for providing ORFRC sediment cores.

CHAPTER 5

THE EFFECT OF URANIUM ON THE HYDROLYSIS OF PHYTATE BY A NEW MICROORGANISM ISOLATED FROM URANIUM-CONTAMINATED SOILS

In preparation for submission to *Geochimica et cosmochimica acta*

5.1 Abstract

Although the chemical immobilization of uranium with phytate has been investigated, the potential for utilizing phytate, the dominant form or organic phosphorus in a variety of soils, as an organophosphate source to promote U(VI)-phosphate biomineralization has only been limitedly explored. In this study, two phytase-positive microorganisms were isolated from contaminated sediments incubated aerobically in soil slurries (described in Chapter 4 of this dissertation), and PCR amplified 16S rRNA sequences revealed these isolates as *Bradyrhizobium* and *Variovorax* species. To determine the effect of uranium on phytate hydrolysis by metal-resistant microorganisms, *Variovorax* sp. was incubated aerobically in pH 5.5 artificial groundwater amended with 1 mM phytate as the sole phosphorus source, 3 mM lactate as the electron donor, and increasing concentrations of uranium. As phytate may chemically precipitate with uranium, live cells were equilibrated with uranium and lactate prior to phytate addition to ensure exposure of *Variovorax* sp. to elevated uranium levels. Lactate consumption was rapid, complete, and accompanied by biomass accumulation in all experimental conditions, even after a 4 hour equilibration with elevated uranium concentrations.

Without uranium, ~ 6 mM inorganic phosphate was liberated by *Variovorax* sp. and almost complete degradation of the initial 1 mM amended phytate was observed after only 2 weeks of incubation. In the presence of uranium, however, total inorganic phosphate production over the two week incubation period decreased linearly with increasing uranium concentrations, suggesting the existence of a significant uranium toxicity effect. In addition, introduction of uranium resulted in earlier onset and more rapid accumulation of inorganic phosphate as well as incomplete degradation of phytate compared to identical reactors without uranium, suggesting acid phytase production by *Variovorax* sp. may represent a uranium detoxification mechanism. Overall, the results of this study suggest that phytate addition to uranium contaminated environments may promote both chemical uranium sequestration and biomineralization of U(VI)-phosphate minerals via microbially-mediated phytate hydrolysis. In addition, bacterial phytate hydrolysis may be enhanced in contaminated environments if microorganisms initiate phytase enzyme expression as a uranium detoxification mechanism.

5.2 Introduction

An estimated 6.4 trillion liters of groundwater and 40 million cubic meters of soil and solid waste contaminated with uranium and other heavy-metals are found at Department of Energy (DOE) legacy nuclear waste sites across the country (Brooks, 2001). Traditional physical remediation techniques such as pump-and-treat and excavation are not feasible for such vast quantities of waste (Dawson and Gilman, 2001; Jardine, 2006; Mackay and Cherry, 1989). The DOE has therefore focused on the investigation of *in situ* uranium remediation strategies, which aim to retard or halt

contaminant migration, as relatively inexpensive and noninvasive alternatives to more traditional remediation methods (NABIR, 2003).

In natural systems, uranium mobility is largely controlled by sorption to iron oxides (Hsi and Langmuir, 1985; Langmuir, 1997; Waite et al., 1994). At higher pH and in the presence of carbonate, however, uranyl only minimally adsorbs to iron oxides due to formation of aqueous carbonate (Katsoyiannis, 2007) or ternary calcium-uranyl-carbonate (Fox et al., 2006; Meleshyn et al., 2009; Stewart et al., 2010) complexes. Alternately, bioreduction has been extensively studied as an *in situ* uranium remediation technique for contaminated subsurfaces (Fredrickson et al., 2000; Ganesh et al., 1999; Lovley and Phillips, 1992b; Lovley et al., 1991; North et al., 2004; Sanford et al., 2007; Wade and DiChristina, 2000). However, U(IV) mineral dissolution may remobilize uranium in both oxidizing (Langmuir, 1997; Murphy and Shock, 1999) and reducing (Beller, 2005; Fredrickson et al., 2002; Moon et al., 2007; Senko et al., 2002; Senko et al., 2005b; Wan et al., 2005; Wu et al., 2010) conditions. Thus, sorption and bioreduction may not represent long-term uranium sinks and alternative remediation strategies with utility in a broad range of geochemical conditions merit investigation.

The biomineralization of insoluble U(VI)-phosphate minerals through the activities of microbial phosphatases represents a possible complementary bioremediation technique to the widely studied bioreduction. U(VI) forms sparingly soluble phosphate minerals in a wide range of geochemical conditions (Ohnuki et al., 2004; Wellman et al., 2007; Zheng et al., 2006). However, direct addition of inorganic phosphate to subsurface environments drastically decreases soil hydraulic conductivity (Wellman et al., 2006) and limits orthophosphate transport throughout the contaminant plume. Consequently,

research has concentrated primarily on the addition of an exogenous organophosphate source to stimulate microbially-mediated orthophosphate production coupled to a chemical precipitation of sparingly soluble U(VI)-phosphate minerals (Beazley et al., 2007, 2009; Macaskie et al., 1995; Martinez et al., 2007; Montgomery et al., 1995; Shelobolina et al., 2009). To fulfill their phosphate requirements, most microorganisms secrete non-specific acid phosphohydrolases (phosphatases), a group of periplasmic or membrane-bound enzymes that catalyze the hydrolysis of organic phosphoester bonds at acidic to circumneutral pH (Rossolini et al., 1998). *Rahnella* sp. Y9602, a facultative anaerobe isolated from the ORFRC, has displayed phosphatase activity coupled to uranium immobilization in both oxidizing and reducing conditions and at both acidic and circumneutral pH (Beazley et al., 2007, 2009; Martinez et al., 2007). In addition, U(VI)-phosphate precipitation promoted by *Citrobacter sp.* in low pH aerobic conditions has been demonstrated (Macaskie et al., 1995; Montgomery et al., 1995). In contaminated sediments, uranium immobilization has been achieved through microbially-mediated organophosphate hydrolysis in aerobic (Beazley et al., 2011; Shelobolina et al., 2009) and, more recently, anaerobic (Salome et al., 2013) conditions, suggesting U(VI)-phosphate biomineralization may compete with bioreduction in environments generally considered favorable to bioreduction. Thus far, biomineralization studies have predominantly investigated the addition of synthetic organophosphates, such as glycerol-2-phosphate (G2P) and glycerol-3-phosphate (G3P), to subsurface environments (Beazley et al., 2007, 2009; Beazley et al., 2011; Martinez et al., 2007; Shelobolina et al., 2009). In contrast, a few studies (Knox et al., 2008; Nash et al., 1998; Seaman et al.,

2003) have examined the efficacy of utilizing naturally-occurring and abundant organophosphates to promote uranium immobilization.

Inositol hexaphosphate (IP_6), also known as phytate (salt) or phytic acid (metal-free), is a phosphorylated inositol with six attached phosphate groups that is synthesized by plants for phosphorus storage (Turner et al., 2002). IP_6 represents the dominant organophosphate in most terrestrial environments (Turner et al., 2002), making it an attractive alternative to synthetically derived substrates. With six pK_as below 3.0 (Costello et al., 1976), phytic acid carries a highly negative charge (-6 to -9) at environmentally relevant pH. As such, phytic acid efficiently chelates multivalent cations, including Ca^{2+}, Zn^{2+}, Mg^{2+}, Mn^{2+}, and Cu^{2+} (Turner et al., 2002; Wodzinski and Ullah, 1996), especially above circumneutral pH (Shvets et al., 1991), and strongly sorbs to soils (Degroot and Golterman, 1993; Johnson et al., 2012). In fact, phytate inhibits orthophosphate sorption and even displaces previously sorbed inorganic phosphate from iron oxides (Degroot and Golterman, 1993). Simultaneously, it has been shown that calcium phytate immobilizes uranium efficiently at pH 7.0 (Knox et al., 2008; Nash et al., 1998; Seaman et al., 2003). In contrast, phytate-promoted biomineralization of U(VI)-phosphate minerals has only recently been demonstrated in pH 5.5 soil slurries containing ORFRC sediments in which sufficient inorganic phosphate was liberated via microbially-mediated phytate hydrolysis to immobilize uranium (chapter 4 of this dissertation).

Although IP_6 remains chemically stable at all environmentally relevant pH and is not hydrolyzed by conventional phosphohydrolases (Turner et al., 2002), enantioselective phytase enzymes may catalyze its hydrolysis to lower inositol derivatives (IP_X, x: 1-5)

and inorganic phosphate (Irving and Cosgrove, 1971; Parthasarathy and Eisenberg, 1991). In addition, once hydrolysis of the initial phosphate group from IP_6 is achieved, hydrolysis of lower inositol derivatives (IP_X, x: 1-5) may be catalyzed either by phytase or any non-specific acid phosphatase (NSAP) (Marko-Varga and Gorton, 1990; Meek and Nicoletti, 1986). Phytase enzymes are a substrate-specific subclass of phosphomonoesterases produced by plants, animals, and microorganisms (Oh et al., 2004) with variable pH optimum, molecular weight, structure, and metal cofactors required for enzyme activation (Shin et al., 2001). Generally, bacterial phytase biosynthesis is triggered in phosphate-limited conditions and thought to be controlled by the *Pho* regulon which regulates expression of genes involved in the uptake and assimilation of phosphate (Mukhametzyanova et al., 2012). However, *E. coli* phytase, the most robustly characterized bacterial phytase, is not under control of the *Pho* regulon (Mullaney and Ullah, 2007), suggesting the function and regulation of bacterial phytases may be highly variable.

Based on their optimum pH, phytases may be classified broadly as either acid or alkaline phytases. Acid phytases include the subclasses purple acid phosphatases (PAPs) and histidine acid phosphatases (HAPs) which both display optimum catalytic activity at acidic pH and exhibit a range of specific phytase activity. In addition, acid phytases are inhibited by elevated concentrations of monovalent and divalent cations (Oh et al., 2004), and the final product of phytase-catalyzed IP_6 hydrolysis is IP_1 as the final phosphate group cannot be hydrolyzed (Turner et al., 2002). HAPs are the most common class of acid phytase and are widespread among microorganisms (Mukhametzyanova et al., 2012). Unlike acid phytases, alkaline phytases consist of a class of enzymes known as β-

propeller phytases (BPPs) which share a sequence identity of 90-98% with each other but display no homology with any other known group of phosphatases (Mullaney and Ullah, 2007; Yao et al., 2012). Although β-propeller phytases have almost exclusively been characterized in *Bacillus* sp., BPPs from *Shewanella oneidensis* MR-1 (Cheng and Lim, 2006) and *Pedobacter nyackenesis* MJ11 CGMCC 2503 (Huang et al., 2009) have also been isolated, and bioinformatic studies indicate BPPs may be widespread in prokaryotes (Cheng and Lim, 2006; Lim et al., 2007). Interestingly, while acid phytases are inhibited by monovalent and divalent cations (Oh et al., 2004), BPPs require calcium for enzyme function (Ha et al., 2000). All BPPs display two phosphate binding sites: one high-affinity binding site which attracts and orients the phytate molecule and a second binding site where cleavage occurs (Ha et al., 2000). As a result, BPPs preferentially hydrolyze inositol phosphates with adjacent bound phosphate groups resulting in a final BPP phytate hydrolysis product of IP_3 with alternating phosphorylated (meta) and dephosphorylated (ortho and para) positions on the inositol ring (Shin et al., 2001).

In this study, phytate-hydrolyzing microorganisms were isolated from soils slurries described in chapter 4 of this dissertation, and the acid phytase activity of one of these isolates was examined. The objectives of this study were to identify these phytate-hydrolyzing microorganisms, determine the electron-donor dependence of this hydrolysis, and characterize the kinetic effect of uranium on phytate hydrolysis and inorganic phosphate production.

5.3 Materials and Methods

Unless otherwise stated, all pure culture incubations were conducted in artificial groundwater buffered at either pH 5.5 or pH 7.0 with 50 mM 2-(N-

Morpholino)ethanesulfonic acid (MES) or 50 mM 4-(2-hydroxyethyl)-1-piperazineethanesulfonic acid (HEPES), respectively. Background ion concentrations in the artificial groundwater were 200 µM Ca^{2+}, 2.0 µM Fe^{2+}, 5.1 µM Mn^{2+}, 7.9 mM K^{+}, 7.5 mM Na^{+}, 8.0 µM MoO_4^{2-}, 410 µM Cl^{-}, 810 µM SO_4^{2-}, and 15.4 mM NO_3^{-} reflective of the composition of ORFRC groundwater (Brooks, 2001). Except when noted, all chemicals were reagent grade (Fisher).

5.3.1 Isolation of ORFRC microorganisms

To isolate ORFRC microorganisms with potential for phytase gene expression, previously described soil slurries (discussed in Chapter 4 of this dissertation) were plated onto three agar plates, each containing different enriched nutrient media (1% tryptone, 1/10 nutrient broth, or sphingobacteria; Table 1S) designed to isolate the maximum diversity of microorganisms. In addition to standard nutrients (Table 1S), each media was amended with 85 mg/L 4-methylumbelliferyl phosphate (MUP, Acros), a compound which fluoresces under ultraviolet (UV) light only after the attached phosphate group is removed via hydrolysis (Adcock and Saint, 2001; Martinez et al., 2007). A microbial colony that fluoresces when grown on MUP-containing medium (MUP-positive) may represent a microbial isolate that is actively growing and hydrolyzing phosphate, either through phosphohydrolases or phytase enzymes . Slurry dilutions were grown for 3 days at room temperature in the dark before being placed under UV light for identification of MUP-positive colonies. Following identification of MUP-positive colonies, several representatives of each MUP-positive phenotype from all slurry treatments were patched onto a fresh agar plate and grown for two days in aerobic conditions. Each isolate was then inoculated into sterile 1.5 mL centrifuge tubes containing the appropriate liquid

medium, grown for one day at room temperature, and stabilized with sterile glycerol for storage at -80°C. A separate 1 µL aliquot of each culture was plated onto phytate agar plates (details in supplementary material) and grown for two days in the dark at room temperature. After two days, each colony was observed for a haloed clearing indicating the possible presence of phytase metabolism (Yu et al., 2012).

5.3.2 Phytase assay

To determine which microorganisms hydrolyze phytate in aqueous solution, isolates that revealed a haloed clearing when grown on phytate-amended agar plates were inoculated from freezer stocks directly into 1.5 mL centrifuge tubes containing 1.0 mL of pH 5.5 artificial groundwater amended with 1 mM Na-phytate (Sigma Aldrich) and 1 mM glycerol (OmniPur) as carbon source. Inorganic phosphate production was quantified after 1 week of incubation in the dark and at room temperature.

5.3.3 DNA extraction and 16S rRNA amplification

To establish purity and identity of phytase-positive ORFRC microorganisms, DNA was extracted from each of these isolates and their 16S rRNA amplified and sequenced. First, each isolate was inoculated into nutrient broth media (NB, Table 1S) and grown overnight in the dark at 30°C. A 1 mL aliquot of each culture was then transferred to a 1.5 mL tube and centrifuged at 4000 rpm for 10 minutes. The supernatant was discarded, and DNA was extracted from the remaining pellets by the standard phenol-chloroform method (Chomczynski and Sacchi, 1987). Pellets were resuspended in 467 µL of pH 8.0 tris–EDTA buffer, 30 µL of 10% (w/v) sodium dodecyl sulfonate (SDS), and 1 µL of RNase A, and the solution was mixed and incubated for 1 h at

37°C. After incubation, 500 µL of a mixture containing phenol, chloroform, and isoamyl alcohol (25:24:1) was added to the EDTA mixture, and the solution was thoroughly mixed before centrifugation at 14,000 × g for 10 minutes. The supernatant was then transferred to a clean tube and extracted twice more with the phenol-chloroform-isoamyl alcohol mixture (25:24:1) to ensure the DNA product was sufficiently cleansed of proteins and organic impurities. Next, 40 µL of 3 M acetate (pH 5.5) and 280 µL of isopropanol were incubated for 1 hour at 4°C to precipitate the DNA. The resulting precipitate was washed in 70 % ethanol to remove impurities, dried, resuspended in 40 µL sterile distilled water, and stored at 4°C until use.

For 16S rRNA gene amplification, polymerase chain reactions (PCR) of reaction mixtures containing 4 ng/µL DNA, 10 µL 10 x DNA polymerase buffer (NEB), 0.5 mM deoxynucleoside triphosphates (dNTPs, NEB), 200 µM forward (8F) and reverse (1489R) primers, and 0.2 µL of *Taq* DNA polymerase (NEB) for a final reaction volume of 50 µL were conducted. The thermocycling regime consisted of a 3 min 95°C initialization step; three short temperature cycles including a 30 sec 95°C denaturation step, a 30 second 59°C annealing step, and a 105 second 72°C elongation step which were cycled through 30 times; and a 7 min long final elongation step at 72°C. PCR products were gel purified (Quiagen) and sequenced (GeneWiz). The resulting sequences were reverse-complemented, and the forward and reverse amplified sequences showed no overlap for either isolate. Due to quality of the PCR product, the sequences for each strain were truncated at 650 base pairs (ES5) and 550 base pairs (IS2), and a nucleotide BLAST (nBLAST) (Altschul et al., 1997) was performed on the resulting sequences (query sequences in supplementary material) to identify each isolate.

5.3.4 Growth characteristics of the new ORFRC isolates

To determine the growth characteristics of the newly isolated strains, freezer stocks of each isolate were streaked onto agar plates containing NB media and grown for two days at 30°C. Single colonies of each isolate were picked and inoculated in duplicate into 5 mL liquid NB and grown overnight in the dark at 200 rpm and 30°C. Each bacterial culture was then diluted 50x in fresh NB and grown at 30°C and 200 rpm. Absorbance at 600 nm (OD_{600}) was monitored over time using a Milton Roy Spectronic 501 spectrophotometer. To correct for the background absorbance of NB at this wavelength, fresh NB media was used as a blank. For select time points, an aliquot of culture was reserved for cell counts as determined by staining with acridine orange to calibrate the OD_{600} measurement.

5.3.5 Carbon-dependent phytase activity of the new isolates

To investigate the dependence of phytate hydrolysis on the type of available carbon source, each isolate was assayed for phytase activity in the presence of lactate, acetate, and formate. For comparison, the well-characterized isolates *Shewanella oneidensis* MR-1, *Shewanella putrefaciens* strain 200, and three metal-resistant bacteria isolated from the ORFRC (*Rahnella* sp. Y9602, *Arthrobacter* sp. X34, and *Bacillus* sp. Y9-2) were assayed for phytase activity using the same procedure as live controls. Freezer stocks of each isolate were streaked onto agar plates containing either NB or *Luria bertani* (LB, Table 1S) media and grown for two days at 30°C. Single colonies from each plate were picked and inoculated into 5 mL liquid NB or LB media (in duplicate) and grown overnight in the dark at 200 rpm and 30°C. Each bacterial culture

was then diluted 25x in fresh NB or LB and grown (30°C, 200 rpm) for ~ 4 hours until cell concentration reached ~ 10^8 cells/mL as determined by OD_{600}. Cells were then pelleted and washed in 0.85% NaCl before inoculation at a final concentration of 10^7 cells/mL into artificial groundwater buffered at either pH 5.5 or 7.0 with 50 mM MES or HEPES, and amended with 1 mM Na-phytate (Sigma Aldrich) and 1 mM lactate, 1 mM acetate, or 1 mM formate as an electron donor. Inorganic phosphate production was quantified after 5 days of incubation at 30°C in the dark and under agitation (200 rpm) to maintain aerobic conditions.

5.3.6 Effect of uranium on phytate hydrolysis.

To determine the effect of uranium on phytate hydrolysis, one of the new isolates was shocked with uranium and incubated aerobically in artificial groundwater amended with phytate for a period of two weeks. The isolate was streaked onto agar plates containing NB media and grown for two days at 30°C. A single colony was inoculated into 5 mL liquid NB (in duplicate) and grown overnight in the dark at 200 rpm and 30°C. Each bacterial culture was then diluted 25x in fresh NB and grown at 30°C and 200 rpm for ~4 hours until OD_{600} reached 0.2, corresponding to a cell concentration of ~ 10^8 cells/mL. Cells were then pelleted, washed in 0.85% NaCl, and inoculated at a final cell concentration of 10^7 cells/mL into artificial groundwater buffered at pH 5.5 with 50 mM MES and amended with 3 mM lactate as electron donor and 0, 25 50, 100, 250, 500, or 1000 µM uranyl acetate (Spectrum). Cells were shocked with uranium at room temperature for a period of 4 hours prior to incubations in the presence of 1 mM Na-phytate (Sigma Aldrich). Triplicate reactors containing cells and otherwise identical abiotic controls without cells were incubated in the dark and at 30°C under aerobic

conditions by agitation at 200 rpm using a Lab-Line 3525 shaker incubator. At each time point, a small aliquot was collected and split for absorbance measurements at 600 nm, as a proxy for cell density, and filtration through a 0.2 μm pore size polyethersulfone (PES) membrane filter (Puradisc, Whatman). A fraction of each filtered sample was preserved in 2% trace metal grade nitric acid for uranium quantification, while another was frozen until measurement of organic acids, inorganic phosphate, and inositol phosphate species. Rate constants, k_{obs}, for inorganic phosphate production were calculated for each experimental treatment assuming pseudo-first-order reactions from the linear regression of the natural log of concentrations as a function of time. Errors reported for rate constants represent the standard error of the slope of linear regressions.

5.3.7 Analytical Techniques

Total dissolved uranium concentration was measured in duplicate using an Agilent 7500a inductively-coupled plasma mass spectrometer (ICP-MS). Samples were diluted in 2% trace metal grade nitric acid (Fisher), and standards ranging from 0 to 10 nM were prepared using uranyl acetate (Spectrum) acidified in 2% trace metal grade nitric acid. Holmium and bismuth were used as internal references in both standards and samples (SPEX certiPrep), and 2% trace metal grade nitric acid blanks and calibration check standards were used as quality controls. Reported errors represent the standard deviation between triplicate reactors and duplicate measurements.

As phytate interferes with the original molybdenum blue spectrophotometric method for orthophosphate detection, inorganic phosphate in the presence of phytate was quantified using a modified spectrophotometric technique (Heinonen and Lahti, 1981).

First, a 0.4 mL aliquot of freshly made molybdate reagent containing 2.5 mL ammonium molybdate (10 mM), 2.5 mL sulfuric acid (2.5 M), and 5.0 mL acetone was combined with 0.2 mL of filtered sample/standard and mixed thoroughly. A 20 µL aliquot of 1.0 M citric acid was then added to each sample/standard, and the yellow color was allowed to develop for 10 minutes prior to spectrophotometric detection at 410 nm using a Milton Roy Spectronic 501 spectrophotometer. Standards ranging from 0 to 1 mM were prepared using NaH_2PO_4 (Fisher) dissolved in Nanopure water (Barnstead). Reported errors represent the standard deviation between triplicate reactors.

Inositol hexaphosphate (IP_6), inositol pentaphosphate (IP_5), inositol tetraphosphate (IP_4), inositol triphosphate (IP_3), and inositol bisphosphate (IP_2) (standards from Sigma Aldrich) were quantified using a modified chromatographic separation coupled to suppressed spectrophotometric detection at 500 nm (Rounds and Nielsen, 1993) with a Dionex ICS-3000 dual pump chromatography system. Separation was achieved with an OmniPac PAX-100 guard column (4 x 40 mm). Eluent flow conditions included a 23 minute linear gradient (0.5 mL/min) from 0.01 M 1-methylpiperazine (pH 4.0) to 0.38 M $NaNO_3$ in 0.01 M 1-methylpiperazine (pH 4.0). Following separation, a solution of 0.015% (w/v) $FeCl_3 \bullet 6H_2O$ in 0.15% (w/v) sulfosalicylic acid (pH 1.8) was introduced (0.5 mL/min) as a post-column reagent. The methylpiperazine/sulfosalicylic acid mixture was then pumped through a reaction coil to ensure thorough mixing. Reported errors for IP_x (x = 1:6) species include analytical error and standard deviation between triplicate incubations.

The consumption of lactate was quantified by ion chromatography using a Dionex GP-50 HPLC pump and conductivity detector (Dionex, CD-20) coupled to an Analytical

Instrument Systems, Inc. integrator (LCC 100). An ion-exclusion column (Dionex IonPac ICE-AS6) was used in line with an AMMS-300 (4-mm, Dionex) suppressor. Operating conditions included a 0.4 mM heptafluorobutyric acid (HFBA) eluent with a 1 mL min^{-1} flow rate and a 5 mN Tetrabutylammonium hydroxide (TBA-OH) regenerant. All reagents and standards were prepared using reagent grade chemicals (Acros) unless otherwise specified. Mixed standards ranging from 0 to 3 mM were prepared using sodium lactate (Fisher) and sodium acetate (Fisher) dissolved in Nanopure water (Barnstead). Typical elution times ranged between 10 and 15 minutes and calibration curves were analyzed at the beginning and end of each run to account for instrument drift.

Table 5.1 Selected results from a nucleotide BLAST of the amplified 16S rRNA of strain ES5 using the National Center for Biotechnology Information (NCBI) genomic database. When available, the environment each strain was isolated from is listed.

Description	Environment	Max Score[a]	Total Score[b]	Query Recovery[c]	E-Value[d]	Max Identity[e]	Accession[f]
Variovorax paradoxus strain S110 16S rRNA, complete sequence	Soil	1171	2303	100%	0.0	100%	NR 074654.1
Variovorax sp. SAP777.1 16S rRNA gene, partial sequence	Floral Nectar	1171	2225	100%	0.0	100%	JX067694.1
Variovorax sp. S2U1 16S rRNA gene, partial sequence	Arctic plants	1171	1461	64%	0.0	100%	HE814658.1
Variovorax paradoxus strain NBRC 15149 16S rRNA gene, partial sequence	N/A	1171	2303	100%	0.0	100%	AB680784.1
Variovorax paradoxus strain DSM 1072 16S rRNA gene, partial sequence	Contaminated soils	1171	2303	100%	0.0	100%	AB622222.1
Variovorax paradoxus strain DSM 647 16S rRNA gene, partial sequence	Contaminated soils	1171	2303	100%	0.0	100%	AB622221.1
Variovorax paradoxus strain DSM 645 16S rRNA gene, partial sequence	Contaminated soils	1171	2303	100%	0.0	100%	AB622220.1
Variovorax paradoxus strain IBP-SL9 16S rRNA gene, partial sequence	Siberian forest soils	1171	2275	100%	0.0	100%	HQ689690.1
Variovorax sp. BZ15 16S rRNA gene, partial sequence	Hydrocarbon contaminated soils	1171	2220	100%	0.0	100%	HQ588854.1
Uncultured *123ariovorax* sp. clone T301B6 16S rRNA gene, partial sequence	Anthracene contaminated soils	1171	2303	100%	0.0	100%	HM438647.1
Uncultured *123ariovorax* sp. clone T9222c6 16S rRNA gene, partial sequence	Soils	1171	2303	100%	0.0	100%	HM447708.1
Variovorax sp. 12DCB 16S rRNA gene, partial sequence	Hydrocarbon contaminated soils	1171	2220	100%	0.0	100%	GU565221.1
Variovorax sp. WPCB174 16S rRNA gene, partial sequence	Wetland	1171	2220	100%	0.0	100%	FJ006917.1
Variovorax paradoxus strain B4 16S rRNA gene, partial sequence	Soils	1171	2292	100%	0.0	100%	EU979529.1
Variovorax sp. RKS7-5 16S rRNA gene, partial sequence	Glacier	1171	2220	100%	0.0	100%	EU934231.1
Variovorax paradoxus strain TBEA6 16S rRNA gene, partial sequence	Contaminated soils	1171	2297	100%	0.0	100%	EF641108.1

[a]The score of the single best aligned sequence
[b]The total score of all aligned sequences
[c]The percentage of the query sequence that overlaps the subject sequence
[d]Represents the statistical significance of a given pairwise alignment, a lower E-value indicates a more significant hit
[e]The percent similarity between the query and the subject sequences over the length of the coverage area
[f]Identification number for a specific strain in Genbank

Table 5.2 Selected results from a nucleotide BLAST of the amplified 16S rRNA of strain IS2 using the National Center for Biotechnology Information (NCBI) genomic database. When available, the environment each strain was isolated from is listed.

Description	Environment	Max Score[a]	Total Score[b]	Query Recovery[c]	E-Value[d]	Max Identity[e]	Accession[f]
Bradyrhizobium sp. ORS 3647 16S rRNA gene, partial sequence	Soil	957	1832	100%	0.0	99%	JN085499.1
Bradyrhizobium elkanii strain USDA4348 16S rRNA gene, partial sequence	Tree nodule	957	1832	100%	0.0	99%	JQ911631.1
Bradyrhizobium elkanii strain B0810 16S rRNA gene, partial sequence	Apple tree leaf	957	1852	99%	0.0	99%	AB695336.1
Bradyrhizobium sp. NBRC 101128 16S rRNA gene, partial sequence	N/A	957	1859	100%	0.0	100%	AB681394.1
Bradyrhizobium elkanii strain STM4804 16S rRNA gene, partial sequence	Soils	957	1651	85%	0.0	100%	FR822764.1
Bradyrhizobium sp. 17-4 16S rRNA gene, partial sequence	River sediment	957	1871	100%	0.0	99%	AB672634.1
Bradyrhizobium genosp. TUXTLAS-31 strain 75m 16S rRNA gene, partial sequence	Sugarcane	957	1815	94%	0.0	100%	JF66670.1
Bradyrhizobium sp. 88 16S rRNA gene, partial sequence	Soils	957	1871	100%	0.0	99%	JF905601.1
Bradyrhizobium elkanii strain CCBAU 25551 16S rRNA gene, partial sequence	Soybean plant	957	1848	100%	0.0	99%	HQ231447.1
Bradyrhizobium sp. LMTR-M60 16S rRNA gene, partial sequence	*Phaseolus lunatus*[h]	957	1848	100%	0.0	99%	HQ704815.1
Bradyrhizobium sp. Z2-YC6861 16S rRNA gene, partial sequence	Soils	957	1848	100%	0.0	99%	GQ369129.1
Bradyrhizobium sp. DG 16S rRNA gene, partial sequence	Legume tree nodule	957	1848	100%	0.0	99%	HM151913.1
Bradyrhizobium sp. CCBAU 051011 16S rRNA gene, partial sequence	Peanut plant nodule	957	1848	100%	0.0	99%	HM107171.1
Bradyrhizobium lablabi strain CCBAU 23160 16S rRNA gene, partial sequence	*Lablab purpureus*[i]	957	1843	100%	0.0	99%	GU433456.1
Bradyrhizobium sp. IV-102 16S rRNA gene, partial sequence	Grassland soils	957	1843	100%	0.0	99%	AB531426.1
Bradyrhizobium sp. UFLA04-289 16S rRNA gene, partial sequence	*Macroptilium atropurpureum*	953	1861	100%	0.0	99%	GQ156917.1

[a]The score of the single best aligned sequence
[b]The total score of all aligned sequences
[c]The percentage of the query sequence that overlaps the subject sequence
[d]Represents the statistical significance of a given pairwise alignment, a lower E-value indicates a more significant hit
[e]The percent similarity between the query and the subject sequences over the length of the coverage area
[f]Identification number for a specific strain in Genbank
[h]Lima bean plant
[i]Hyacinth bean

5.4 Results

5.4.1 Isolation of phytate-hydrolyzing ORFRC microorganisms

A total of 107 colonies were isolated from diluted soil slurries using the MUP assay (Figure 5.1a-5.1c). When each of these isolates was grown on enriched nutrient media agar plates amended with phytate, a haloed clearing was observed around 88 colonies (82%), indicating the possible expression of phytate-hydrolyzing enzymes by these microorganisms (Figure 5.2a-5.2b) (Yu et al., 2012).

Only two colonies (#83 and #85 named hereafter ES5 and IS2) liberated significant inorganic phosphate over a period of 1 week in pH 5.5 artificial groundwater amended with 1 mM phytate and 1 mM glycerol (Figure 5.3). The other colonies hydrolyzed less than 0.1 mM orthophosphate in solution, slightly above background concentrations. The sequenced PCR-amplified 16S rRNA of both ES5 and IS2 revealed high quality chromatograms with definitive peaks for each nucleotide base (Figures 5.4, C.1, C.2, C.3). The resulting nBLAST of the PCR amplified 16S rRNA from isolate ES5 revealed high sequence similarity with several strains of *Variovorax paradoxus* along with other *Variovorax* species (Table 1), while the nBLAST of 16S rRNA from isolate IS2 showed high sequence similarity with *Bradyrhizobium* species (Table 2), strongly implicating these two isolates as members of the genus *Variovorax* and *Bradyrhizobium*, respectively. Interestingly, many of the best matches for strain ES5 were isolated from contaminated environments (Table 1). As *Bradyrhizobium* sp. commonly forms root nodules on plants (Vanrhijn and Vanderleyden, 1995), a large fraction of the matches for strain I.S.2 were isolated from soils or plants (Table 2).

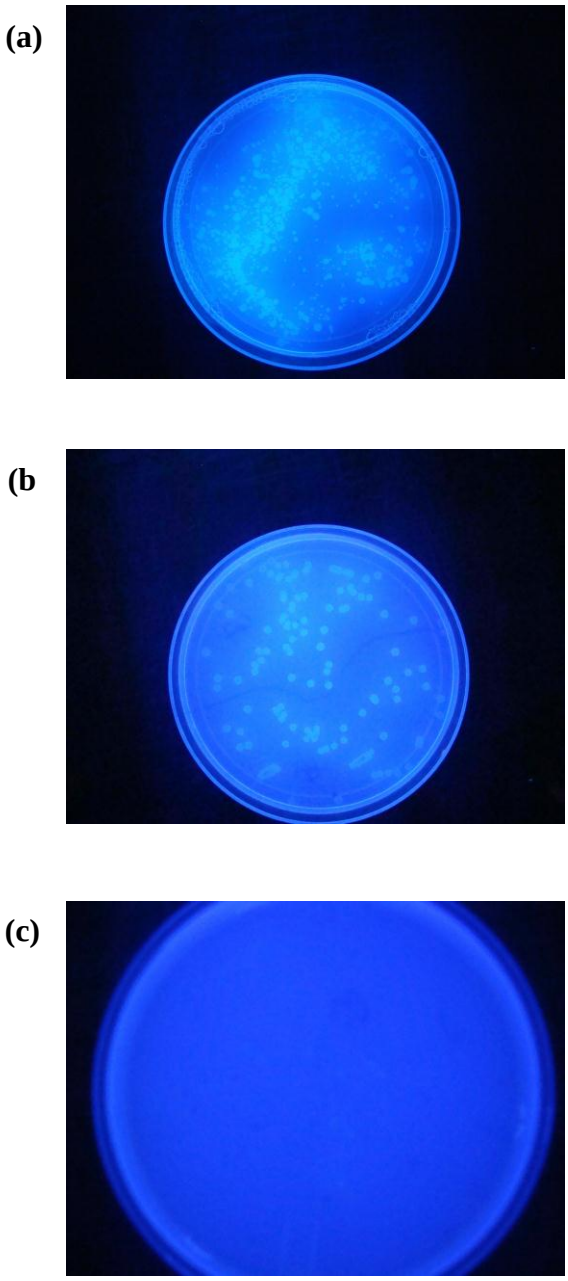

Figure 5.1 Fluorescence under UV light of soils slurries (see Chapter 4 of this dissertation) serially diluted 10^4 times and grown onto agar plates containing enriched nutrient medium amended with 4-methylumbelliferyl phosphate (MUP), a compound which fluoresces upon hydrolysis of the phosphate group. (a) pH 7.0 slurries amended with uranium, glycerol, and phytate (sphingobacteria medium), (b) pH 5.5 slurries amended with uranium and phytate (1/10 nutrient broth medium), and (c) pH 7.0 soils slurries amended with uranium and glycerol, but no phytate (1% tryptone medium). Dilutions were plated and allowed to grow at room temperature in the dark for ~ 3 days.

(a)

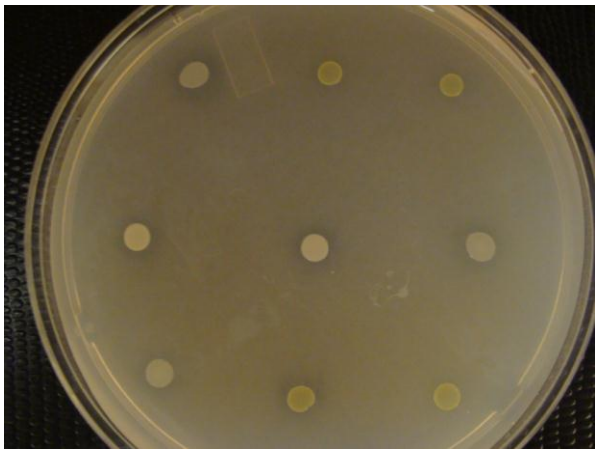

(b

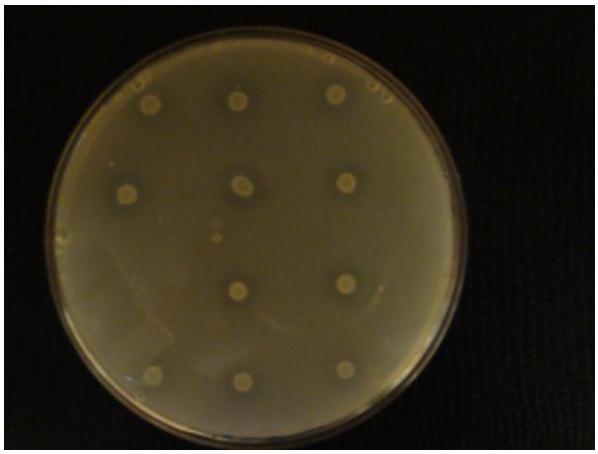

Figure 5.2 Microbial isolates from (a) pH 7.0 and (b) pH 5.5 soil slurries amended with uranium and phytate (see Chapter 4 of this dissertation) plated onto enriched nutrient medium amended with phytate at pH 7.0. Isolates were allowed to grow at room temperature in the dark. After 3 days, a clear halo was noticed around the colonies, indicating the possible expression of phytase activity (Yu et al., 2012).

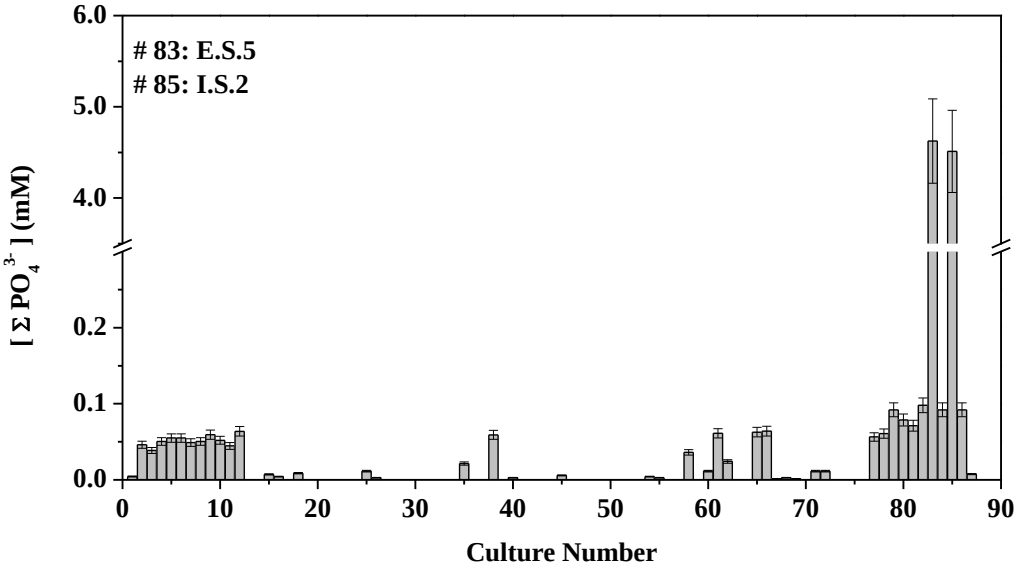

Figure 5.3 Inorganic phosphate (ΣPO_4^{3-}) production after 1.5 weeks of incubation in aerobic pure cultures of MUP-positive microorganisms isolated from aerobic soil slurries containing contaminated soils from the Oak Ridge Field Research Center (discussed in Chapter 4 of this dissertation). Incubations were conducted at pH 5.5 in artificial groundwater amended with 1 mM glycerol and 1 mM inositol hexaphosphate. Error bars represent the variation between triplicate incubations and the analytical error on duplicate measurements.

5.4.2 Characterization of phytate-hydrolyzing microorganisms

The optical density (OD_{600}) of both *Variovorax* sp. and *Bradyrhizobium* sp. showed a similar evolution over the 18-hour incubation period (Figure 5.5). Although these strains displayed similar growth curves, equivalent absorbance values represented different cell concentrations as determined by staining with acridine orange. For example, *Variovorax* sp. displayed cell concentrations of ~ 1(± 0.1) 10^8 cells/mL at an OD_{600} of ~ 0.1, while *Bradyrhizobium* sp. displayed cell concentrations of only ~ 1(± 0.1) 10^7 cells/mL. This trend was similar at higher absorbance values, yet maximum cell concentrations seem to approach 10^{10} cells/mL for both strains.

Comparison of inorganic phosphate production by *Variovorax* sp. and *Bradyrhizobium* sp. in the presence of various carbon sources revealed no significant differences between incubations amended with glycerol (Figure 5.3), lactate, acetate, or formate (Figure 5.6) as electron donors. Interestingly, the ORFRC metal-resistant isolates *Rahnella* sp. Y9602, *Athrobacter* sp. X34, and *Bacillus* sp. Y9-2 did not liberate inorganic phosphate from phytate hydrolysis after 5 days of incubation (Figure 5.6). In fact, the concentration of inorganic phosphate produced by these organisms was much lower than in the abiotic controls, suggesting they assimilated phosphate from the background medium. While the well-characterized bacteria *Shewanella oneidensis* MR-1 and *Shewanella putrefaciens* strain 200 liberated about 2-6 times more inorganic phosphate than the chemical controls (Figure 5.6)

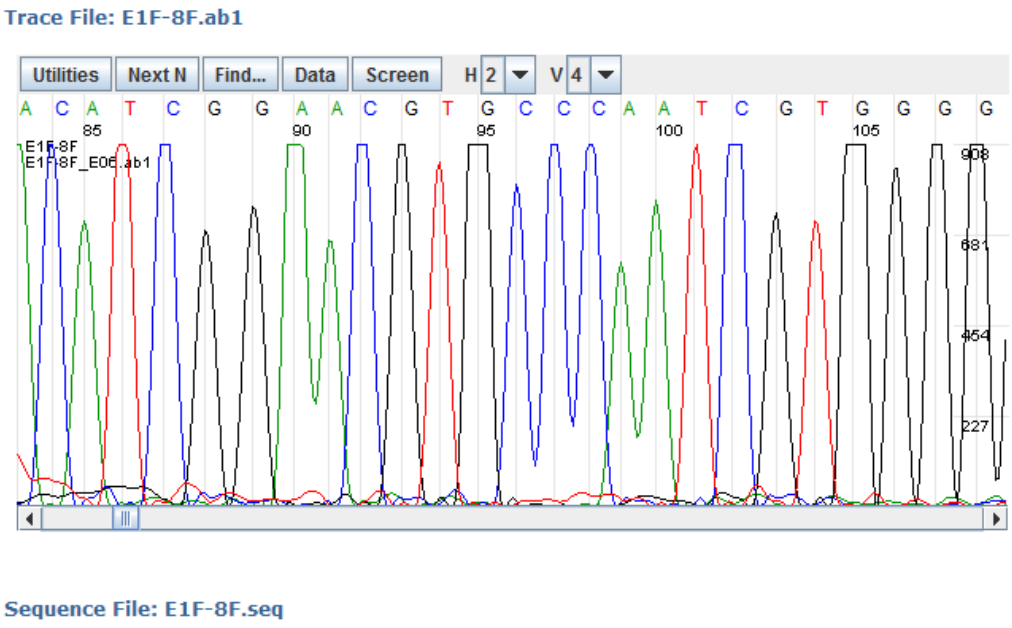

Figure 5.4 Representative chromatogram of the sequenced 16S rRNA from isolate ES5 amplified by PCR with forward primer 8F. DNA was sequenced by Genewiz, and the sequences for isolate ES5 were truncated at 650 base pairs due to the poor quality of data above this number.

5.4.3 Effect of U on phytate hydrolysis by *Variovorax* sp.

The pH of the incubations increased slightly from 5.5 to ~ 5.75 over the first 35 hours of incubation despite the presence of 50 mM MES as buffer (Figure 5.7a). This pH increase was not mirrored in the chemical control incubations (data not shown), indicating it was likely a result of microbial respiration. Indeed, a marked rise in OD_{600} was observed in all incubations over the same time interval (Figure 5.7b). An inverse correlation ($R^2 = 0.989$) between the initial rate of biomass production (calculated from OD_{600} between 0 and 36 hours) and the uranium concentration used to shock the cells (Figure 5.7c) was observed up to a uranium concentration of 500 µM (Figure 5.7c). Interestingly, biomass production rates leveled off for cells exposed to uranium concentrations above 500 µM. The rise in pH (Figure 5.7a) and biomass production (Figure 5.7b) occurred concomitantly with a sharp decrease in lactate concentrations (Figure 5.8a), and lactate was completely consumed by *Variovorax* sp. within 85 hours, while lactate consumption was not observed in the abiotic controls over the duration of the incubations (Figure 5.8a). Initial lactate consumption rates mirrored the trend displayed by initial biomass production rates as a function of uranium concentrations (Figure 5.8b). The initial rate of lactate consumption decreased linearly ($R^2 = 0.978$) as uranium concentrations were raised up to 500 µM (Figure 5.8b). As with biomass production, however, exposure of the cells to uranium concentrations above 500 µM did not change lactate consumption rates (Figure 5.8b).

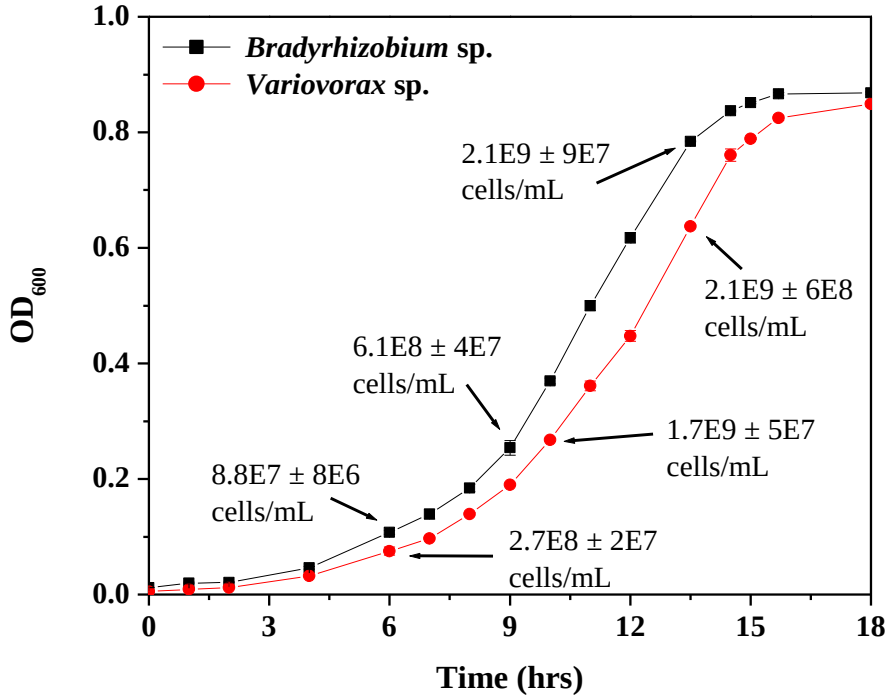

Figure 5.5 Absorbance at 600 nm (OD_{600}) as a function of time in aerobic pure culture incubations with *Bradyrhizobium* sp. and *Variovorax* sp. conducted at pH 7.0 in nutrient broth media. Cell counts as determined by staining with acridine orange are provided at select time points. Error bars on absorbance measurements represent the variation between triplicate incubations and the analytical error on duplicate measurements.

Uranium in the chemical controls was completely precipitated from solution immediately upon addition of 1 mM phytate (Figure 5.9a) for all initial uranium concentrations. Regardless of its concentration, uranium remained in solution before phytate addition, even after 4 hours of equilibration with *Variovorax* sp. (Figure 5.9b), indicating little uranium uptake by cells during the uranium exposure period. As observed with chemical control incubations, however, uranium was immediately removed from solution upon addition of 1 mM phytate (Figure 5.9b). Regardless of the initial uranium concentrations used to shock the cells, orthophosphate was released by Variovorax sp. in all incubations, even when cells were exposed to 1 mM uranium

(Figure 5.10a). In contrast, no detectable inorganic phosphate was produced over the duration of the incubations in the chemical controls (Figure 5.10a). The extent of orthophosphate production, however, was highly affected by the concentration of uranium used to initially shock the cells (Figure 5.10a): Phytate was completely hydrolyzed (i.e. 6 mM phosphate produced from 1 mM phytate) in incubations without uranium while the least phosphate was produced in incubations amended with 1 mM uranium. Interestingly, the initial rate of phosphate production was less for incubations without uranium than in incubations exposed to up to 500 µM uranium (Figure 5.10a). This observation was reflected in the pseudo-first-order rate constants for inorganic phosphate production (Figure 5.10b). Rate constants for orthophosphate production in incubations amended with between 25 and 500 µM uranium were more than 1.5 times greater than in otherwise identical reactors without uranium (Figure 5.10b). For incubations where cells were exposed to 1 mM uranium, however, the pseudo-first-order rate constant decreased by more than 2 folds compared to otherwise identical reactors without uranium (Figure 5.10b). Surprisingly, the net production of orthophosphate by all uranium-exposed cells only lasted about 136 hours and was followed by an apparent lack of production for about 50 hours (Figure 5.10a). After ~ 187 hours, inorganic phosphate production resumed at a much slower rate than initially observed (Figure 5.10a).

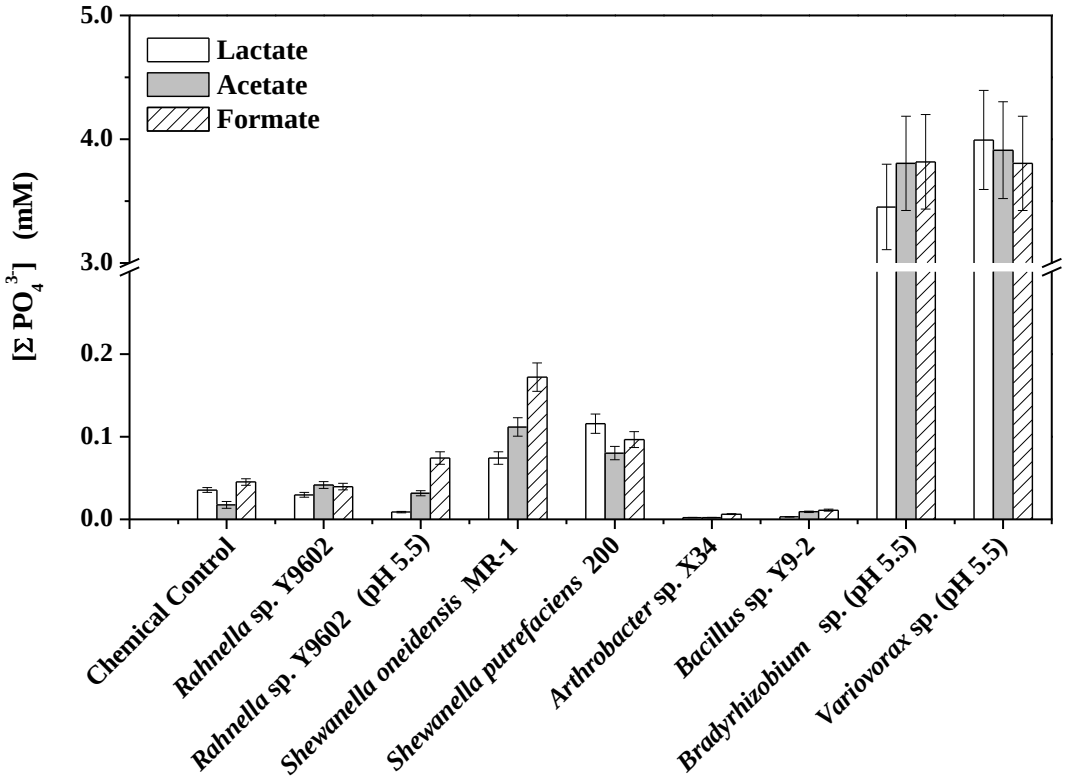

Figure 5.6 Inorganic phosphate (ΣPO_4^{3-}) production after 1 week of incubation in chemical controls and aerobic pure cultures of *Rahnella* sp. Y9602, *Shewanella oneidensis* MR-1, *Shewanella putrefaciens* strain 200, *Arthrobacter* sp. X34, *Bacillus* sp. Y9-2, *Bradyrhizobium* sp., and *Variovorax* sp.. Incubations were conducted at pH 7.0 (unless otherwise noted) in artificial groundwater amended with 1 mM inositol hexaphosphate and 1 mM lactate, 1 mM acetate, or 1 mM formate as electron donors. Error bars represent the variation between triplicate incubations and the analytical error on duplicate measurements.

A similar relationship exists between the observed lag phase in the onset of inorganic phosphate production and uranium concentrations (Figure 5.11a). Without uranium, inorganic phosphate accumulated in solution after 61 hours of incubation (Figure 5.11a). Exposure of the cells to 25, 50, or 100 µM uranium, however, resulted in a shortened lag phase of about 35 hours (Figure 5.11a). In turn, the lag phase in inorganic phosphate production increased above 100 µM uranium compared to identical experiments without uranium, and orthophosphate accumulation did not occur until 187 hours of incubation when cells were exposed to 1 mM uranium (Figure 5.11a). As expected, the lag phase in IP_6 consumption as the cells were exposed to increasing uranium concentrations varied similarly. The onset of IP_6 consumption occurred sooner in reactors amended with low concentrations of uranium than in reactors without uranium (Figure 5.11b). When exposed to 1 mM uranium, however, phytate hydrolysis was significantly delayed compared to all other experimental conditions (Figure 5.11b).

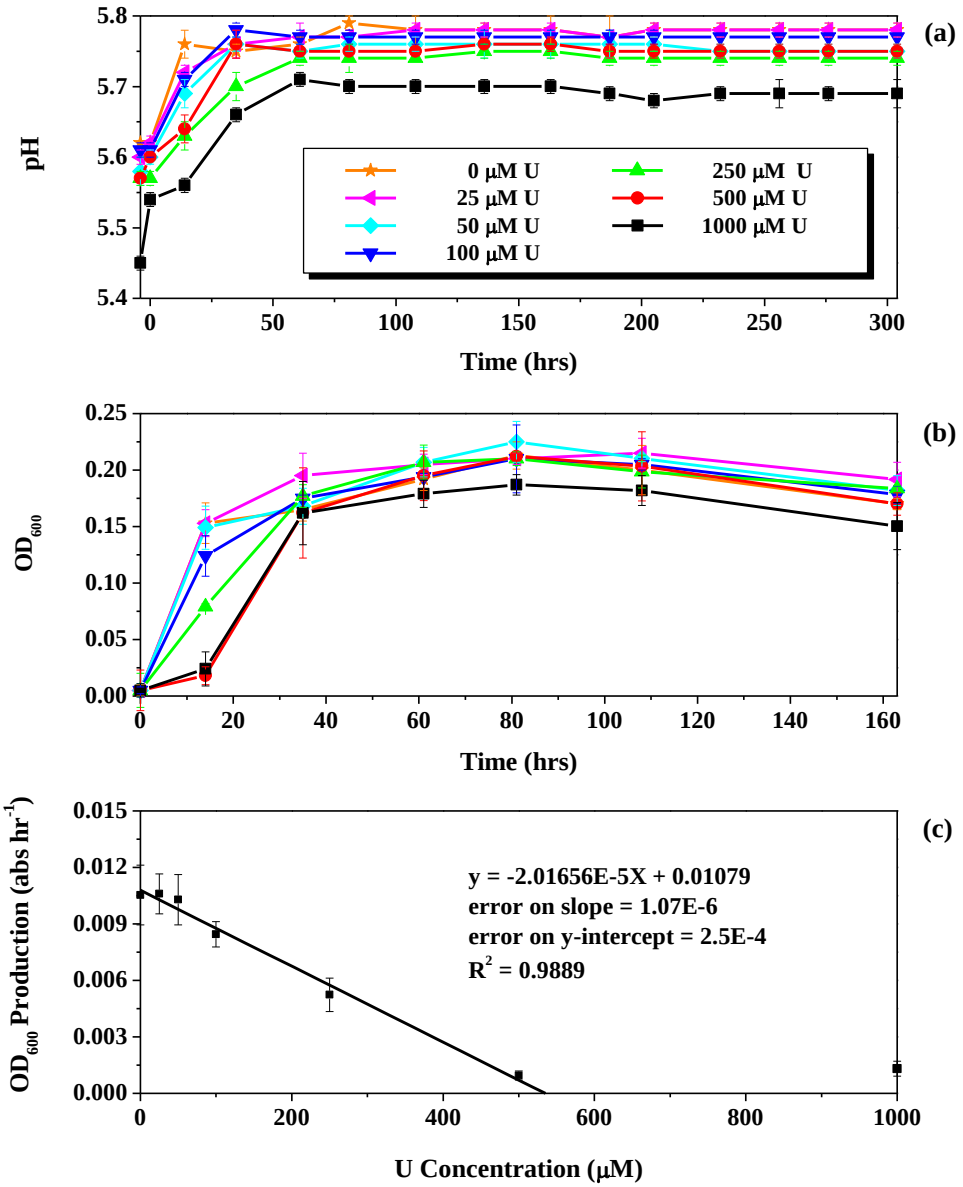

Figure 5.7 Evolution of (a) pH and (b) absorbance at 600 nm (OD_{600}) function of time in aerobic incubations of *Variovorax paradoxus* sp. initially exposed to increasing concentrations of UO_2^{2+} for 4 hours. Incubations were conducted at pH 5.5 in artificial groundwater amended with 3 mM lactate and 1 mM inositol hexaphosphate. OD_{600} was corrected for the background absorbance of the abiotic controls to account for the light scattering of U-IP_6 precipitates. (c) Initial rate of biomass production (OD_{600}) as a function of initial uranium concentration. The linear fit (black line) does not include the data point for incubations amended with 1000 µM uranium. Error bars represent the variation between triplicate incubations and the analytical error on duplicate measurements.

The phytate concentration measured initially in incubations of cells exposed to low concentrations of uranium (0 – 250 μM) was relatively close (~95%) to the concentration added (Figure 5.12a-e). In these incubations, IP_5 reached a maximum concentration of ~ 300 μM after 61 hours and was completely consumed over the course of 1 to 2 days (Figure 5.12a-f). Without uranium, complete sequential transformation of IP_6, IP_5, IP_4, and IP_3 occurred (Figure 5.12a). When exposed to uranium concentrations between 25 and 500 μM, however, IP_4 and IP_3 accumulated but were not completely consumed, and little IP_2 was detected (Figure 5.12 b-f). Initial phytate concentrations in incubations of cells exposed to high uranium concentrations (500 μM and 1 mM) were much lower (80% and 52%) than the concentration of IP_6 amended (Figure 5.12f-g), indicating IP_6 was immediately removed from solution by another mechanism than hydrolysis. Interestingly, phytate hydrolysis did not occur in any of the abiotic control incubations (Figure 5.12a-g), suggesting that this mechanism was bacterially driven. Inositol phosphate transformations in incubations of cells exposed to 1 mM uranium were significantly different from all other treatments (Figure 5.12a-g). In these conditions, IP_6 was consumed slowly with a gradual accumulation of IP_5 and IP_4 but not IP_3 or IP_2 over the duration of the incubations (Figure 5.12g). After 232 hours of incubation, however, IP_6 concentrations rapidly decreased to zero and IP_4 accumulated to 600 μM (Figure 5.12g).

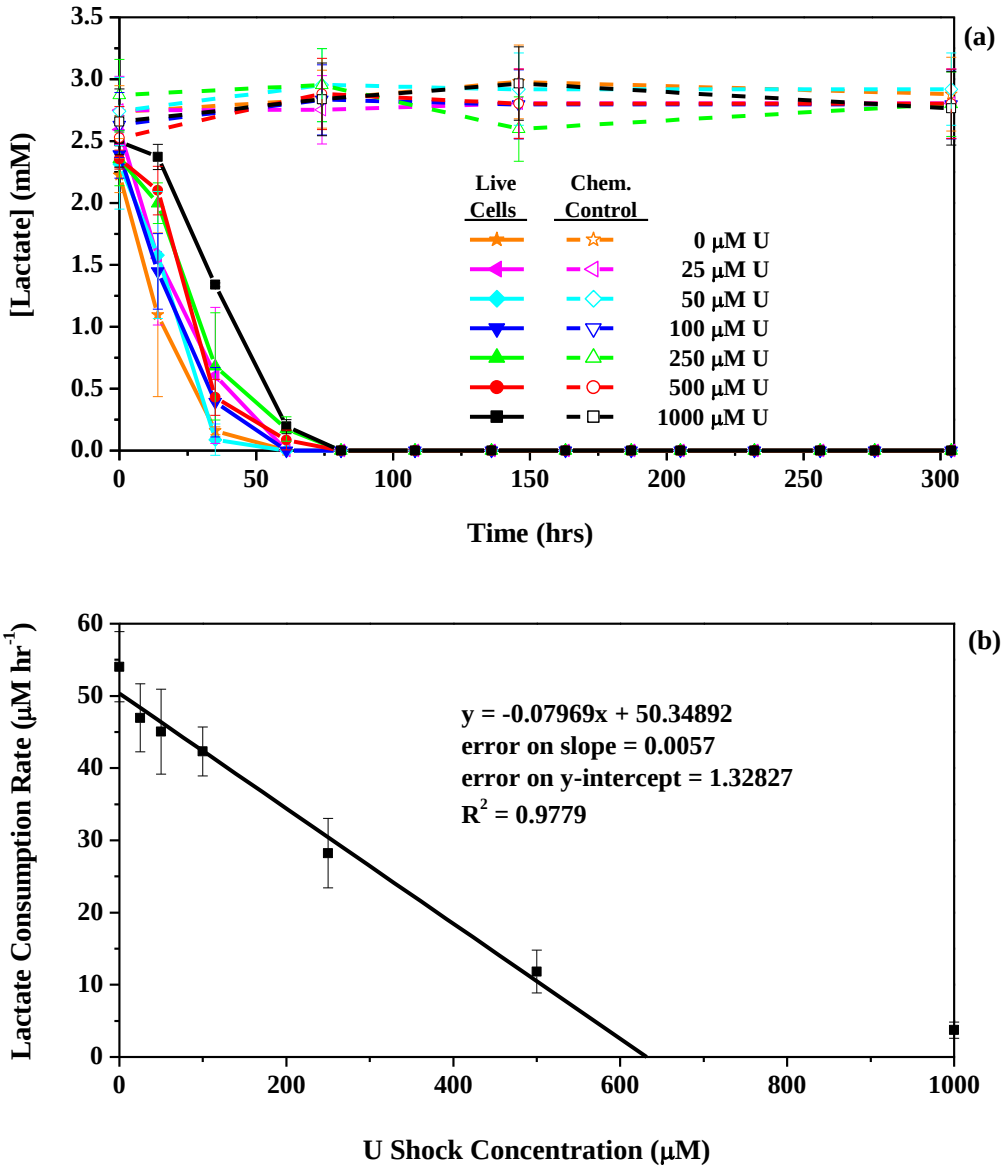

Figure 5.8 (a) Consumption of lactate as a function of time by *Variovorax* sp. initially exposed to increasing concentrations of UO_2^{2+} incubated in aerobic conditions at pH 5.5 in artificial groundwater amended with 3 mM lactate and 1 mM inositol hexaphosphate. Solid symbols with solid lines represent incubations inoculated with live cells, and open symbols with dashed lines represent abiotic control incubations. (b) Initial rate of lactate consumption as a function of the uranium concentration used to shock the cells. The linear fit (black line) does not include the data point of the incubations conducted with cells exposed to 1000 µM uranium. Error bars represent the variation between triplicate incubations and the analytical error on duplicate measurements.

5.5 Discussion

While biomineralization of U(VI)-phosphate minerals has been demonstrated with synthetic organophosphates, the use of a natural phosphorus source to promote this process has only recently been investigated (see Ch. 4 of this dissertation). Hydrolysis of phytate by the ORFRC natural microbial community was previously demonstrated in low pH contaminated soils. In this study, two strains were isolated from the same sediment slurry incubations, and one of these strains was investigated for its ability to not only survive but also catalyze phytate hydrolysis in the presence of uranium. To our knowledge, this is the first study to examine phytate-hydrolysis in pure culture experiments for uranium bioremediation applications.

5.5.1 ORFRC phytate-mineralizing microorganisms

A large proportion of microorganisms enriched from the soil slurries amended with phytate fluoresced in the presence of MUP (Figure 5.1a, 5.1b) regardless of whether or not phytate hydrolysis occurred in the slurry incubations, suggesting that phosphatase activity determined via MUP assays (Adcock and Saint, 2001) is not a good predictor of phytase enzyme activity in the original slurries. While significant microbial growth arose from dilutions of slurries without phytate, no fluorescent colonies were observed in these incubations (Figure 5.1c), indicating that the apparent phosphorus limitation present in these conditions was not sufficient to prime subsurface microorganisms for phosphatase expression. Together, these results demonstrate that the presence of phytate, rather than phytate hydrolysis, promoted ORFRC microbial phosphatase metabolism. The exact mechanism for this phenomenon is unclear, however, it may indicate that alkaline phytase enzyme production was indeed activated in pH 7.0 soil slurries, but that enzyme

function was inhibited by pH (Greiner, 2007), multivalent metals (i.e. Zn^{2+}, Cu^{2+}, Al^{3+}) (Yoon et al., 1996), or a Ca^{2+} limitation (Shimizu, 1992; Shin et al., 2001). Similarly, a large percentage (82%) of MUP-positive isolates displayed a haloed clearing when grown on agar plates amended with phytate (Figure 5.2a, 5.2b). When inoculated into liquid media, however, only two isolates (E.S.5, I.S.2) liberated inorganic phosphate from phytate (Figure 5.3), indicating that regulation of phytase enzyme production may be highly variable in the 82% of MUP-positive isolates that produced a haloed clearing. Indeed, bacterial phytase biosynthesis is generally thought to be triggered in phosphate-limiting conditions and assumed to be controlled by the *Pho* regulon (Mukhametzyanova et al., 2012). At the same time, however, *E. coli* phytase, the most robustly characterized bacterial phytase, is not under control of the *Pho* regulon (Mullaney and Ullah, 2007), demonstrating that the function and regulation of bacterial phytases may be highly variable between bacterial species.

The nBLAST of the PCR-amplified 16S rRNA of the isolates indicated that the phytate-mineralizing bacterium E.S.5 is a member of the genus *Variovorax* and possibly the species *paradoxus*, while strain I.S.2 is likely a member of the genus *Bradyrhizobium*. Both *Variovorax* sp. (Jiang et al., 2012) and *Bradyrhizobium* sp. (Vanrhijn and Vanderleyden, 1995) are known to form symbiotic relationships with plants in the rhizosphere. Thus, the ability of isolates E.S.5 and I.S.2 to hydrolyze phytate may stem evolutionarily from their proximal relationship to plants, which commonly synthesize phytate for phosphorus storage (Turner et al., 2002).

The genus *Bradyrhizobium* represents a class of gram-negative *alphaproteobacteria* from the family *Bradyrhizobiaceae* (Jordan, 1982) and has been

well-characterized as a nitrogen-fixing symbiotic bacterium that nodulates the roots of leguminous plants (Wielbo, 2012). The type of plant nodulated is highly variable between bacterial species. However, the process of plant nodule formation, which involves signaling by plants to induce *nod* gene expression by nodulating rhizobacteria, is highly conserved by all nodulating *Bradyrhizobiaceae* (Fisher and Long, 1992). Recently, *Bradyrhizobium* sp. strain FRC01 was isolated from background ORFRC sediments (Wang et al., 2013a). Strain FRC01 was the sole bacterial strain in ORFRC denitrifying enrichments that survived treatment with 312 nM Hg(II) as determined by terminal restriction fragment length polymorphism (tRFLP) (Wang et al., 2013a). The survival of *Bradyrhizobium* sp. may be attributed to expression of *merA* (Wang et al., 2013a), a mercuric iron reductase which catalyzes the reduction of toxic Hg(II) to volatile Hg(0) (Barkay et al., 2003; Summers and Sugarman, 1974) .

The genus *Variovorax* is a class of gram-negative *Betaproteobacteria* belonging to the family *Comamonadaceae* (Willems et al., 2005). *Variovorax* sp. are common inhabitants of soil and water (Willems et al., 2005) and have been isolated from environments all over the world (Satola et al., 2013), possibly due to their ability to survive on airborne particles during transport (Ravva et al., 2012). In addition, *Variovorax* sp. display chemoorganotrophic metabolisms and are well-known for their diverse and unique metabolic capabilities, particularly in the species *Paradoxus* (Satola et al., 2013). *Paradoxus* strains are facultative anaerobes and are known to degrade a large number of complex organic substrates for carbon assimilation (Satola et al., 2013). They frequently occur in environments polluted with organic contaminants (Dejonghe et al., 2003; Futamata et al., 2001; Futamata et al., 2005; Greene et al., 2000; Nogales et al.,

1999; Snellinx et al., 2003; Suyama et al., 1998), arsenite (Macur et al., 2004), and other heavy metals (Belimov et al., 2001). In fact, two strains of *Variovorax paradoxus* have been isolated from Oak Ridge Waste Area Grouping 5 (WAG5) site groundwater (Gao et al., 2010), which has been investigated for its role in the formation of the Oak Ridge tritium plume (Jardine et al., 1999; Lenczewski et al., 2003). Currently, the only *Variovorax paradoxus* strain with a published whole genome sequence is S110 (Han et al., 2011). Interestingly, this strain does not show any identifiable phytase genes within its genome. However, it does display genome regions which code for inositol monophosphatase (Gene Vapar_3566) and inositol phosphatase/fructose-16-bisphosphatase (Gene Vapar_3026), enzymes involved in *myo*-inositol biosynthesis which are usually found in plants or eukaryotes (Majumder et al., 2003). In all identified inositol-synthesizing organisms, *myo*-inositol biosynthesis is achieved via dephosphorylation of *myo*-inositol 1-phosphate generated from glucose-6-phosphate by L-*myo*-inositol 1-phosphate synthase (MIPS) (Majumder et al., 2003).

Inorganic phosphate liberated from phytate by *V. paradoxus* sp. and *Bradyrhizobium* sp. was not significantly affected by the type of available electron donor. In the presence of glycerol (Figure 5.3), lactate, acetate, and formate (Figure 5.6), both *Variovorax* sp. and *Bradyrhizobium* sp. released over 50% of available organic phosphate as orthophosphate. With extracellular orthophosphate in excess of 1 mM, intracellular orthophosphate concentrations accumulate as high as 80 mM in *Streptococcus Lactis* (Poolman et al., 1987) and 13 mM in *Escherichia Coli* (Vershinina and Znamenskaya, 2002). However, intracellular accumulation of phosphate only depleted extracellular orthosphosphate by ~ 100 µM (Poolman et al., 1987), suggesting that cell lysis by

Variovorax sp. and *Bradyrhizobium* sp. should not account for a significant fraction of the observed 4 mM orthophosphate accumulation. These observations suggest orthophosphate liberation by *Variovorax* sp. and *Bradyrhizobium* sp. was most likely due to phytate-hydrolysis that may apparently be coupled to oxidation of a wide variety of carbon sources. Although not the degree of *V. paradoxus* or *Bradyrhizobium* sp., *Shewanella oneidensis* MR-1, which is known to possess phytase enzymes (Cheng and Lim, 2006), and *Shewanella putrefaciens* strain 200 also liberated significant levels of inorganic phosphate compared to chemical control experiments (Figure 5.6), suggesting either that hydrolysis of IP_6 was minimal, that inorganic phosphate produced was immediately acquired by the cells, or that the phosphate produced in the cultures originated from different sources (e.g. lysis of cell material).

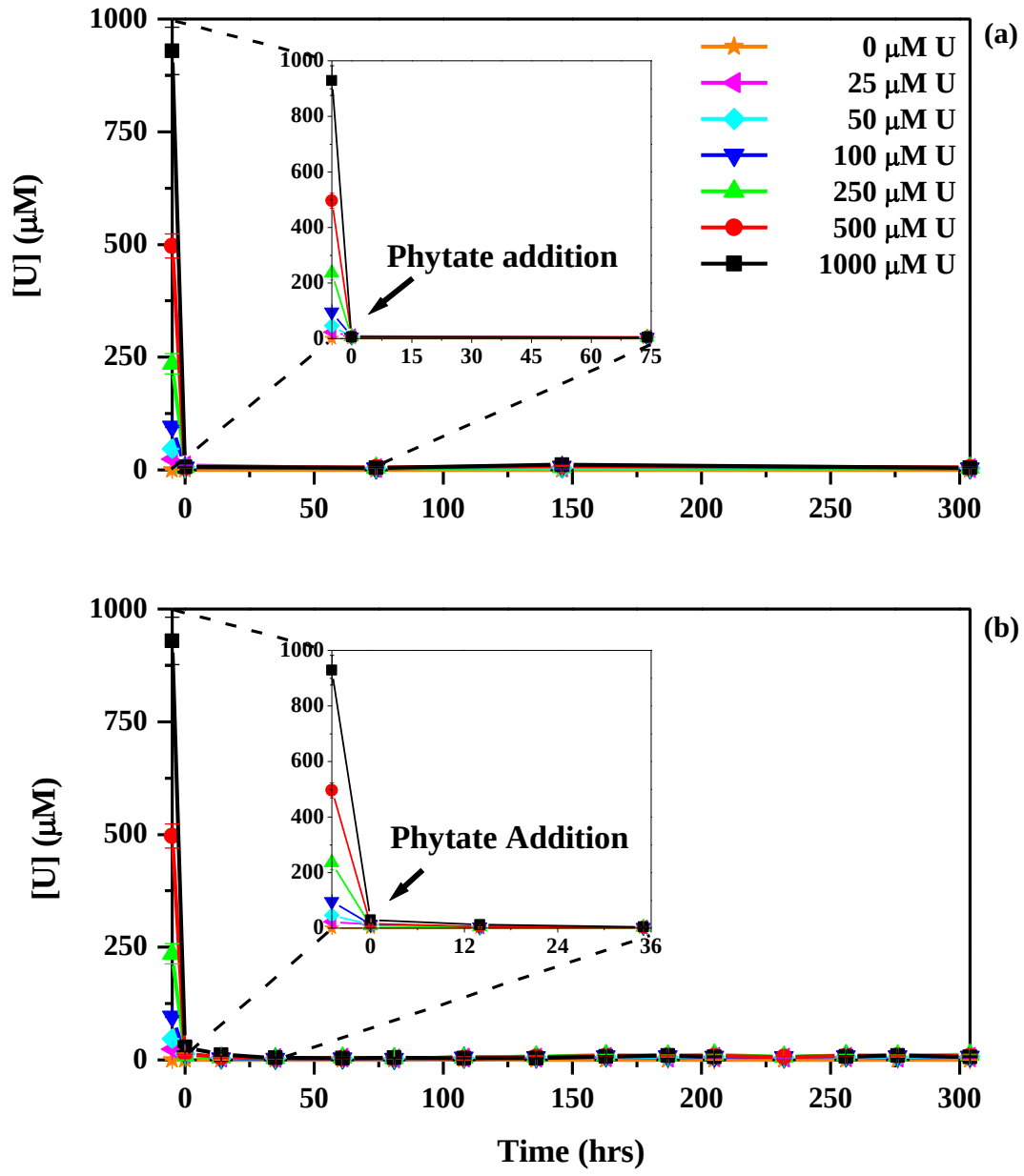

Figure 5.9 Dissolved uranium as a function of time in (a) chemical control incubations and (b) aerobic pure culture incubations of *Variovorax* sp. initially exposed to increasing concentration of UO_2^{2+}. Incubations were conducted at pH 5.5 in artificial groundwater amended with 3 mM lactate and 1 mM inositol hexaphosphate. Error bars represent the variation between triplicate incubations and the analytical error on duplicate measurements.

5.5.2 Effect of uranium exposure on phytate hydrolysis by Variovorax sp.

At pH 5.5, phytate exhibits an approximately equal mixture of species with either a -6 or -7 charge and, thus, is expected to interact strongly with multivalent cations (Turner et al., 2002; Wodzinski and Ullah, 1996). Prior to phytate addition, uranium remained in solution in both abiotic control experiments (Figure 5.9a) and live incubations with *Variovorax* sp. (Figure 5.9b). However, upon phytate addition uranium was immediately removed from solution (Figure 5.9a, 5.9b). As essentially identical uranium removal behavior was observed in chemical control and live cell incubations for all concentrations of uranium, this precipitation mechanism cannot be attributed to cellular processes. Thus, the rapid initial U removal in these incubations was likely due to a chemical precipitation of uranium with phytate. While previous research revealed uranium should remain soluble with $[IP_6]$:[U] ratios above 10:1 (Ch. 4 of this dissertation, Figure 4.1b), uranium was only sparingly soluble in all experimental treatments after phytate addition, even with [U]:$[IP_6]$ ratios as high as [40]:[1] (Figure 5.9a, 5.9b), indicating uranium solubility in the presence of IP_6 is driven by steric hindrances produced at elevated phytate concentrations rather than by the relative concentrations of these species. Previous investigations have demonstrated chemical uranium immobilization with Ca-phytate (Knox et al., 2008; Nash et al., 1998; Seaman et al., 2003) either through a coprecipitation with Ca-Phytate or exchange between calcium in the phytate solid and UO_2^{2+} (Nash et al., 1998). In addition, metals such as lead have been shown to sorb strongly to Ca-phytate precipitates (Wise, 1986). As calcium concentrations in the artificial groundwater were relatively low and constant at 200 μM in all incubations, precipitation with calcium cannot account for the markedly decreased

solubility of phytate in incubations containing elevated concentrations of uranium (Figure 5.12f, 5.12g). Thus, the removal of uranium in these experiments is attributed to direct precipitation with phytate.

In live-cell control experiments where *Variovorax* sp. was inoculated into pH 5.5 artificial groundwater amended with increasing concentrations of uranium but no added organophosphate, cell growth only occurred in incubations without uranium over the 81 hour incubation period (see Figure C.4 in Appendix). As background phosphate was not limiting in these conditions, these findings suggest that uranium may produce a toxicity effect on *Variovorax* sp.. Contrastingly, in the presence of phytate, *Variovorax* sp. growth rates (Figure 5.7c) and lactate consumption rates (Figure 5.8b) were initially negligible but later rebounded (Figure 5.7b, 5.8a) with a concurrent rise in pH (Figure 5.7a) likely attributable to the production of CO_2 during microbial respiration. These results indicate the apparent uranium toxicity effect on *Variovorax* sp. was reversible in these conditions. *Pseudomonas fluorescens*, a gram-negative subsurface denitrifier, displayed a similar behavior (Bencheikh-Latmani and Leckie, 2003). Although citrate degradation by *P. fluorescens* was inhibited by uranyl, 30% of cell metabolism was restored after desorption of cell-associated U(VI) by a carbonate wash. In addition, the presence of a strong chelator such as EDTA at acidic pH was found to decrease the inhibitory effect of uranyl on iron oxidation by *Thiobacillus ferrooxidans* (Tuovinen and Kelly, 1974). Similarly, uranyl sorption to the cell surface may have a toxicity effect on *Variovorax* sp.. At pH 5.5 in the absence of phytate, the dominant uranyl species in artificial groundwater are free uranyl and positively charged hydroxide complexes (Figure 1.3d) which should interact strongly with negatively charged phosphate and

carboxylate functional groups (Suzuki and Banfield, 1999) on gram-negative (Haas et al., 2001) and gram-positive cell surfaces (Fowle et al., 2000). Phytate, like EDTA, efficiently chelates metals and likely desorbed uranyl from cell surfaces and precipitated U(VI) phytate outside the cells, which restored metabolic activity. Interestingly, when the cells were exposed to uranium concentrations above 500 µM, the toxicity effect on *Variovorax* sp. was not exacerbated (Figure 5.7c, 5.8b), suggesting sorption sites on cell surfaces were possibly saturated with uranyl around a uranium concentration of 500 µM. In contrast, if uranium toxicity observed for *Variovorax* sp. was due to uptake of U(VI) by the cells, addition of 1 mM uranium should have been even more toxic than addition of 500 µM U, and uranium toxicity should have been irreversible.

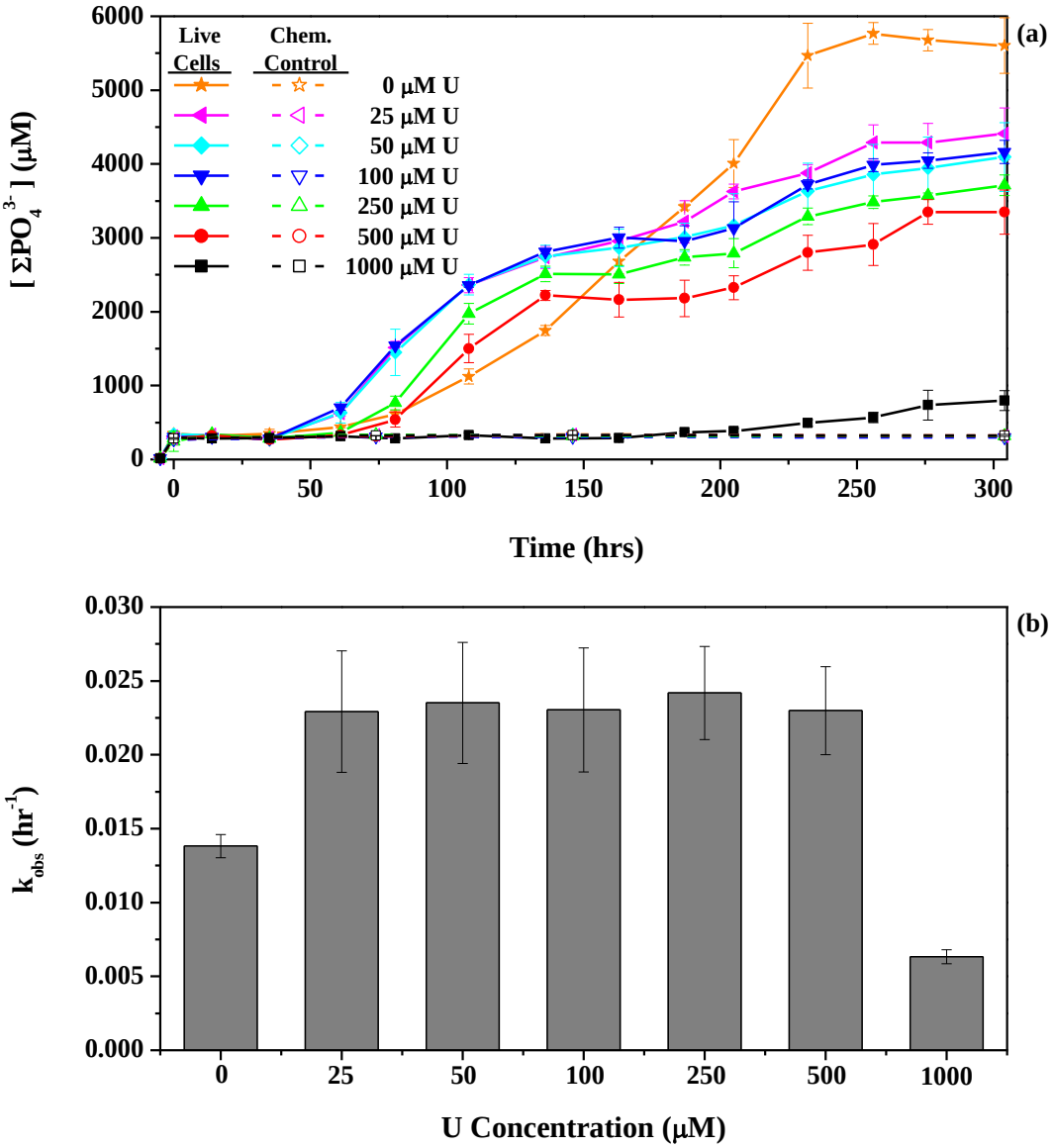

Figure 5.10 (a) Production of inorganic phosphate (ΣPO_4^{3-}) as a function of time by *Variovorax* sp. exposed to increasing concentrations of UO_2^{2+} initially. Incubations were conducted in aerobic conditions at pH 5.5 in artificial groundwater amended with 3 mM lactate and 1 mM inositol hexaphosphate. Solid symbols with solid lines represent incubations inoculated with live cells, and open symbols with dashed lines represent chemical controls. Error bars represent the variation between triplicate incubations and the analytical error on duplicate measurements. (b) Calculated pseudo-first-order rates constants (k_{obs}) for inorganic phosphate (ΣPO_4^{3-}) production by *Variovorax* sp. exposed to increasing uranium concentrations. Error bars represent the standard error of the slope of the linear regression used to calculate k_{obs}.

Variovorax sp. cells unexposed to uranium completely hydrolyzed phytate over a 2 week incubation period (Figure 5.10a) with a calculated pseudo-first order rate constant for initial inorganic phosphate production of 0.014 ± 0.001 hr^{-1} (Figure 5.10b) suggesting phytate hydrolysis catalyzed by phytase enzymes may have been induced by phosphate limitation (Mukhametzyanova et al., 2012) in these conditions. Interestingly, the calculated pseudo-first order rate constant for initial orthophosphate production nearly doubled upon introduction of 25 µM UO_2^{2+} and remained elevated until uranium concentrations reached 1 mM (Figure 5.10b). In addition, the lag phase in the onset of phytate hydrolysis (Figure 5.11b) and inorganic phosphate production (Figure 5.11a) decreased significantly in incubations of cells exposed to 25 µM uranium, indicating phytate hydrolysis by *Variovorax* sp. may represent a uranium detoxification mechanism in these conditions. Hydrolysis of organophosphates as uranium detoxification mechanism has been proposed before for *Citrobacter* sp. in low-pH aerobic conditions (Macaskie et al., 1995; Montgomery et al., 1995) and for the facultative anaerobe *Rahnella* sp. Y9602 in both aerobic and anaerobic conditions and at both circumneutral and acidic pH (Beazley et al., 2007, 2009; Martinez et al., 2007). As IP_6 hydrolysis at pH 5.5 requires catalysis by phytase enzymes (Irving and Cosgrove, 1974), it may also be surmised that *Variovorax* sp. might activate phytase enzyme production partly in response to perceived uranium toxicity.

While inorganic phosphate production when cells were exposed to uranium occurred more rapidly and earlier than in otherwise identical experiments with unexposed cells, the net production of orthophosphate by all uranium-exposed cells temporarily ceased and then resumed but at a much slower rate than initially observed (Figure 5.10a).

In addition, this drastic shift in phosphate accumulation observed in the presence of uranium was not conserved in incubations without uranium (Figure 5.10a). Together, these results suggest a possible shift in the impetus for enzyme production by cells exposed to uranium after 136 hours of incubation that was not apparent for experiments with unexposed cells. To our knowledge, the effect of uranium on orthophosphate production via microbially-mediated phytate hydrolysis has not been previously examined. However, uranyl detoxification through intracellular (Strandberg et al., 1981; Suzuki and Banfield, 2004) and extracellular (Beazley et al., 2007; Macaskie et al., 2000) precipitation with phosphate has been demonstrated. In addition, bacterial up-regulation of the gene CC1295, an extracellular protein containing a phytase domain known to bind Ca^{2+} and IP_6 (Oh et al., 2001), was demonstrated through comparative analysis of genome-wide transcriptional activities in *Caulobacter crescentus* both before and after exposure to 200 µM uranium (Hu et al., 2005), suggesting phytase gene expression may indeed play a role in uranium detoxification by heavy-metal resistant microorganisms.

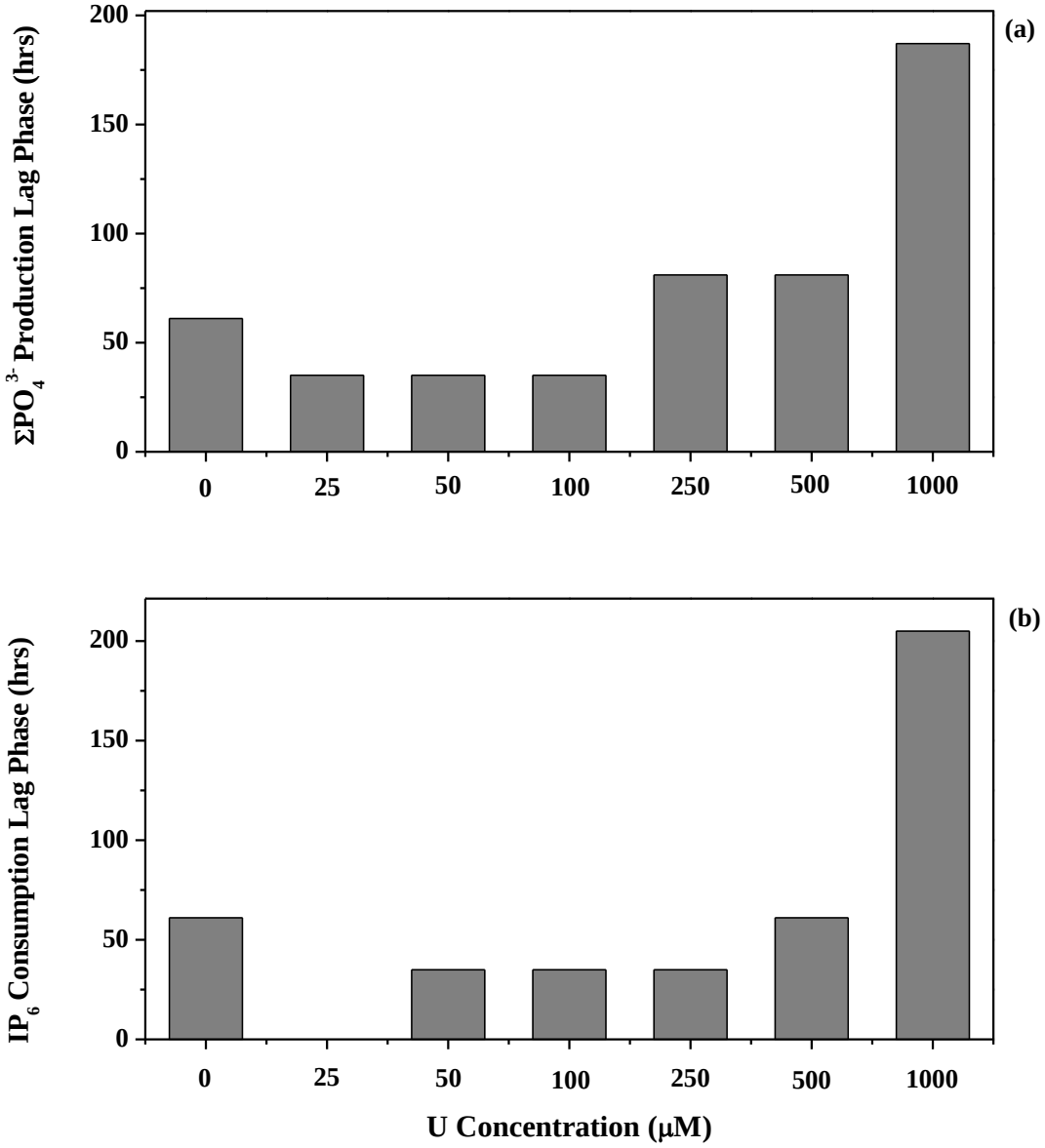

Figure 5.11 Lag phase in the onset of (a) inorganic phosphate (ΣPO_4^{3-}) production and (b) inositol hexaphosphate (IP_6) consumption by *Variovorax* sp. exposed to increasing concentrations of UO_2^{2+} for 4 hours prior to incubation in pH 5.5 artificial groundwater amended with 3 mM lactate and 1 mM inositol hexaphosphate.

Examination of the extent of orthophosphate production also reveals an interesting relationship between uranium exposure levels and the concentration of inorganic phosphate measured at the end of the incubations. Excluding incubations not amended with uranium in which phytate degradation proceeded almost to completion (Figure 5.12a), the extent of orthophosphate accumulation after 2 weeks of incubation decreased linearly with exposure to increasing uranium concentrations (Figure C.5). As uranium was precipitated with phytate prior to phytate hydrolysis and inorganic phosphate production in these incubations (Figure 5.9a, 5.9b), this decrease in overall orthophosphate accumulation cannot solely be explained by the precipitation of U(VI)-phosphate minerals. Alternatively, the decrease in orthophosphate production, which occurred well after uranium immobilization, may represent a hysteresis effect on *Variovorax* sp. whereby the toxic effects of uranium on microbial metabolism are not completely reversible upon removal of the toxic substance. This phenomenon has also been demonstrated with other microorganisms and a range of contaminants including U, Ni, Cu, and various organic compounds (Bencheikh-Latmani and Leckie, 2003; Czechowska and van der Meer, 2012; Huang et al., 1998; Mueller and Steiner, 1992; Tuovinen and Kelly, 1974).

As expected, the trend in IP_6 hydrolysis lag phase mirrored that observed for orthophosphate production in all experimental treatments (Figure 5.11a, 5.11b), further supporting the premise that *Variovorax* sp. may produce acidic phytase enzymes to detoxify uranium. In addition, the incomplete transformation of lower inositol phosphate degradation products observed for uranium-amended incubations did not occur in identical experiments without uranium addition (Figure 5.12a-5.12g), indicating either

an inhibition of phytase enzyme function in the presence of uranium or a shift in the dominant hydrolysis mechanism in cells exposed to uranium. At acidic pH, bacterial acid phytase activity is inhibited by negatively charged oxyanions which interact with positively charged arginine, lysine, and histidine residues in the enzyme active site (Ullah et al., 2011). As uranium predominantly carries a positive charge at pH 5.5, it should not disrupt acid phytase enzyme function in this system. Therefore, the decrease in rate of inositol phosphate hydrolysis evident in uranium-exposed cells likely reflects a shift in the mechanism of hydrolysis rather than the effect of direct enzyme inhibition.

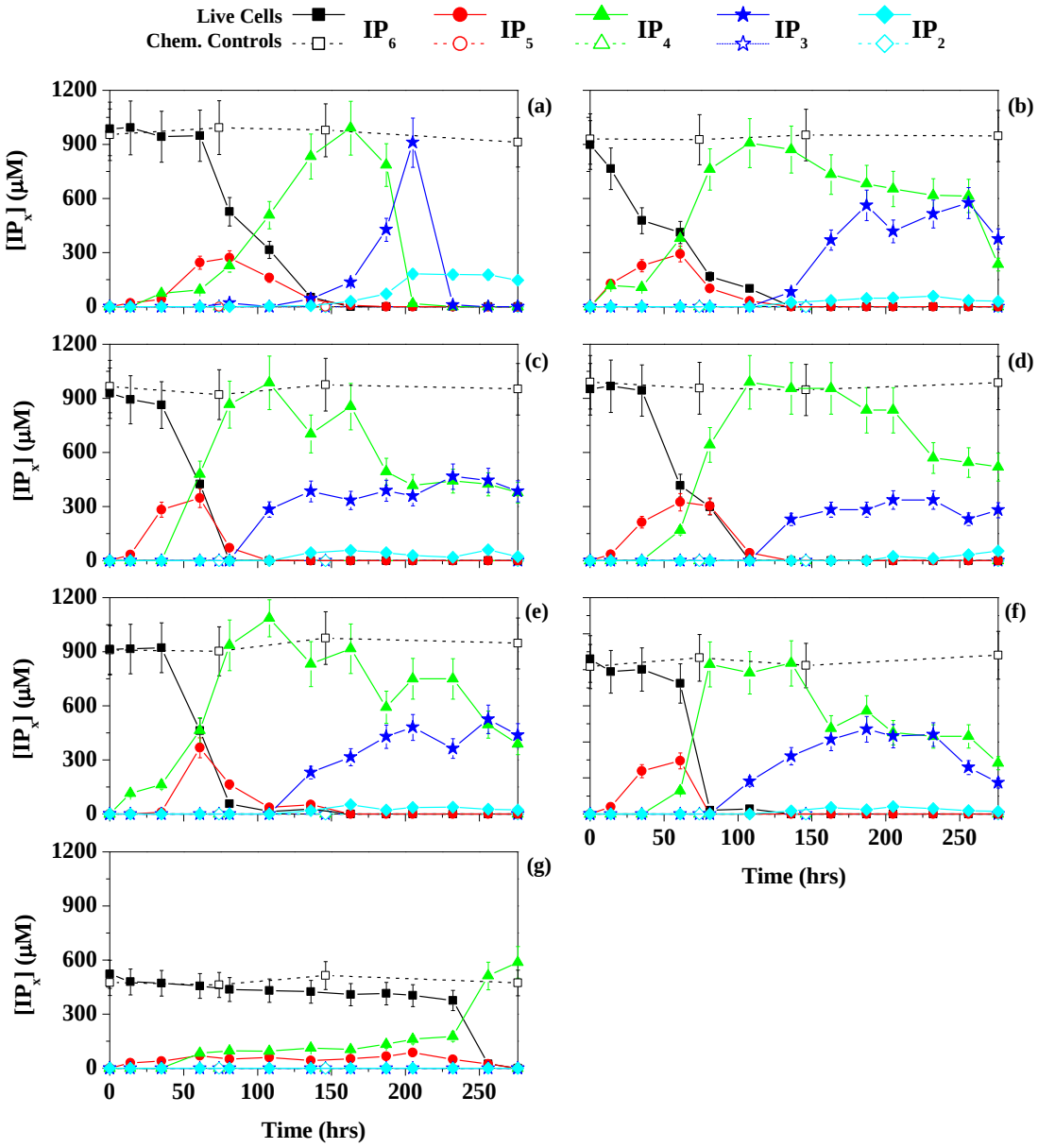

Figure 5.12 Transformation of inositol hexaphosphate (IP_6), inositol pentaphosphate (IP_5), inositol tetraphosphate (IP_4), inositol triphosphate (IP_3), and inositol bisphosphate (IP_2) as a function of time by *Variovorax* sp. exposed to: (a) 0 μM UO_2^{2+}, (b) 25 μM UO_2^{2+}, (c) 50 μM UO_2^{2+}, (d) 100 μM UO_2^{2+}, (e) 250 μM UO_2^{2+}, (f) 500 μM UO_2^{2+}, or (g) 1000 μM UO_2^{2+} for 4 hours before the beginning of the incubations. Cells were incubated in aerobic conditions, at pH 5.5, and in artificial groundwater amended with 3 mM lactate and 1 mM inositol phosphate. Closed symbols with solid lines represent incubations inoculated with live cells, and open symbols with dashed lines represent

chemical control incubations. Error bars represent the variation between triplicate incubations and the analytical error from calibrations.

In situ uranium immobilization promoted via U(VI)-phosphate biomineralization is a promising remediation strategy due to its utility in a range of environments, including at contaminated sites such as the ORFRC where fluctuating redox-conditions, elevated nitrate concentrations, and low pH complicate bioreduction. Phytate, a naturally occurring and abundant compound in soils, represents an ideal organophosphate to promote this process. Yet, microbially-mediated phytate hydrolysis coupled to chemical precipitation of U(VI)-phosphate minerals was only recently investigated in soils slurries with ORFRC sediments. In this study, phytate hydrolysis by bacteria isolated from contaminated sediments was demonstrated. IP_6 was hydrolyzed by *Variovorax* sp., even after exposure to elevated uranium levels, indicating *Variovorax* sp. may actively hydrolyze phytate *in situ* and, thus, represent a model organism for in-depth examination of phytate-promoted U(VI)-phosphate biomineralization. More importantly, phytate hydrolysis was coupled to liberation of significant inorganic phosphate, demonstrating that phytate hydrolysis by *Variovorax* sp. is not inhibited at high phosphate concentrations. In addition, the incomplete degradation of IP_x (x = 2:4) intermediates may stimulate other subsurface microorganisms with conventional phosphohydrolases that could process these compounds and further enhance inorganic phosphate production. Thus, phytate-promoted U(VI)-phosphate biomineralization strategies represent an attractive method to immobilize uranium in a variety of low pH environments.

5.6 Conclusions

The biomineralization of U(VI)-phosphate minerals represents an attractive uranium bioremediation strategy in low pH environments with elevated concentrations of

bioreduction-inhibiting co-contaminants. U(VI)-phosphate biomineralization has been successfully demonstrated, yet studies have primarily investigated addition of exogenous organophosphates to contaminated environments which may be both expensive and difficult to implement for *in situ* field applications. The use of phytate, a naturally-occurring and abundant organophosphate in soils, as an alternative to synthetic substrates has only recently been considered. While phytate hydrolysis promoted by soil slurries containing contaminated ORFRC sediments has been demonstrated (Chapter 4 of this dissertation), pure cultures studies with metal-tolerant phytate-hydrolyzing microorganisms are still lacking. In this study, phytate-hydrolyzing isolates were enriched from uranium-contaminated sediments, and the effect of exposure to increasing concentrations of uranium on phytate-hydrolysis promoted by *Variovorax* sp. was investigated in aerobic conditions at pH 5.5 to determine its potential as a model organism for investigations of the mechanism of phytate-promoted U(VI)-phosphate biomineralization.

Without uranium, *Variovorax* sp. completely hydrolyzed phytate and released all inorganic phosphate in solution as confirmed by the lack of phytate hydrolysis by-products. When the cells were initially exposed to increasing uranium concentrations, however, total inorganic phosphate production over the two week incubation period decreased linearly with increasing U(VI) concentration, suggesting the existence of a significant uranium toxicity effect. In addition, introduction of uranium resulted in earlier onset of both IP_6 degradation and inorganic phosphate production, along with more rapid inorganic phosphate production compared to identical reactors without uranium, suggesting phytase enzymes produced by *Variovorax* sp. generate phosphate to

immobilize uranium under the form of uranium phosphate minerals as a detoxification mechanism. Interestingly, this behavior was observed in spite of the almost instantaneous precipitation of uranium with phytate, suggesting the existence of a memory effect whereby the influence of uranium toxicity was observed well after removal of the toxic substance. Overall, the results of this study suggest that phytate addition to uranium contaminated environments may promote both chemical uranium sequestration and biomineralization of U(VI)-phosphate minerals via microbially-mediated phytate hydrolysis. This process may be complemented by hydrolysis of phytate degradation by-products by other organisms that express conventional phosphohydrolases, especially when the concentration of uranium reaches toxic levels in contaminated environments.

5.7 Acknowledgements

This research was supported by the Office of Science (BER), US Department of Energy Grant No. DE-FG02-04ER63906. We thank Dave Watson of Oak Ridge National Laboratory for providing ORFRC sediment cores.

CHAPTER 6

DEVELOPMENT OF A DIAGNOSTIC KINETIC MODEL FOR MICROBIALLY-MEDIATED PHYTATE HYDROLYSIS IN CONTAMINATED ENVIRONMENTS

In preparation for submission to *Environmental Science and Technology*

6.1 Abstract

For phytate-promoted U(VI)-phosphate biomineralization to be implemented as bioremediation strategy, predictive models describing the mechanism of microbial phytate hydrolysis must first be developed. In this study, the exposure of *Variovorax* sp. to varying uranium concentrations in the presence of phytate was used to validate a kinetic model for the enzymatic hydrolysis of phytate and its inositol intermediate products. Cell growth, the transformation of phytate and its inositol phosphate intermediates, and the production of inorganic phosphate were successfully modeled with Michaelis-Menten type kinetics adjusted to account for the competition between all inositol phosphate species for a single phytase enzyme. Kinetic parameters indicate the affinity of the enzyme for each inositol phosphate and their rates of hydrolysis depend on the stability of the substrate and the steric hindrance between enzyme and substrate. Comparison of several incubations conducted with the same microorganism exposed to increasing uranium concentrations suggests that exposure to uranium increases the production of phytase enzymes by *Variovorax* to enhance phytate hydrolysis and precipitate uranium phosphate minerals, possibly as a detoxification mechanism.

6.2 Introduction

Large-scale uranium contamination remains a pressing problem at Department of Energy (DOE) managed waste sites throughout the United States. The existence of these sites, along with the projected increase in nuclear power production, requires that an effective remediation strategy be developed for these contaminants. The biomineralization of U(VI)-phosphate minerals represents a promising uranium bioremediation strategy which has gained popularity in recent years (Beazley et al., 2007, 2009; Beazley et al., 2011; Macaskie et al., 1994; Macaskie et al., 2000; Martinez et al., 2007; Salome et al., 2013; Shelobolina et al., 2009). This technique requires addition of an organophosphate to contaminated subsurface environments to stimulate microbially-mediated organophosphate hydrolysis that is coupled to the chemical precipitation of U(VI)-phosphate minerals. For all contaminant remediation strategies, predictive capabilities which incorporate transport and reactive transformation of contaminants are vital for the successful field implementation of laboratory-tested techniques. Rapid chemical reactions such as adsorption, oxidation, and sometimes precipitation/dissolution are usually transport limited processes, and reaction networks may use a thermodynamic approach that is easily implemented in reactive transport models (Steefel and Van Cappellen, 1990). In turn, microbially-mediated reactions are often reaction limited and required to be implemented as kinetic rate laws in reactive transport models (e.g. Regnier et al., 2005; Thullner et al., 2005; Wang and Van Cappellen, 1996). Rate laws are based on mechanistic considerations, and while the kinetics of chemical reactions are relatively well known, the kinetics of most microbial reactions remains poorly understood and have to be validated for implementation in reactive transport models (Thullner et al., 2007).

Microbial organophosphate hydrolysis is an enzymatically controlled process. Phosphohydrolases, or phosphatases, are found widely in the environment and are primarily of bacterial origin (Rossolini et al., 1998). To fulfill their phosphate requirements, subsurface microorganisms often produce phosphohydrolase enzymes which catalyze the hydrolysis of organic phosphoester bonds in a broad range of chemical conditions (Rossolini et al., 1998). Previous research has primarily investigated the use of the synthetic organophosphates glycerol-3-phosphate (G3P) (Beazley et al., 2007, 2009; Martinez et al., 2007; Shelobolina et al., 2009) and glycerol-2-phosphate (G2P) (Beazley et al., 2011; Macaskie et al., 2000; Salome et al., 2013) to promote microbial phosphatase expression and organophosphate hydrolysis. However, recent studies have investigated the use of phytate, a naturally-occurring and abundant organophosphate (Turner et al., 2002), to promote U(VI)-phosphate biomineralization (see Chapters 4 and 5 of this dissertation). Phytate, also known as inositol hexaphosphate (IP_6) or phytic acid, presents a unique enzymatic challenge for subsurface microorganisms as conventional phosphohydrolases cannot catalyze its hydrolysis (Turner et al., 2002). Instead, enantioselective phytase enzymes are required to initiate IP_6 degradation to lower inositol derivatives (IP_x, x = 1-5) and orthophosphate (Irving and Cosgrove, 1971; Parthasarathy and Eisenberg, 1991). Once hydrolysis of the initial phosphate group from IP_6 is achieved, however, hydrolysis of lower inositol derivatives (IP_x, x= 1-5) may be catalyzed either by phytase or any phosphohydrolase (Marko-Varga and Gorton, 1990; Meek and Nicoletti, 1986).

In natural systems, uranium mobility is controlled by a complex combination of sorption, reductive or non-reductive precipitation, and ligand complexation reactions.

Thermodynamic models, which predict the fate of uranium assuming chemical equilibrium is reached, have been widely used in combination with laboratory techniques to elucidate the dominant processes controlling uranium mobility in a given system (e.g. Beazley et al., 2007; Bruno et al., 1995; Han et al., 2007; Salome et al., 2013). As natural environments represent dynamic systems that are seldom at equilibrium, however, thermodynamic models may not capture the effect of transport and reactive transformations on the spatial and temporal distribution of uranium in soils and sedimentary environments. In these cases, kinetic models better reflect the dominant chemical reactions and transport processes that drive the complex biogeochemical dynamics prevalent in the environment, and these models are typically used as predictive tools (Steefel et al., 2005) when the biogeochemical mechanism of uranium transformation is known, as in the case of uranium reduction (Luo et al., 2007a; Zhang et al., 2010), sorption (Katsoyiannis, 2007), dissolution (Liu et al., 2004), and precipitation (Beazley et al., 2011). When the microbial or geochemical mechanism is unknown, however, as in the case of the microbial hydrolysis of phytate and its role in the immobilization of uranium, kinetic models are used as diagnostic tools to test the different possible mechanisms involved (Thullner et al., 2005; Yabusaki et al., 2008). Rate laws obtained from these experiments are then incorporated in more complex models that include both transport and reactive transformations (Beazley et al., 2011).

In this study, enzymatic transformation of inositol phosphates by *Variovorax* sp. in batch reactors was described using Michaelis-Menten enzyme kinetics modified to reflect enzymatic competition. The goal of this exercise is to elucidate the mechanism of phytate hydrolysis by the model phytate-hydrolyzing bacterium *Variovorax* sp. and to

derive kinetic parameters for microbially catalyzed phytate hydrolysis. If successful, the development of predictive capabilities for phytate hydrolysis by natural microbial communities in contaminated environments could represent an important advance towards determining contaminant mobility in U(VI)-phosphate biomineralization strategies. The data sets used below were reported in Salome et al. (2013) (Chapter 5 of this dissertation).

6.3 Modeling phytate hydrolysis by *Variovorax* sp.

6.3.1 Governing Equations

The kinetic equations governing biomass production, lactate consumption, and IP_6 consumption in batch reactor experiments conducted with a pure culture of *Variovorax* sp. isolated in Chapter 5 of this dissertation were primarily derived from the reaction described in Equation 6-1. This governing equation assumes Michaelis-Menten enzyme kinetics (Equation 6-2) whereby the rate of substrate (*S*) degradation or product (*P*) accumulation is dependent on the initial concentration of enzyme (included in the maximum rate, R_x), the substrate concentration, and the Michaelis-Menten equilibrium constant (K_x).

$$S_x + E \rightleftharpoons_{k_{-x}}^{k_x} ES_x \xrightarrow{k_{hx}} P + E \tag{6-1}$$

$$\frac{d[S_x]}{dt} = -\frac{R_x[S_x]}{K_x + [S_x]}$$

$$where\ K_x = \frac{k_{-x} + k_{hx}}{k_x}\ \ and\ R_x = k_{hx}[E_0] \tag{6-2}$$

Assuming the hydrolysis of all inositol phosphates (IP_x, x = 2 – 5) is catalyzed solely by phytase enzymes, it follows that the mathematical model used to describe their degradation should account for the competition between each IP_x species for a fixed concentration of enzymes. In addition, it was assumed that only more highly phosphorylated inositol phosphates compete with hydrolysis of a given IP_x species as their phosphate groups are more likely to come into contact with available phytase enzymes than less phosphorylated inositol phosphates. For example, IP_4 hydrolysis should only be outcompeted by IP_5 and IP_6 hydrolysis. Thus, inositol phosphate degradation was modeled using Michaelis-Menten enzyme kinetics modified to reflect this competition between a given IP_x species (S_x) and the competing inositol phosphates (S_{x+1}) (Equations 6-3 to 6-7).

$$S_x + E \rightleftharpoons_{k_{-x}}^{k_x} ES_x \tag{6-3}$$

$$S_{x+1} + E \rightleftharpoons_{k_{-(x+1)}}^{k_{x+1}} ES_{x+1} \tag{6-4}$$

$$ES_x \xrightarrow{k_{hx}} S_{x-1} + E \tag{6-5}$$

$$ES_{x+1} \xrightarrow{k_{h(x+1)}} S_x + E \tag{6-6}$$

$$\frac{d[S_x]}{dt} = -\frac{R_x[S_x]}{K_x\left(1 + \frac{[S_{x+1}]}{K_{x+1}}\right) + [S_x]}$$

$$where \;\; R_x = k_{hx}[E_0], \;\; K_x = \frac{k_{-x} + k_{hx}}{k_x}, \; and \; K_{x+1} = \frac{k_{-(x+1)} + k_{h(x+1)}}{k_{x+1}} \tag{6-7}$$

6.3.2 Reactions and Rates

The reactions taking place in this system are presented in Table 6.1, and the accompanying rate laws for each chemical species of interest are described by equations

6-8 through 6-12. The governing reactions for this system were derived assuming a single enzyme (i.e. phytase) hydrolyzes all inositol phosphate species and the IP_x degradation rate is a function of microbial abundance (i.e. [*X*]). The effect of pH was neglected as the system was buffered at pH 5.5 using MES (see Chapter 5 of this dissertation).

Table 6.1 Reactions governing inositol phosphate transformation by phytase enzymes produced by *Variovorax* sp. during aerobic respiration. *Lac*$^-$ denotes lactate ($C_3O_3H_5^-$) and *X* represents biomass (i.e. *Variovorax* sp. cell growth).

$Lac^- + O_2 + H^+ \overset{K_{Lac}}{\longleftrightarrow} CO_2 + H_2O + X$	Lactate Respiration
$IP_6 + E \rightleftharpoons^{k_6}_{k_{-6}} EIP_6 \overset{k_{h6}}{\longrightarrow} IP_6 + E + P_i$	IP_6 Degradation
$IP_5 + E \rightleftharpoons^{k_5}_{k_{-5}} EIP_5 \overset{k_{h5}}{\longrightarrow} IP_4 + E + P_i$	IP_5 Degradation
$IP_4 + E \rightleftharpoons^{k_4}_{k_{-4}} EIP_4 \overset{k_{h4}}{\longrightarrow} IP_3 + E + P_i$	IP_4 Degradation
$IP_3 + E \rightleftharpoons^{k_3}_{k_{-3}} EIP_3 \overset{k_{h3}}{\longrightarrow} IP_2 + E + P_i$	IP_3 Degradation
$IP_2 + E \rightleftharpoons^{k_2}_{k_{-2}} EIP_2 \overset{k_{h2}}{\longrightarrow} IP_1 + E + P_i$	IP_2 Degradation
$IP_x + E \rightleftharpoons^{k_x}_{k_{-x}} EIP_2 \overset{k_{hx}}{\longrightarrow} IP_1 + E + P_i$	IP_x Degradation

Simultaneously, consumption of inorganic phosphate by biomass was assumed to be negligible compared to orthophosphate production via inositol phosphate hydrolysis. In addition, precipitation of U(VI)-phosphate minerals was neglected as uranium was initially removed from solution upon phytate addition after the 4 hour exposure period.

As incubations were under constant agitation and open to the atmosphere (see Chapter 5 of this dissertation), oxygen concentration was assumed to remain constant and was, thus, incorporated into the constant term R_{Lac} (maximum rate of lactate oxidation). In order to account for the steady state IP_2 concentrations observed for these incubations (See Chapter 5 of this dissertation), a reversible first order rate law for the formation of IP_2 from IP_1 was included in the rate law for IP_2 transformation. This term was also accounted for in the rate law for inorganic phosphate production as a phosphorus sink.

$$\frac{d[X]}{dt} = Y * [O_2] * \frac{R_{Lac}*[Lac]}{K_{Lac} + [Lac]} \quad (6\text{-}8)$$

$$\frac{d[Lac]}{dt} = -[X] * [O_2] * \frac{R_{Lac}*[Lac]}{K_{Lac} + [Lac]} \quad (6\text{-}9)$$

$$\frac{d[IP_6]}{dt} = -[X] * \frac{R_6*[IP_6]}{K_6 + [IP_6]} \quad (6\text{-}10)$$

$$\frac{d[IP_{x-1}]}{dt} = \frac{d[IP_x]_{degradation}}{dt} - [X] * \frac{R_{x-1} * [IP_{x-1}]}{K_{x-1}\left(1 + \sum_{i=x}^{6} \frac{[IP_i]}{K_i}\right) + [IP_{x-1}]} \quad (6\text{-}11)$$

$$\frac{d[\Sigma PO_4^{3-}]}{dt} = \sum_{i=2}^{6} \frac{d[IP_i]_{degradation}}{dt} \quad (6\text{-}12)$$

where Y represents the yield coefficient, R_x represents the maximum rate of transformation for a given species, K_x represents the Michaelis constant for a given species, and X represents the concentration of biomass.

6.3.3 Numerical Treatment

The set of coupled ordinary differential equations shown above (Equations 6-8 to 6-12) was solved numerically utilizing a variable step Runge-Kutta method (ode45) available in Matlab™ (see Appendix D for code). Initial concentrations of lactate, biomass, ΣPO_4^{3-}, IP_6, IP_5, IP_4, IP_3, and IP_2 taken from experimental data (Chapter 5 of

this dissertation) were introduced into the model as initial conditions, and these values were adjusted depending on which incubation treatment was modeled. Lag phase in the onset of inositol phosphate hydrolysis and inorganic phosphate production was also variable between experimental treatments and was adjusted accordingly. Due to the number of constants, Michaelis constants (K_x) and maximum rates (R_x) were adjusted to fit available data for phytate hydrolysis by *Variovorax* sp. without uranium. Once a suitable fit was achieved for this system, the model was adjusted for incubations amended with increasing concentrations of uranium by manipulating maximum rates (R_x). Experimental results discussed in Chapter 5 of this dissertation suggest that *Variovorax* sp. enhances the production of phytase enzymes to precipitate uranium- phosphate minerals as a detoxification mechanism. Thus, exposure to uranium may affect the rate of production of phytase enzymes even if uranium does not directly interact with or inhibit these enzymes. As rate constants are by definition concentration- independent, the Michaelis constants describing EIP_x (x = 2-6) transformations should be unaffected by the suspected increase in the rate of enzyme production upon exposure of cells to uranium. In other words, Michaelis constants should be conserved between incubations with and without uranium. Contrastingly, maximum rates (R_x) incorporate initial enzyme concentration (E_0) which may be affected by uranium addition if *Variovorax* sp. does in fact increase phytase enzyme production after uranium exposure as a uranium detoxification mechanism. Therefore, only maximum rates (R_x) were manipulated to account for observed differences between incubations with and without uranium.

6.4 Results and Discussion

6.4.1 Model Validation

The model was validated by studying the effect of increasing the maximum rates of lactate (Figure 6.1) or IP_6 (Figure 6.2) degradation on cell growth, phytate hydrolysis, and the temporal evolution of inositol phosphate intermediates and orthophosphate production. The model behavior was tested for maximum lactate consumption rates (R_{Lac}) of 0, 0.01, 0.1, 1, and 10 mmole L^{-1} h^{-1}. As lactate consumption is directly related to biomass growth which in turn affects inositol phosphate hydrolysis, inositol phosphate hydrolysis rates should increase as the maximum rate of lactate consumption increases as is indeed observed (Figure 6.1a-6.1h). If the maximum rate of lactate oxidation is negligible ($R_{Lac} = 0$), lactate is not consumed and little IP_6 is hydrolyzed as biomass does not grow. As the maximum rate of lactate oxidation (R_{Lac}) is increased, however, cell growth rates and the sequential hydrolysis of IP_6 and its inositol phosphate intermediates are increased (Figure 6.1a-6.1h). As lactate is the sole electron donor for microorganisms in the experimental system, inositol phosphate degradation should be limited by lack of cell growth if the rate of lactate oxidation (R_{Lac}) is zero. Lactate consumption, however, does not necessarily result in inositol phosphate transformation. Thus, manipulation of the maximum rate of IP_6 degradation (R_6) should not affect lactate consumption or cell growth. Comparison of model results with increasing maximum IP_6 degradation rates of 0, 0.001, 0.01, 0.1, and 1 mmole L^{-1} h^{-1} confirms that lactate degradation and cell growth react independently of inositol phosphate degradation rates. In addition, the degree and rate of modeled lower inositol phosphate accumulation (IP_2-IP_5) is driven by IP_6 degradation rates (Figure 6.2a-6.2h). These results demonstrate that the model responds as expected when rate constants for lactate consumption and IP_6 degradation are manipulated.

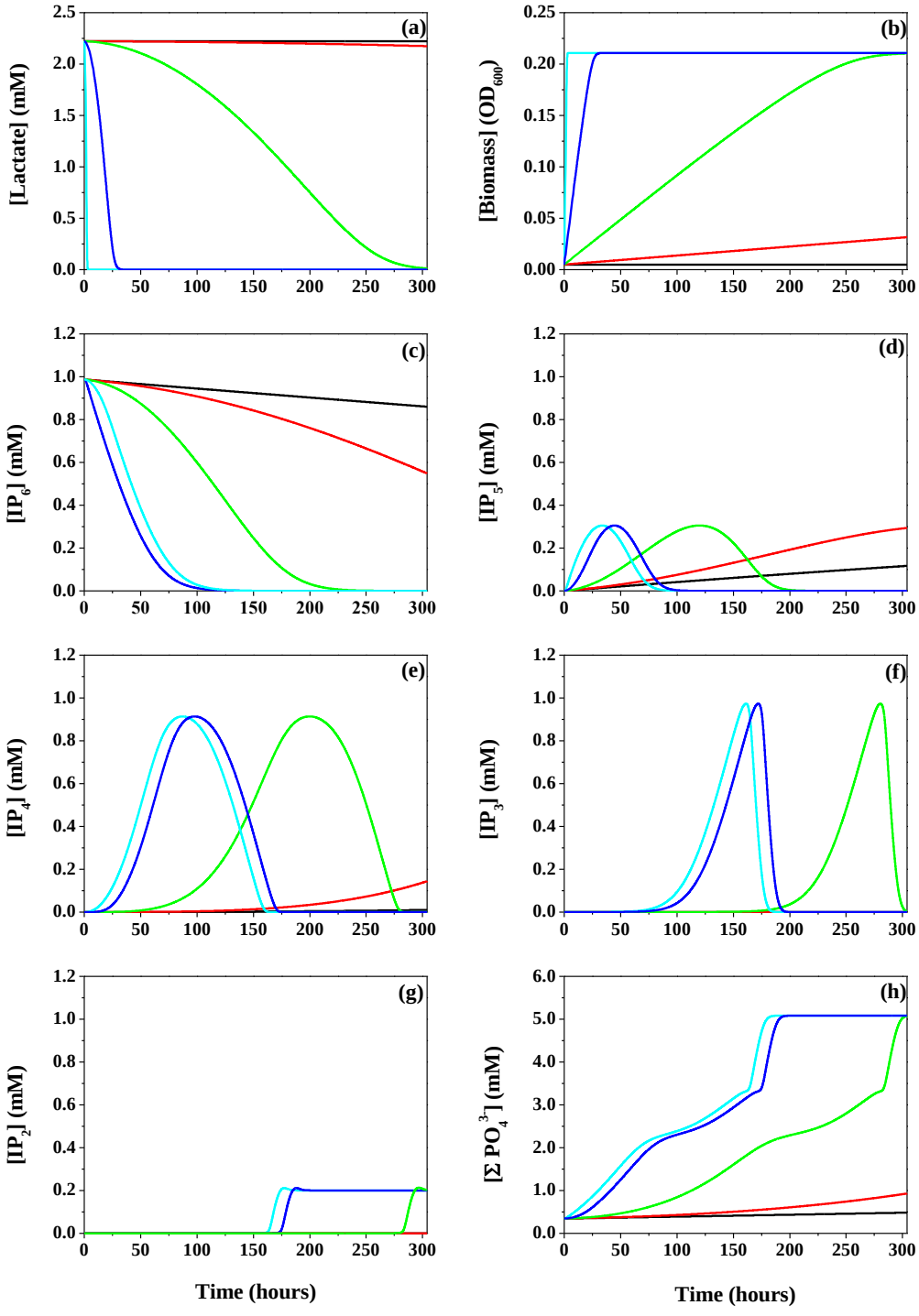

Figure 6.1 Model predicted (a) lactate oxidation, (b) biomass production, (c) IP_6 decomposition, (d) IP_5, (e) IP_4, (f), IP_3, and (g) IP_2 transformations, and (h) inorganic phosphate production as a function of time for maximum lactate consumption rates (R_{Lac}) of 0 (black), 0.01 (red), 0.1 (green), 1 (blue), and 10 (teal) mmole L^{-1} h^{-1}.

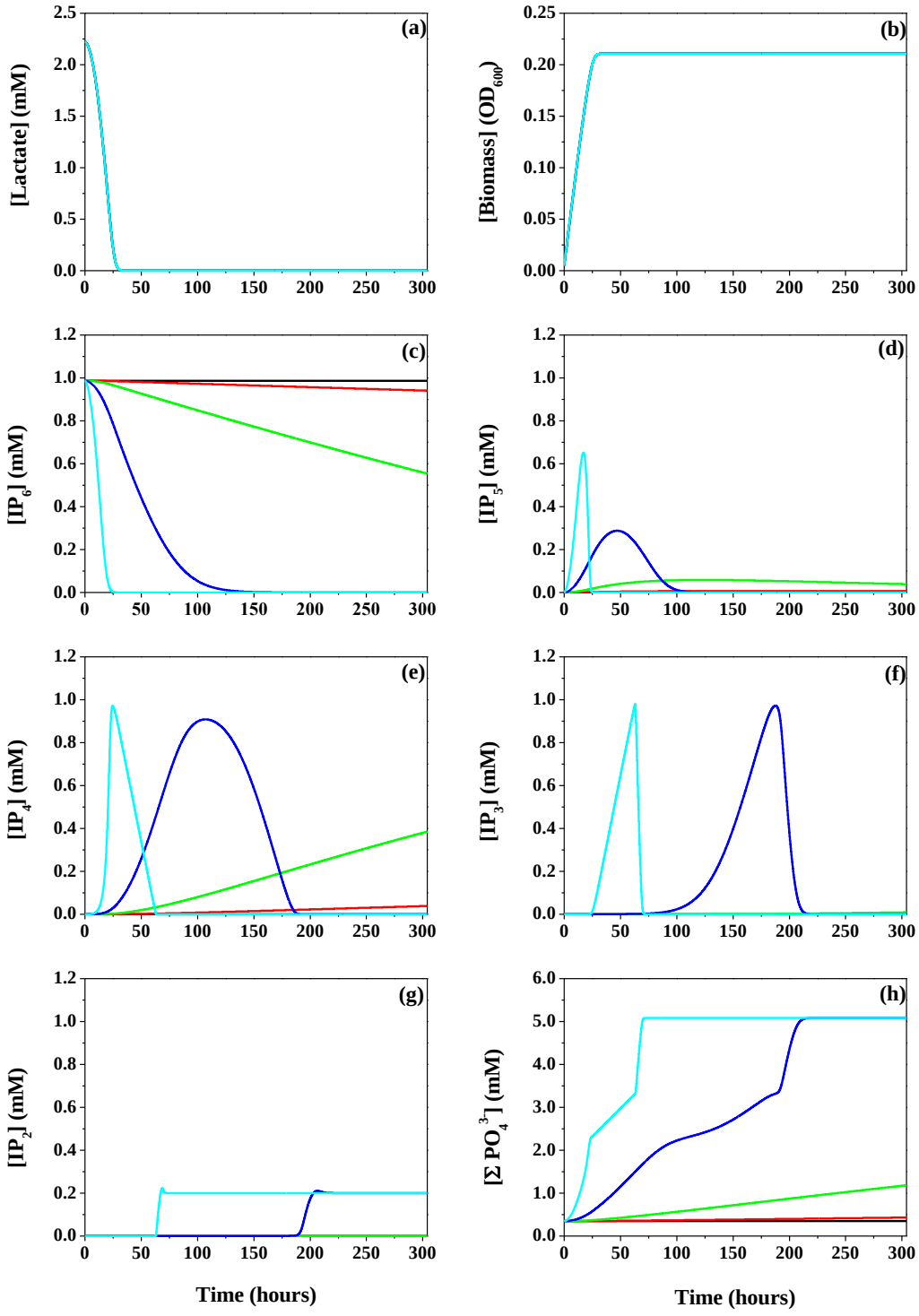

Figure 6.2 Model predicted (a) lactate oxidation, (b) biomass production, (c) IP_6 decomposition, (d) IP_5, (e) IP_4, (f), IP_3, and (g) IP_2 transformations, and (h) inorganic phosphate production as a function of time for maximum lactate consumption rates (R_{Lac}) of 0 (black), 0.001 (red), 0.01 (green), 0.1 (blue), and 1 (teal) mmole L^{-1} h^{-1}.

6.4.2 Phytate hydrolysis by *Variovorax* species

The results of this kinetic model (summarized in Table 6.2) reveal some important insights into the enzymatic processes that may control phytate hydrolysis by *Variovorax* species. Without uranium, modeled results closely mirror experimental data for lactate consumption (Figure 6.3a), cell growth (Figure 6.3a), inositol phosphate species (Figures 6.3b), and inorganic phosphate (Figure 6.3c) with some key divergences. Cell growth was reproduced well by the model until 150 hours of incubation when OD_{600} began to decrease (Figure 6.3a), indicating that cell death was not balanced by cell growth after this point in the pure culture incubations. The model, however, was not expected to reproduce this feature as cell death was not incorporated into the governing equations that control the behavior of biomass (Equation 6-8). In addition, cell counts were relatively high (corresponding to approximately ~ 10^9 cell mL^{-1}) even after 150 hours, suggesting that cell death should not significantly affect the hydrolysis of inositol phosphate and the production of inorganic phosphate.

As this model does not account for inorganic phosphate sinks (i.e. cellular uptake, precipitation reactions), the predicted concentrations for orthophosphate production should represent a theoretical maximum assuming IP_6 was the only P source in this system. Interestingly, the model slightly overestimated inorganic phosphate concentrations before ~ 150 hours while it underestimated them after ~ 150 hours regardless of the presence or not of uranium in different concentrations (Figures 6.3c, and 6.4c, and Figures D.1c, D.2c, D.3c, and D.4c in Appendix D). This observation suggests that additional phosphate sinks (before ~ 150 hrs) and sources (after ~ 150 hours) were not accounted for in the model. As uranium was removed prior to liberation of inorganic

phosphate accumulation, and as calcium concentrations in the artificial groundwater were not sufficient to precipitate apatite, it is unlikely that phosphate mineral precipitation was significant in this system. Alternately, cell uptake of orthophosphate could be responsible for the removal of phosphate produced extracellularly during phytate hydrolysis. Indeed, *Streptococcus Lactis* and *Escherichia Coli* have been shown to accumulate as much as 80 mM (Poolman et al., 1987) and 13 mM (Vershinina and Znamenskaya, 2002) inorganic phosphate, respectively, from micromolar phosphate concentrations in the medium.

Table 6.2 Rate constants calculated from a kinetic model of phytate hydrolysis by *Variovorax* sp. in pH artificial groundwater amended with 3 mM lactate, 1 mM inositol hexaphosphate (IP_6), and increasing concentration of uranium. Rates (R_x) are reported in units of µmoles L^{-1} h^{-1} and rate constants (K_x) are reported in units of h^{-1}.

	Uranium Exposure Concentration					
Parameter	**0 µM U**	**25 µM U**	**50 µM U**	**100 µM U**	**250 µM U**	**500 µM U**
Y	10^{-5}	10^{-5}	10^{-5}	10^{-5}	10^{-5}	10^{-5}
R_{Lac}	10^{3}	$10^{2.8}$	$10^{2.8}$	$10^{2.9}$	$10^{2.7}$	$10^{2.8}$
K_{Lac}	$10^{2.5}$	$10^{2.5}$	$10^{2.5}$	$10^{2.5}$	$10^{2.5}$	$10^{2.5}$
R_6	$10^{2.05}$	$10^{2.05}$	$10^{2.25}$	$10^{2.0}$	$10^{2.3}$	$10^{2.5}$
K_6	$10^{2.5}$	$10^{2.5}$	$10^{2.5}$	$10^{2.5}$	$10^{2.5}$	$10^{2.5}$
R_5	10^{6}	$10^{5.8}$	$10^{5.8}$	$10^{5.8}$	$10^{5.8}$	$10^{6.1}$
K_5	10^{2}	10^{2}	10^{2}	10^{2}	10^{2}	10^{2}
R_4	$10^{1.1}$	$10^{1.25}$	$10^{1.15}$	$10^{1.15}$	$10^{1.05}$	$10^{1.15}$
K_4	$10^{0.3}$	$10^{0.3}$	$10^{0.3}$	$10^{0.3}$	$10^{0.3}$	$10^{0.3}$
R_3	10^{3}	10^{5}	10^{5}	$10^{5.5}$	$10^{4.5}$	$10^{5.2}$
K_3	10^{2}	10^{2}	10^{2}	10^{2}	10^{2}	10^{2}
R_2	$10^{4.2}$	$10^{2.4}$	$10^{2.4}$	$10^{2.1}$	$10^{2.0}$	$10^{2.5}$
K_2	$10^{1.6}$	$10^{1.6}$	$10^{1.6}$	$10^{1.6}$	$10^{1.6}$	$10^{1.6}$

These considerations suggest the overprediction of orthophosphate concentrations during the phase of rapid cell growth (<150 hours) (Figure 6.3a) was likely caused by the omission of cellular uptake of inorganic phosphate in the model. In addition, *Variovorax* sp. was grown in enriched nutrient media (including high phosphate concentrations) prior to incubation in artificial groundwater (described in Chapter 5 of this dissertation) and may have therefore accumulated elevated intracellular orthophosphate reserves before inoculation. As the concentration of orthophosphate was underpredicted by the model after 150 hours when cell density decreased significantly (Figure 6.3a), cell lysis may have been sufficient to provide additional phosphate to the medium. Thus, the assumptions that cellular uptake of phosphate and cell death should not significantly affect model results may not be valid.

Michaelis constants (K_x) and maximum rates of degradation (R_x) for inositol phosphate transformation were initially optimized for incubations without uranium (Table 6.1) with good results (Figure 6.3b). Closer examination of Michaelis constants (K_x) for inositol phosphate degradation, however, reveals important information on the relative strength of the interaction between a given IP_x (x = 2-6) species and the phytase enzyme. Based on the derivation of equations governing competitive inositol phosphate degradation (Equation 6-7), the Michaelis constant for a given inositol species should reflect the ratio between rate constants for degradation (i.e. $k_{-x} + k_{hx}$) and formation (i.e. k_x) of the enzyme-inositol complex (Equation 6-13). Assuming that conversion of the enzyme-inositol complex is efficient (i.e. $k_{hx} >> k_{-x}$), the Michaelis constants should only represent the ratio of the rate constant for the degradation of the enzyme-IP_x complex to form IP_{x-1} and inorganic phosphate (k_{hx}) to the rate constant for the formation of the

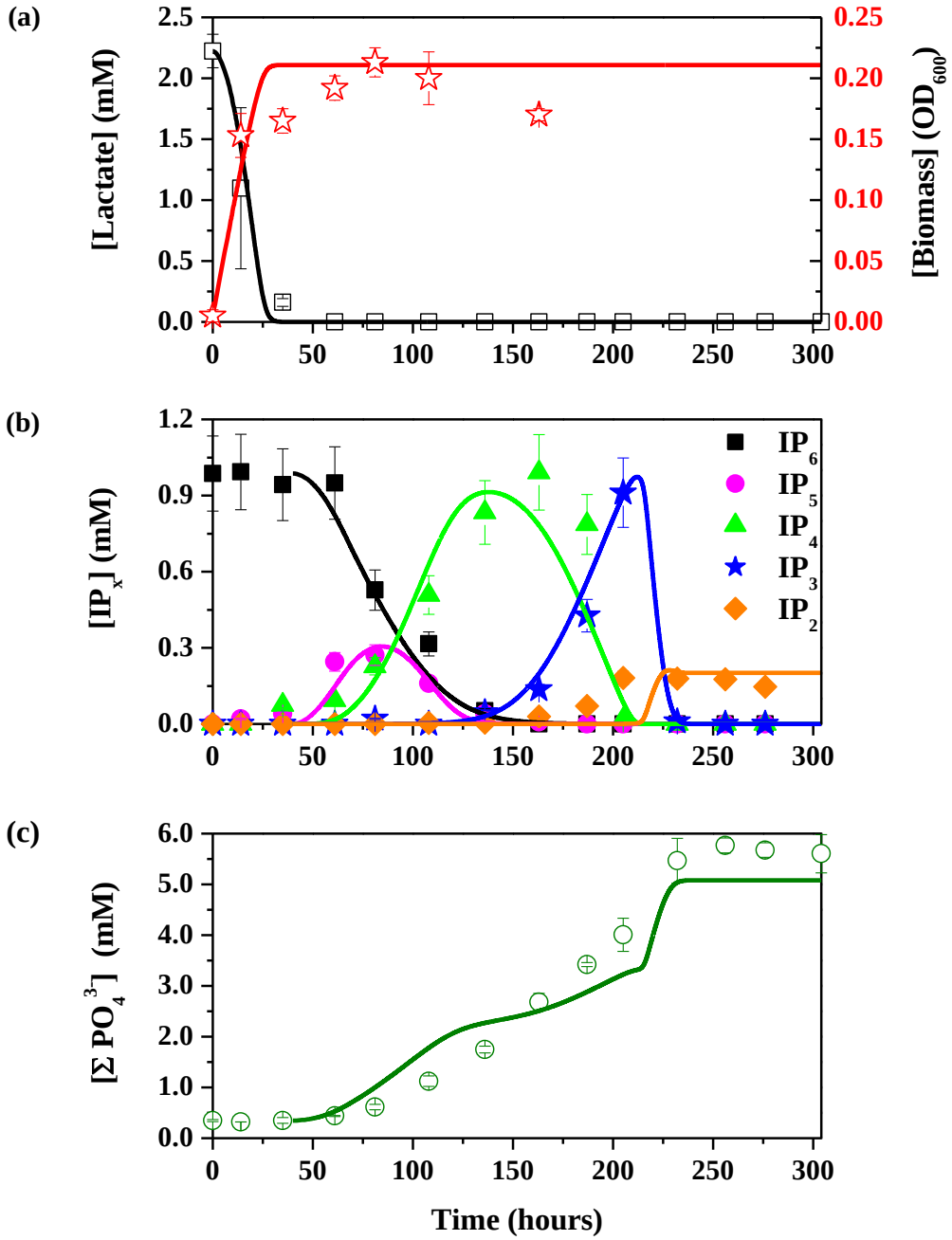

Figure 6.3 Comparison of experimental (symbols) and modeled (solid lines) concentrations or (a) lactate (black), (a) biomass (red), (b) inositol phosphate species (IP_x with x = 6 (back), 5 (magenta), 4 (green), 3 (blue), 2 (orange)), and (c) inorganic phosphate (green) as a function of time obtained in aerobic incubations of *Variovorax* sp. in pH 5.5 artificial groundwater amended with 3 mM lactate and 1 mM inositol hexaphosphate (IP_6).

enzyme-IP_x complex (k_x) (Equation 6-14). Substituting k_{hx} in Equation 6-14 with the maximum rate of IP_x hydrolysis (Equation 6-7) reveals a relationship between k_x, the initial enzyme concentration, the maximum rate of degradation, and Michaelis constant (Equation 6-15 to 6-16). This relationship was used to calculate $k_x[E_0]$ using model results for R_x and K_x (Table 6.3). As $[E_0]$ is constant in each incubation, variations of the $k_x[E_0]$ product associated with the hydrolysis of each inositol phosphate (IP_x) represent variations in the relative strength of the interaction between the phytase enzymes and the different IP_x species. Applying this logic to the results of incubations conducted without uranium (Table 6.3 Top) reveals a five-order of magnitude difference between the weakest (IP_6, $k_6[E_0]=10^{-0.45}$) and strongest (IP_5, $k_5[E_0]=10^4$) enzyme-inositol interaction, suggesting that enzyme interaction with different inositol phosphates depends on inositol phosphate stability. As IP_6 is symmetrical and highly stable, it presents the lowest affinity for the enzyme, and the R_6/K_6 ratio is the lowest of all hydrolysis reactions (Table 6.3 Top). In turn, IP_5 is asymmetrical which destabilizes the molecule enough to increase its affinity for the enzyme and is reflected in the four-order of magnitude higher R_5/K_5 ratio. Similarly, IP_4 formed by hydrolysis of IP_5 should be highly symmetrical which dramatically decreases its affinity for the enzyme (low R_4/K_4 in Table 6.3 Top). The poor symmetry of IP_3 must explain its slightly higher affinity for the enzyme, while the hydrolysis of IP_2 and IP_1 are probably catalyzed due to the large decrease in steric hindrance between these inositol compounds and phytase subsequent to removal of the first four phosphate groups. The good agreement between the simulations of the temporal evolution of the entire suite of inositol phosphate intermediates and the logical variations in the binding affinity of the enzyme obtained for each of these intermediates strongly

suggest that the same phytase enzyme is involved in the hydrolysis of phytate and its inositol derivatives.

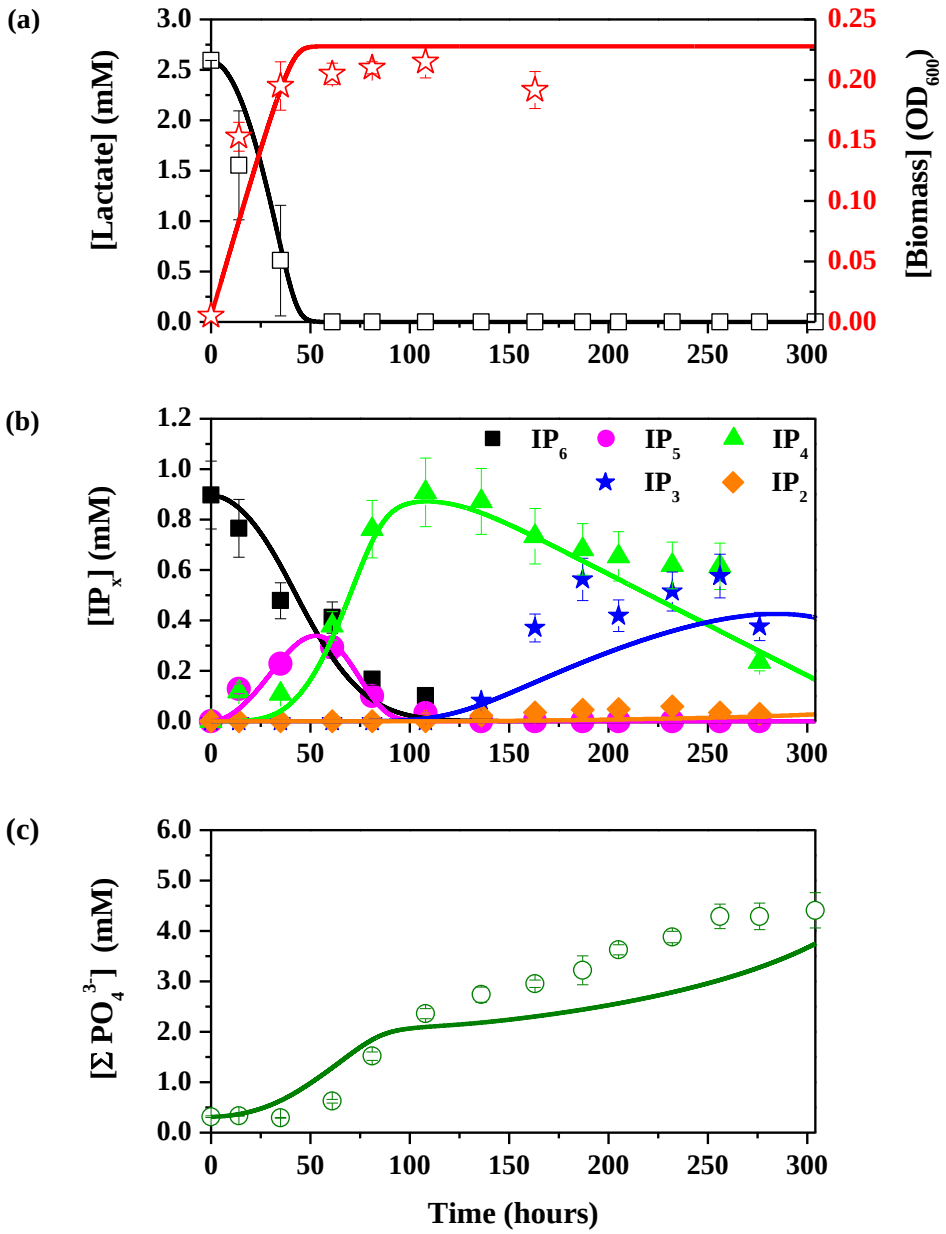

Figure 6.4 Comparison of experimental (symbols) and modeled (solid lines) concentrations or (a) lactate (black), (a) biomass (red), (b) inositol phosphate species (IP_x with x = 6 (back), 5 (magenta), 4 (green), 3 (blue), 2 (orange)), and (c) inorganic phosphate (green) as a function of time obtained in aerobic incubations of *Variovorax* sp. in pH 5.5 artificial groundwater amended with 3 mM lactate, 1 mM inositol hexaphosphate (IP_6), and 25 µM uranium.

Table 6.3 (Top) Ratios of Michaelis constants (K_x) to maximum degradation rates (R_x) for IP_x (x = 2-6) degradation in incubations without uranium. (Middle) Ratios of maximum degradation rates of IP_6 (R_6) relative to these of lower inositol phosphates (R_x, x = 2-5). (Bottom) Ratios of the maximum degradation rate of IP_x (R_{xu}) for a given concentration of uranium relative to that of the same species without uranium (R_x).

	Uranium Exposure Concentration					
Ratio	**0 µM U**	**25 µM U**	**50 µM U**	**100 µM U**	**250 µM U**	**500 µM U**
R_6/K_6	$10^{-0.45}$	-	-	-	-	-
R_5/K_5	$10^{4.0}$	-	-	-	-	-
R_4/K_4	$10^{0.8}$	-	-	-	-	-
R_3/K_3	$10^{1.0}$	-	-	-	-	-
R_2/K_2	$10^{2.6}$	-	-	-	-	-
R_6/R_5	9091	5556	3571	6250	3125	4000
R_6/R_4	0.11	0.16	0.08	0.14	0.06	0.04
R_6/R_3	9.1	1000	500	1000	100	500
R_6/R_2	100	2.2	1.4	1.25	0.5	1.0
R_{6u}/R_6	-	1	1.6	0.89	1.8	2.8
R_{5u}/R_5	-	0.63	0.63	0.63	0.63	1.3
R_{4u}/R_4	-	1.4	1.1	1.1	0.9	1.1
R_{3u}/R_3	-	100	100	316	31	158
R_{2u}/R_2	-	0.02	0.02	0.01	0.01	0.02

$$K_x = \frac{k_{-x} + k_{hx}}{k_x} \tag{6-13}$$

$$If\ k_{hx} \gg k_{-x} \Rightarrow K_x = \frac{k_{hx}}{k_x} \tag{6-14}$$

$$Since \quad R_x = k_{hx}[E_0] \Rightarrow k_{hx} = \frac{R_x}{[E_0]} \tag{6-15}$$

$$K_x = \left(\frac{1}{k_x}\right)\left(\frac{R_x}{[E_0]}\right) \Rightarrow k_x[E_0] = \left(\frac{R_x}{K_x}\right) \tag{6-16}$$

Information on the kinetics of degradation of the different enzyme-inositol phosphate complexes may also be gleaned from the model results by examining the ratio of the maximum rate of degradation of the lower inositol phosphate compounds (R_x, x = 2-5) relative to the maximum degradation rates of IP_6 (Table 6.3 Middle). As the initial concentration of enzyme can be assumed constant within a given incubation, the rate constants for the degradation of the intermediate enzyme-inositol phosphate complexes can be evaluated relative to the rate constant of degradation of the phytate-enzyme intermediate (Equations 6-17 and 6-18).

$$R_x = k_{hx}[E_0] \qquad R_{x-1} = k_{h(x-1)}\,[E_0] \tag{6-17}$$

$$\frac{R_x}{R_{x-1}} = \frac{k_{hx}[E_0]}{k_{h(x-1)}[E_0]} = \frac{k_{hx}}{k_{h(x-1)}} \tag{6-18}$$

These calculations reveal that the IP_5-phytase complex hydrolyses the fastest compared to all the other inositol phosphate species (Table 6.3 Middle), likely because its asymmetry destabilizes IP_5. The effect of the geometry and steric hindrance of the intermediate inositol phosphate compounds is also reflected in their relative kinetics of degradation obtained with the model. The rate constant of hydrolysis of IP_2 is higher than that of IP_3, and that of IP_4 is the lowest as this inositol phosphate compound is the most symmetrical of all the intermediate inositol phosphate compounds. These ratios are generally conserved irrespective of the exposure of *Variovorax* sp. to various uranium concentrations (Table 6.3 Middle), suggesting that uranium does not directly interact with or inhibit the phytase enzyme. These findings are in agreement with the fact that uranium is precipitated immediately upon addition of phytate and does not affect the growth of the organism (see chapter 5 of this dissertation). Indeed, the relative ratios of maximum rates

of degradation of each inositol phosphate compound in the presence of various concentrations of uranium (R_{xu}) compared to the maximum rates obtained in the absence of uranium (R_x) do generally not vary significantly when the cells are exposed to increasing uranium concentrations (Table 6.3 Bottom), except for IP_3 and IP_2 which are increased and decreased significantly when exposed to uranium. These exceptions for the hydrolysis of the low inositol phosphate compounds may reflect a delayed response of the organism to the exposure of uranium. As rate constants are concentration-independent and should only be affected by a change in mechanism, changes in the maximum rate of inositol phosphate degradation (R_x) between incubations with and without uranium should only be affected by differences in the initial concentration of phytase enzyme. Thus, the increase in the relative maximum rate of hydrolysis of IP_3 in the presence of uranium indicates that the initial enzyme concentration generally increased upon uranium exposure, suggesting *Variovorax* sp. may have increased phytase enzyme synthesis to precipitate uranium-phosphate minerals as detoxification mechanism (see detailed discussion in Chapter 5 of this dissertation). The observation that the increase in phytase production only occurs for the hydrolysis of IP_3 (i.e. 5 days after exposure to uranium) reflects a delayed response, probably related to the time it takes to sense environmental conditions. The decrease in enzyme concentration seemingly associated with the hydrolysis of IP_2, however, suggests the organism reacted by shutting down enzyme production as if it realized that the toxic compound was removed from solution.

6.5 Insights on biogeochemical cycling of phytate

Predictive models represent a key component of any successful remediation strategy. Prior to the current study, only limited information was available on the mechanism of inositol phosphate hydrolysis *in vivo*(see Chapters 4 and 5 of this dissertation). In addition, the effect of uranium on phytate hydrolysis by pure culture microorganisms had, to our knowledge, never been examined. Detailed examination of the parameters describing inositol phosphate transformation revealed that *Variovorax* sp. likely catalyzed IP_x hydrolysis with a single phytase enzyme rather than a combination of phytase and phosphohydrolases. In addition, the model clearly indicated that the affinity of the enzyme for each inositol phosphate and its rate of hydrolysis depend on the stability of the substrate and the steric hindrance between the enzyme and the substrate. More importantly, the mechanism of hydrolysis was not affected significantly upon exposure of the organism to uranium. In fact, the modeling results indicate that phytase production by *Variovorax* sp. may have been enhanced as a result of uranium toxicity. Finally, as the predicted evolution of inositol phosphate transformation and inorganic phosphate accumulation closely followed experimental results, this model may be applied to more complex systems involving in parallel solid-mediated processes (e.g. phytate adsorption and its effect on hydrolysis) and substrate transport. Overall, the development of a diagnostic model for phytate hydrolysis by metal-resistant microorganisms isolated from contaminated environments represents an important step towards implementing phytate-promoted U(VI)-phosphate biomineralization in field studies.

6.6 Acknowledgements

This research was supported by the Office of Science (BER), US Department of Energy Grant No. DE-FG02-04ER63906.

CHAPTER 7

GEOCHEMICAL CONTROLS ON URANIUM-PHOSPHATE SOLUBILITY AND ORGANOPHOSPHATE BIOAVAILABILITY: IMPLICATIONS FOR UTILIZING PHYTATE IN URANIUM BIOREMEDIATION STRATEGIES

In preparation for submission to *Environmental Science and Technology*

7.1 Abstract

For U(VI)-phosphate biomineralization via microbially-mediated phytate hydrolysis to be an effective remediation strategy, the U(VI)-phosphate mineral product must remain stable over a broad range of chemical conditions and phytate must remain bioavailable to subsurface microorganisms. In this study, the stability of U(VI)-phosphate minerals exposed to varying pH and dissolved inorganic carbon (DIC) concentrations in artificial groundwater was examined. In low pH conditions representative of the Oak Ridge Field Research Center (ORFRC), U(VI)-phosphate minerals remain stable for at least 6 months. At higher pH, however, U(VI)-phosphate minerals were destabilized after 12 days, indicating that U(VI)-phosphate biomineralization is an appropriate remediation strategy for low pH or low DIC environments. Although phytate strongly sorbed to ORFRC soils, a significant fraction of added phytate remained soluble, suggesting phytate may be an acceptable substrate to promote biomineralization of U(VI)-phosphate minerals over significant distances in subsurface environments. In addition, extracted wheat bran was found to contain large concentrations of acid-extractable phytate,

demonstrating that wheat bran may be a cost-effective phytate source for use in bioremediation. Overall, the results of this study indicate that phytate-promoted biomineralization of U(VI)-phosphate minerals may be an effective remediation strategy for uranium contamination in low pH contaminated subsurface environments.

7.2 Introduction

Due to the vast quantities of uranium-containing waste present at DOE managed facilities (DOE, 1997; NABIR, 2003), *in situ* uranium remediation techniques have been investigated as alternatives to cost-prohibitive traditional remediation methods (Dawson and Gilman, 2001; Jardine, 2006; Mackay and Cherry, 1989) which require physical removal of contaminants. Bioreduction, or the biologically-mediated reductive precipitation of U(IV) minerals, represents the most widely studied *in situ* bioremediation technique for immobilization of uranium in contaminated environments (Fredrickson et al., 2000; Ganesh et al., 1999; Lovley and Phillips, 1992b; Lovley et al., 1991; North et al., 2004; Sanford et al., 2007; Wade and DiChristina, 2000). However, the uraninite mineral product of bioreduction is oxidized and remobilized upon reintroduction of oxygen in areas of groundwater recharge (Langmuir, 1997; Murphy and Shock, 1999) or in the presence of NO_2^- (Beller, 2005; Moon et al., 2007; Wu et al., 2010), MnO_2 (Fredrickson et al., 2002), or $Fe(OH)_3$ (Senko et al., 2002; Senko et al., 2005b; Wan et al., 2005) in reducing conditions. In addition, bioreduction is inhibited at low pH or in the presence of common co-contaminants such as nitrate (Finneran et al., 2002b; Wu et al., 2006a; Wu et al., 2006b), a more energetically-favorable terminal electron acceptor than uranium. Thus, *in situ* biomineralization of U(VI)- phosphate minerals has recently gained popularity as an alternative remediation technique for contaminated sites

characterized by low pH and/or high nitrate where bioreduction is not suitable (Finneran et al., 2002b; Wu et al., 2006a; Wu et al., 2006b).

Biomineralization of U(VI)-phosphate minerals aims to capitalize on the low solubility of the uranyl ion (UO_2^{2+}) in the presence of phosphate over a broad range of environmental conditions (Ohnuki et al., 2004; Wellman et al., 2007; Zheng et al., 2006), including at low pH when bioreduction is not favorable. Direct addition of inorganic phosphate to subsurface environments typically results in rapid orthophosphate precipitation and, consequently, drastic decrease in soil hydraulic conductivity (Wellman et al., 2006) which prevents dissemination of the phosphorus substrate throughout the contaminant plume. Research has therefore focused on addition of organophosphate substrates to contaminated environments to promote microbially-mediated organophosphate hydrolysis coupled to a chemical precipitation of U(VI)-phosphate minerals (Beazley et al., 2007, 2009; Macaskie et al., 1995; Martinez et al., 2007; Montgomery et al., 1995; Shelobolina et al., 2009). In phosphate limiting conditions, microorganisms secrete soluble periplasmic or membrane-bound non-specific phosphatase enzymes which catalyze organophosphate hydrolysis and release of inorganic phosphate for cell uptake (Rossolini et al., 1998). Uranium immobilization coupled to microbial phosphatase expression has been demonstrated both in aerobic and anaerobic conditions via experiments with pure culture isolates (Beazley et al., 2007, 2009; Macaskie et al., 1995; Martinez et al., 2007; Montgomery et al., 1995) and natural microbial communities in contaminated sediments (Beazley et al., 2011; Shelobolina et al., 2009).

Even if the biomineralization of U(VI)-phosphate minerals may be promoted by

organophosphate hydrolysis, the long-term stability of the U(VI)-phosphate biomineralization product is vital to ensuring permanent contaminant mitigation. Previous research identified the mineral product of biomineralization as part of the autunite/meta-autunite group minerals (Beazley et al., 2007) which are generally composed of sheets of square bipyramidal uranyl and tetrahedral phosphate polyhedra linked by interlayer charge-balancing cations [i.e. autunite, $Ca(UO_2)_2(PO_4)_{2\ (s)}$] (Catalano and Brown, 2004; Locock and Burns, 2003). Above pH 7.0, elevated bicarbonate concentrations promote autunite mineral dissolution (Liu et al., 2004; Sowder et al., 2001). In addition, carbonates inhibit U(VI) sorption to iron oxides at this pH (Katsoyiannis, 2007) through the formation of highly soluble uranyl-carbonate complexes (Langmuir, 1997), further enhancing contaminant mobility. Chernikovite [$(UO_2)H(PO_4)\bullet 4H_2O$] and meta-autunite ($Ca[(UO_2)(PO_4)]_2\bullet xH_2O$), however, remain stable in 1 mM carbonate (pH 8.3) for at least 100 days (Sowder et al., 2001), and the rate of carbonate-promoted autunite dissolution is lowest at acidic pH (Wellman et al., 2007). Microbially enhanced autunite dissolution has been demonstrated in the presence of *Arthrobacter* sp. (Katsenovich et al., 2012) and *Shewanella putrefaciens* 200R (Smeaton et al., 2008), apparently promoted to access inorganic phosphate in nutrient-limiting conditions. This process, however, has only been assessed above circumneutral pH, and the observed dissolution was more likely an indirect effect of carbonate production during microbial respiration. Thus, further characterization of the effect of carbonates on U(VI)-phosphate mineral dissolution for the range of conditions present at the ORFRC is warranted.

While previous biomineralization studies have demonstrated uranium immobilization coupled to hydrolysis of primarily synthetic organophosphates (Beazley et al., 2007, 2009; Beazley et al., 2011; Martinez et al., 2007; Shelobolina et al., 2009), the use of a naturally-occurring and abundant organophosphate to promote this process has not been thoroughly examined. Inositol hexaphosphate (IP_6), also known as phytate (salt) or phytic acid (metal-free), is a phosphorylated inositol with six attached phosphate groups that is synthesized by plants for phosphorus storage and, thus, comprises the main organic phosphorus fraction in most terrestrial environments (Turner et al., 2002). As phytate carries a highly negative charge at all environmentally relevant pH (Costello et al., 1976), it interacts strongly with soils sorbents (Degroot and Golterman, 1993; Johnson et al., 2012) which may limit phytate transport throughout the contaminant plume. In addition, phytate forms sparingly soluble complexes with metals (Martin and Evans, 1987; Turner et al., 2002) which has led to examination of chemical sequestration of mobile U(VI) with phytate (Knox et al., 2008; Nash et al., 1998; Seaman et al., 2003). However, very limited information is available on the biomineralization of U(VI)-phosphate minerals via microbially-mediated phytate hydrolysis (discussed thoroughly in Chapter 4 and 5 of this dissertation).

Although phytate represents a common soil constituent, it is only naturally available in surficial soils. Thus, bioremediation strategies utilizing phytate would require injection of exogenous dissolved IP_6, likely extracted from plant materials, into contaminated subsurfaces. Phytate synthesis represents the primary phosphorus storage mechanism for cereals, legumes, and oleaginous seeds (Gibson et al., 2010), and phytate composes up to 2.2% (w/w) of cereals (Gibson et al., 2010), 9.15% (w/w) of legumes

(Gibson et al., 2010), and 1.6% (w/w) of seeds (Abebe et al., 2007). In addition, 90% of phytic acid in cereals is concentrated in the bran (Gibson et al., 2010). Extraction of phytate from cereals typically involves water or acid solvents (Kolchev, 1978), with between 0.01 and 2.4 M HCl commonly used (Han, 1988; Makower, 1970; Park et al., 2006), and room temperature acid extractions are more effective than similar extractions at high temperature (Canan et al., 2011). Thus, cereal bran may represent an excellent source of inexpensive and easily extractable phytate for use in biomineralization strategies.

The objective of this study was to define the geochemical controls on U(VI)-phosphate mineral stability and phytate bioavailability in conditions representative of acidic contaminated soils in order to optimize *in situ* uranium remediation techniques reliant on microbially-mediated phytate hydrolysis. The stability of autunite over a range of pH in the presence of carbonate and alternative phosphate sources was determined, and a sequential extraction technique for differentiation of U(VI)-phosphate and U(VI)-phytate precipitates was validated. In addition, phytate sorption to ORFRC soils was investigated, and the phytate content of inexpensive grains was examined.

7.3 Materials and Methods

Unless otherwise noted, all chemicals used were Fisher reagent grade. U(VI)-phosphate precipitation and batch phytate sorption experiments were conducted in artificial groundwater designed to reflect geochemical conditions at the ORFRC (Brooks, 2001). Background ion concentrations in the artificial groundwater were 200 µM Ca^{2+}, 2.0 µM Fe^{2+}, 5.1 µM Mn^{2+}, 7.9 mM K^{+}, 7.5 mM Na^{+}, 8.0 µM MoO_4^{2-}, 410 µM Cl^{-}, 810

μM SO_4^{2-}, and 15.4 mM NO_3^-, and groundwater was buffered at pH 5.5 using 50 mM 2-(N-Morpholino)ethanesulfonic acid (MES).

7.3.1 U(VI)-phosphate mineral stability

To examine stability of uranium precipitates potentially formed during *in situ* biomineralization of U(VI)-phosphate minerals, increasing concentrations of dissolved inorganic carbon (DIC) and various phosphate substrates were equilibrated with abiotically precipitated uranium phosphate minerals. Calcium autunite $Ca(UO_2)_2(PO_4)_2$ (Beazley et al., 2007) was chemically precipitated in pH 5.5 artificial groundwater amended with 1 mM NaH_2PO_4 and 200 μM uranyl acetate (Spectrum). After 24 hours of equilibration, the mineral groundwater mixture was centrifuged at 3300 rpm for 5 minutes, and the supernatant was removed. The mineral was then resuspended in pH 4.5, 5.5, 7.0, or 8.0 artificial groundwater amended with either sodium bicarbonate (0-20 mM) or 10 mM phytic acid sodium salt hydrate (Sigma), sodium triphosphate (Sigma), or sodium metaphosphate (Sigma) as phosphate sources. Triplicate samples were agitated continuously in the dark on a rotary wheel at 30 rpm for 10 days prior to analysis. A long-term (6 month) set of experiments was also conducted using the above protocol. Just before analyses, samples were filtered through a 0.2 μm polyethersulfone (PES) membrane filter. A small aliquot of filtered sample was diluted in 2% trace metal grade nitric acid for uranium analysis, and the remainder was reserved for analysis of total dissolved phosphate (ΣPO_4^{3-}).

7.3.2 Sequential extraction of U(VI)-phosphate and U(VI)-phytate precipitates

To determine solid-phase uranium speciation in contaminated sediments treated for bioremediation, sequential extraction profiles for pure phases have to be accurately defined. Calcium autunite $Ca(UO_2)_2(PO_4)_2$ (Beazley et al., 2007) was precipitated as described above. U(VI)-phytate precipitates were formed from pH 5.5 artificial groundwater amended with 500 µM phytic acid sodium salt hydrate and 200 µM uranyl acetate. All artificial groundwater mixtures were allowed to equilibrate for 24 hours. To create mixtures of both uranium solids, artificial groundwater containing either autunite or U(VI)-phytate precipitates were combined after equilibration. The mineral-groundwater mixtures were centrifuged at 3300 rpm for 5 minutes. An aliquot of supernatant for each mineral was filtered (0.2 µm, PES) and acidified in 2% trace metal grade nitric acid for uranium quantification, and the remainder of the supernatant was discarded. The following modified sequential extraction procedure (Tessier et al., 1979) was performed in triplicate on autunite minerals, U(VI)-phytate precipitates, and mixtures of these two uranium solids: (1) 1.0 M $MgCl_2$ in 10 mM nitrilotriacetic acid (NTA) (pH 4.5) was added and agitated at 20°C for 1 hour to extract the loosely adsorbed fraction; (2) 1.0 M acetic acid (pH 5.0) was added and agitated at 20°C for 5 hours to dissolve uranium minerals; (3) 0.04 M $NH_2OH \cdot HCl$ in 25% (v/v) Acetic Acid was agitated at 96°C for 6 hours to remove Fe- and Mn-associated uranium; and (4) 1.5 mL of 0.02 M HNO_3 and 2.5 mL of 30% H_2O_2 (pH 2.0) were agitated at 96°C for 2 hours, a second 1.5 mL aliquot of 30% H_2O_2 (pH 2.0) was added and agitated at 96°C for 3 hours, and a third 5 mL aliquot of 2.5 M NH_4OAc in 20% (v/v) HNO_3 was agitated at 20°C for 1 hour to extract the uranium fraction bound to organics. After each extraction step, samples were

centrifuged, and supernatants were filtered (0.2 µm, PES) and acidified for uranium analysis.

7.3.3 Sorption of phytate to ORFRC soils

To characterize sorption of phytate onto Oak Ridge sediments, pH 5.5 artificial groundwater amended with increasing concentrations of phytic acid sodium salt hydrate (0-10 mM) was equilibrated in triplicate with ORFRC soils (10 g/L) for a period of 4 days. Soils were collected during installation of a monitoring well in Area 3 (well number: FWB134-08-03, core depth: 6.5 – 7.5 m). Due to their proximity to the S-3 waste disposal ponds, Area-3 soils are generally characterized by low pH high nitrate, and high uranium concentrations (Brooks, 2001) making this area an ideal field-site for investigations on the biomineralization of U(VI)-phosphate minerals. In addition, ORFRC soils display bulk Mn and Fe contents of 0.36 g kg^{-1} and 25.8 g kg^{-1}, respectively (Barnett et al., 2002). Soil samples were agitated continuously on a rotary wheel and kept in the dark during equilibration. In addition, soils were autoclaved for 1 hour at 121°C prior to equilibration to ensure microbial activity did not affect phytate in this system. After equilibration, soil-groundwater mixtures were centrifuged at 3300 rpm for 10 minutes, and the supernatant was filtered (0.2 µm, PES) and frozen for preservation until analysis of dissolved IP_6. The data were represented using Langmuir isotherms (Eq. 7-1) where Γ represents the concentration of sorbed phytate (mol g^{-1} soil), Γ_{max} the maximum concentration of sorbed phytate (mol g^{-1} soil), K_{ads} is the equilibrium constant for phytate sorption onto ORFRC soils, and C represents the aqueous concentration of phytate. If phytate sorption to ORFRC soils follows a Langmuir isotherm, a linear trend should be apparent when sorption data is represented graphically after a double-inverse

linearization procedure (Eq. 7-2). The y-intercept and slope of the resulting linear curve represent Γ_{max}^{-1} and $(\Gamma_{max}K_{ads})^{-1}$, respectively, and these values were used to derive the isotherm for phytate sorption onto ORFRC soils. The reported errors on Γ_{max} and K_{ads} were derived from the standard error of the y-intercept and slope of the linear regressions.

$$\Gamma = \Gamma_{max}\left(\frac{K_{ads}C}{1 + K_{ads}C}\right) \quad (7\text{-}1)$$

$$\frac{1}{\Gamma} = \frac{1}{\Gamma_{max}} + \left(\frac{1}{\Gamma_{max}K_{ads}}\right)\left(\frac{1}{C}\right) \quad (7\text{-}2)$$

7.3.4 Extraction of inositol phosphates from cereal bran

To determine if sufficient phytate can be extracted from natural cereals as affordable alternative source of phytate, both oat bran and wheat bran were examined for their extractable phytate content. Oat and wheat bran, purchased from a large national grocer, were added to deionized water or 1.0 M hydrochloric acid to a final solids concentration of 90 g/L. Extraction vials were agitated continuously on a rotary wheel and kept in the dark for 4 days. After extraction, vials were centrifuged, and the supernatant was filtered (0.2 µm, PES) and frozen until quantification of phytate.

7.3.5 Analytical Techniques

Dissolved uranium was measured using an Agilent 7500a Series system inductively coupled plasma mass spectrometer (ICP-MS). Standards ranging from 0 to 10 nM were prepared using uranyl acetate (Spectrum) acidified in 2% trace metal grade nitric acid (Fisher). Holmium and bismuth were used as internal standards (SPEX certiPrep), and 2% trace metal grade nitric acid blanks and calibration check standards

were used as quality controls. Error bars represent the standard deviation between triplicate incubations and the analytical error on duplicate measurements.

Dissolved inorganic phosphate was quantified by ion chromatography (IC) using a Dionex GP-50 high-performance liquid chromatography (HPLC) pump and conductivity detector (Dionex, CD-20) coupled to an Analytical Instrument Systems, Inc. integrator (LCC 100). An anion exchange analytical column (Dionex AS14, 4 x 250mm) and guard column (Dionex AG14, 4 x 50mm) were used in line with an AMMS-300 (4-mm, Dionex) suppressor. Operating conditions included a carbonate buffer eluent (1 mM $NaHCO_3$/ 3 mM Na_2CO_3) with a 1 mL min^{-1} flow rate and a 25 mN H_2SO_4 regenerant. All reagents and standards were prepared using reagent grade chemicals (Fisher) unless otherwise specified.

Inositol hexaphosphate (Sigma) was quantified using a modified chromatographic separation coupled to suppressed spectrophotometric detection at 500 nm (Rounds and Nielsen, 1993) with a Dionex ICS-3000 dual pump chromatography system. Separation was achieved with an OmniPac PAX-100 guard column (4 x 40 mm), and eluent flow conditions included a 23 minute linear gradient (0.5 mL/min) from 0.01 M 1-methylpiperazine (pH 4.0) to 0.38 M $NaNO_3$ in 0.01 M 1-methylpiperazine (pH 4.0). Following separation, 0.015% (w/v) $FeCl_3 \cdot 6H_2O$ in 0.15% (w/v) sulfosalicylic acid (pH 1.8) was introduced (0.5 mL/min) as a post-column reagent through a reaction coil to ensure thorough mixing. Reported errors for IP_6 include analytical error and standard deviation between triplicate incubations.

7.4 Results and Discussion

7.4.1 Autunite Mineral Stability

Above pH 6.0, when carbonate is deprotonated, elevated DIC promotes the dissolution of oxidized and reduced uranium minerals (De Pablo et al., 1999; Liu et al., 2004; Sowder et al., 2001; Ulrich et al., 2009). Indeed, autunite remained stable at pH 4.5 and 5.5 at all concentrations of carbonate (Figure 7.1). In addition, autunite remained stable in the presence of low concentration of DIC (ca. 2 mM) at all pHs (Figure 7.1), indicating carbonate levels were not sufficient to promote mineral dissolution. Even at pH 7.0 with 5 mM DIC, only about 10% of total uranium was remobilized through mineral dissolution, and this percentage increased to 25% with 10 mM DIC. Mineral dissolution was more drastic at pH 8.0, however, with up to 70% U(VI) produced in solution at a DIC of 15 mM. The carbonate-promoted oxidative dissolution of U(IV) minerals has been proposed to occur via binding of bicarbonate to the previously oxidized uranium surface followed by detachment of the U(VI)-bicarbonate surface complex (Liu et al., 2004). Likely, a similar mechanism can explain the dissolution of autunite in the presence of carbonate. Below pH 6.4, carbonate is predominantly neutral (Stumm and Morgan, 1996) and does not interact with positively charged autunite surfaces. Above pH 6.4, however, negatively charged bicarbonate interacts strongly with autunite resulting in detachment of highly soluble uranyl-carbonate complexes.

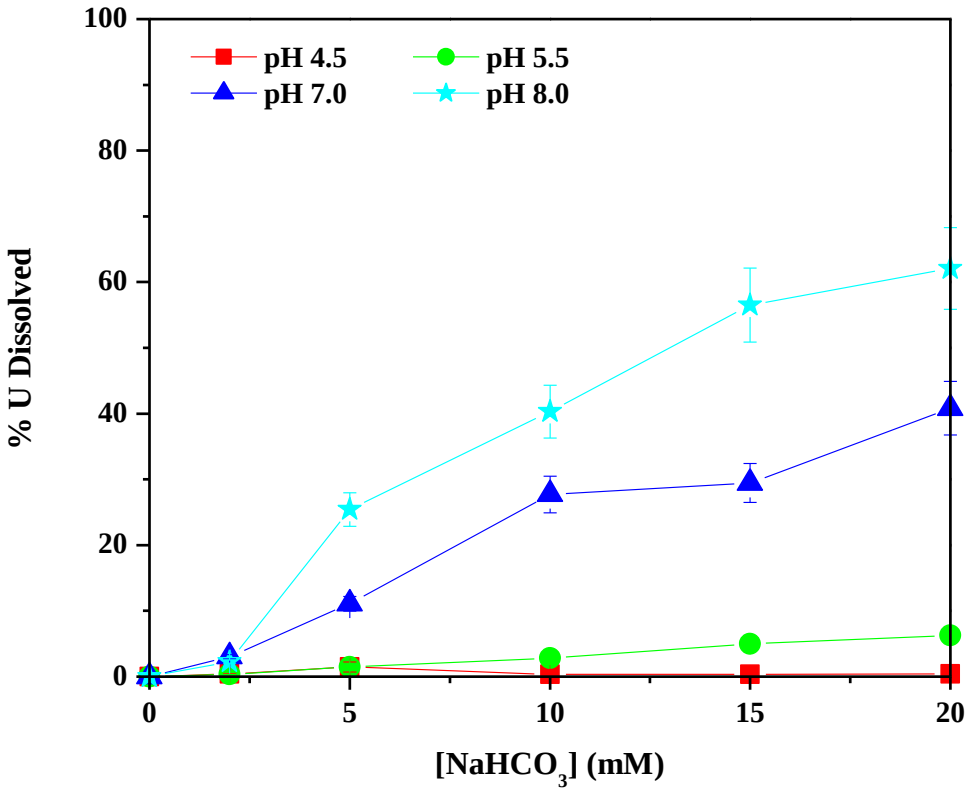

Figure 7.1 Percent dissolution of autunite as a function of carbonate concentration in pH 4.5, 5.5, 7.0, and 8.0 artificial groundwater after a 10 day equilibration. Error bars represent the variation between triplicate experiments and the analytical error on duplicate measurements.

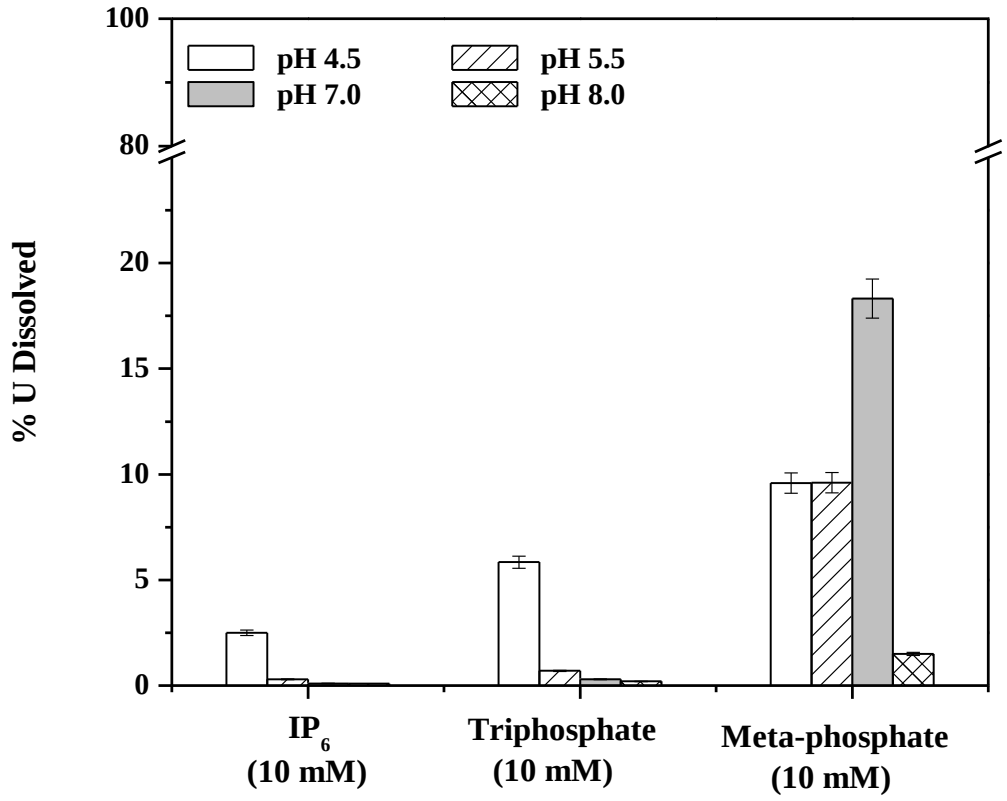

Figure 7.2 Dissolution of autunite after a 10 day equilibration in pH 4.5, 5.5, 7.0, and 8.0 artificial groundwater amended with 10 mM inositol hexaphosphate (IP_6), 10 mM triphosphate, or 10 mM meta-phosphate. Error bars represent the variation between triplicate experiments and the analytical error on duplicate measurements.

The effect of polyphosphate compounds on U-P dissolution was not as drastic as observed with carbonates (Figure 7.2). A maximum dissolution of 20% occurred in the presence of sodium metaphosphate at pH 7.0 (Figure 7.2), while minimal dissolution occurred in the presence of sodium phytate (Figure 7.2). Interestingly, uranium dissolution in the presence of these polyphosphate and organophosphate compounds exhibited a positive correlation with the concentration of inorganic phosphate produced in solution (Figure 7.3). The production of inorganic phosphate in this system far exceeded concentrations expected solely from autunite dissolution (i.e. 200 μM) (Figure

7.3), indicating polyphosphates and/or organophosphates were hydrolyzed. While the most significant autunite dissolution occurred in metaphosphate-amended systems, uranium minerals dissolved only when phosphate was produced in excess of 3 mM (Figure 7.3), presumably due to chemical hydrolysis of metaphosphate at pH 4.5, 5.5 and 7.0. At pH 8.0, however, when less than 1 mM orthophosphate accumulated and pH had no effect on autunite stability (Figure 7.1), metaphosphate did not promote autunite dissolution (Figure 7.3), suggesting this process was promoted by orthophosphates rather than the polyphosphate source. Thus, the small dissolution of autunite observed at low pH for triphosphate and pH < 8 for meta-phosphate was likely promoted dissolved inorganic phosphate that accumulated in solution. Indeed, elevated phosphate concentrations have been shown to increase the solubility of autunite minerals either by acting as a stabilizing ligand for uranium upon released from the autunite mineral or by actively binding uranium in the positively charged autunite structure and catalyzing release of soluble uranium-phosphate aqueous complexes (Mattigod et al., 2008). As the first dissolution mechanism should not be enhanced by elevated phosphate concentrations, uranium release via direct interaction of phosphate with the autunite mineral surface represents the most likely dissolution mechanism.

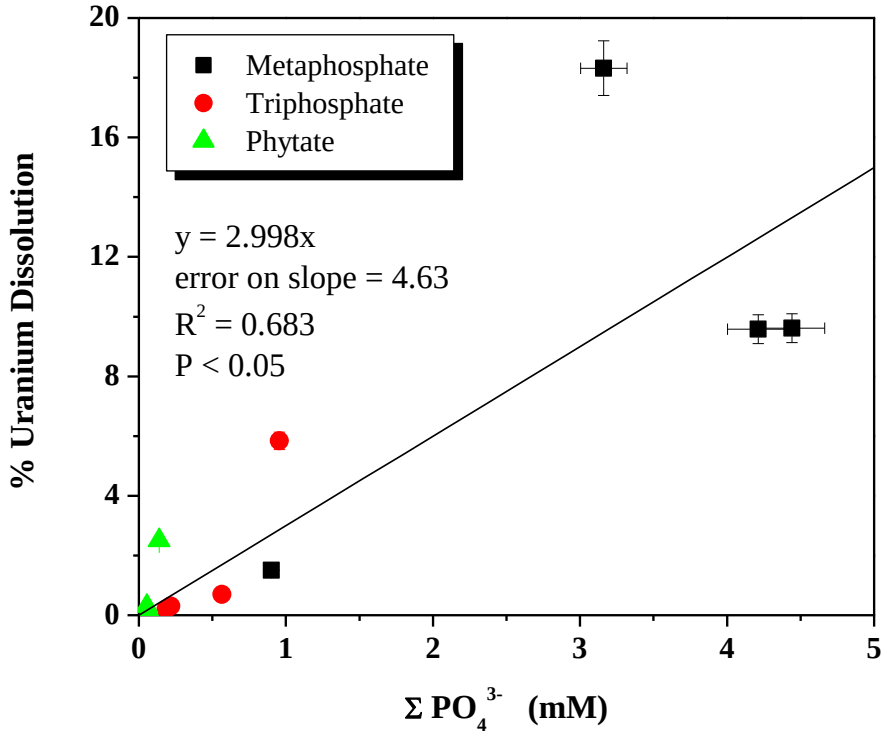

Figure 7.3 Relationship between autunite dissolution and inorganic phosphate concentrations after a 10 day equilibration in pH 4.5, 5.5, 7.0, and 8.0 artificial groundwater amended with 10 mM inositol hexaphosphate (phytate, green triangles), 10 mM triphosphate (red circles), or 10 mM meta-phosphate (black squares). Error bars represent the variation between triplicate experiments and the analytical error on duplicate measurements.

7.4.2 Sequential extraction of U(VI)-phosphate and U(VI)-phytate precipitates

Tessier's sequential extraction technique has long been used to elucidate solid-phase metal speciation (Tessier et al., 1979), and the dissolution of U(VI)-phosphate minerals in the presence of ORFRC soils promoted by pH 5.0 acetic acid, the second step of this extraction technique, has been demonstrated (Beazley et al., 2011). In this study, abiotically precipitated autunite was extractable by acetate (Figure 7.4), confirming that dissolved uranium detected in the acetate extractable fraction is attributable to the dissolution of uranium phosphate minerals. Comparatively, U(VI)-phytate precipitates

were not dissolved by acetate but were instead divided between the hydroxylamine (~20%) and peroxide extractable (~80%) fractions (Figure 7.4) revealing that U(VI)-phytate solids are likely resistant to dissolution by acetic acid. Indeed, acetate extractable uranium in contaminated sediments drastically decreased after treatment with both Ca-phytate and Na-phytate (Seaman et al., 2003) suggesting treatment with IP_6 decreases the leachability of uranium. It is unclear why U(VI)-phytate precipitates were distributed between both the hydroxylamine and peroxide extractable fractions. To our knowledge, uranium precipitates have not previously been identified in the peroxide extractable fraction using this technique. However, as peroxide should oxidize organic carbon to carbon dioxide, it is surmised that the mechanism behind this dissolution involves oxidation of inositol within the phytate molecule. Hydroxylamine is known to extract Fe- and Mn-occluded uranium through reductive dissolution of these metal oxides (Tessier et al., 1979). As only pure uranium mineral phases were present, however, Fe- or Mn- associated uranium cannot account for the hydroxylamine-extracted U fraction in this system. In addition, hydroxylamine does not reduce U(VI) (Paiva and Malik, 2004), suggesting that the uranium extracted by this step is not U(IV), which remains soluble at acidic pH (Casas et al., 1998). In turn, autunite dissolution rates are highest in low pH groundwater (Wellman et al., 2007), suggesting that the partial dissolution of U(VI)-phytate minerals by hydroxylamine was most likely caused by the low pH of the extractant. Nonetheless, mixtures of autunite and U(VI)-phytate precipitates displayed extraction profiles very similar to those predicted from extraction of their isolated mineral phases (Figure 7.4). Thus, this extraction technique should accurately differentiate between U(VI)-phosphate and U(VI)-phytate precipitates in defined matrices.

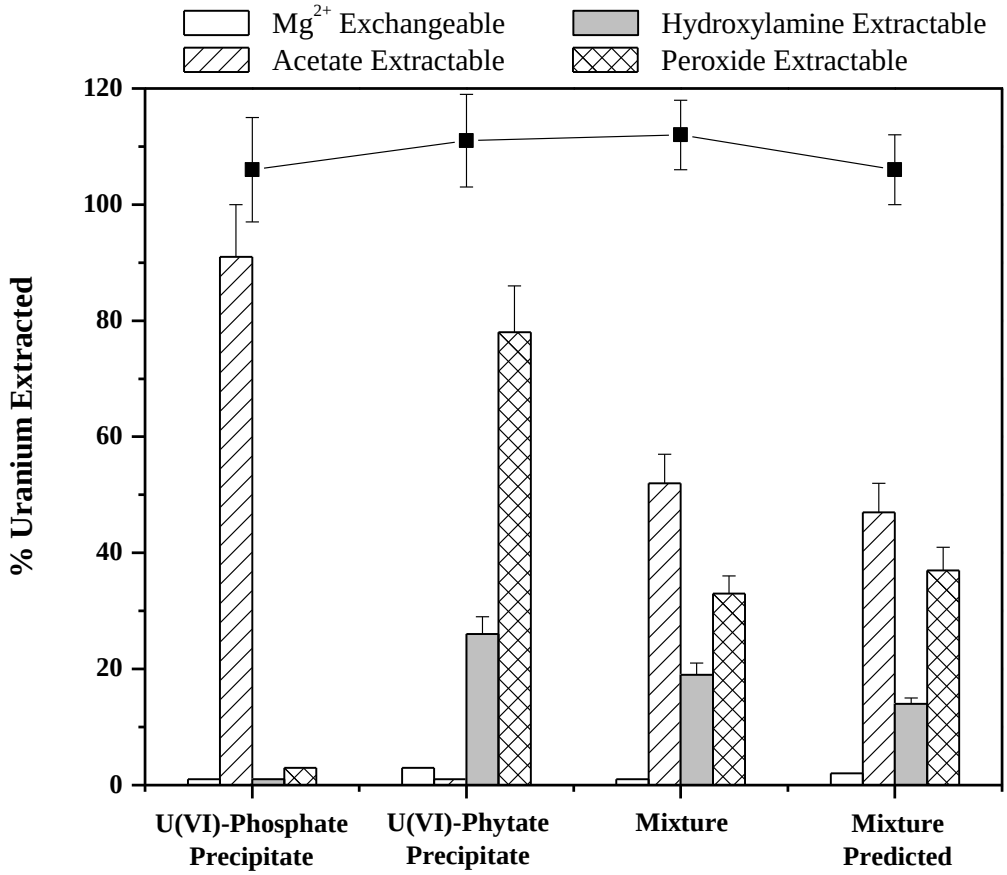

Figure 7.4 Sequential extraction of U(VI)-phosphate, U(VI)-phytate, and mixtures of these precipitates using the technique of Tessier et al. (1979). The extraction profile of the precipitate mixture was predicted from the extraction profiles of each individual precipitate. Square symbols represent the total percentage of uranium recovered for each mineral. Error bars represent the variation between triplicate extractions and the analytical error on duplicate measurements.

7.4.3 Interaction of phytate with ORFRC soils

To represent a successful bioremediation strategy in contaminated environments, the phytate-promoted immobilization of uranium depends on the transport of phytate throughout contaminant plumes. Phytate carries a highly negative charge at all environmentally relevant pH and, thus, interacts strongly with soil sorbents such as metal oxides and organic matter (Borie et al., 1989; Degroot and Golterman, 1993; Johnson et

al., 2012; Shang et al., 1992). In fact, phytate is so strongly attracted to soil surfaces that it will displace previously sorbed orthophosphate (Anderson and Malcolm, 1974; Berg and Joern, 2006; Bowman et al., 1967). In this study, adsorption of phytate to ORFRC Area 3 soils at pH 5.5 followed a Langmuir-type sorption isotherm (Figure 7.5) with a calculated K_{ads} and Γ_{max} of 679 ± 178 M^{-1} and 28 ± 6 μmol IP_6 g^{-1} soil, respectively. Comparatively, phytate adsorbed to goethite at pH 5.5 was determined to be an outer-sphere complex with a K_{ads} of 5.04 M^{-1} and a Γ_{max} of 36 ± 2 μmol IP_6 g^{-1} (Johnson et al., 2012). While the maximum sorption capacities for phytate sorption onto ORFRC soils and goethite are comparable, the K_{ads} for phytate sorption onto ORFRC soils is much higher than for phytate sorption onto goethite, indicating ORFRC soils contain much stronger sorbents than goethite at this pH. Adsorption of uranium to ORFRC soils has been successfully modeled assuming ferrihydrite to be the dominant soil sorbent (Barnett et al., 2002). While goethite displays a pH_{ZPC} between 5.9 and 6.7 (Langmuir, 1997; Stumm and Morgan, 1996), ferrihydrite displays a much higher pH_{ZPC} of ~ 8.5 (Sverjensky and Fukushi, 2006). Thus, at pH 5.5 when ferrihydrite surfaces are overall positively charged and the net charge on goethite surfaces is nearly neutral, negatively charged phytate should interact more strongly with ferrihydrite than goethite, explaining the vastly different calculated K_{ads} for phytate sorption to ORFRC soils (this study) and goethite (Johnson et al., 2012) in these conditions.

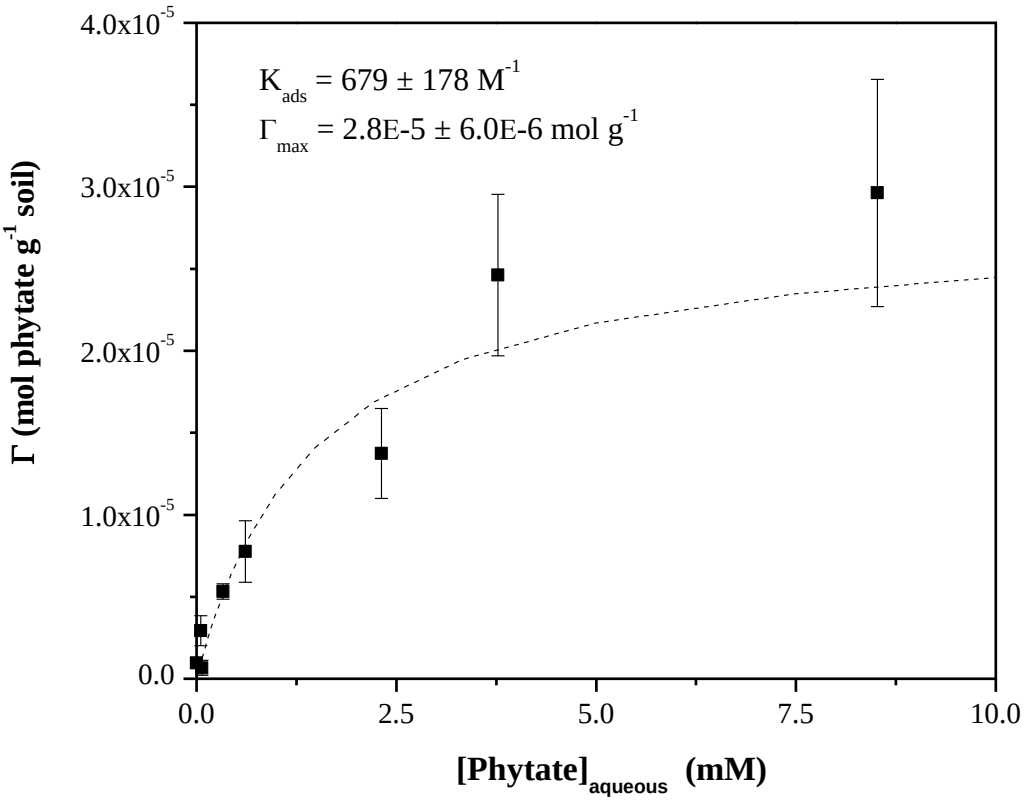

Figure 7.5 Adsorption of phytate to ORFRC soils in pH 5.5 artificial groundwater. The equilibrium constant for phytate sorption, K_{ads}, and the maximum sorption capacity of ORFRC soils, Γ_{max}, were calculated from the Langmuir sorption isotherm for this system. Error bars represent the variation between triplicate experiments and the analytical error on duplicate measurements.

7.4.4 Phytate content of commercial cereal bran

Inositol hexaphosphate is synthesized by plants for phosphorus storage and, thus, represents the dominant organic phosphorus in many soils (Turner et al., 2002). In particular, phytate is the principal phosphorus storage mechanism in cereals, legumes, and oleaginous seeds (Gibson et al., 2010). Due to the propensity of phytate to chelate metals and prevent absorption of micronutrients, it is considered a potent anti-nutrient, especially in low-income countries where diets are largely built around affordable grains

and legumes (Gibson et al., 2010) As such, the phytate content of dietary staples like cereals and legume has been well characterized with phytate comprising up to 2.22% (w/w) of cereals and up to 9.15%(w/w) of legumes (Reddy, 2001). In addition, cereal phytate is primarily concentrated in the bran of the grain (Odell et al., 1972). Thus, wheat bran and oat bran may represent inexpensive sources of phytate for use in U(VI)-phosphate bioremediation strategies. After 4 days of extraction with deionized water (DI) and hydrochloric acid (HCl), inositol hexaphosphate was detected in both oat bran and wheat bran extracts, while inositol pentaphosphate (IP_5) was present in extracts of oat bran but not wheat bran (Figure 7.6). Extractions with HCl improved phytate yield for both oat and wheat bran as compared to similar extractions with DI (Figure 7.7), indicating acid extractions are more efficient for concentrating phytate from cereal bran than water extractions. Commercial wheat brans contain on average 64.2 μmol g^{-1} dry weight phytate, which is in average double the amount of phytate as oat brans (Garcia-Estepa et al., 1999). Acid extractions of wheat bran performed in the current study provided ~ 50 μmol IP_6 g^{-1} dry weight, 5 times more IP_6 than similar extractions with oat bran (Figure 7.7), confirming that wheat bran represents a better source of acid-extractable phytate than oat bran and demonstrating that digestion with 1.0 M HCl is sufficient to extract the majority of available phytate from wheat bran.

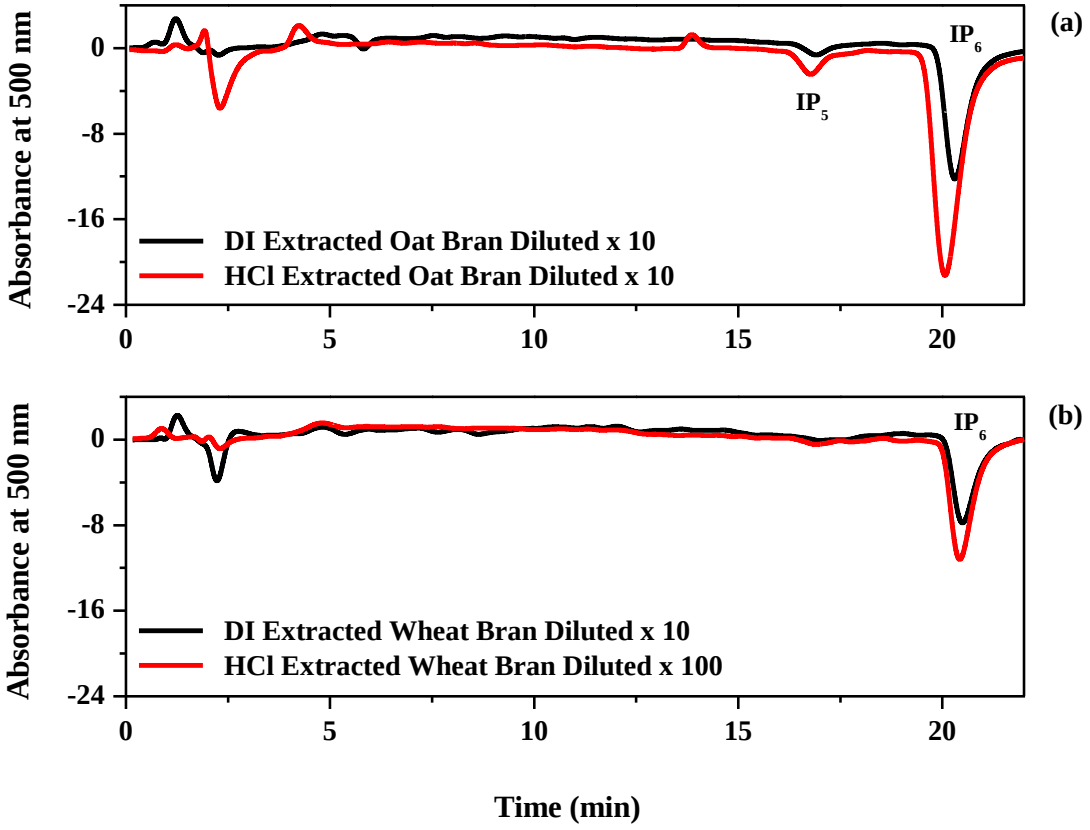

Figure 7.6 Chromatographic separation coupled to spectrophotometric detection of inositol phosphates (Rounds and Nielsen, 1993) in deionized water (DI) and acid (HCl) used to extract commercially available (a) oat bran and (b) wheat bran. Concentration of inositol species is proportional to peak area of suppressed absorbance peaks. Inositol pentaphosphate (IP_5) elutes from the column at ~ 17 minutes, while inositol hexaphosphate (IP_6) elutes from the column at ~ 21 minutes. No other inositol phosphates (IP_x with x = 2, 3, and 4) were detected.

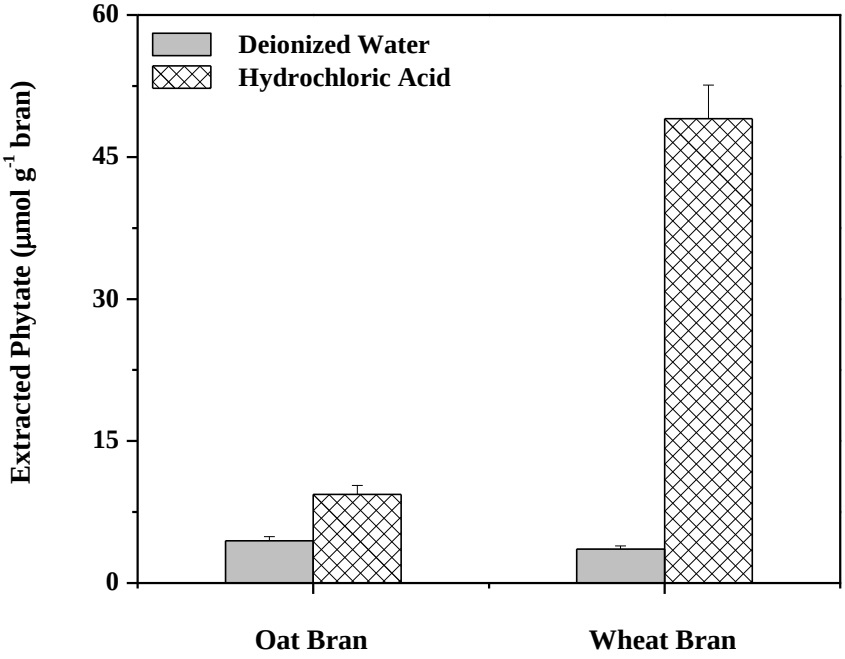

Figure 7.7 Phytate content normalized to the mass of oat bran and wheat bran extracted with deionized water or hydrochloric acid. Cereal bran was extracted for 4 days prior to filtration and quantification of inositol phosphates. Error bars represent the variation between triplicate extractions.

7.5 Implications for U(VI)-Phosphate Biomineralization Strategies

For biomineralization of U(VI)-phosphate minerals to be an effective remediation strategy, parameters surrounding the stability of the mineral product and the bioavailability of the organophosphate substrate must first be characterized. In this study, the stability of the autunite mineral product of U(VI)-phosphate biomineralization was demonstrated in conditions representative of the ORFRC. At alkaline pH and high DIC, however, significant autunite dissolution was observed, indicating that biomineralization is a plausible bioremediation technique for the ORFRC but may not be appropriate at contaminated sites exhibiting more alkaline pH like the Hanford 300 Area facility. In

addition, autunite remained stable in the presence of IP_6, suggesting biomineralization strategies utilizing phytate as an organophosphate source will not compromise the stability of the mineral product. Phytate interacted strongly with ORFRC Area 3 soils, yet significant fractions of phytate remained in solution, suggesting phytate should spread over large areas upon injection into contaminated sediments. In addition to promoting U(VI)-phosphate biomineralization, phytate may also chemically precipitate with uranium, generating a need for an accurate means of differentiating between these two precipitates. Sequential chemical extractions of U(VI)-phosphate and U(VI)-phytate precipitates revealed different extraction profiles for each of these solids, and extraction profiles for mixtures of these precipitates closely resembled predicted results. Thus, sequential extractions should accurately differentiate between these two solid-phase uranium species. The abundance of phytate in soils suggests that natural attenuation is likely ongoing in a variety of contaminated environments. The efficient extraction of phytate from bran, however, may represent an alternative source of phytate which could be used in U(VI)-phosphate biomineralization strategies. Given the concentration of phytate extracted in commercially available wheat bran and its current cost, 1 kg of phytate could be extracted from approximately $90 worth of wheat bran, while it would cost upwards of $1500 to purchase the same mass of purified phytate from a major chemical manufacturer. Thus, the ability to extract phytate directly from plant sources represents a potential cost savings of over 94%.

7.6 Acknowledgements

This research was supported by the Office of Science (BER), US Department of Energy Grant No. DE-FG02-04ER63906. We thank Dave Watson of Oak Ridge National Laboratory for providing ORFRC sediment cores.

CHAPTER 8

CONCLUSIONS

The large quantities of contaminated groundwater and soils at DOE facilities have spurred research on *in situ* remediation methods for immobilizing uranium in the subsurface. This dissertation examined the efficacy of phytate-promoted U(VI)-phosphate biomineralization as a uranium remediation technique. The strategy involves addition of phytate to a contaminated subsurface to promote microbial phytase activity with subsequent liberation of inorganic phosphate, which chemically precipitates with uranium. The main hypotheses explored in this dissertation include:

1. U(VI)-phosphate biomineralization outcompetes uranium bioreduction in anaerobically-maintained contaminated sediments.
2. ORFRC microorganisms hydrolyze phytate and liberate inorganic phosphate when fed phytate as sole phosphorus source.
3. Inorganic phosphate liberated via microbially-catalyzed phytate hydrolysis promotes U(VI)-phosphate biomineralization.
4. The U(VI)-phosphate mineral product formed during biomineralization remains stable in a broad range geochemical conditions.

First, the competition dynamic between U(VI) bioreduction, U(VI)-phosphate biomineralization, and adsorption in the presence of G2P and alternate terminal electron acceptors was studied in anaerobically-maintained sediment microcosms containing ORFRC contaminated soils at two different pHs. The objectives of this work were to

determine whether (1) nitrate-, iron-, or sulfate-reducing conditions are most conducive to U(VI)-phosphate biomineralization through the activities of endogenous ORFRC microbial phosphatases and (2) the biomineralization of U(VI)-phosphate minerals outcompetes uranium bioreduction in conditions typically favorable to bioreduction (i.e. pH 7.0, low nitrate). The addition of G2P to ORFRC Area 3 sediments was sufficient to stimulate reduction of nitrate but not sulfate, even after complete removal of nitrate, suggesting the lack of a suitable terminal electron donor for sulfate-reducing bacteria in these incubations. Although more efficient at pH 7.0, G2P-independent anaerobic respiration of iron oxides occurred at both pHs, even in the presence of elevated nitrate concentrations. In turn, nitrate reduction depended on G2P hydrolysis and was enhanced at circumneutral pH, suggesting that G2P bioavailability may drive anaerobic nitrate respiration in these sediments. The magnitude of G2P hydrolysis was much greater than the availability of uranium at both pHs, suggesting that organophosphate hydrolysis in these sediments was activated by a nutrient limitation rather than as a uranium detoxification mechanism. XANES analysis of incubated sediments demonstrated uranium was not reduced. In addition, wet chemical extractions and EXAFS spectroscopy indicated the presence of U(VI)-P species in reactors amended with G2P at both pHs. Thus, uranium was likely precipitated as U(VI)-phosphate minerals in sediments amended with G2P. Overall, these results not only suggested that biomineralization of U(VI)-phosphate minerals may be complementary to bioreduction in reducing conditions, but also that U(VI)-phosphate biomineralization may be dominant in certain environments due to its utility in a wide range of geochemical and redox conditions.

As glycerol-2-phosphate is synthetic and would be expensive to apply over a large field area, the ability of the ORFRC natural microbial community to promote U(VI)-phosphate biomineralization in aerobic conditions via hydrolysis of phytate, a naturally-occurring organophosphate, was tested in soil slurries at two different pHs. The objectives of this work were to (1) explore the phytase activity of the ORFRC natural microbial community at pH 5.5 and 7.0, (2) determine the dependence of this activity on the addition of glycerol as electron donor, and (3) examine the biomineralization of U(VI)-phosphate minerals coupled to microbial phytase activity. While phytate hydrolysis was not evidenced at pH 7.0, complete hydrolysis was observed at pH 5.5, suggesting indigenous microorganisms express acidic but not alkaline phytases in these soils. More importantly, this hydrolysis occurred both with and without added glycerol, indicating endogenous electron donors were sufficient to support microbial metabolism. The presence of uranium accelerated phytate hydrolysis and decreased the rate of hydrolysis of inositol intermediates as a result of a possible toxicity effect on the indigenous population. Inorganic phosphate production from phytate hydrolysis at pH 5.5 enhanced uranium immobilization via biomineralization of U(VI)-phosphate minerals and formation of ternary sorption complexes as determined by wet chemical extractions and EXAFS spectroscopy of incubated sediments. This work demonstrated for the first time the ability of natural microbial communities to liberate phosphate from phytate in acidic soils and the potential utility of phytate-promoted biomineralization of U(VI)-phosphate minerals as a uranium immobilization strategy.

The phytase activity of ORFRC microorganisms isolated from the above soil slurries was then determined in pH 5.5 pure culture incubations amended with increasing

concentrations of uranium. The objectives of this work were to (1) isolate phytate-hydrolyzing microorganisms from these sediments, (2) determine what geochemical conditions induce phytase expression by one of the isolates, and (3) investigate the effect of exposure to increasing uranium concentrations on the production of phytase enzymes. Two microorganisms that hydrolyze phytate in artificial groundwater were identified, and PCR amplified 16S rRNA sequences revealed these isolates as *Bradyrhizobium* and *Variovorax* species. *Variovorax* sp. was exposed to increasing concentrations of uranium for a four-hour period and incubated aerobically in pH 5.5 artificial groundwater amended with phytate as sole phosphorus source and lactate as electron donor. In both abiotic controls and live cell incubations, uranium was immediately removed from solution upon addition of phytate, likely due to formation of U(VI)-phytate precipitates. The organism grew, though at lower rates than without uranium, even in the presence of as much as 1 mM uranium. Without uranium, the almost complete degradation of phytate by *Variovorax* sp. after only 2 weeks of incubation was accompanied by the stoichiometric production of inorganic phosphate. When the cells were exposed to uranium, however, total inorganic phosphate production over the same period decreased linearly with increasing uranium concentrations, suggesting the existence of a significant uranium toxicity effect. Introduction of uranium also resulted in incomplete degradation of phytate and an earlier onset and more rapid accumulation of inorganic phosphate compared to identical reactors without uranium, indicating acid phytase enzyme production by *Variovorax* sp. may represent a uranium detoxification mechanism. These results demonstrate that phytate addition to uranium contaminated environments may promote both chemical uranium sequestration and biomineralization of U(VI)-phosphate

minerals via microbially-mediated phytate hydrolysis and that bacterial phytate hydrolysis may be enhanced in contaminated systems if microorganisms initiate phytase enzyme expression as a uranium detoxification mechanism. A diagnostic kinetic model was then developed to confirm the mechanism of phytate hydrolysis by ORFRC microorganisms.

Finally, the chemical reactivity of uranium-phosphate minerals was tested in a variety of geochemical conditions, and the phytate content of commercial cereal grains was determined to identify alternative inexpensive phytate sources. The objectives of this work were to (1) demonstrate the stability of U(VI)-phosphate minerals in a wide range of geochemical conditions, (2) validate a sequential extraction technique for differentiating between U(VI)-phosphate and U(VI)-phytate precipitates, (3) characterize phytate sorption to ORFRC soils, and (4) investigate the potential of utilizing an inexpensive phytate source in U(VI)-phosphate biomineralization strategies. While U(VI)-phosphate minerals were not dissolved significantly by other phosphorus sources, including phytate at any pH, they were destabilized by relatively high carbonate concentrations after a few days above circumneutral pH, confirming that the biomineralization of U(VI) phosphate minerals may be better suited in low pH conditions or low DIC environments. Indeed, U(VI)-phosphate minerals remained stable for at least 6 months even in the presence of high carbonate concentrations in low pH conditions representative of the ORFRC subsurface. U(VI)-phytate precipitates were extracted primarily by peroxide, demonstrating sequential chemical extraction techniques may successfully differentiate between U(VI)-phosphate and U(VI)-phytate precipitates in defined systems, which will be useful in future investigations. Although phytate strongly

sorbed to ORFRC soils, significant fractions of added phytate remained soluble and, thus, bioavailable, suggesting phytate may be an acceptable amendment to promote biomineralization of U(VI)-phosphate minerals. Finally, extracted wheat bran was found to contain large concentrations of acid-extractable phytate, indicating that it may be a cost-effective phytate source for use in biomineralization techniques. These results demonstrate that phytate-promoted biomineralization of U(VI)-phosphate minerals may be an effective uranium remediation strategy for low pH, low DIC contaminated sites such as the ORFRC.

Overall, the results of this study reveal the utility of U(VI)-phosphate biomineralization strategies in a wide range of geochemical conditions, including anaerobic environments where bioreduction was previously thought to be the only biological mechanism of removal of uranium, and low pH environments where bioremediation strategies currently require *ex situ* treatment of groundwater. In addition, the efficacy of UVI)-phosphate biomineralization promoted by microbially-mediated phytate hydrolysis was demonstrated for the first time in soil slurries and pure culture incubations. Thus, phytate hydrolysis catalyzed by the natural microbial community at contaminated waste sites may represent a highly-efficient and cost-effective method for the bioremediation of uranium contaminations.

8.1 Recommendations for future research

The results presented in this dissertation have brought to light new questions which are addressed below as recommendations for future research. This study examined the stability of U(VI)-phosphate minerals over a range of pH and dissolved inorganic carbon concentrations. As phytate chemically precipitates with uranium, the stability of

U(VI)-phytate precipitates must also be demonstrated to ensure long-term uranium immobilization in contaminated environments. Adsorption of phytate onto ORFRC soils was determined at pH 5.5. However, to properly model substrate bioavailability in contaminated subsurfaces, phytate sorption as a function of pH should also be characterized. Such information will be useful to predict the behavior of phytate injected in subsurface environments.

To fully examine the effect of phytate sorption on orthophosphate release by the natural microbial community at Oak Ridge, phytate hydrolysis should be investigated in flow-through reactors. While flow-through reactor experiments are more difficult to set up, they present the advantage of maintaining inorganic phosphate concentrations to low levels in the reactors to evaluate fully the long-term role of adsorbed phytate as potential source of inorganic phosphate. In parallel, the ability to ORFRC microorganisms to hydrolyze phytate extracted from cereal bran should be examined both in slurries and pure culture incubations to determine whether cereal bran could provide an inexpensive source of phytate for bioremediation studies.

Finally, the kinetics of phytate hydrolysis by *Variovorax* sp. was only investigated at pH 5.5 and in aerobic conditions. The ideal pH conditions that promote this process should be therefore established, and it would be useful to determine whether this organism is an obligate aerobe as other *Variovorax* strains are also known to reduce nitrate. These kinetic experiments should also be repeated with *Bradyrhizobium* sp., the other phytase-positive microorganism isolated from the ORFRC, and the respiratory phenotype of this organism should be determined. If the genome of each of these microorganisms is fully sequenced, gene deletion experiments should also be designed to

determine the molecular mechanism controlling phytase expression as uranium detoxification process.

APPENDIX A

SUPPLEMENTAL INFORMATION FOR CHAPTER 3

A.1 Calculation of pseudo-first order rate constants

Pseudo-first order rate constants were calculated for uranium, nitrate, G2P, and Fe(III) removal utilizing a linearization of the data in the form of Eq. C-1.

$$\ln\left(\frac{C}{C_0}\right) = -kt \qquad \text{(C-1)}$$

Data was transformed and graphically represented as $\ln(C/C_0)$ vs. time, where C represents concentration of each species at time x, and C_0 represents the initial concentration of each species at the time observed removal begins. An unweighted linear regression was fit for each species of interest in each reactor, and the slope of the regression was reported as the rate constant (Figure 2B and S1). For reactor treatments where no change in species concentration was observed for the duration of the experiment, the rate constant was reported as zero. For uranium removal, two separate removal phases were fit with linear regressions for pH 5.5 reactors (Figure 2B). The initial removal phase occurred between days 0 and 4, and the secondary removal phase occurred between days 7 and 39. For pH 7.0 reactors, only one uranium removal phase was observed (Figure 2B). A single removal phase was also observed for nitrate, Fe(III), and G2P (Figure S1). Errors were reported as the standard error of the slope found by performing a linear regression on the above data.

Table A.1 Composition of trace elements solution as reported in Widdel and Bak (1992).

Species	*Concentration (mM)*
HCl	100
$FeSO_4 \cdot 7H_2O$	7.5
H_3BO_3	0.5
$MnCl_4 \cdot 4H_2O$	0.5
$CoCl_2 \cdot 6H_2O$	0.8
$NiCl_2 \cdot 6H_2O$	0.1
$CuCl_2 \cdot 2H_2O$	0.01
$ZnSO_4 \cdot 7H_2O$	0.5
$Na_2MoO_4 \cdot 2H_2O$	0.15

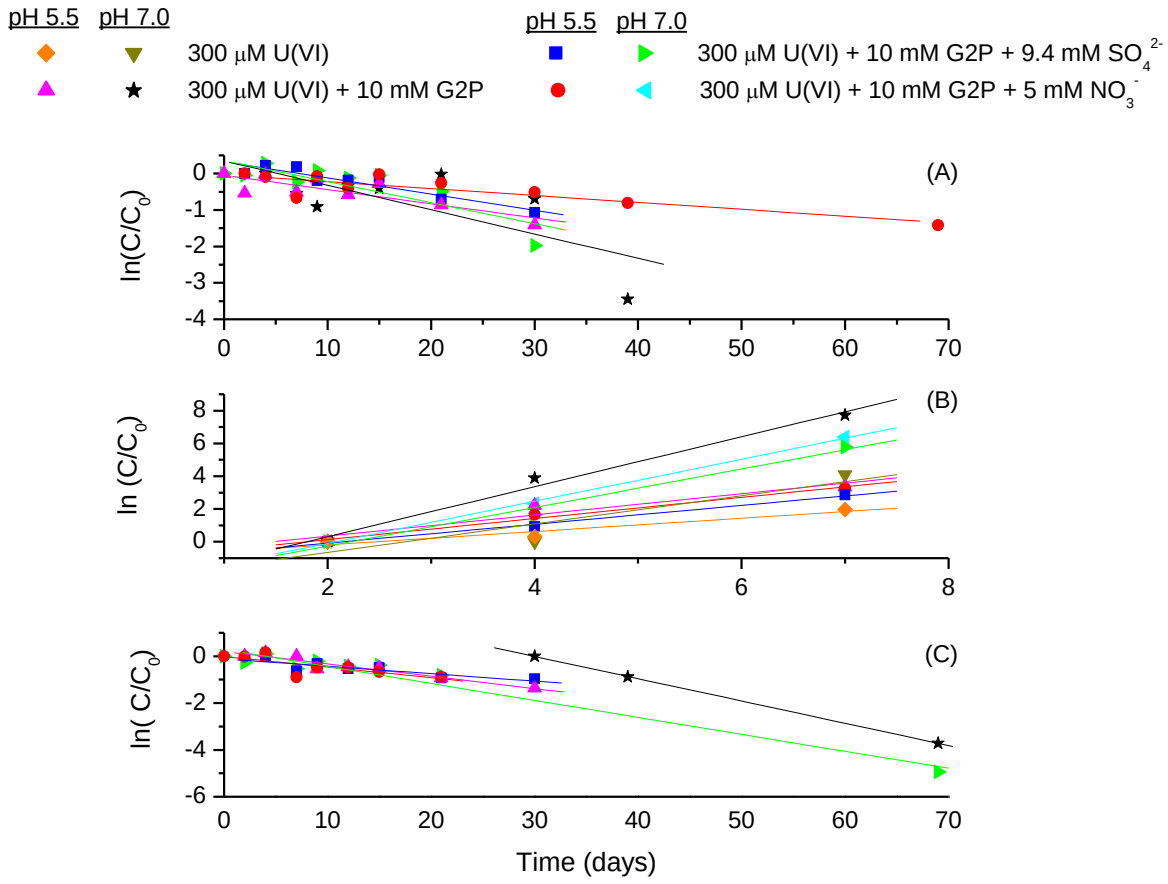

Figure A.1 Linearization of static microcosm data for A) NO_3^-, B) Fe(III), and C) G2P for pH 5.5 and 7.0 reactors amended with 300 μM UO_2^{2+} only; 300 μM UO_2^{2+} and 7 mM NO_3^- (pH 7.0 only); 300 μM UO_2^{2+} and 5 mM G2P; 300 μM UO_2^{2+}, 5 mM G2P, and 7 mM NO_3^- (pH 5.5 only); or 300 μM UO_2^{2+}, 5 mM G2P, and 9.4 mM SO_4^{2-}. For each chemical species, treatments not shown exhibited no discernable change in concentrations of that species for the duration of the experiment, and rate constants for these reactors were reported as zero. Errors on rate constants from these calculations were reported as the standard error of the slope.

APPENDIX B

SUPPLEMENTAL INFORMATION FOR CHAPTER 4

Table B.1 Background ion concentrations in the artificial groundwater reflective of the composition of groundwater at the Oak Ridge Field Research Center in Oak Ridge, TN (Brooks, 2001).

Ion	*Concentration*
Ca^{2+}	200 µM
Fe^{2+}	2.0 µM
Mn^{2+}	5.1 µM
K^{+}	7.9 mM
Na^{+}	7.5 mM
MoO_4^{2-}	8.0 µM
Cl^{-}	410 µM
SO_4^{2-}	810 µM
NO_3^{-}	15.4 mM

Table B.2 Predicted solution equilibrium and solid phase saturation indices using MINEQL+ (Schecher and McAvoy, 2001) in pH 5.5 and 7.0 soil slurries. Solution concentrations are reported in percent of total species. For solid phase species, values reported represent saturation indices for each mineral phase, and numbers in parentheses represent the percentage of uranium precipitated as each respective mineral. Each treatment was modeled as an open system using the maximum measured inorganic phosphate concentration and initial conditions as input for all other species. A double layer sorption model onto amorphous Fe-oxide (0.41 g/L, 600 m^2/g surface area) was included in the calculations. Unless otherwise noted, log K values are as reported in Schecher and McAvoy (2001).

		Treatment			
U(VI) Species	*Log K*	*pH 5.5 0 mM ΣPO_4^{3-} 200 µM UO_2^{2+}*	*pH 5.5 40 mM ΣPO_4^{3-} 200 µM UO_2^{2+}*	*pH 7.0 0 mM ΣPO_4^{3-} 200 µM UO_2^{2+}*	*pH 7.0 40 mM ΣPO_4^{3-} 200 µM UO_2^{2+}*
Aqueous					
UO_2^{2+}		1.4%	0.0%	0.0%	0.0%
$(UO_2)_2OH_2^{2+}$	-5.62[a,b]	1.2%	0.0%	0.0%	0.0%
UO_2OH^+	-5.20[a,b]	1.8%	0.0%	0.0%	0.0%
$(UO_2)_3(OH)_5^+$	-15.55[a,b]	5.6%	0.0%	0.0%	0.0%
$UO_2PO_4^-$	13.23[b]	0.0%	0.0%	0.0%	0.0%
Fe(wk)OH-$UO_2(OH)_2$	-6.28[c]	6.5%	0.0%	24.4%	0.0%
Fe(st)OH-$UO_2(OH)_2$	-2.57[c]	11.4%	0.0%	11.6%	0.0%
Solid Phase					
Schoepite	-5.2[a]	0(71.6% U)	-5.5	0(63.7% U)	-5.965
Na-Autunite	47.4	-28.5	0 (100% U)	-29.1	0 (100% U)
Ca-Autunite	27.2[a]	-30.8	-2.5	-31.5	-3.503

[a] (Langmuir, 1997), [b] (Guillamont et al., 2003), [c] (Waite et al., 1994)

Table B.3 Fitting Parameters for U L_{III}-edge EXAFS derived using SIXPACK (Webb, 2005) in soil slurries treated with a (pH 5.5, 200 µM U), b (pH 5.5, 200 µM U + 10 mM IP_6), c (pH 5.5, 200 µM U + 10 mM IP_6 + 10 mM glycerol), d (pH 7.0, 200 µM U + 10 mM DIC), e (pH 7.0, 200 µM U + 10 mM DIC +10 mM IP_6), and f (pH 7.0, 200 µM U + 10 mM IP_6 + 10 mM glycerol + 10 mM DIC). N represents U-ligand coordination number, R(Å) represents U-ligand distance.

Treatment	*Shell*	*N*	*R(Å)*	$\sigma^2(Å^2)$	ΔE_0 *(eV)*	*R factor*
A	O_{ax}	2.0	1.78(0.01)	0.005(0.001)	6.21(3.90)	0.0098
	O_{eq}	3.26(1.43)	2.26(0.03)	0.009		
	O_{eq}	1.77(0.64)	2.42(0.03)	0.003		
	Mn/Fe	0.77(0.39)	3.38(0.06)	0.003		
B	O_{ax}	2.0	1.79 (0.01)	0.004(0.001)	10.0(2.13)	0.0159
	O_{eq}	4.04(0.95)	2.34(0.02)	0.009		
	Mn/Fe	0.63(0.23)	3.46(0.02)	0.003		
	P	0.39(0.44)	3.88(0.06)	0.002		
C	O_{ax}	2.0	1.78(0.01)	0.004(0.001)	8.72(2.29)	0.0122
	O_{eq}	3.79(0.93)	2.34(0.02)	0.009		
	Mn/Fe	0.58(0.22)	3.45(0.02)	0.003		
	P	0.55(0.45)	3.89(0.05)	0.002		
D	O_{ax}	2.0	1.78(0.02)	0.006(0.001)	3.99(4.37)	0.0085
	O_{eq}	3.28(1.23)	2.25(0.04)	0.009		
	O_{eq}	1.20(0.46)	2.41(0.04)	0.003		
	C	0.60(0.24)	2.90(0.03)	0.009		
	Mn/Fe	0.24(0.14)	3.43(0.04)	0.003		
E	O_{ax}	2.0	1.77(0.02)	0.003(0.002)	4.70(3.51)	0.0336
	O_{eq}	4.70(1.90)	2.29(0.03)	0.009		
	C	1.59(0.63)	2.94(0.03)	0.009		
	Mn/Fe	0.31(0.35)	3.49(0.06)	0.003		
F	O_{ax}	2.0	1.77(0.01)	0.004(0.001)	7.10(2.55)	0.0145
	O_{eq}	4.91(1.32)	2.29(0.02)	0.009		
	C	0.74(0.32)	2.92(0.03)	0.009		
	Mn/Fe	0.66(0.23)	3.45(0.02)	0.003		

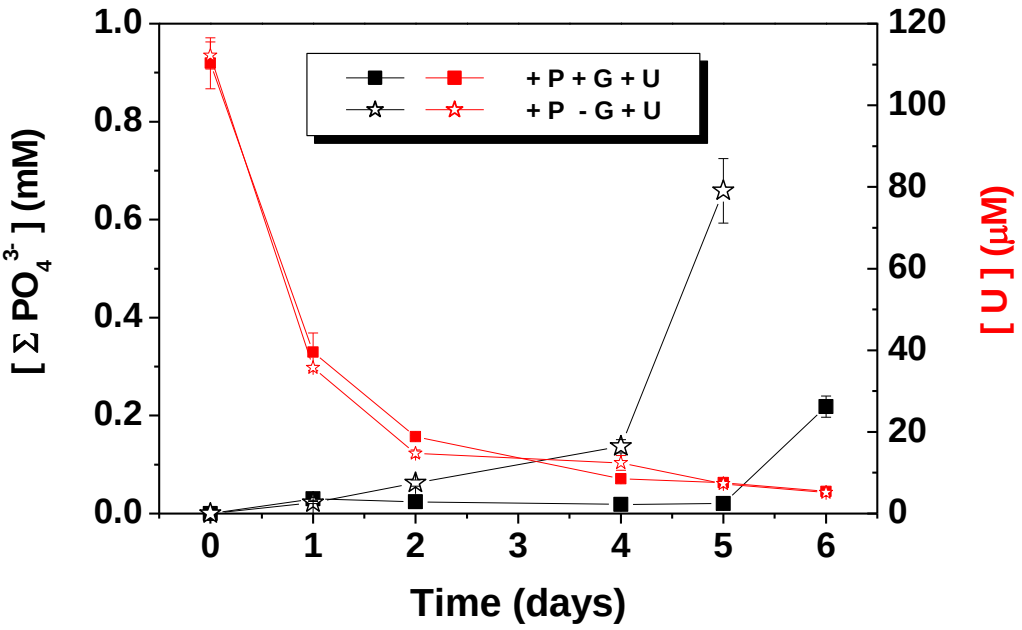

Figure B.1 Inorganic phosphate production (black) and uranium removal (red) in selected soil slurries containing 16 g/L Area 3 Oak Ridge Field Research Center soils and pH 5.5 buffered artificial groundwater amended with 10 mM phytate, 10 mM glycerol, and 200 µM UO_2^{2+} (+ P + G + U) or 10 mM phytate and 200 µM UO_2^{2+} (+ P – G + U). Closed symbols represent slurries amended with glycerol. Error bars include variation between triplicate reactors and the analytical error on duplicate measurements.

APPENDIX C

SUPPLEMENTAL INFORMATION FOR CHAPTER 5

C.1 Preparation of MUP-amended Enriched Nutrient Media Plates

Unless otherwise stated, all chemicals used to prepare MUP-amended enriched nutrient media plates were purchased from Becton, Dickinson and Company (BD), and all media were made using nanopure water (Barnstead). To prepare enriched nutrient media plates, 1 L each of 1% tryptone media, 1/10 nutrient broth media, and sphingobacteria media (Table C1) were made and autoclaved. After sterilization, solutions were allowed to cool before an aliquot of filter-sterile MUP (final concentration 85 mg/L) was added. Each medium was poured into sterile petri dishes (Fisher) and allowed to dry at room temperature in the dark for 2 days.

C.2 Preparation of Phytate Media Plates

To prepare phytate media plates, two 500 mL solutions containing on one hand 2 g/L $MgSO_4$, 2 g/L NaCl, and 10 g/L NH_4Cl and on the other hand 20 g/L agar were prepared using nanopure water (Barnstead) and adjusted to pH 7.0 using 1 N HCl (Fisher) and/or 1N NaOH (Fisher). Each solution was autoclaved separately, allowed to cool slightly, and then mixed together. After mixing, aliquots of sterile glycerol (pH 7.0, final concentration 10 g/L) and sterile Na-phytate (pH 7.0, final concentration 5 g/L) were also added and mixed thoroughly. The resulting media was then poured into sterile petri dishes (Fisher) and allowed to dry at room temperature in the dark for two days.

C.3 16S rRNA sequence of isolate IS2 as queried with nBLAST

TCGAGCGGGCATAGCAATATGTCNNCGGCAGACGGGTGAGTAACGCNNNNN
NNNNNNNCTTTTGGTTCGGAACAACACAGGGAAACTTGTGCTAATACCGGAT
AAGCCCTTACGGGGAAAGATTTATCGCCGAAAGATCGGCCCGCGTCTGATTA
GCTAGTTGGTGAGGTAATGGCTCACCAAGGCGACGATCAGTAGCTGGTCTGA
GAGGATGATCAGCCACATTGGGACTGAGACACGGCCCAAACTCCTACGGGA
GGCAGCAGTGGGGAATATTGGACAATGGGCGCAAGCCTGATCCAGCCATGCC
GCGTGAGTGATGAAGGCCCTAGGGTTGTAAAGCTCTTTTGTGCGGGAAGATA
ATGACGGTACCGCAAGAATAAGCCCCGGCTAACTTCGTGCCAGCAGCCGCGG
TAATACGAAGGGGGCTAGCGTTGCTCGGAATCCTGGGCGTAAAGGGTGCGTA
GGCGGGTCTTTAAGTCAGGGGTGAAATCCTGGAGCTCAACTCCAGAACTGCC
TTTTCGGTTAGCGCACCGTCTTCAGGTAAAACCAACTCCCATGGTGTGACGGG
NGGTGTGTACAAGGCCCGGGAACGTATTCACCGTGGCGTGCTGATCCACGAT
TACTAGCGATTCCAACTTCATGGGCTCGAGTTGCAGAGCCCAATCCGAACTG
AGACGGCTTTTTGAGATTTGCGAAGGGTCGCCCCTTAGCATCCCATTGTCACC
GCCATTGTAGCACGTGTGTAGCCCAGCCCGTAAGGGCCATGAGGACTTGACG
TCATCCCCACCTTCCTCGCGGCTTATCACCGGCAGTCTCCTTAGAGTGCTCAA
CTAAATGGTAGCAACTAAGGACGGGGGTTGCGCTCGTTGCGGGACTTAACCC
AACATCTCACGACACGAGCTGACGACAGCCATGCAGCACCTGTCTCCGGTCC
AGCCGAACTGAAGAACTCCGTCTCTGGAGTCCGCGACCGGGATGTCAAGGGC
TGGTAAGGTTCTGCGCGTTGCGTCNAATTAAACCACATGCTCCACCGCTTGT

C.4 16S rRNA sequence of isolate ES5 as queried with nBLAST

TCGAACGGCAGCGCGGGAGCAATCCTGGCGGCGAGTGGCGAACGGGTGAGT
AATACATCGGAACGTGCCCAATCGTGGGGGATAACGCAGCGAAAGCTGTGCT
AATACCGCATACGATCTACGGATGAAAGCAGGGGATCGCAAGACCTTGCGCG
AATGGAGCGGCCGATGGCAGATTAGGTAGTTGGTGAGGTAAAGGCTCACCAA
GCCTTCGATCTGTAGCTGGTCTGAGAGGACGACCAGCCACACTGGGACTGAG
ACACGGCCCAGACTCCTACGGGAGGCAGCAGTGGGGAATTTTGGACAATGGG
CGAAAGCCTGATCCAGCCATGCCGCGTGCAGGATGAAGGCCTTCGGGTTGTA
AACTGCTTTTGTACGGAACGAAACGGCCTTTTCTAATAAAGAGGGCTAATGA
CGGTACCGTAAGAATAAGCACCGGCTAACTACGTGCCAGCAGCCGCGGTAAT
ACGTAGGGTGCAAGCGTTAATCGGAATTACTGGGCGTAAAGCGTGCGCAGGC
GGTAATGTAAGACAGTTGTGAAATCCCCGGGCTCAACCTGGGAACTGCATCT
GTGACTGCATTGCTGGAGTACGGCAGAGGGGGATGGAATTCATCGCCCTCCT
TGCGGTTAAGCTAACTACTTCTGGCAGAACCCGCTCCCATGGTGTGACGGGC
GGTGTGTACAAGACCCGGGAACGTATTCACCGTGACATTCTGATCCACGATT
ACTAGCGATTCCGACTTCACGCAGTCGAGTTGCAGACTGCGATCCGGACTAC
GACTGGTTTTATGGGATTAGCTCCCCCTCGCGGGTTGGCAACCCTTTGTACCA
GCCATTGTATGACGTGTGTAGCCCCACCTATAAGGGCCATGAGGACTTGACG
TCATCCCCACCTTCCTCCGGTTTGTCACCGGCAGTCTCATTAGAGTGCCCAAC
TAAATGTAGCAACTAATGACAAGGGTTGCGCTCGTTGCGGGACTTAACCCAA
CATCTCACGACACGAGCTGACGACAGCCATGCAGCACCTGTGTTACGGTTCT
CTTTCGAGCACTAAGCCATCTCTGGCGAATTCCGTACATGTCAAAGGTGGGTA
AGGTTTTTCGCGTTGCATCGAATTAAACCACATCATCCACCGCTTGTGCGGGT
CCCCGTCAATTCCTTTGAGTTTCAACCTTGCGGCCGTACTCCCCAGGCGGTCA
ACTTCACGCGTTAGCTTCGTTACTGAGTCAGTGAAGACCCAACAAC

Table C.1 Composition of the enriched nutrient media used to grow the new isolates. For plate cultures, 15 g/L agar was added.

Media	**Recipe**
Nutrient broth (NB)	3 g/L beef extract, 5 g/L peptone
Luria bertani (LB)	10 g/L tryptone, 10 g/L NaCl, 5 g/L yeast extract
1/10 nutrient broth	0.3 g/L beef extract, 0.5 g/L peptone
Sphingobacteria	10 g/L tryptone, 5 g/L NaCl, 3 g/L yeast extract
1% tryptone	10 g/L tryptone

Trace File: E1R-1439R.ab1

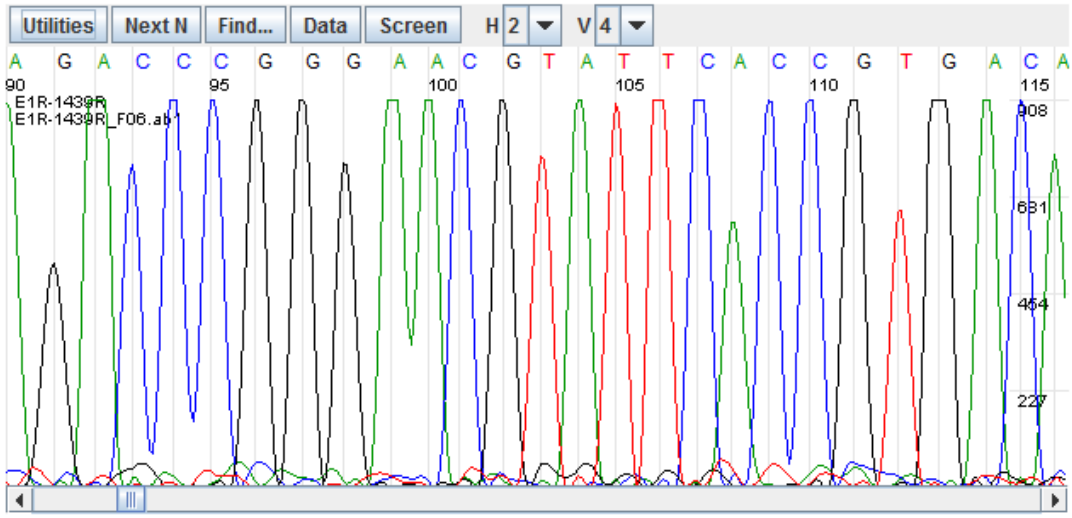

Sequence File: E1R-1439R.seq

>E1R-1439R_F06.ab1
NNNNNNNNNNNNNNNNATCGCCCTCCTTGCGGTTAAGCTAACTACTTCTGGCAGAACCCGCTCCCATGGTGTGACGGGCG
GTGTGTACAAGACCCGGGAACGTATTCACCGTGACATTCTGATCCACGATTACTAGCGATTCCGACTTCACGCAGTCGAG
TTGCAGACTGCGATCCGGACTACGACTGGTTTTATGGGATTAGCTCCCCCTCGCGGGTTGGCAACCCTTTGTACCAGCCA
TTGTATGACGTGTGTAGCCCCACCTATAAGGGCCATGAGGACTTGACGTCATCCCCACCTTCCTCCGGTTTGTCACCGGC
AGTCTCATTAGAGTGCCCAACTAAATGTAGCAACTAATGACAAGGGTTGCGCTCGTTGCGGGACTTAACCCAACATCTCA
CGACACGAGCTGACGACAGCCATGCAGCACCTGTGTTACGGTTCTCTTTCGAGCACTAAGCCATCTCTGGCGAATTCCGT
ACATGTCAAAGGTGGGTAAGGTTTTTCGCGTTGCATCGAATTAAACCACATCATCCACCGCTTGTGCGGGTCCCCGTCAA
TTCCTTTGAGTTTCAACCTTGCGGCCGTACTCCCCAGGCGGTCAACTTCACGCGTTAGCTTCGTTACTGAGTCAGTGAAG
ACCCAACAACCAGTTGACATCGTTTAGGGCGTGGACTACCAGGGTATCTAATCCTGTTTGCTCCCCACGCTTTCGTGCAT
GAGCGTCAGTACAGGCCCAGGGGATTGCCTTCGCCATCGGTGTTCCTCCGCATATCTACGCATTTCACTGCTACACGCGG
AATTCCATCCCCCTCTGCCGTACTCCAGCAATGCAGTCACAGATGCAGTTCCCAGGTTGAGCCCGGGGATTTCACAACTG
TCTTACATTACCGCCTGCGCACGCTTTACGCCCAGTAATTCCGANNACGCTTGCACCCTACGTATTACCGCNGCTGCTGG
CACGTAGTTAGCCGGNGNTTATTCTTACGGTACCGTCATTANCCNNCNTTNNTANAAAANGNCCGTTTCNTTCCGNANNN
AAAANCNNN

Figure C.1 Representative chromatogram of the sequenced 16S rRNA from isolate ES5 amplified by PCR with reverse primer 1489R. DNA was sequenced by Genewiz, and the sequences for isolate ES5 were truncated at 650 base pairs due to the poor quality of data above this number.

.

Trace File: IF-8F.ab1

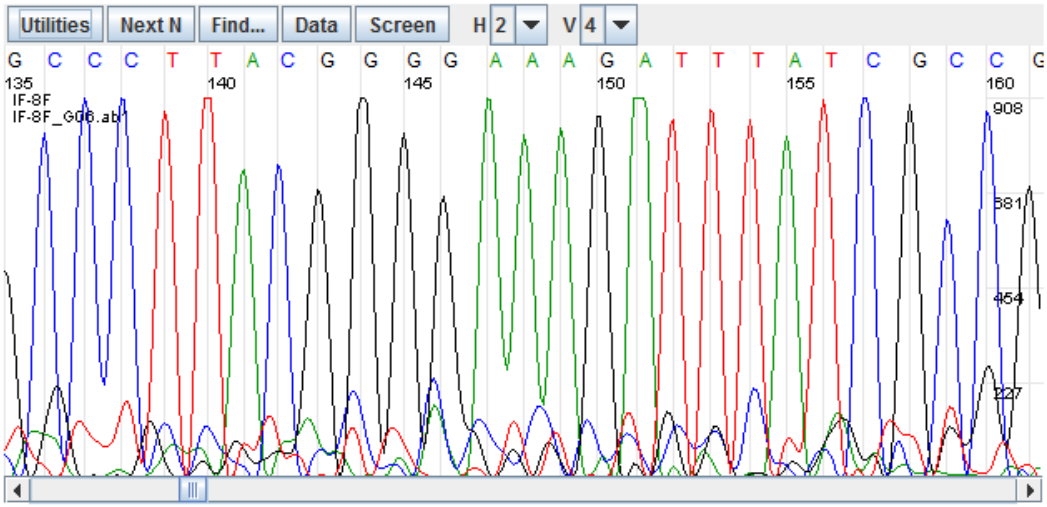

Sequence File: IF-8F.seq

```
>IF-8F_G06.ab1
NNNNNNNNNNNNNNNNNNNNNANNNNNNANTCGAGCGGGCATAGCAATATGTCNNCGGCAGACGGGTGAGTAACGCNNNNN
NNNNNNNCTTTTGGTTCGGAACAACACAGGGAAACTTGTGCTAATACCGGATAAGCCCTTACGGGGAAAGATTTATCGCC
GAAAGATCGGCCCGCGTCTGATTAGCTAGTTGGTGAGGTAATGGCTCACCAAGGCGACGATCAGTAGCTGGTCTGAGAGG
ATGATCAGCCACATTGGGACTGAGACACGGCCCAAACTCCTACGGGAGGCAGCAGTGGGGAATATTGGACAATGGGCGCA
AGCCTGATCCAGCCATGCCGCGTGAGTGATGAAGGCCCTAGGGTTGTAAAGCTCTTTTGTGCGGGAAGATAATGACGGTA
CCGCAAGAATAAGCCCCGGCTAACTTCGTGCCAGCAGCCGCGGTAATACGAAGGGGGCTAGCGTTGCTCGGAATCACTGG
GCGTAAAGGGTGCGTAGGCGGGTCTTTAAGTCAGGGGTGAAATCCTGGAGCTCAACTCCAGAACTGCCTTTGATACTGAA
GATCTTGAGTTCGGGAGAGGTGAGTGGAACTGCGAGTGTAGAGGTGNNTTCGNAGATATTCGCANNAACACCAGTGGCGA
NNGNGGCTCACTGGCCCCGATACTGACGCTGAGGCACGAAAGCNTGGGGGAGCAAATAGGATTAGNNCCCTGGTGTCCAC
GCCGCAAACGATGAATGCAGCCGTTNANGGNTTACTCNCTANTGGNGCACCTNANNCTNANNNTTTCCGCCCTNGGGNGA
TAGNNCTAAGNTNNNAATTTANNGGNNATGACGGGNNNCCCCCCNTCCGGTGGANACATGTTNNTTTAAATTCAACCTN
```

Figure C.2 Representative chromatogram of the sequenced 16S rRNA from isolate IS2 amplified by PCR with forward primer 8F. DNA was sequenced by Genewiz, and the sequences for isolate IS2 were truncated at 550 base pairs due to the poor quality of data above this number.

Trace File: IR-1439R.ab1

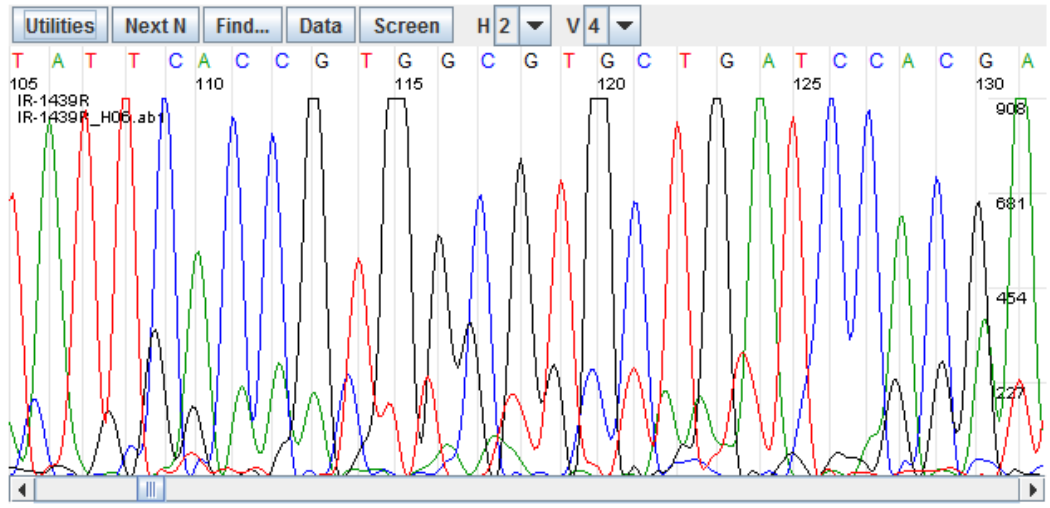

Sequence File: IR-1439R.seq

```
>IR-1439R_H06.ab1
NNNNNNNNNNNNNNNNNNNNGGNTGCCNNTTCGGTTAGCGCACCGTCTTCAGGTAAAACCAACTCCCATGGTGTGACGGG
NGGTGTGTACAAGGCCCGGGAACGTATTCACCGTGGCGTGCTGATCCACGATTACTAGCGATTCCAACTTCATGGGCTCG
AGTTGCAGAGCCCAATCCGAACTGAGACGGCTTTTTGAGATTTGCGAAGGGTCGCCCCTTAGCATCCCATTGTCACCGCC
ATTGTAGCACGTGTGTAGCCCAGCCCGTAAGGGCCATGAGGACTTGACGTCATCCCCACCTTCCTCGCGGCTTATCACCG
GCAGTCTCCTTAGAGTGCTCAACTAAATGGTAGCAACTAAGGACGGGGGTTGCGCTCGTTGCGGGACTTAACCCAACATC
TCACGACACGAGCTGACGACAGCCATGCAGCACCTGTCTCCGGTCCAGCCGAACTGAAGAACTCCGTCTCTGGAGTCCGC
GACCGGGATGTCAAGGGCTGGTAAGGTTCTGCGCGTTGCGTCNAATTAAACCACATGCTCCACCGCTTGTGCGGGCCCCC
GTCAATTCCTTTGAGTTTTAATCTTGCGACCGTACTCCCCAGGCGGAATGCTTAAAGCGTTAGCTGCGCCACTAGTGAGT
AAACCCACTAACGGCTGGCATTCATCGTTTACGGCGTGNACTACCAGGNTATCTAATCCTGTTTGCTCCCCACGCTTTCG
TGCCTCAGCGTCAGTATCGGGCCAGTGAGCCGCCTTCGCCACTGNTGTTCTTGCNAATATCTACGAATTTCACCTCTACA
CTCGCAGTTCCACTCACCTCTCCNNAANTCAAGATCTTCAGTATCAAAGGCAGTTCTGGAGTTGAGCTNNNNGATTTCAC
NCCTGANNNNAANACCCGCCTANGCNNNNTTTACGCCNANNGNTTNNNANCNACGNCTAGCCCNNNTNGTANTACNNNNG
NTGCNGGCNNNAANNTTANNCNGGGGNTTNNTNNNNNNNN
```

Figure C.3 Representative chromatogram of the sequenced 16S rRNA from isolate IS2 amplified by PCR with reverse primer 1489R. DNA was sequenced by Genewiz, and the sequences for isolate IS2 were truncated at 550 base pairs due to the poor quality of data above this number.

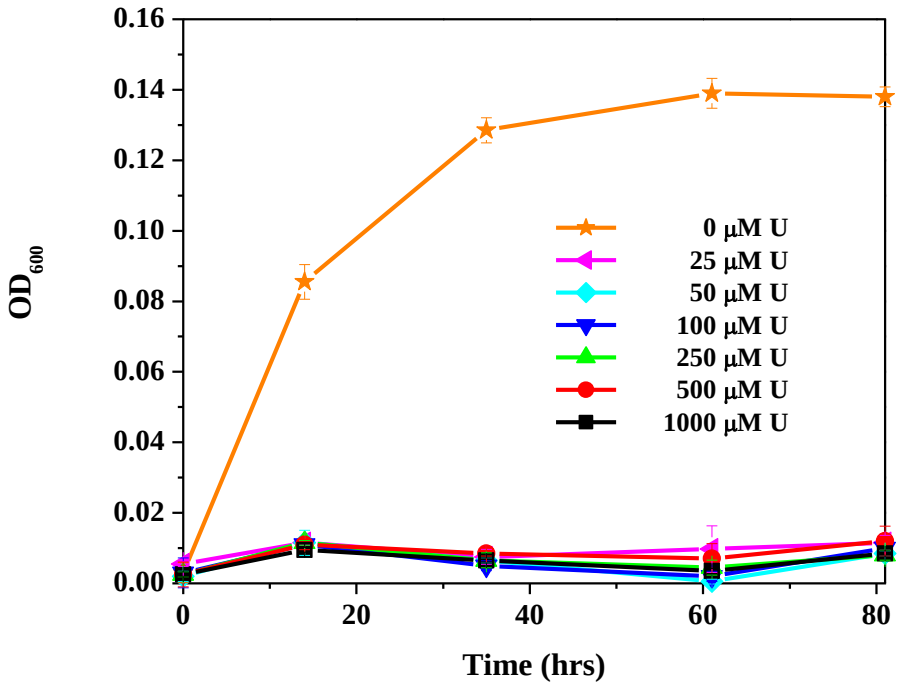

Figure C.4 Growth curve of *Variovorax* sp. exposed to increasing concentrations of UO_2^{2+} for 4 hours at pH 5.5 in aerobic artificial groundwater amended with 3 mM lactate. Growth was measured by absorbance at 600 nm (OD_{600}). No phosphate source was added to these incubations. Error bars represent the variation between triplicate incubations and the analytical error on duplicate measurements.

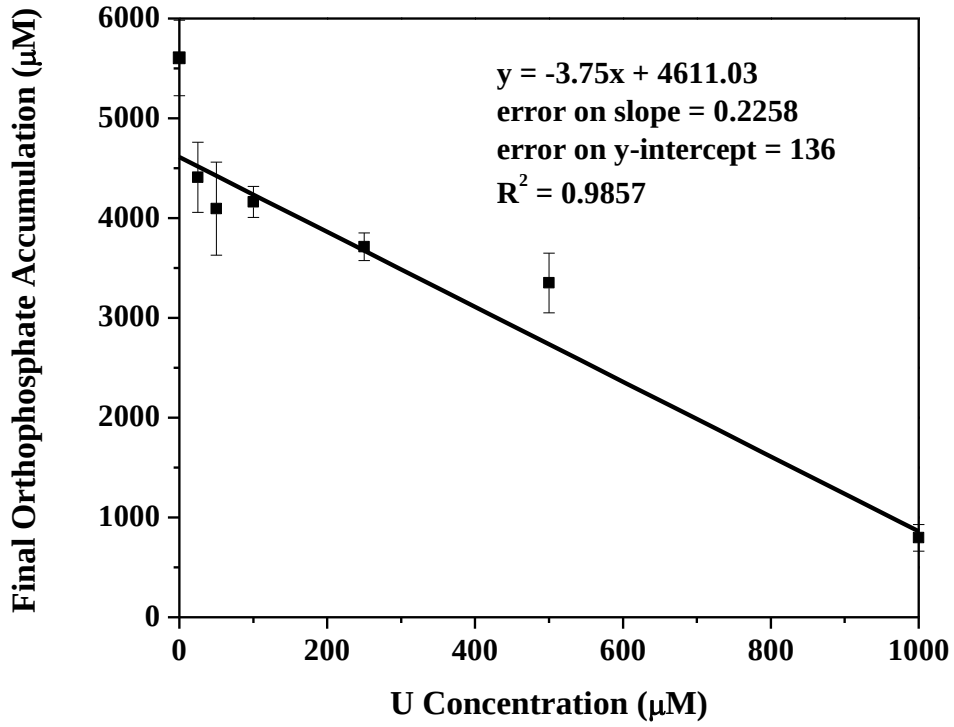

Figure C.5 Dissolved orthophosphate concentration produced from phytate hydrolysis by *Variovorax* sp. after 2 weeks of incubation as a function of the uranium concentrations used to shock the cells. The linear fit (black line) does not include cells unexposed to uranium. Error bars represent the variation between triplicate incubations and the analytical error on duplicate measurements.

APPENDIX D

SUPPLEMENTAL INFORMATION FOR CHAPTER X

D.1 Matlab™ code RungeKutta.m

```
clear
global constant

% Solving for pure culture incubations without uranium

% Constants

Y = 10^-5;          % Growth yield coefficient
Rprimemax = 10^3;   % Rate constant for lactate consumption
Km1 = 10^2.5;       % lactate consumption and cell growth

Rmax6 = 10^1.62;    % IP6 consumption
Km6 = 10^0;         % IP6 consumption

Rmax5 = 10^2.2;     % IP5 degradation
Km5 = 10^0;         % IP5 degradation

Rmax4 = 10^2.5;     % IP4 degradation
Km4 = 10^3;         % IP4 degradation


Rmax3 = 10^3;       % IP3 degradation
Km3 = 10^2;         % IP3 degradation


Rmax2 = 10^4.2;     % IP2 degradation
Km2 = 10^1.6;       % IP2 degradation


K1 = 10^0.55;       % IP2 reforming from IP1

Kb = 10^1;          % Biomass consumption of PO4


% Initial Concentrations

Xi = 0.005;         % Initial OD600
Laci = 2223.071;    % Initial Lactate concentration
```

```
IP6i = 987;          % Initial IP6 Concentration
IP5i = 0;            % Initial IP5 Concentration
IP4i = 0;            % Initial IP4 concentration
IP3i = 0;            % Initial IP3 concentration
IP2i = 0;            % Initial IP2 concentration
PO4i = 347;          % Initial PO4 concentration
IP1i = 0;

constant = [Y; Rprimemax; Km1; Rmax6; Km6; Rmax5; Km5; Rmax4; Km4; Rmax3;
   Km3; Rmax2; Km2; K1; Kb];

% y0 is vector of initial concentrations

y0(1) = Xi;
y0(2) = Laci;
y0(3) = IP6i;
y0(4) = IP5i;
y0(5) = IP4i;
y0(6) = IP3i;
y0(7) = IP2i;
y0(8) = PO4i;
y0(9) = IP1i;


dt = 1;
t = [0:dt:304]';
tspan = [0, max(t)];


[T, y] = ode45('RK4odes1', tspan, y0);

% IP1 by mass balance

a = y(:,3)+y(:,4)+y(:,5)+y(:,6)+y(:,7);

IP1 = y(:,3) + y(:,4) + y(:,5) + y(:,6)+ y(:,7);

% Pure Culture Data


TdataBio = [0, 14, 35, 61, 81, 108, 136];
Xdata = [0.005, 0.153, 0.165, 0.192, 0.213, 0.2, 0.17];
Tdata = [0, 14, 35, 61, 81, 108, 136, 163, 187, 205, 232, 256, 276];
LacData = [2223, 1097, 160, 0, 0, 0, 0, 0, 0, 0, 0, 0, 0];
IP6Data = [986, 992, 942, 949, 527, 315, 53, 0, 0, 0, 0, 0, 0];
IP5Data = [0, 19, 40, 244, 270, 160, 6, 1.2, 0, 0, 0, 0, 0];
```

```
IP4Data = [0, 0, 74, 94, 227, 508, 833, 991, 787, 17, 0, 0, 0];
IP3Data = [0, 0, 0, 0, 20, 0, 45, 136, 427, 911, 9, 0, 0];
IP2Data = [0, 0, 0, 0, 0, 4, 5, 30, 70, 181, 179, 176, 147];
TPData = [0, 14, 35, 61, 81, 108, 136, 163, 187, 205, 232, 256, 276, 304];
PO4Data = [347, 320, 349, 438, 611, 1122, 1746, 2683, 3419, 4007, 5466, 5767, 5675,
5604];

% Plot model data vs. pure culture data

subplot(5,2,1)
plot(T, y(:,1), 'b-', TdataBio, Xdata, 'ko')
xlabel('Time(hrs)')
ylabel('Biomass')

subplot(5,2,2)
plot(T,y(:,2), 'b-', Tdata, LacData, 'ko')
xlabel('Time(hrs)')
ylabel('Lactate')

TIP6 = T + 30;

subplot(5,2,3)
plot(TIP6,y(:,3), 'b-', Tdata, IP6Data, 'ko')
xlabel('Time(hrs)')
ylabel('IP6')

TIP5 = T + 30;

subplot(5,2,4)
plot(TIP6,y(:,4), 'b-', Tdata, IP5Data, 'ko')
xlabel('Time(hrs)')
ylabel('IP5')


subplot(5,2,5)
plot(TIP6,y(:,5), 'b-', Tdata, IP4Data, 'ko')
xlabel('Time(hrs)')
ylabel('IP4')


subplot(5,2,6)
plot(TIP6,y(:,6), 'b-', Tdata, IP3Data, 'ko')
xlabel('Time(hrs)')
ylabel('IP3')

subplot(5,2,7)
```

```
plot(TIP6,y(:,3), 'b-', T, y(:,4), 'g-', T, y(:,5), 'r-', T,y(:,6),'m-' , T, y(:, 7), 'k-', T, a(:,1), 'r-')
xlabel('Time(hrs)')
ylabel('IP3')

subplot(5,2,8)
plot(TIP6,y(:,7), 'b-', Tdata, IP2Data, 'ko')
xlabel('Time(hrs)')
ylabel('IP2')

subplot(5,2,9)
plot(TIP6,y(:,8), 'b-', TPData, PO4Data, 'ko')
xlabel('Time(hrs)')
ylabel('PO4')

subplot(5,2,10)
plot(TIP6,y(:,9), 'b-')
xlabel('Time(hrs)')
ylabel('IP1')

% Write the data and time to text files with user input for filenames

timefile = input('Please enter desired time file name:  ');
datafile = input('Please enter desired data file name:  ');


dlmwrite(timefile,T)
dlmwrite(datafile,y)
```

D.2 Matlab Code RK4Odes1.m

```
function RK4odes1 = RK4odes1(T,y)

global constant

Y = constant(1);
Rprimemax = constant(2);
Km1 = constant(3);
Rmax6 = constant(4);
Km6 = constant(5);
Rmax5 = constant(6);
Km5 = constant(7);
Rmax4 = constant(8);
Km4 = constant(9);
Rmax3 = constant(10);
Km3 = constant(11);
Rmax2 = constant(12);
Km2 = constant(13);
K1 = constant(14);
Kb = constant(15);


 % Biomass

RK4odes1(1,1) = Y*(Rprimemax*y(2))/(Km1+y(2));

% Lactate

RK4odes1(2,1) = -Rprimemax*y(2)*y(1)/(Km1+y(2));

% IP6

RK4odes1(3,1) = -y(1)*Rmax6*y(3)/(Km6 + y(3));

% IP5

RK4odes1(4,1) = y(1)*Rmax6*y(3)/(Km6 + y(3)) - y(1)*(Rmax5*y(4)/(Km5* (1 +
((y(3))/Km6))+ y(4)));

% IP4

RK4odes1(5,1) = y(1)*(Rmax5*y(4)/(Km5*(1 + ((y(3))/Km6))+ y(4))) -
y(1)*(Rmax4*y(5)/(Km4*(1+(((y(3)/Km6) + (y(4)/Km5)))) + y(5)));

% IP3
```

```
RK4odes1(6,1) = y(1)*(Rmax4*y(5)/(Km4*(1+(((y(3)/Km6) + (y(4)/Km5)))) + y(5)))-
y(1)*(Rmax3*y(6)/(Km3*(1+(((y(3)/Km6)+(y(4)/Km5)+(y(5)/Km4)))) + y(6)));

% IP2

RK4odes1(7,1) =  (1)*(Rmax3*y(6)/(Km3*(1+(((y(3)/Km6)+(y(4)/Km5)+(y(5)/Km4))))
+ y(6)))  -y(1)*(Rmax2*y(7)/(Km2*(1+(((y(3)/Km6)+(y(4)/Km5) +(y(5)/Km4) +(y(6)/
Km3)))) +y(7))) + K1*y(9) ;

% PO4

RK4odes1(8,1) =  y(1)*Rmax6*y(3)/(Km6 + y(3)) +  y(1)*(Rmax5*y(4)/(Km5*(1 +
((y(3))/Km6))+ y(4))) + y(1)*(Rmax4*y(5)/(Km4*(1+(((y(3)/Km6) + (y(4)/Km5)))) +
y(5)))+ y(1)*(Rmax3*y(6)/(Km3*(1+(((y(3)/Km6)+(y(4)/Km5)+(y(5)/Km4)))) + y(6)))
+  y(1)*(Rmax2*y(7)/(Km2*(1+(((y(3)/Km6)+(y(4)/Km5)+(y(5)/Km4)+(y(6)/Km3)))) +
y(7)))- K1*y(9);

% IP1

RK4odes1(9,1) = -K1*y(9) + y(1)*(Rmax2*y(7)/(Km2*(1 +(((y(3)/Km6)+ (y(4)/Km5)+
(y(5)/Km4)+(y(6)/Km3)))) + y(7)));
```

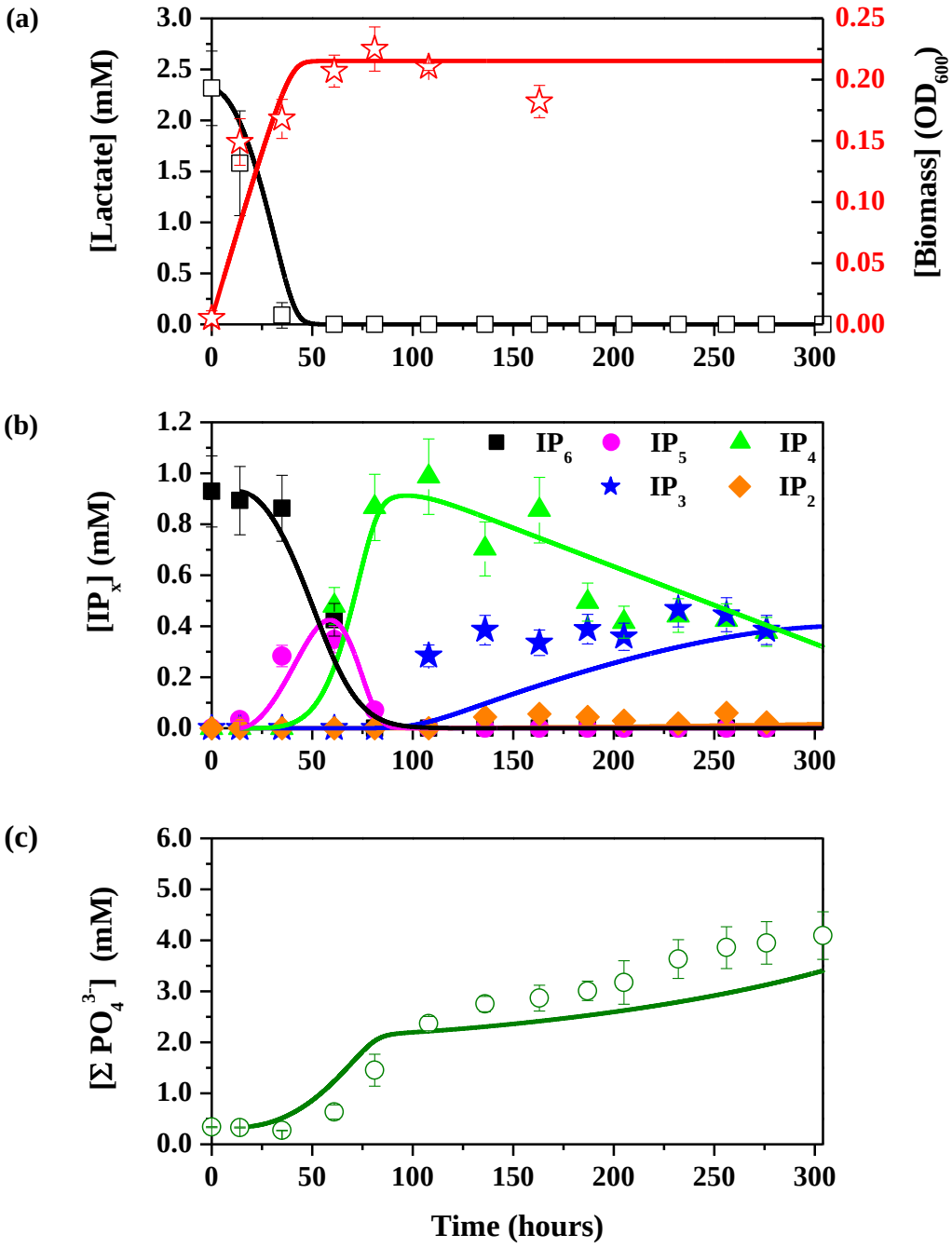

Figure D.1 Comparison of experimental (symbols) and modeled (solid lines) concentrations or (a) lactate (black), (a) biomass (red), (b) inositol phosphate species (IP_x with x = 6 (back), 5 (magenta), 4 (green), 3 (blue), 2 (orange)), and (c) inorganic phosphate (green) as a function of time obtained in aerobic incubations of *Variovorax* sp. in pH 5.5 artificial groundwater amended with 3 mM lactate, 1 mM inositol hexaphosphate (IP_6), and 50 µM uranium.

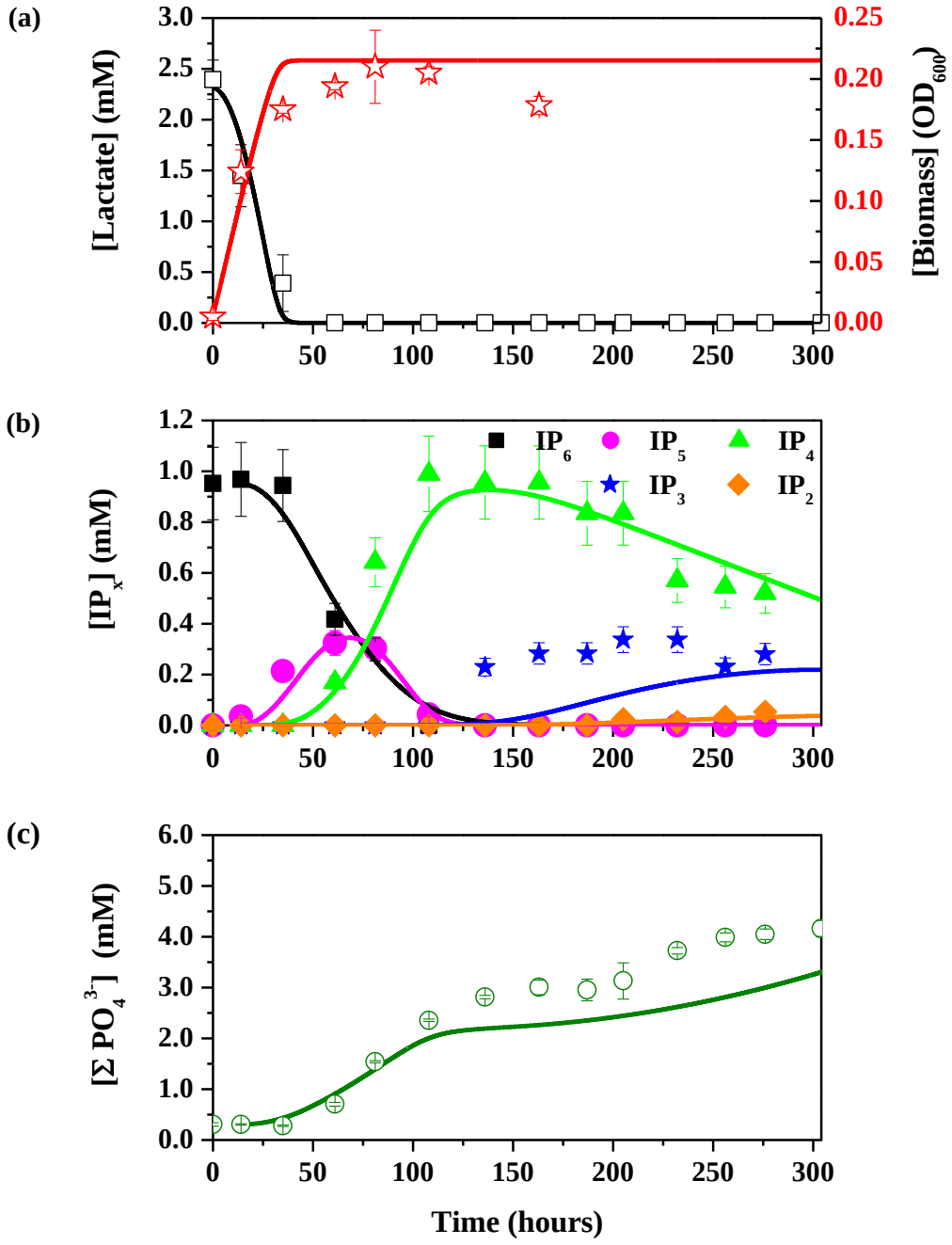

Figure D.2 Comparison of experimental (symbols) and modeled (solid lines) concentrations or (a) lactate (black), (a) biomass (red), (b) inositol phosphate species (IP_x with x = 6 (back), 5 (magenta), 4 (green), 3 (blue), 2 (orange)), and (c) inorganic phosphate (green) as a function of time obtained in aerobic incubations of *Variovorax* sp. in pH 5.5 artificial groundwater amended with 3 mM lactate, 1 mM inositol hexaphosphate (IP_6), and 100 µM uranium.

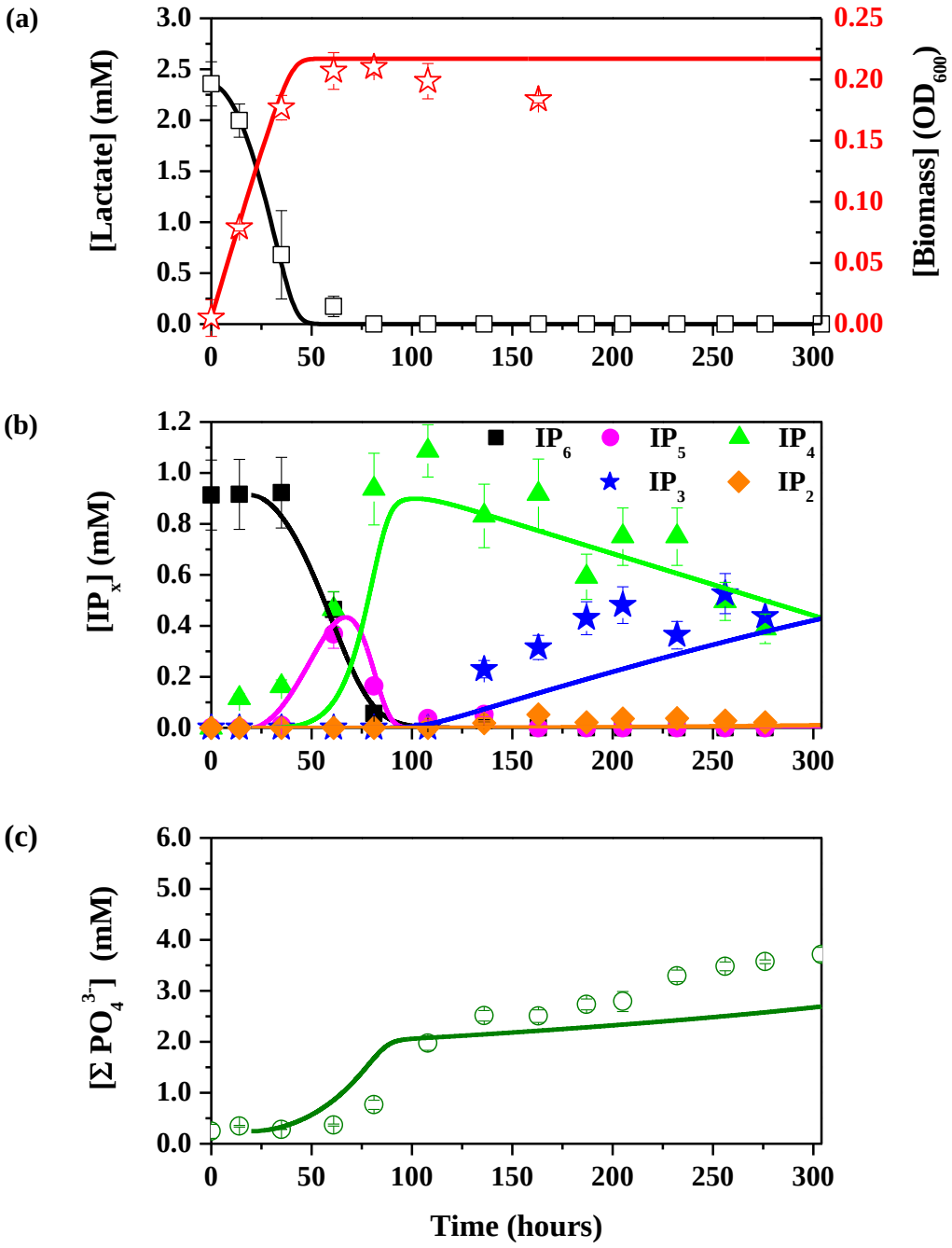

Figure D.3 Comparison of experimental (symbols) and modeled (solid lines) concentrations or (a) lactate (black), (a) biomass (red), (b) inositol phosphate species (IP_x with x = 6 (back), 5 (magenta), 4 (green), 3 (blue), 2 (orange)), and (c) inorganic phosphate (green) as a function of time obtained in aerobic incubations of *Variovorax* sp. in pH 5.5 artificial groundwater amended with 3 mM lactate, 1 mM inositol hexaphosphate (IP_6), and 250 µM uranium.

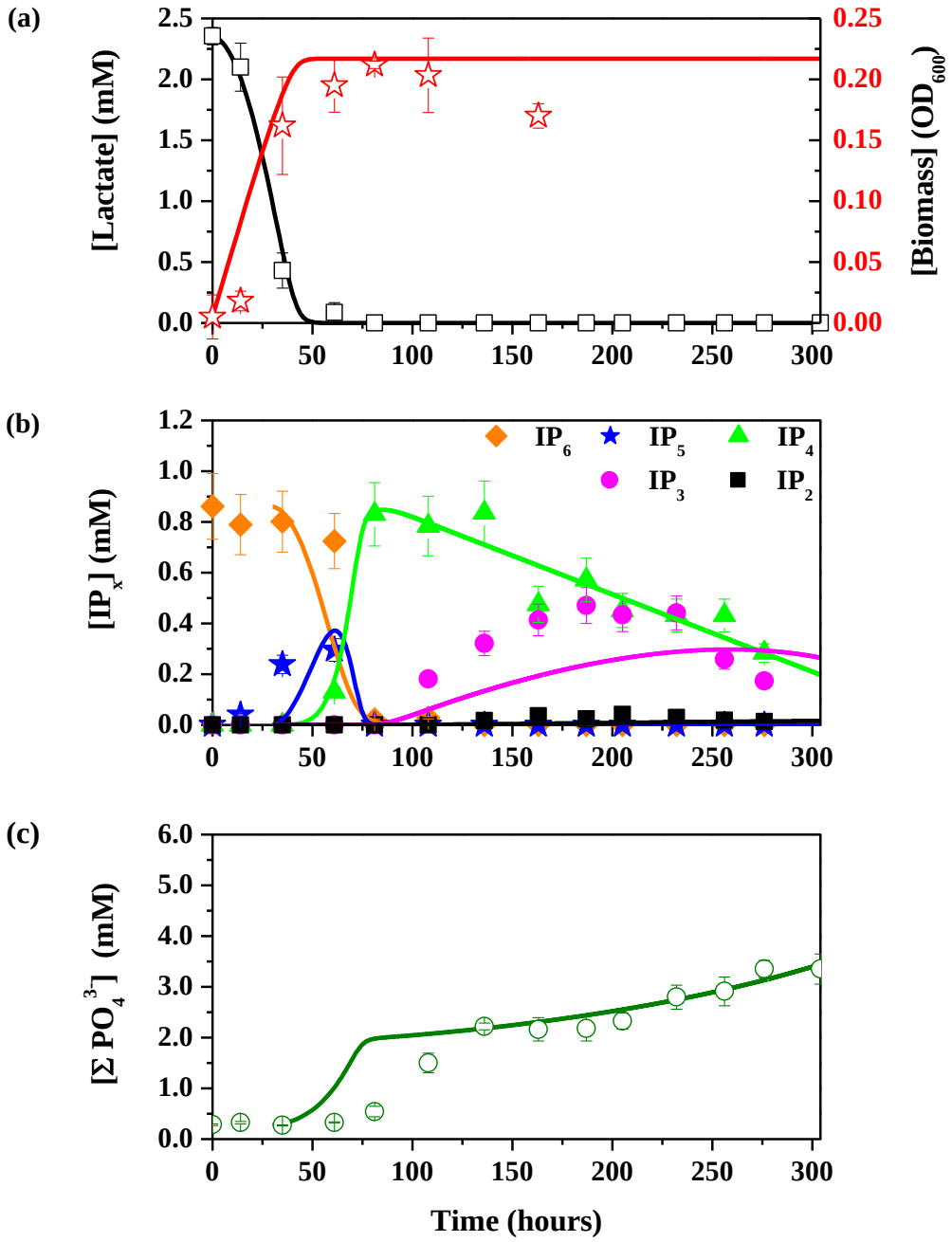

Figure D.4 Comparison of experimental (symbols) and modeled (solid lines) concentrations or (a) lactate (black), (a) biomass (red), (b) inositol phosphate species (IP_x with x = 6 (back), 5 (magenta), 4 (green), 3 (blue), 2 (orange)), and (c) inorganic phosphate (green) as a function of time obtained in aerobic incubations of *Variovorax* sp. in pH 5.5 artificial groundwater amended with 3 mM lactate, 1 mM inositol hexaphosphate (IP_6), and 500 µM uranium.

REFERNCES

Abebe, Y., Bogale, A., Hambidge, K.M., Stoecker, B.J., Bailey, K., Gibson, R.S., 2007. Phytate, zinc, iron and calcium content of selected raw and prepared foods consumed in rural Sidama, Southern Ethiopia, and implications for bioavailability. Journal of Food Composition and Analysis 20, 161-168.

Adcock, P.W., Saint, C.P., 2001. Rapid confirmation of Clostridium perfringens by using chromogenic and fluorogenic substrates. Applied and Environmental Microbiology 67, 4382-4384.

Akob, D.M., Mills, H.J., Gihring, T.M., Kerkhof, L., Stucki, J.W., Anastacio, A.S., Chin, K.J., Kusel, K., Palumbo, A.V., Watson, D.B., Kostka, J.E., 2008. Functional diversity and electron donor dependence of microbial populations capable of U(VI) reduction in radionuclide-contaminated subsurface sediments. Applied and Environmental Microbiology 74, 3159-3170.

Akob, D.M., Mills, H.J., Kostka, J.E., 2007. Metabolically active microbial communities in uranium-contaminated subsurface sediments. Fems Microbiology Ecology 59, 95-107.

Allen, P.G., Shuh, D.K., Bucher, J.J., Edelstein, N.M., Palmer, C.E.A., Silva, R.J., Nguyen, S.N., Marquez, L.N., Hudson, E.A., 1996. Determinations of uranium structures by EXAFS: Schoepite and other U(VI) oxide precipitates. Radiochimica Acta 75, 47-53.

Altschul, S.F., Madden, T.L., Schaffer, A.A., Zhang, J.H., Zhang, Z., Miller, W., Lipman, D.J., 1997. Gapped BLAST and PSI-BLAST: a new generation of protein database search programs. Nucleic Acids Research 25, 3389-3402.

Anderson, G., Malcolm, R.E., 1974. Nature of alkali-soluble soil organic phosphates. Journal of Soil Science 25, 282-297.

Ankudinov, A.L., Ravel, B., Rehr, J.J., Conradson, S.D., 1998. Real-space multiple-scattering calculation and interpretation of x-ray-absorption near-edge structure. Physical Review B 58, 7565.

Appelo, C.A.J., Van der Weiden, M.J.J., Tournassat, C., Charlet, L., 2002. Surface complexation of ferrous iron and carbonate on ferrihydrite and the mobilization of arsenic. Environmental Science & Technology 36, 3096-3103.

Arai, Y., Marcus, M.K., Tamura, N., Davis, J.A., Zachara, J.M., 2007. Spectroscopic evidence for uranium bearing precipitates in vadose zone sediments at the Hanford 300-area site. Environmental Science & Technology 41, 4633-4639.

Bak, W.a., 1992. Gram-negative mesophilic sulfate-reducing bacteria, in: A. Balows, H.G.T., M. Dworkin, W. Harder, and K.-H. Schleifer (Ed.), The Prokaryotes, 2 ed. Springer, New York, pp. 3352-3378.

Bargar, J.R., Reitmeyer, R., Lenhart, J.J., Davis, J.A., 2000. Characterization of U(VI)-carbonato ternary complexes on hematite: EXAFS and electrophoretic mobility measurements. Geochimica Et Cosmochimica Acta 64, 2737-2749.

Barkay, T., Miller, S.M., Summers, A.O., 2003. Bacterial mercury resistance from atoms to ecosystems. Fems Microbiology Reviews 27, 355-384.

Barnett, M.O., Jardine, P.M., Brooks, S.C., 2002. U(VI) adsorption to heterogeneous subsurface media: Application of a surface complexation model. Environmental Science & Technology 36, 937-942.

Barnett, M.O., Jardine, P.M., Brooks, S.C., Selim, H.M., 2000. Adsorption and transport of uranium(VI) in subsurface media. Soil Science Society of America Journal 64, 908-917.

Beazley, M.J., Martinez, R.J., Sobecky, P.A., Webb, S.M., Taillefert, M., 2007. Uranium biomineralization as a result of bacterial phosphatase activity: Insights from bacterial isolates from a contaminated subsurface. Environmental Science & Technology 41, 5701-5707.

Beazley, M.J., Martinez, R.J., Sobecky, P.A., Webb, S.M., Taillefert, M., 2009. Nonreductive Biomineralization of Uranium(VI) Phosphate Via Microbial Phosphatase Activity in Anaerobic Conditions. Geomicrobiology Journal 26, 431-441.

Beazley, M.J., Martinez, R.J., Webb, S.M., Sobecky, P.A., Taillefert, M., 2011. The effect of pH and natural microbial phosphatase activity on the speciation of uranium in subsurface soils. Geochimica Et Cosmochimica Acta 75, 5648-5663.

Becerra, C.A., Lopez-Luna, E.L., Ergas, S.J., Nuesslein, K., 2009. Microcosm-based Study of the Attenuation of an Acid Mine Drainage-Impacted Site through Biological Sulfate and Iron Reduction. Geomicrobiology Journal 26, 9-20.

Behrends, T., Van Cappellen, P., 2005. Competition between enzymatic and abiotic reduction of uranium(VI) under iron reducing conditions. Chemical Geology 220, 315-327.

Belimov, A.A., Safronova, V.I., Sergeyeva, T.A., Egorova, T.N., Matveyeva, V.A., Tsyganov, V.E., Borisov, A.Y., Tikhonovich, I.A., Kluge, C., Preisfeld, A., Dietz, K.J., Stepanok, V.V., 2001. Characterization of plant growth promoting rhizobacteria isolated from polluted soils and containing 1-aminocyclopropane-1-carboxylate deaminase. Canadian Journal of Microbiology 47, 642-652.

Beller, H.R., 2005. Anaerobic, nitrate-dependent oxidation of U(IV) oxide minerals by the chemolithoautotrophic bacterium Thiobacillus denitrificans. Applied and Environmental Microbiology 71, 2170-2174.

Bencheikh-Latmani, R., Leckie, J.O., 2003. Association of uranyl with the cell wall of Pseudomonas fluorescens inhibits metabolism. Geochimica Et Cosmochimica Acta 67, 4057-4066.

Berg, A.S., Joern, B.C., 2006. Sorption dynamics of organic and inorganic phosphorus compounds in soil. Journal of Environmental Quality 35, 1855-1862.

Bernier-Latmani, R., Veeramani, H., Vecchia, E.D., Junier, P., Lezama-Pacheco, J.S., Suvorova, E.I., Sharp, J.O., Wigginton, N.S., Bargar, J.R., 2010. Non-uraninite Products of Microbial U(VI) Reduction. Environmental Science & Technology 44, 9456-9462.

Beyenal, H., Sani, R.K., Peyton, B.M., Dohnalkova, A.C., Amonette, J.E., Lewandowski, Z., 2004. Uranium immobilization by sulfate-reducing biofilms. Environmental Science & Technology 38, 2067-2074.

Blakeney, M.D., Moulaei, T., DiChristina, T.J., 2000. Fe(III) reduction activity and cytochrome content of Shewanella putrefaciens grown on ten compounds as sole terminal electron acceptor. Microbiological Research 155, 87-94.

Bollag, J.M., Henninger, N.M., 1978. Effects of nitrite toxicity on soil bacteria under aerobic and anaerobic conditions. Soil Biology & Biochemistry 10, 377-381.

Borch, T., Masue, Y., Kukkadapu, R.K., Fendorf, S., 2007. Phosphate imposed limitations on biological reduction and alteration of ferrihydrite. Environmental Science & Technology 41, 166-172.

Borie, F., Zunino, H., Martinez, L., 1989. Macromolecule-P-associations and inositol phosphates in some Chilean volcanic soils of temperate regions. Communications in Soil Science and Plant Analysis 20, 1881-1894.

Bowman, B.T., Thomas, R.L., Elrick, D.E., 1967. Movement of phytic acid in soil cores. Soil Science Society of America Proceedings 31, 477-&.

Boyanov, M.I., Fletcher, K.E., Kwon, M.J., Rui, X., O'Loughlin, E.J., Loeffler, F.E., Kemner, K.M., 2011. Solution and Microbial Controls on the Formation of Reduced U(IV) Species. Environmental Science & Technology 45, 8336-8344.

Brooks, S.C., 2001. Waste Characteristics of the Former S-3 Ponds and Outline of Uranium Chemistry Relevant to NABIR Field Research Center Studies. NABIR FRC.

Brooks, S.C., Fredrickson, J.K., Carroll, S.L., Kennedy, D.W., Zachara, J.M., Plymale, A.E., Kelly, S.D., Kemner, K.M., Fendorf, S., 2003. Inhihition of bacterial U(VI) reduction by calcium. Environmental Science & Technology 37, 1850-1858.

Bruno, J., Depablo, J., Duro, L., Figuerola, E., 1995. Experimental study and modeling of the U(VI)-Fe(OH)(3) surface precipitation coprecipitation equilibria. Geochimica Et Cosmochimica Acta 59, 4113-4123.

Burns, P.C., 1999. The crystal chemistry of uranium, in: Burns, P.C.a.F., R. (Ed.), Uranium: Mineralogy, Geochemistry and the Environment. Mineralogical Society of America, Washington, D.C., pp. 23-90.

Canan, C., Lisboa Cruz, F.T., Delaroza, F., Casagrande, R., Mendes Sarmento, C.P., Shimokomaki, M., Ida, E.I., 2011. Studies on the extraction and purification of phytic acid from rice bran. Journal of Food Composition and Analysis 24, 1057-1063.

Cardenas, E., Wu, W.-M., Leigh, M.B., Carley, J., Carroll, S., Gentry, T., Luo, J., Watson, D., Gu, B., Ginder-Vogel, M., Kitanidis, P.K., Jardine, P.M., Zhou, J., Criddle, C.S., Marsh, T.L., Tiedje, J.M., 2010. Significant Association between Sulfate-Reducing Bacteria and Uranium-Reducing Microbial Communities as

Revealed by a Combined Massively Parallel Sequencing-Indicator Species Approach. Appl. Environ. Microbiol. 76, 6778-6786.

Casas, I., de Pablo, J., Gimenez, J., Torrero, M.E., Bruno, J., Cera, E., Finch, R.J., Ewing, R.C., 1998. The role of pe, pH, and carbonate on the solubility of UO_2 and uraninite under nominally reducing conditions. Geochimica Et Cosmochimica Acta 62, 2223-2231.

Catalano, J.G., Brown, G.E., 2004. Analysis of uranyl-bearing phases by EXAFS spectroscopy: Interferences, multiple scattering, accuracy of structural parameters, and spectral differences. American Mineralogist 89, 1004-1021.

Catalano, J.G., McKinley, J.P., Zachara, J.M., Heald, S.M., Smith, S.C., Brown, G.E., 2006. Changes in uranium speciation through a depth sequence of contaminated Hanford sediments. Environmental Science & Technology 40, 2517-2524.

Chakraborty, S., Favre, F., Banerjee, D., Scheinost, A.C., Mullet, M., Ehrhardt, J.-J., Brendle, J., Vidal, L., Charlet, L., 2010. U(VI) Sorption and Reduction by Fe(II) Sorbed on Montmorillonite. Environmental Science & Technology 44, 3779-3785.

Cheng, C.W., Lim, B.L., 2006. Beta-propeller phytases in the aquatic environment, Archives of Microbiology, pp. 1-13.

Cheng, T., Barnett, M.O., Roden, E.E., Zhuang, J.L., 2004. Effects of phosphate on uranium(VI) adsorption to goethite-coated sand. Environmental Science & Technology 38, 6059-6065.

Chernyaev, I.I., 1966. Complex compounds of uranium. Israel Program for Scientiic Translations, Jerusalem.

Chomczynski, P., Sacchi, N., 1987. Single-step method of RNA isolation by acid guanidinium thiocyanate phenol chloroform extraction. Analytical Biochemistry 162, 156-159.

Cosgrove, D.J., 1980. Inositol phosphates : their chemistry, biochemistry, and physiology. Elsevier Scientific Pub. Co. ;, Amsterdam ;.

Costello, A.J.R., Glonek, T., Myers, T.C., 1976. P-31 Nuclear magnetic resonance - pH titrations of myoinositol hexaphosphate. Carbohydrate Research 46, 159-171.

Cotton, F.A., Wilkinson, G., Murillo, C.A., Bochmann, M., 1999. Advanced Inorganic Chemistry. John Wiley & Sons, Inc., New York.

Czechowska, K., van der Meer, J.R., 2012. Reversible and Irreversible Pollutant-Induced Bacterial Cellular Stress Effects Measured by Ethidium Bromide Uptake and Efflux. Environmental Science & Technology 46, 1201-1208.

Davis, J.A., Kent, D.B., 1990. Surface complexation modeling in aqueous geochemistry. Reviews in Mineralogy 23, 177-260.

Dawson, G.W., Gilman, J., 2001. Land reclamation technology - expanding the geotechnical engineering envelope. Proceedings of the Institution of Civil Engineers-Geotechnical Engineering 149, 49-61.

De Pablo, J., Casas, I., Gimenez, J., Molera, M., Rovira, M., Duro, L., Bruno, J., 1999. The oxidative dissolution mechanism of uranium dioxide. I. The effect of temperature in hydrogen carbonate medium. Geochimica Et Cosmochimica Acta 63, 3097-3103.

Degroot, C.J., Golterman, H.L., 1993. On the presence of organic phosphate in some camargue sediments-evidence for the importance of phytate. Hydrobiologia 252, 117-126.

Dejonghe, W., Berteloot, E., Goris, J., Boon, N., Crul, K., Maertens, S., Hofte, M., De Vos, P., Verstraete, W., Top, E.M., 2003. Synergistic degradation of linuron by a bacterial consortium and isolation of a single linuron-degrading Variovorax strain. Applied and Environmental Microbiology 69, 1532-1541.

Dichristina, T.J., 1992. Effects of nitrate and nitrite on dissimilatory iron reduction by shewanella-putrefaciens-200. Journal of Bacteriology 174, 1891-1896.

Dideriksen, K., Stipp, S.L.S., 2003. The adsorption of glyphosate and phosphate to goethite: A molecular-scale atomic force microscopy study. Geochimica Et Cosmochimica Acta 67, 3313-3327.

DOE, 1997. Linking Legacies - Connecting the Cold War Nuclear Weapons Production Processes to Their Environmental Consequences Office of Environmental Management - The U.S. Department of Energy Washington, D.C.

Dong, W.M., Brooks, S.C., 2006. Determination of the formation constants of ternary complexes of uranyl and carbonate with alkaline earth metals (Mg2+, Ca2+, Sr2+, and Ba2+) using anion exchange method. Environmental Science & Technology 40, 4689-4695.

Edwards, L., Kusel, K., Drake, H., Kostka, J.E., 2007. Electron flow in acidic subsurface sediments co-contaminated with nitrate and uranium. Geochimica Et Cosmochimica Acta 71, 643-654.

Finch, R., Murakami, T., 1999a. Systematics and paragenesis of uranium minerals, in: Burns, P.C.a.F., R. (Ed.), Uranium: Mineralogy, Geochemistry and the Environment. Mineralogical Society of America, Washington, D.C., pp. 91-180.

Finch, R., Murakami, T., 1999b. Systematics and paragenesis of uranium minerals. Reviews in Mineralogy and Geochemistry 38, 91-179.

Finneran, K.T., Anderson, R.T., Nevin, K.P., Lovley, D.R., 2002a. Potential for Bioremediation of uranium-contaminated aquifers with microbial U(VI) reduction. Soil & Sediment Contamination 11, 339-357.

Finneran, K.T., Housewright, M.E., Lovley, D.R., 2002b. Multiple influences of nitrate on uranium solubility during bioremediation of uranium-contaminated subsurface sediments. Environmental Microbiology 4, 510-516.

Fisher, R.F., Long, S.R., 1992. Rhizobium-plant signal exchange. Nature 357, 655-660.

Fletcher, K.E., Boyanov, M.I., Thomas, S.H., Wu, Q.Z., Kemner, K.M., Loffler, F.E., 2010. U(VI) Reduction to Mononuclear U(IV) by Desulfitobacterium Species. Environmental Science & Technology 44, 4705-4709.

Fowle, D.A., Fein, J.B., Martin, A.M., 2000. Experimental study of uranyl adsorption onto Bacillus subtilis. Environmental Science & Technology 34, 3737-3741.

Fox, P.M., Davis, J.A., Zachara, J.M., 2006. The effect of calcium on aqueous uranium(VI) speciation and adsorption to ferrihydrite and quartz. Geochimica Et Cosmochimica Acta 70, 1379-1387.

Fredrickson, J.K., Zachara, J.M., Kennedy, D.W., Duff, M.C., Gorby, Y.A., Li, S.M.W., Krupka, K.M., 2000. Reduction of U(VI) in goethite (α-FeOOH) suspensions by a dissimilatory metal-reducing bacterium. Geochimica Et Cosmochimica Acta 64, 3085-3098.

Fredrickson, J.K., Zachara, J.M., Kennedy, D.W., Liu, C.X., Duff, M.C., Hunter, D.B., Dohnalkova, A., 2002. Influence of Mn oxides on the reduction of uranium(VI) by the metal-reducing bacterium Shewanella putrefaciens. Geochimica Et Cosmochimica Acta 66, 3247-3262.

Fu, S.J., Sun, J.Y., Qian, L.C., Li, Z.Y., 2008. Bacillus phytases: Present scenario and future perspectives. Applied Biochemistry and Biotechnology 151, 1-8.

Futamata, H., Harayama, S., Watanabe, K., 2001. Group-specific monitoring of phenol hydroxylase genes for a functional assessment of phenol-stimulated trichloroethylene bioremediation. Applied and Environmental Microbiology 67, 4671-4677.

Futamata, H., Nagano, Y., Watanabe, K., Hiraishi, A., 2005. Unique kinetic properties of phenol-degrading Variovoyax strains responsible for efficient trichloroethylene degradation in a chemostat enrichment culture. Applied and Environmental Microbiology 71, 904-911.

Ganesh, R., Robinson, K.G., Chu, L.L., Kucsmas, D., Reed, G.D., 1999. Reductive precipitation of uranium by Desulfovibrio desulfuricans: Evaluation of cocontaminant effects and selective removal. Water Research 33, 3447-3458.

Gao, W.M., Gentry, T.J., Mehlhorn, T.L., Carroll, S.L., Jardine, P.M., Zhou, J.Z., 2010. Characterization of Co(III) EDTA-Reducing Bacteria in Metal- and Radionuclide-Contaminated Groundwater. Geomicrobiology Journal 27, 93-100.

Garcia-Estepa, R.M., Guerra-Hernandez, E., Garcia-Villanova, B., 1999. Phytic acid content in milled cereal products and breads. Food Research International 32, 217-221.

Gavrilescu, M., Pavel, L.V., Cretescu, I., 2009. Characterization and remediation of soils contaminated with uranium. Journal of Hazardous Materials 163, 475-510.

Gibson, R.S., Bailey, K.B., Gibbs, M., Ferguson, E.L., 2010. A review of phytate, iron, zinc, and calcium concentrations in plant-based complementary foods used in low-income countries and implications for bioavailability. Food and Nutrition Bulletin 31, S134-S146.

Gihring, T.M., Zhang, G., Brandt, C.C., Brooks, S.C., Campbell, J.H., Carroll, S., Criddle, C.S., Green, S.J., Jardine, P., Kostka, J.E., Lowe, K., Mehlhorn, T.L., Overholt, W., Watson, D.B., Yang, Z., Wu, W.-M., Schadt, C.W., 2011. A Limited Microbial Consortium Is Responsible for Extended Bioreduction of Uranium in a Contaminated Aquifer. Applied and Environmental Microbiology 77, 5955-5965.

Gleyzes, C., Tellier, S., Astruc, M., 2002. Fractionation studies of trace elements in contaminated soils and sediments: a review of sequential extraction procedures. Trac-Trends in Analytical Chemistry 21, 451-467.

Grasshoff, K., 1983. Determination of Nitrite, in: Grasshoff, K., Ehrhardt, M., Kremling, K., Almgren, T. (Eds.), Methods of seawater analysis, 2nd, rev. and extended ed. ed. Verlag Chemie GmbH, Weinheim

Green, S.J., Prakash, O., Gihring, T.M., Akob, D.M., Jasrotia, P., Jardine, P.M., Watson, D.B., Brown, S.D., Palumbo, A.V., Kostka, J.E., 2010. Denitrifying Bacteria Isolated from Terrestrial Subsurface Sediments Exposed to Mixed-Waste Contamination. Applied and Environmental Microbiology 76, 3244-3254.

Green, S.J., Prakash, O., Jasrotia, P., Overholt, W.A., Cardenas, E., Hubbard, D., Tiedje, J.M., Watson, D.B., Schadt, C.W., Brooks, S.C., Kostka, J.E., 2012. Denitrifying Bacteria from the Genus Rhodanobacter Dominate Bacterial Communities in the Highly Contaminated Subsurface of a Nuclear Legacy Waste Site. Applied and Environmental Microbiology 78, 1039-1047.

Greene, E.A., Beatty, P.H., Fedorak, P.M., 2000. Sulfolane degradation by mixed cultures and a bacterial isolate identified as a Variovorax sp. Archives of Microbiology 174, 111-119.

Greiner, R., 2007. Phytate-Degrading Enzymes: Regulation of Synthesis in Microorganisms and Plants, in: Turner, B.L., Richardson, A.E., Mullaney, E.J.

(Eds.), Inositol phosphates: Linking Agriculture and the Environment. CAB International, pp. 78-96.

Greiner, R., Sajidan, 2008. Production of D-myo-inositol(1,2,4,5,6)pentakisphosphate using alginate-entrapped recombinant Pantoea agglomerans glucose-1-phosphatase. Brazilian Archives of Biology and Technology 51, 235-246.

Grenthe, I., Fuger, J., Konings, R.J.M., Lemire, R.J., Mueller, A.B., Nguyen-Trung, C., Wanner, H., 1992. Chemical Thermodynamics of Uranium. Nuclear Energy Agency, Paris, France.

Gu, B.H., Wu, W.M., Ginder-Vogel, M.A., Yan, H., Fields, M.W., Zhou, J., Fendorf, S., Criddle, C.S., Jardine, P.M., 2005. Bioreduction of uranium in a contaminated soil column. Environmental Science & Technology 39, 4841-4847.

Guillaumont, R., Fanghänel, T., Fuger, J., Grenthe, I., Neck, V., Palmer, D.A., Rand, M.H., 2003. Chemical Thermodynamics 5. Update on the Checmical Thermodynamics of Uranium, Neptunium, Plutonium, Americium and Technetium.

Elsevier, Amsterdam.

Guo, Z.L., Guo, F.H., Tao, Z.Y., 2006. Effects of phosphate and ionic strength upon uranium(VI) sorption onto alumina as a function of pH. Radiochimica Acta 94, 223-228.

Ha, N.C., Oh, B.C., Shin, S., Kim, H.J., Oh, T.K., Kim, Y.O., Choi, K.Y., Oh, B.H., 2000. Crystal structures of a novel, thermostable phytase in partially and fully calcium-loaded states. Nature Structural Biology 7, 147-153.

Haas, J.R., Dichristina, T.J., Wade, R., 2001. Thermodynamics of U(VI) sorption onto Shewanella putrefaciens. Chemical Geology 180, 33-54.

Han, J.I., Choi, H.K., Lee, S.W., Orwin, P.M., Kim, J., Laroe, S.L., Kim, T.G., O'Neil, J., Leadbetter, J.R., Lee, S.Y., Hur, C.G., Spain, J.C., Ovchinnikova, G., Goodwin, L., Han, C., 2011. Complete Genome Sequence of the Metabolically Versatile Plant Growth-Promoting Endophyte Variovorax paradoxus S110. Journal of Bacteriology 193, 1183-1190.

Han, R.P., Zou, W.H., Wang, Y., Zhu, L., 2007. Removal of uranium(VI) from aqueous solutions by manganese oxide coated zeolite: discussion of adsorption isotherms and pH effect. Journal of Environmental Radioactivity 93, 127-143.

Han, Y.W., 1988. Removal of phytic acid from soybean and cottonseed meals. Journal of Agricultural and Food Chemistry 36, 1181-1183.

Heinonen, J.K., Lahti, R.J., 1981. A new and convenient colorimetric determination of inorganic ortho-phosphate and its application to the assay of inorganic pyrophosphatase. Analytical Biochemistry 113, 313-317.

Herbert, R.A., 1999. Nitrogen cycling in coastal marine ecosystems. Fems Microbiology Reviews 23, 563-590.

Ho, C.H., Miller, N.H., 1986. Formation of uranium oxide sols in bicarbonate solutions Journal of Colloid and Interface Science 113, 232-240.

Hsi, C.K.D., Langmuir, D., 1985. Adsorption of uranyl onto ferric oxyhydroxides - Application of the surface complexation site-binding model. Geochimica Et Cosmochimica Acta 49, 1931-1941.

Hu, P., Brodie, E.L., Suzuki, Y., McAdams, H.H., Andersen, G.L., 2005. Whole-genome transcriptional analysis of heavy metal stresses in Caulobacter crescentus. Journal of Bacteriology 187, 8437-8449.

Huang, F.Y.C., Brady, P.V., Lindgren, E.R., Guerra, P., 1998. Biodegradation of uranium-citrate complexes: Implications for extraction of uranium from soils. Environmental Science & Technology 32, 379-382.

Huang, H.Q., Shao, N., Wang, Y.R., Luo, H.Y., Yang, P.L., Zhou, Z.G., Zhan, Z.C., Yao, B., 2009. A novel beta-propeller phytase from Pedobacter nyackensis MJ11 CGMCC 2503 with potential as an aquatic feed additive. Applied Microbiology and Biotechnology 83, 249-259.

Hudson, E.A., Allen, P.G., Terminello, L.J., Denecke, M.A., Reich, T., 1996. Polarized x-ray-absorption spectroscopy of the uranyl ion: Comparison of experiment and theory. Physical Review B 54, 156.

Hyun, S.P., Davis, J.A., Sun, K., Hayes, K.F., 2012. Uranium(VI) Reduction by Iron(II) Monosulfide Mackinawite. Environmental Science & Technology 46, 3369-3376.

Irving, G., Cosgrove, D., 1971. Inositol Phosphate Phosphatases of Microbiological Origin. Some Properties of a Partially Purified Bacterial (Pseudomonas Sp.) Phytase. Australian Journal of Biological Sciences 24, 547-558.

Irving, G.C., Cosgrove, D.J., 1974. Inositol phosphate phosphatases of microbiological origin: Some properties of the partially purified phosphatases of *Aspergillus ficuum* NRRL 3135. Australian Journal of Biological Sciences 27, 361-368.

Istok, J.D., Senko, J.M., Krumholz, L.R., Watson, D., Bogle, M.A., Peacock, A., Chang, Y.J., White, D.C., 2004. In situ bioreduction of technetium and uranium in a nitrate-contaminated aquifer. Environmental Science & Technology 38, 468-475.

Jardine, P.M., Sanford, W.E., Gwo, J.P., Reedy, O.C., Hicks, D.S., Riggs, J.S., Bailey, W.B., 1999. Quantifying diffusive mass transfer in fractured shale bedrock. Water Resources Research 35, 2015-2030.

Jardine, P.M., Watson, D.B , Blake, D.A. , Beard, L.P., Brooks, S.C., Carley, J.M., Criddle, C.S., Doll, W.E., Fields, M.W., Fendorf, S.E., Geesey, G.G., Ginder-Vogel, M., Hubbard, S.S., Istok, J.D., Kelly, S., Kemner, K.M., Peacock A.D., Spalding, B.P., White, D.C., Wolfe, A., Wu, W., Zhou, J., 2006. Techniques for assessing the performance of in situ bioreduction and immobilization of metals and radionuclides in contaminated subsurface envionments. Technical Report; NABIR FRC.

Jeon, B.H., Dempsey, B.A., Burgos, W.D., Barnett, M.O., Roden, E.E., 2005. Chemical reduction of U(VI) by Fe(II) at the solid-water interface using natural and synthetic Fe(III) oxides. Environmental Science & Technology 39, 5642-5649.

Jeon, B.H., Kelly, S.D., Kemner, K.M., Barnett, M.O., Burgos, W.D., Dempsey, B.A., Roden, E.E., 2004. Microbial reduction of U(VI) at the solid-water interface. Environmental Science & Technology 38, 5649-5655.

Jerden, J.L., Sinha, A.K., 2003. Phosphate based immobilization of uranium in an oxidizing bedrock aquifer. Applied Geochemistry 18, 823-843.

Jiang, F., Chen, L., Belimov, A.A., Shaposhnikov, A.I., Gong, F., Meng, X., Hartung, W., Jeschke, D.W., Davies, W.J., Dodd, I.C., 2012. Multiple impacts of the plant

growth-promoting rhizobacterium Variovorax paradoxus 5C-2 on nutrient and ABA relations of Pisum sativum. Journal of Experimental Botany 63, 6421-6430.

Johnson, B.B., Quill, E., Angove, M.J., 2012. An investigation of the mode of sorption of inositol hexaphosphate to goethite. Journal of Colloid and Interface Science 367, 436-442.

Jordan, D.C., 1982. Transfer of *Rhizobium-japonicum* buchanan 1980 to *Bradyrhizobium* Gen-nov, a genus of slow-growing, root nodule bacteria from leguminous plants. International Journal of Systematic Bacteriology 32, 136-139.

Katsenovich, Y.P., Carvajal, D.A., Wellman, D.M., Lagos, L.E., 2012. Enhanced U(VI) release from autunite mineral by aerobic Arthrobacter sp in the presence of aqueous bicarbonate. Chemical Geology 308, 1-9.

Katsoyiannis, I.A., 2007. Carbonate effects and pH-dependence of uranium sorption onto bacteriogenic iron oxides: Kinetic and equilibrium studies. Journal of Hazardous Materials 139, 31-37.

Kelly, S.D., Kemner, K.M., Carley, J., Criddle, C., Jardine, P.M., Marsh, T.L., Phillips, D., Watson, D., Wu, W.M., 2008. Speciation of uranium in sediments before and after in situ biostimulation. Environmental Science & Technology 42, 1558-1564.

Kelly, S.D., Kemner, K.M., O'Loughlin, E.J., Boyanov, M.I., Watson, D.B., Jardine, P.M., Phillips, D.H., 2005. U L_3-Edge EXAFS Measuerments of Sediment Samples from Oak Ridge National Laboratory, Tennessee, U.S.A. Technical Report.

Kelly, S.D., Wu, W.-M., Yang, F., Criddle, C.S., Marsh, T.L., O'Loughlin, E.J., Ravel, B., Watson, D., Jardine, P.M., Kemner, K.M., 2009. Uranium Transformations in Static Microcosms. Environmental Science & Technology 44, 236-242.

Kerovuo, J., Lauraeus, M., Nurminen, P., Kalkkinen, N., Apajalahti, J., 1998. Isolation, characterization, molecular gene cloning, and sequencing of a novel phytase from Bacillus subtilis. Applied and Environmental Microbiology 64, 2079-2085.

Kertesz, M.A., Cook, A.M., Leisinger, T., 1994. Microbial-metabolism of sulfur-containing and phosphorus-containing xenobiotics. Fems Microbiology Reviews 15, 195-215.

Kim, O.-H., Kim, Y.-O., Shim, J.-H., Jung, Y.-S., Jung, W.-J., Choi, W.-C., Lee, H., Lee, S.-J., Kim, K.-K., Auh, J.-H., Kim, H., Kim, J.-W., Oh, T.-K., Oh, B.-C., 2010. beta-Propeller Phytase Hydrolyzes Insoluble Ca(2+)-Phytate Salts and Completely Abrogates the Ability of Phytate To Chelate Metal Ions. Biochemistry 49, 10216-10227.

Kim, Y.O., Kim, H.K., Bae, K.S., Yu, J.H., Oh, T.K., 1998. Purification and properties of a thermostable phytase from Bacillus sp. DS11. Enzyme and Microbial Technology 22, 2-7.

Klabunde, T., Strater, N., Frohlich, R., Witzel, H., Krebs, B., 1996. Mechanism of Fe(III)-Zn(II) purple acid phosphatase based on crystal structures. Journal of Molecular Biology 259, 737-748.

Knox, A.S., Brimon, R.L., Kaplan, D.I., Paller, M.H., 2008. Interactions among phosphate amendments, microbes and uranium mobility in contaminated sediments. Science of the Total Environment 395, 63-71.

Kolchev, L.A., 1978. Method for producing phytin. United States Patent. N. 4070422.

Kostka, J.E., Green, S.J., 2011. Microorganisms and processes linked to uranium reduction and immobilization, in: Stolz, J.F., Oremland, R.S. (Eds.), Microbial Metal and Metalloid Metabolism: Advances and Applications. ASM Press, Washington, D.C., pp. 117-138.

Kosztolanyi, K., Nguyen, T.C., Lhote, F., Vernet, M., 1996. Reduction of uranyl complexes and precipitation of uranium oxides by means of hydrogen sulphide gas. Magyar Kemiai Folyoirat 102, 180-187.

Kuang, R.B., Chan, K.H., Yeung, E., Lim, B.L., 2009. Molecular and Biochemical Characterization of AtPAP15, a Purple Acid Phosphatase with Phytase Activity, in Arabidopsis. Plant Physiology 151, 199-209.

Langmuir, D., 1978. Uranium solution-mineral equilibria at low-temperatures with applications to sedimentary ore-deposits. Geochimica Et Cosmochimica Acta 42, 547-569.

Langmuir, D., 1997. Aqueous Environmental Geochemistry. Prentice Hall, Upper Saddle River, New Jersey.

Lehto, J., Hou, X., 2011. Chemistry and Analysis of Radionuclides: Laboratory Techniques and Methodology. WILEY-VCH, Weinheim, Germany.

Lenczewski, M., Jardine, P., McKay, L., Layton, A., 2003. Natural attenuation of trichloroethylene in fractured shale bedrock. Journal of Contaminant Hydrology 64, 151-168.

Ler, A., Stanforth, R., 2003. Evidence for surface precipitation of phosphate on goethite. Environmental Science & Technology 37, 2694-2700.

Li, L., Stanforth, R., 2000. Distinguishing adsorption and surface precipitation of phosphate on goethite (alpha-FeOOH). Journal of Colloid and Interface Science 230, 12-21.

Liger, E., Charlet, L., Van Cappellen, P., 1999. Surface catalysis of uranium(VI) reduction by iron(II). Geochimica Et Cosmochimica Acta 63, 2939-2955.

Lim, B.L., Yeung, P., Cheng, C., Hill, J.E., 2007. Distribution and diversity of phytate-mineralizing bacteria. Isme Journal 1, 321-330.

Liu, C.X., Zachara, J.M., Fredrickson, J.K., Kennedy, D.W., Dohnalkova, A., 2002. Modeling the inhibition of the bacterial reduction of U(VI) by beta-MnO2(S)(g). Environmental Science & Technology 36, 1452-1459.

Liu, C.X., Zachara, J.M., Qafoku, O., McKinley, J.P., Heald, S.M., Wang, Z.M., 2004. Dissolution of uranyl microprecipitates in subsurface sediments at Hanford site, USA. Geochimica Et Cosmochimica Acta 68, 4519-4537.

Locock, A.J., Burns, P.C., 2003. The crystal structure of synthetic autunite, $Ca[(UO_2)(PO_4)]_2(H_2O)_{11}$. American Mineralogist 88, 240-244.

Lovley, D.R., 1993. Dissimilatory Metal Reduction. Annual Review of Microbiology 47, 263-290.

Lovley, D.R., Phillips, E.J.P., 1992a. Bioremediation of uranium contamination with enzymatic uranium reduction. Environmental Science & Technology 26, 2228-2234.

Lovley, D.R., Phillips, E.J.P., 1992b. Reduction of uranium by desulfovibrio-desulfuricans. Applied and Environmental Microbiology 58, 850-856.

Lovley, D.R., Phillips, E.J.P., Gorby, Y.A., Landa, E.R., 1991. Microbial reduction of uranium Nature 350, 413-416.

Luo, J., Weber, F.A., Cirpka, O.A., Wu, W.M., Nyman, J.L., Carley, J., Jardine, P.M., Criddle, C.S., Kitanidis, P.K., 2007a. Modeling in-situ uranium(VI) bioreduction by sulfate-reducing bacteria. Journal of Contaminant Hydrology 92, 129-148.

Luo, W., Wu, W.-M., Yan, T., Criddle, C., Jardine, P., Zhou, J., Gu, B., 2007b. Influence of bicarbonate, sulfate, and electron donors on biological reduction of uranium and microbial community composition. Applied Microbiology and Biotechnology 77, 713-721.

Macaskie, L.E., Basnakova, G., 1998. Microbially enhanced chemisorption of heavy metals: A method for the bioremediation of solutions containing long lived isotopes of neptunium and plutonium. Environmental Science & Technology 32, 184-187.

Macaskie, L.E., Bonthrone, K.M., Rouch, D.A., 1994. Phosphatase-mediated heavy metal accumulation by a Citrobacter sp. and related enterobacteria. Fems Microbiology Letters 121, 141-146.

Macaskie, L.E., Bonthrone, K.M., Yong, P., Goddard, D.T., 2000. Enzymically mediated bioprecipitation of uranium by a Citrobacter sp.: a concerted role for exocellular lipopolysaccharide and associated phosphatase in biomineral formation. Microbiology-Uk 146, 1855-1867.

Macaskie, L.E., Empson, R.M., Cheetham, A.K., Grey, C.P., Skarnulis, A.J., 1992. Uranium bioaccumulation by a c*itrobacter* sp as a result of enzymatically mediated growth of polycrystalline HUO_2PO_4 Science 257, 782-784.

Macaskie, L.E., Hewitt, C.J., Shearer, J.A., Kent, C.A., 1995. Biomass production for the removal of heavy-metals from aqueous-solutions at low pH using growth-decoupled cells of a citrobacter sp. International Biodeterioration & Biodegradation 35, 73-92.

Mackay, D.M., Cherry, J.A., 1989. Groundwater contamination: pump-and-treat remediation part 2. Environmental Science & Technology 23, 630-636.

Macur, R.E., Jackson, C.R., Botero, L.M., McDermott, T.R., Inskeep, W.P., 2004. Bacterial populations associated with the oxidation and reduction of arsenic in an unsaturated soil. Environmental Science & Technology 38, 104-111.

Madden, A.S., Palumbo, A.V., Ravel, B., Vishnivetskaya, T.A., Phelps, T.J., Schadt, C.W., Brandt, C.C., 2009. Donor-dependent Extent of Uranium Reduction for Bioremediation of Contaminated Sediment Microcosms. Journal of Environmental Quality 38, 53-60.

Madden, A.S., Smith, A.C., Balkwill, D.L., Fagan, L.A., Phelps, T.J., 2007. Microbial uranium immobilization independent of nitrate reduction. Environmental Microbiology 9, 2321-2330.

Majumder, A.L., Chatterjee, A., Dastidar, K.G., Majee, M., 2003. Diversification and evolution of L-myo-inositol 1-phosphate synthas. Febs Letters 553, 3-10.

Makower, R.U., 1970. Extraction and determination of phytic acid in beans (*Phaseolus-vulgaris*). Cereal Chemistry 47, 288-&.

Marko-Varga, G., Gorton, L., 1990. Postcolumn derivitization in liquid-chromatography using immobilized enzyme reactors and amperometric detection. Analytica Chimica Acta 234, 13-29.

Marsili, E., Beyenal, H., Di Palma, L., Merli, C., Dohnalkova, A., Amonette, J.E., Lewandowski, Z., 2007. Uranium immobilization by sulfate-reducing biofilms grown on hematite, dolomite, and calcite. Environmental Science & Technology 41, 8349-8354.

Martin, C.J., Evans, W.J., 1987. Phytic acid-divalent cation interactions. V. Titrimetric, calorimetric, and binding-studies with Cobalt(II) and Nickel(II) and their comparison with ohter metal-ions Journal of Inorganic Biochemistry 30, 101-119.

Martinez, R.J., Beazley, M.J., Taillefert, M., Arakaki, A.K., Skolnick, J., Sobecky, P.A., 2007. Aerobic uranium (VI) bioprecipitation by metal-resistant bacteria isolated from radionuclide- and metal-contaminated subsurface soils. Environmental Microbiology 9, 3122-3133.

Martinez, R.J., Wang, Y.L., Raimondo, M.A., Coombs, J.M., Barkay, T., Sobecky, P.A., 2006. Horizontal gene transfer of P-IB-type ATPases among bacteria isolated

from radionuclide- and metal-contaminated subsurface soils. Applied and Environmental Microbiology 72, 3111-3118.

Mattigod, S., Wellman, D.M., Glovack, J.N., Arey, B., Wood, M., 2008. Meta-Autunite Solubility as Related to Uranium Minerals in Concrete Waste Forms, Actinides IV---Basic Science, Applications, and Technology. Materials Research Society, San Francisco, CA.

Meek, J.L., Nicoletti, F., 1986. Detection of inositol trisphosphate and other organic-phosphates by high-performance liquid-chromatography using an enzyme-loaded postcolumn reactor. Journal of Chromatography 351, 303-311.

Meijer, E.M., Vanderzwaan, J.W., Wever, R., Stouthamer, A.H., 1979. Anaerobic respiration and energy-conservation in paracoccus-denitrificans - Functioning of iron-sulfur centers and the uncoupling effect of nitrite. European Journal of Biochemistry 96, 69-76.

Meleshyn, A., Azeroual, M., Reeck, T., Houben, G., Riebe, B., Bunnenberg, C., 2009. Influence of (Calcium-)Uranyl-Carbonate Complexation on U(VI) Sorption on Ca- and Na-Bentonites. Environmental Science & Technology 43, 4896-4901.

Merroun, M.L., Nedelkova, M., Ojeda, J.J., Reitz, T., Fernandez, M.L., Arias, J.M., Romero-Gonzalez, M., Selenska-Pobell, S., 2011. Bio-precipitation of uranium by two bacterial isolates recovered from extreme environments as estimated by potentiometric titration, TEM and X-ray absorption spectroscopic analyses. Journal of Hazardous Materials 197, 1-10.

Mohagheghi, A., Updegraff, D.M., Goldhaber, M.B., 1985. The role of sulfate-reducing bacteria in the deposition of sedimentary uranium ores. Geomicrobiology Journal 4, 153-173.

Mohanty, S.R., Kollah, B., Hedrick, D.B., Peacock, A.D., Kukkadapu, R.K., Roden, E.E., 2008. Biogeochemical processes in ethanol stimulated uranium-contaminated suhsurface sediments. Environmental Science & Technology 42, 4384-4390.

Montgomery, D.M., Dean, A.C.R., Wiffen, P., Macaskie, L.E., 1995. Phosphatase production and activity in citrobacter-freundii and a naturally-occurring, heavy-metal-accumulating citrobacter sp. Microbiology-Uk 141, 2433-2441.

Moon, H.S., Komlos, J., Jaffe, P.R., 2007. Uranium reoxidation in previously bioreduced sediment by dissolved oxygen and nitrate. Environmental Science & Technology 41, 4587-4592.

Mueller, R.F., Steiner, A., 1992. Inhibition of anaerobic-digestion caused by heavy-metals. Water Science and Technology 26, 835-846.

Mukhametzyanova, A., Akhmetova, A., Sharipova, M., 2012. Microorganisms as phytase producers. Microbiology 81, 267-275.

Mullaney, E.J., Ullah, A.H.J., 2007. Attributes, Catalytic Mechanisms and Applications, in: Turner, B.L., Richardson, A.E., Mullaney, E.J. (Eds.), Inositol Phosphates: Linking Agriculture and the Environment. CAB International, Cambridge, MA, pp. 97-110.

Murphy, Riley, 1962. A modified single solution method for determination of phosphate in natural waters. Analytica Chimica Acta 26.

Murphy, W.M., Shock, E.L., 1999. Environmental aqueous geochemistry of actinides, in: Burns, P.C.a.F., R. (Ed.), Uranium: Mineralogy, Geochemistry and the Environment. Mineralogical Society of America, Washington, D.C., pp. 221-254.

NABIR, 2003. Bioremediation of Metals and Radionuclides, DOE.

Nash, K.L., Jensen, M.P., Schmidt, M.A., 1998. Actinide immobilization in the subsurface environment by in-situ treatment with a hydrolytically unstable organophosphorus complexant: Uranyl uptake by calcium phytate. Journal of Alloys and Compounds 271, 257-261.

Nogales, B., Moore, E.R.B., Abraham, W.R., Timmis, K.N., 1999. Identification of the metabolically active members of a bacterial community in a polychlorinated biphenyl polluted moorland soil. Environmental Microbiology 1, 199-212.

North, N.N., Dollhopf, S.L., Petrie, L., Istok, J.D., Balkwill, D.L., Kostka, J.E., 2004. Change in bacterial community structure during in situ Biostimulation of subsurface sediment cocontaminated with uranium and nitrate. Applied and Environmental Microbiology 70, 4911-4920.

Nriagu, J.O., 1972. Stability of vivianite and ion-pair formation in system $Fe_3(PO_4)_2$-H_3PO_4-H_2O. Geochimica Et Cosmochimica Acta 36, 459-&.

Nyman, J.L., Marsh, T.L., Ginder-Vogel, M.A., Gentile, M., Fendorf, S., Criddle, C., 2006. Heterogeneous response to biostimulation for U(VI) reduction in replicated sediment microcosms. Biodegradation 17, 303-316.

Odell, B.L., Deboland, A.R., Koirtyoh.Sr, 1972. Distribution of phytate and nutritionally important elements among morphological components of cereal grains. Journal of Agricultural and Food Chemistry 20, 718-&.

Oh, B.C., Chang, B.S., Park, K.H., Ha, N.C., Kim, H.K., Oh, B.H., Oh, T.K., 2001. Calcium-dependent catalytic activity of a novel phytase from Bacillus amyloliquefaciens DS11. Biochemistry 40, 9669-9676.

Oh, B.C., Choi, W.C., Park, S., Kim, Y.O., Oh, T.K., 2004. Biochemical properties and substrate specificities of alkaline and histidine acid phytases. Applied Microbiology and Biotechnology 63, 362-372.

Ohnuki, I., Kozai, N., Samadfam, M., Yasuda, R., Yamamoto, S., Narumi, K., Naramoto, H., Murakami, T., 2004. The formation of autunite ($Ca(UO_2)_2(PO_4)_2$•nH_2O)within the leached layer of dissolving apatite: incorporation mechanism of uranium by apatite. Chemical Geology 211, 1-14.

Paiva, A.P., Malik, P., 2004. Recent advances on the chemistry of solvent extraction applied to the reprocessing of spent nuclear fuels and radioactive wastes. Journal of Radioanalytical and Nuclear Chemistry 261, 485-496.

Park, H.R., Ahn, H.J., Kim, S.H., Lee, C.H., Byun, M.W., Lee, G.W., 2006. Determination of the phytic acid levels in infant foods using different analytical methods. Food Control 17, 727-732.

Parthasarathy, R., Eisenberg, F., 1991. Biochemistry, stereochemistry, and nomenclature of the inositol phosphates. Acs Symposium Series 463, 1-19.

Payne, T.E., Davis, J.A., Waite, T.D., 1996. Uranium adsorption on ferrihydrite - Effects of phosphate and humic acid. Radiochimica Acta 74, 239-243.

Petrie, L., North, N.N., Dollhopf, S.L., Balkwill, D.L., Kostka, J.E., 2003. Enumeration and characterization of iron(III)-reducing microbial communities from acidic subsurface sediments contaminated with uranium(VI). Applied and Environmental Microbiology 69, 7467-7479.

Poolman, B., Nijssen, R.M.J., Konings, W.N., 1987. Dependence of *Streptococcus Lactis* phosphate transport on internal phosphate concentration and internal pH. Journal of Bacteriology 169, 5373-5378.

Powers, L.G., Mills, H.J., Palumbo, A.V., Zhang, C.L., Delaney, K., Sobecky, P.A., 2002. Introduction of a plasmid-encoded phoA gene for constitutive overproduction of alkaline phosphatase in three subsurface Pseudomonas isolates. Fems Microbiology Ecology 41, 115-123.

Qatibi, A.I., Niviere, V., Garcia, J.L., 1991. *Desulfovibrio-alcoholovorans* sp. nov., a sulfate-reducing bacterium able to grow on glycerol, 1,2-propanediol and 1,3-propanediol. Archives of Microbiology 155, 143-148.

Rake, J.B., Eagon, R.G., 1980. Inhibition, but not uncoupling, of respiratory energy coupling of 3 bacterial species by nitrite. Journal of Bacteriology 144, 975-982.

Rao, D., Rao, K.V., Reddy, T.P., Reddy, V.D., 2009. Molecular characterization, physicochemical properties, known and potential applications of phytases: An overview. Critical Reviews in Biotechnology 29, 182-198.

Ravva, S.V., Hernlem, B.J., Sarreal, C.Z., Mandrell, R.E., 2012. Bacterial communities in urban aerosols collected with wetted-wall cyclonic samplers and seasonal fluctuations of live and culturable airborne bacteria. Journal of Environmental Monitoring 14, 473-481.

Reddy, N.R., 2001. Occurrence, Distribution, Content, and Dietary Intake of Phytate, Food Phytates. CRC Press.

Regenspurg, S., Schild, D., Schafer, T., Huber, F., Malmstrom, M.E., 2009. Removal of uranium(VI) from the aqueous phase by iron(II) minerals in presence of bicarbonate. Applied Geochemistry 24, 1617-1625.

Regnier, P., Dale, A.W., Pallud, C., Lith, Y., Bonneville, S., Hyacinthe, C., Thullner, M., Laverman, A.M., Cappellen, P., 2005. Incorporating geomicrobial processes in reactive transport models of subsurface environments, in: Nützmann, G., Viotti,

P., Aagaard, P. (Eds.), Reactive Transport in Soil and Groundwater. Springer Berlin Heidelberg, pp. 109-125.

Roh, Y., Lee, S.R., Choi, S.K., Elless, M.P., Lee, S.Y., 2000. Physicochemical and mineralogical characterization of uranium-contaminated soils. Soil & Sediment Contamination 9, 463-486.

Romero-Gonzalez, M.R., Cheng, T., Barnett, M.O., Roden, E.E., 2007. Surface complexation modeling of the effects of phosphate on uranium(VI) adsorption. Radiochimica Acta 95, 251-259.

Rossolini, G.M., Schippa, S., Riccio, M.L., Berlutti, F., Macaskie, L.E., Thaller, M.C., 1998. Bacterial nonspecific acid phosphohydrolases: physiology, evolution and use as tools in microbial biotechnology. Cellular and Molecular Life Sciences 54, 833-850.

Rounds, M.A., Nielsen, S.S., 1993. Anion-exchange high-performance liquid chromatography with post-column detection for the analysis of phytic acid and other inositol phosphates. Journal of Chromatography A 653, 148-152.

Salome, K.R., Green, S.J., Beazley, M.J., Webb, S.M., Kostka, J.E., Taillefert, M., 2013. The role of anaerobic respiration in the immobilization of uranium through biomineralization of phosphate minerals. Geochimica Et Cosmochimica Acta 106, 344-363.

Sanford, R.A., Wu, Q., Sung, Y., Thomas, S.H., Amos, B.K., Prince, E.K., Loffler, F.E., 2007. Hexavalent uranium supports growth of Anaeromyxobacter dehalogenans and Geobacter spp. with lower than predicted biomass yields. Environmental Microbiology 9, 2885-2893.

Sato, T., Murakami, T., Yanase, N., Isobe, H., Payne, T.E., Airey, P.L., 1997. Iron nodules scavenging uranium from groundwater. Environmental Science & Technology 31, 2854-2858.

Satola, B., Wubbeler, J.H., Steinbuchel, A., 2013. Metabolic characteristics of the species Variovorax paradoxus. Applied Microbiology and Biotechnology 97, 541-560.

Schecher, W.D., McAvoy, D.C., 2001. MINEQL+: A Chemical Equilibrium Modeling System, Version 4.5 for Windows, User's Manual. Research Software, Hallowell, Maine.

Seaman, J.C., Hutchison, J.M., Jackson, B.P., Vulava, V.M., 2003. In situ treatment of metals in contaminated soils with phytate. Journal of Environmental Quality 32, 153-161.

Senko, J.M., Istok, J.D., Suflita, J.M., Krumholz, L.R., 2002. In-situ evidence for uranium immobilization and remobilization. Environmental Science & Technology 36, 1491-1496.

Senko, J.M., Mohamed, Y., Dewers, T.A., Krumholz, L.R., 2005a. Role for Fe(III) minerals in nitrate-dependent microbial U(IV) oxidation. Environmental Science & Technology 39, 2529-2536.

Senko, J.M., Suflita, J.M., Krumholz, L.R., 2005b. Geochemical controls on microbial nitrate-dependent U(IV) oxidation. Geomicrobiology Journal 22, 371-378.

Shan, Y., McKelvie, I.D., Hart, B.T., 1994. Determination of alkaline phosphatase-hydrolyzable phosphorus in natural-water systems by enzymatic flow-injection. Limnology and Oceanography 39, 1993-2000.

Shang, C., Stewart, J.W.B., Huang, P.M., 1992. pH effect on kinetics of adsorption of organic and inorganic phosphates by short-range ordered aluminum and iron precipitates. Geoderma 53, 1-14.

Sharp, J.O., Lezama-Pacheco, J.S., Schofield, E.J., Junier, P., Ulrich, K.-U., Chinni, S., Veeramani, H., Margot-Roquier, C., Webb, S.M., Tebo, B.M., Giammar, D.E., Bargar, J.R., Bernier-Latmani, R., 2011. Uranium speciation and stability after reductive immobilization in aquifer sediments. Geochimica Et Cosmochimica Acta 75, 6497-6510.

Shelobolina, E.S., Konishi, H., Xu, H.F., Roden, E.E., 2009. U(VI) Sequestration in Hydroxyapatite Produced by Microbial Glycerol 3-Phosphate Metabolism. Applied and Environmental Microbiology 75, 5773-5778.

Shelobolina, E.S., O'Neill, K., Finneran, K.T., Hayes, L.A., Lovley, D.R., 2003. Potential for in situ bioremediation of a low-pH, high-nitrate uranium-contaminated groundwater. Soil & Sediment Contamination 12, 865-884.

Shimizu, M., 1992. Purification and characterization of phytase from *Bacillus subtilis (natto)* N-77. Bioscience Biotechnology and Biochemistry 56, 1266-1269.

Shimizu, M., 1993. Purification and characterization of phytase and acid-phosphatase produced by *Aspergillus oryzae* K1. Bioscience Biotechnology and Biochemistry 57, 1364-1365.

Shin, S., Ha, N.C., Oh, B.C., Oh, T.K., Oh, B.H., 2001. Enzyme mechanism and catalytic property of beta propeller phytase. Structure 9, 851-858.

Shvets, V.I., Stepanov, A.E., Schmitt, L., Spiess, B., Schlewer, G., 1991. Synthesis and complexation properties of inositol phosphates. Acs Symposium Series 463, 155-171.

Sijbesma, W.F.H., Almeida, J.S., Reis, M.A.M., Santos, H., 1996. Uncoupling effect of nitrite during denitrification by Pseudomonas fluorescens: An in vivo P-31-NMR study. Biotechnology and Bioengineering 52, 176-182.

Singer, P.C., Stumm, W., 1970. Solubility of ferrous iron in carbonate-bearing waters. Journal American Water Works Association 62, 198-&.

Sitte, J., Akob, D.M., Kaufmann, C., Finster, K., Banerjee, D., Burkhardt, E.M., Kostka, J.E., Scheinost, A.C., Buchel, G., Kuesel, K., 2010. Microbial Links between Sulfate Reduction and Metal Retention in Uranium- and Heavy Metal-Contaminated Soil. Applied and Environmental Microbiology 76, 3143-3152.

Sivaswamy, V., Boyanov, M.I., Peyton, B.M., Viamajala, S., Gerlach, R., Apel, W.A., Sani, R.K., Dohnalkova, A., Kemner, K.M., Borch, T., 2011. Multiple Mechanisms of Uranium Immobilization by Cellulomonas sp Strain ES6. Biotechnology and Bioengineering 108, 264-276.

Smeaton, C.M., Weisener, C.G., Burns, P.C., Fryer, B.J., Fowle, D.A., 2008. Bacterially enhanced dissolution of meta-autunite. American Mineralogist 93, 1858-1864.

Snellinx, Z., Taghavi, S., Vangronsveld, J., van der Lelie, D., 2003. Microbial consortia that degrade 2,4-DNT by interspecies metabolism: isolation and characterisation. Biodegradation 14, 19-29.

Sobecky, P.A., Schell, M.A., Moran, M.A., Hodson, R.E., 1996. Impact of a genetically engineered bacterium with enhanced alkaline phosphatase activity on marine phytoplankton communities. Applied and Environmental Microbiology 62, 6-12.

Sowder, A.G., Clark, S.B., Fjeld, R.A., 2001. The impact of mineralogy in the U(VI)-Ca-PO_4 system on the environmental availability of uranium. Journal of Radioanalytical and Nuclear Chemistry 248, 517-524.

Spain, A.M., Krumholz, L.R., 2011. Nitrate-Reducing Bacteria at the Nitrate and Radionuclide Contaminated Oak Ridge Integrated Field Research Challenge Site: A Review. Geomicrobiology Journal 28, 418-429.

Steefel, C.I., DePaolo, D.J., Lichtner, P.C., 2005. Reactive transport modeling: An essential tool and a new research approach for the Earth sciences. Earth and Planetary Science Letters 240, 539-558.

Steefel, C.I., Van Cappellen, P., 1990. A new kinetic approach to modeling water-rock interaction: The role of nucleation, precursors, and Ostwald ripening. Geochimica Et Cosmochimica Acta 54, 2657-2677.

Stewart, B.D., Mayes, M.A., Fendorf, S., 2010. Impact of Uranyl−Calcium−Carbonato Complexes on Uranium(VI) Adsorption to Synthetic and Natural Sediments. Environmental Science & Technology 44, 928-934.

Stookey, L.L., 1970. Ferrozine- A new spectrophotometric reagent for iron. Anal. Chem. 42, 779-781.

Strandberg, G.W., Shumate, S.E., Parrott, J.R., 1981. MICROBIAL-CELLS AS BIOSORBENTS FOR HEAVY-METALS - ACCUMULATION OF URANIUM BY SACCHAROMYCES-CEREVISIAE AND PSEUDOMONAS-AERUGINOSA. Applied and Environmental Microbiology 41, 237-245.

Strater, N., Klabunde, T., Tucker, P., Witzel, H., Krebs, B., 1995. Crystal-structure of a purple acid-phosphatase containing a dinuclear Fe(III)-Zn(II) active-site. Science 268, 1489-1492.

Stubbs, J.E., Elbert, D.C., Veblen, D.R., Zhu, C., 2006. Electron microbeam investigation of uranium-contaminated soils from Oak Ridge, TN, USA. Environmental Science & Technology 40, 2108-2113.

Stumm, W., Morgan, J.J., 1996. Aquatic chemistry : chemical equilibria and rates in natural waters, 3rd ed. ed. Wiley, New York :.

Summers, A.O., Sugarman, L.I., 1974. Cell-free mercury(II)-reducing activity in a plasmid-bearing strain of *Escherichia coli*. Journal of Bacteriology 119, 242-249.

Suyama, T., Hosoya, H., Tokiwa, Y., 1998. Bacterial isolates degrading aliphatic polycarbonates. Fems Microbiology Letters 161, 255-261.

Suzuki, Y., Banfield, J.F., 1999. Geomicrobiology of uranium, in: Burns, P.C.a.F., R. (Ed.), Uranium: Mineralogy, Geochemistry and the Environment. Mineralogical Society of America, Washington, D.C., pp. 393-432.

Suzuki, Y., Banfield, J.F., 2004. Resistance to, and accumulation of, uranium by bacteria from a uranium-contaminated site. Geomicrobiology Journal 21, 113-121.

Sverjensky, D.A., Fukushi, K., 2006. A predictive model (ETLM) for As(III) adsorption and surface speciation on oxides consistent with spectroscopic data. Geochimica Et Cosmochimica Acta 70, 3778-3802.

Tessier, A., Campbell, P.G.C., Bisson, M., 1979. Sequential extraction procedure for the speciation of particulate trace-metals. Anal. Chem. 51, 844-851.

Tessier, A., Fortin, D., Belzile, N., DeVitre, R.R., Leppard, G.G., 1996. Metal sorption to diagenetic iron and manganese oxyhydroxides and associated organic matter: Narrowing the gap between field and laboratory measurements. Geochimica Et Cosmochimica Acta 60, 387-404.

Thullner, M., Regnier, P., Van Cappellen, P., 2007. Modeling microbially induced carbon degradation in redox-stratified subsurface environments: Concepts and open questions. Geomicrobiology Journal 24, 139-155.

Thullner, M., Van Cappellen, P., Regnier, P., 2005. Modeling the impact of microbial activity on redox dynamics in porous media. Geochimica Et Cosmochimica Acta 69, 5005-5019.

Tuovinen, O.H., Kelly, D.P., 1974. Studies on the growth of *Thiobacillus ferrooxidans*. II. Toxicity of uranium to growing cultures and tolerance conferred by mutation, other metal cations, and EDTA. Archives of Microbiology 95, 153-164.

Turner, B.L., Paphazy, M.J., Haygarth, P.M., McKelvie, I.D., 2002. Inositol phosphates in the environment. Philosophical Transactions of the Royal Society of London Series B-Biological Sciences 357, 449-469.

Ullah, A.H., Sethumadhavan, K., Mullaney, E.J., 2011. Vanadate Inhibition of Fungal PhyA and Bacterial AppA2 Histidine Acid Phosphatases. Journal of Agricultural and Food Chemistry 59, 1739-1743.

Ulrich, K.U., Ilton, E.S., Veeramani, H., Sharp, J.O., Bernier-Latmani, R., Schofield, E.J., Bargar, J.R., Giammar, D.E., 2009. Comparative dissolution kinetics of biogenic and chemogenic uraninite under oxidizing conditions in the presence of carbonate. Geochimica Et Cosmochimica Acta 73, 6065-6083.

Van Haverbeke, L., Vochten, R., Van Springel, K., 1996. Solubility and spectrochemical characteristics of synthetic chernikovite and meta-ankoleite. Mineralogical Magazine 60, 759-766.

Van Nostrand, J.D., Wu, L., Wu, W.-M., Huang, Z., Gentry, T.J., Deng, Y., Carley, J., Carroll, S., He, Z., Gu, B., Luo, J., Criddle, C.S., Watson, D.B., Jardine, P.M., Marsh, T.L., Tiedje, J.M., Hazen, T.C., Zhou, J., 2011. Dynamics of Microbial Community Composition and Function during In Situ Bioremediation of a Uranium-Contaminated Aquifer. Applied and Environmental Microbiology 77, 3860-3869.

Vanrhijn, P., Vanderleyden, J., 1995. The *Rhizobium*-plant symbiosis. Microbiological Reviews 59, 124-142.

Vershinina, O.A., Znamenskaya, L.V., 2002. The Pho regulons of bacteria. Microbiology 71, 497-511.

Vincent, J.B., Crowder, M.W., Averill, B.A., 1992. Hydrolysis of phosphate monoesters - A biological problem with multiple chemical solutions. Trends in Biochemical Sciences 17, 105-110.

Wade, R., DiChristina, T.J., 2000. Isolation of U(VI) reduction-deficient mutants of Shewanella putrefaciens. Fems Microbiology Letters 184, 143-148.

Waite, T.D., Davis, J.A., Payne, T.E., Waychunas, G.A., Xu, N., 1994. Uranium(VI) adsorption to ferrihydrite- application of a surface complexation model. Geochimica Et Cosmochimica Acta 58, 5465-5478.

Wan, J.M., Tokunaga, T.K., Brodie, E., Wang, Z.M., Zheng, Z.P., Herman, D., Hazen, T.C., Firestone, M.K., Sutton, S.R., 2005. Reoxidation of bioreduced uranium under reducing conditions. Environmental Science & Technology 39, 6162-6169.

Wang, Y., Van Cappellen, P., 1996. A multicomponent reactive transport model of early diagenesis: Application to redox cycling in coastal marine sediments. Geochimica Et Cosmochimica Acta 60, 2993-3014.

Wang, Y.P., Wiatrowski, H.A., John, R., Lin, C.C., Young, L.Y., Kerkhof, L.J., Yee, N., Barkay, T., 2013a. Impact of mercury on denitrification and denitrifying microbial communities in nitrate enrichments of subsurface sediments. Biodegradation 24, 33-46.

Wang, Z.M., Lee, S.W., Kapoor, P., Tebo, B.M., Giammar, D.E., 2013b. Uraninite oxidation and dissolution induced by manganese oxide: A redox reaction between two insoluble minerals. Geochimica Et Cosmochimica Acta 100, 24-40.

Wanner, B.L., 1993. Gene-regulation by phosphate in enteric bacteria. Journal of Cellular Biochemistry 51, 47-54.

Webb, S.M., 2005. SIXpack: a graphical user interface for XAS analysis using IFEFFIT. Physica Scripta T115, 1011-1014.

Webb, S.M., Fuller, C.C., Tebo, B.M., Bargar, J.R., 2006. Determination of uranyl incorporation into biogenic manganese oxides using X-ray absorption spectroscopy and scattering. Environmental Science & Technology 40, 771-777.

Webb, S.M., Tebo, B.M., Bargat, J.R., 2005. Structural characterization of biogenic Mn oxides produced in seawater by the marine bacillus sp strain SG-1. American Mineralogist 90, 1342-1357.

Wellman, D.M., Gunderson, K.M., Icenhower, J.P., Forrester, S.W., 2007. Dissolution kinetics of synthetic and natural meta-autunite minerals, $X_{3-n}^{(n)+}$ $[(UO_2)(PO_4)]_2 \bullet xH_2O$, under acidic conditions. Geochemistry Geophysics Geosystems 8.

Wellman, D.M., Icenhower, J.P., Owen, A.T., 2006. Comparative analysis of soluble phosphate amendments for the remediation of heavy metal contaminants: Effect on sediment hydraulic conductivity. Environmental Chemistry 3, 219-224.

Wersin, P., Hochella, M.F., Persson, P., Redden, G., Leckie, J.O., Harris, D.W., 1994. Interaction between aqueous uranium(VI) and sulfide minerals - spectroscopic evidence for sorption and reduction. Geochimica Et Cosmochimica Acta 58, 2829-2843.

Wielbo, J., 2012. Rhizobial communities in symbiosis with legumes: genetic diversity, competition and interactions with host plants. Central European Journal of Biology 7, 363-372.

Wielinga, B., Bostick, B., Hansel, C.M., Rosenzweig, R.F., Fendorf, S., 2000. Inhibition of bacterially promoted uranium reduction: Ferric (hydr)oxides as competitive electron acceptors. Environmental Science & Technology 34, 2190-2195.

Willems, A., Mergaert, J., Swings, J., 2005. Genus X. *Variovorax*., in: Brenner, D.J., Kreig, N.R., Staley, J.T., Garrity, G.M. (Eds.), Bergey's manual of systematic bacteriology. Second Edition, Volume Two: The *Proteobacteria*. Part C: The *Alpha-*, *Beta-*, *Delta-*, and *Epsilonproteobacteria*. Springer, New York, pp. 732-735.

Wise, A., 1986. Influence of calcium on trace metal interactions with phytate, in: Graf, E. (Ed.), Phytic acid: Chemistry and applications. Pilatus Press, Minneapolis, MN, pp. 151-160.

Wodzinski, R.J., Ullah, A.H.J., 1996. Phytase. Advances in Applied Microbiology, Vol 42 42, 263-302.

Wu, W.M., Carley, J., Fienen, M., Mehlhorn, T., Lowe, K., Nyman, J., Luo, J., Gentile, M.E., Rajan, R., Wagner, D., Hickey, R.F., Gu, B.H., Watson, D., Cirpka, O.A., Kitanidis, P.K., Jardine, P.M., Criddle, C.S., 2006a. Pilot-scale in situ bioremediation of uranium in a highly contaminated aquifer. 1. Conditioning of a treatment zone. Environmental Science & Technology 40, 3978-3985.

Wu, W.M., Carley, J., Gentry, T., Ginder-Vogel, M.A., Fienen, M., Mehlhorn, T., Yan, H., Caroll, S., Pace, M.N., Nyman, J., Luo, J., Gentile, M.E., Fields, M.W., Hickey, R.F., Gu, B.H., Watson, D., Cirpka, O.A., Zhou, J.Z., Fendorf, S., Kitanidis, P.K., Jardine, P.M., Criddle, C.S., 2006b. Pilot-scale in situ bioremedation of uranium in a highly contaminated aquifer. 2. Reduction of U(VI) and geochemical control of U(VI) bioavailability. Environmental Science & Technology 40, 3986-3995.

Wu, W.M., Carley, J., Green, S.J., Luo, J.A., Kelly, S.D., Van Nostrand, J., Lowe, K., Mehlhorn, T., Carroll, S., Boonchayanant, B., Lofller, F.E., Watson, D., Kemner, K.M., Zhou, J.Z., Kitanidis, P.K., Kostka, J.E., Jardine, P.M., Criddle, C.S., 2010. Effects of Nitrate on the Stability of Uranium in a Bioreduced Region of the Subsurface. Environmental Science & Technology 44, 5104-5111.

Yabusaki, S.B., Fang, Y., Waichler, S.R., 2008. Building conceptual models of field-scale uranium reactive transport in a dynamic vadose zone-aquifer-river system. Water Resources Research 44, W12403.

Yao, M.Z., Zhang, Y.H., Lu, W.L., Hu, M.Q., Wang, W., Liang, A.H., 2012. Phytases: crystal structures, protein engineering and potential biotechnological applications. Journal of Applied Microbiology 112, 1-14.

Yong, P., Macaskie, L.E., 1995. Enhancement of uraium bioaccumulation by a *Citrobacter* sp. via enzymatically-mediated growth of polycrystalline NH4UO2PO4. Journal of Chemical Technology and Biotechnology 63, 101-108.

Yoon, S.J., Choi, Y.J., Min, H.K., Cho, K.K., Kim, J.W., Lee, S.C., Jung, Y.H., 1996. Isolation and identification of phytase-producing bacterium, Enterobacter spz 4, and enzymatic properties of phytase enzyme. Enzyme and Microbial Technology 18, 449-454.

Yu, S., Cowieson, A., Gilbert, C., Plumstead, P., Dalsgaard, S., 2012. Interactions of phytate and myo-inositol phosphate esters (IP1-5) including IP5 isomers with dietary protein and iron and inhibition of pepsin. J. Anim. Sci. 90, 1824-1832.

Zabinsky, S.I., Rehr, J.J., Ankudinov, A., Albers, R.C., Eller, M.J., 1995. Multiple-scattering calculations of X-ray absorption spectra. Physical Review B 52, 2995-3009.

Zeng, H., Giammar, D.E., 2011. U(VI) reduction by Fe(II) on hematite nanoparticles. Journal of Nanoparticle Research 13, 3741-3754.

Zhang, F., Wu, W.-M., Parker, J.C., Mehlhorn, T., Kelly, S.D., Kemner, K.M., Zhang, G., Schadt, C., Brooks, S.C., Criddle, C.S., Watson, D.B., Jardine, P.M., 2010. Kinetic analysis and modeling of oleate and ethanol stimulated uranium (VI) bio-reduction in contaminated sediments under sulfate reduction conditions. Journal of Hazardous Materials 183, 482-489.

Zheng, Z.P., Tokunaga, T.K., Wan, J.M., 2003. Influence of calcium carbonate on U(VI) sorption to soils. Environmental Science & Technology 37, 5603-5608.

Zheng, Z.P., Wan, J.M., Song, X.Y., Tokunaga, T.K., 2006. Sodium meta-autunite colloids: Synthesis, characterization, and stability. Colloids and Surfaces a-Physicochemical and Engineering Aspects 274, 48-55.